DEPARTMENT OF PHYSICS
UNIVERSITY OF JYVÄSKYLÄ
RESEARCH REPORT No. 1/2009

A NEW GAMMA-RAY SPECTROMETRY SYSTEM FOR MEASUREMENTS OF RADIOACTIVITY IN THE MICRO-BECQUEREL RANGE

BY
J.S. ELISABETH WIESLANDER

Academic Dissertation
for the Degree of
Doctor of Philosophy

To be presented, by permission of the
Faculty of Mathematics and Natural Sciences
of the University of Jyväskylä,
for public examination in Auditorium FYS-1 of the
University of Jyväskylä on February 27, 2009
at 12 o'clock noon

Jyväskylä, Finland
February 2009

Preface

The work on this thesis would not have been possible without the help and contributions of other people and I hereby offer them my thanks, in the hope that I do not leave anyone out.

I would like to thank my local supervisor Docent *Mikael Hult* at IRMM in Belgium for the opportunity to work on this interesting project in the Radionuclide Measurements group (IM Unit) at the European Commission - JRC - IRMM, Belgium. Thank you for the guidance into the world of low-background measurements, interesting application projects, discussions about physics and many other things, as well as for always cheerfully answering my questions - of which I had many.

During my PhD I have had the great pleasure of working with two supervisors at the University of Jyväskyklä: this has worked incredibly well!

- If Professor *Harry J Whitlow* had not convinced me that I was "PhD-material" on the phone during the spring of 2005, I would never had done this work. For this I am forever grateful to *Harry* - the positive, dynamic and cheerful supervisor who always solves the various kinds of problems I serve him, whether academic or practical in nature. The PhD programme that he planned together with Professor Rauno Julin has been fun, interesting and exactly as tough as it should be.
- My second supervisor, Professor *Rauno Julin*, is one of the best teachers I have ever come across. He basically knows everything, asks all the right questions that I haden't thought of and discussions with him are always interesting, positive and intellectually challenging. It is easy and fun to study with such a Professor and *Rauno* has helped me to gain more knowledge in these three short years than I thought possible to get into my head. Thank you for your kind guidance towards the gaps in my knowledge and for the interesting discussions that lead to an even stronger interest in physics.

I would like to thank Dr. *Göran Lövestam* for making it possible for me to conduct the neutron activation experiments at PTB in Germany, two visits that turned out to be as interesting as the experiment itself. I am also grateful that you took the extra time to discuss the details of the experiments, theory and calculations at the end of my PhD.

I would like to thank my *colleagues* in the RN sector at IRMM for the pleasant discussions around the coffee table and general help whenever I was a bit lost in the new country and its ways of working. A special thanks to the *friends* and *colleagues* around the whole institute for the cheerful moments and interesting conversations

during the three years in Belgium and especially those that put so much effort into the choir and orchestra in the *music club* at IRMM - hard work but also lots of fun!

I would like to thank Dr. *Marcin Misiaszek* at the Jagiellonian University in Krakow (Poland) for all the help with the development of the ROOT code used for the data analysis. During Marcin's visits to Belgium we worked long hours, but we also had many interesting discussions about physics and other things. In this work we have proven that it is possible to collaborate well even when the only communication channel available is a variety of online chat programs.

The fond memories I have from Jyväskylä University are also a result of the positive, creative and open ambience in the research group. A special thanks to my fellow external PhD student Dr. *Ren Min-Qin* from Singapore for all the cheerful moments during hard studies and leisure time during the first and second year visits to Jyväskylä. Thank you *Ananda Sagari Arcot Rajashekar* for all the kind help, pleasant discussions and experiences of Indian culture! I also thank *Liping Wang*, *Somjai Sangyuenyongpipat*, *Mikko Laitinen*, and the senior assistant *Timo Sajavaara* for the pleasant discussions, help and good company during my visits to Jyväskylä.

I thank the *European Commission - Joint Research Centre - Institute for Reference Materials and Measurements*, Belgium, for the three-year contract offering financial support and resources that made this interesting and valuable work possible at IRMM.

I am grateful for financial support from the *Department of Physics, University of Jyväskylä*, the *Graduate School of Particle and Nuclear Physics (GRASPAND)* and the *Academy of Finland* (Centre of Excellence in Nuclear and Accelerator Based Physics, Ref. 213503). I am especially grateful for the financial support to finish my PhD given to me during the last three months, which shows how flexible you are. I would also like to express my general gratitude towards the Physics Department for running such a good department, as my visits to Finland have been some of my most productive. It is easy to be efficient in the quiet, bright and welcoming environment of Jyväskyklä University.

Finally, I thank my family at home, my parents *Birgitta & Gunnar* and my brother *Johan*, for the constant support not only during the PhD years. I appreciate the continuous, lively discussions in the diverse topics that we all seem to agree are a part of an interesting life and that have contributed to where I am today. I am grateful to my parents for their overall encouragement (even when they do not know where my latest idea might lead) and for the creative, free upbringing that challenged and educated us children intellectually as well as in practical matters such as home renovation techniques and gardening - the only strict requirement being that we should always use our head. Finally, I am especially grateful for the occasional computer and technology support that *Johan* has provided during these years, since it is a part of the fundament on which I and my computer stand - both professionally and privately.

Abstract

In this work a new ultra low-level γ-ray spectrometer has been designed, implemented, characterised and, finally, employed to detect radionuclides in samples with very low levels of activity. The spectrometer includes two high purity germanium (HPGe) detectors placed face-to-face inside a thick radiopure lead shield with an inner lining of electrolytic, radiopure copper. An active muon shield consisting of two plastic scintillators and one coincidence circuit is installed on top of the lead shield. The muon spectrum is gated with the coincidence signal between the two scintillators, which ensures that mainly high-energy events (i.e. muon-induced events) are collected. All data from the two germanium detectors is collected and the muon-induced events in the background spectra are identified and eliminated from the germanium spectra using offline software-based data analysis. In this way the background of the germanium detectors is reduced and lower detection limits achieved.

The spectrometer was in this work used in the following applications: the first detection and quantitative determination of charged particles escaping fusion plasma inside a tokamak, a new method for neutron dosimetry and spectrometry of environmental neutrons using thick metal discs, improvements of rare decay data of the world's rarest primordial isotope ^{180m}Ta and, finally, the quantitative low-uncertainty determination of the partial half-life and branching ratio for ^{115}In from which a theoretical value of the lower bound of the $Q_{\beta-}$ could be determined by a research group at Jyväskylä University. This Q-value was then compared to that determined by new mass measurements by another research group at the same University. The combined efforts of these three research groups lead to the discoveries that this transition may have the lowest known Q value of any nuclear decay discovered so far and the theory for such an ultra-low $Q_{\beta-}$-value must be further developed.

General introduction in Swedish - Översikt på svenska

Intresset för mätningar av radioaktivitet har på senare år ökat. Framför allt har det blivit viktigt att övervaka och kvantifiera olika typer av radioaktiva utsläpp i miljön, men med tiden har det tillkommit många ytterligare tillämpningsområden. De bland allmänheten mest välbekanta är mätningar av radionuklider från bombtester, produktionsprocesser av kärnbränsle och plutonium, tillverkning av vapen och tyvärr också olyckor, varav den mest kända är härdsmältan i Chernobyls kärnkraftverk 1986. Det finns radioaktivitetsmätningar som är en del av vårt dagliga liv utan att vi kanske tänker på det. Några av dessa är detektion och kvantifiering av

- olika typer av utsläpp i miljön,
- tillsatser och kontaminering av födoämnen och vatten,
- radioaktiv dos vid vid olika typer av medicinsk behandling,
- isotopsammansättning och nivå av radioaktivitet i material för tillverkningsindustrin,
- narkotiska preparat, kemikalier, materialkontroll för industriellt bruk (tex metallavfall), typiskt vid tull och flygplatskontroller, samt
- neutronemission kring alla typer av installationer med kärnfysikaliska processer.

I de här sammanhangen är det viktigt att utveckla internationellt erkända standardmetoder för mätningar och att framställa referensmaterial. Många organisationer arbetar med just detta, inte bara inom radioaktiva mätningar. Förutom att ge möjlighet till skydd mot farliga ämnen i mat, vatten och i miljön, är standardmetoder och referensmaterial basen för transaktioner i samhället av olika slag och utgör det fundament på vilket motsvarande lagar och förordningar vilar. Utan referensmaterial och tillförlitliga, etablerade mätmetoder kan vi egentligen inte veta om vi har detekterat den verkliga nivån av radioaktivitet i provet och huruvida denna nivå är farlig eller inte.

1999 inträffade en större olycka vid en kärnbränsleanläggning i Japan [Gasp04] och området runt anläggningen blev bestrålat med neutroner. Vid tillfället för olyckan fanns det ingen neutrondetektor i bruk som direkt kunde mäta neutronflödet. Istället samlade man in olika metaller, till exempel matskedar och guldsmycken, som blivit aktiverade av neutronstrålningen i byggnader kring anläggningen och mätte nivåerna av inducerad radioaktivitet i dem. På så sätt kunde man i efterhand bestämma neutronflödet från anläggningen på olika platser. Olyckan visade på behovet av en enkel, passiv neutrondetektor som skulle kunna installeras i förväg kring byggnader

där kärnfysikaliska processer är i bruk. En sådan enkel neutrondetektor beskrivs och testas i den här doktorsavhandlingen.

Ett exempel på ett internationellt samarbete kring detektion av luftburna radionuklider i miljön är den verksamhet som CTBTO (comprehensive nuclear-test-ban treaty organization) bedriver. För att kontrollera bombtestning runt om i världen använder CTBTO ett internationellt övervakningsystem som kombinerar ett världsomspännande nätverk för provinsamling med en serie laboratorier för analys av luftburna radionuklider [Mile09].

Med tiden har intresset ökat för utveckling och användning av mätutrustning med mycket låga bakgrundsnivåer på grund av: (i) låga nivåer av radioaktivitet i proverna, (ii) den ökande mängden av olika radionuklider som ska mätas samt (iii) kravet på snabbare mätningar. En stor fördel med låga nivåer av bakgrundstrålning i en detektor är att detektionsgränsen sjunker och följdaktligen kan mättiden kortas i vissa fall.

Gemensamt för många av de nämnda tillämpningarna är att radioaktivitetsmätningarna med fördel kan göras med γ-spektrometrar designade för att ha låg bakgrundsaktivitet. Gammaspektrometri erbjuder dessutom ett enkelt och i princip icke-förstörande sätt att förbereda prover, till skillnad från radiokemisk provframställning. En annan fördel är, eftersom γ-strålning enkelt penetrerar materia, att topparna i de uppmätta energispektra är skarpa även från tjocka prover, vilket vanligtvis inte är fallet vid detektion av laddade partiklar.

Idag är germaniumdetektorn den vanligast förekommande inom γ-spektrometri. De första germaniumdetektorerna dök upp i början på 1960-talet [Frec62], men då var germaniumkristallerna mycket små och detektionseffektiviteten låg. Med tiden har dock detektorerna såväl som de olika teknikerna kring γ-spektrometri utvecklats. HPGe-detektorn (high purity germanium) är idag arbetsmyran i de flesta γ-spektrometrilaboratorierna över hela världen. Dessa detektorer finns i många varianter och storlekar för såväl generella tillämpningar som mycket specifika, ovanliga mätningar.

Ett område inom γ-spektrometri som växer snabbt är mätningar i underjordiska laboratorier där bidraget till bakgrunden från den kosmiska bakgrundstrålningen är effektivt reducerad. Kombinationen av underjordisk placering, extremt noggrann design av HPGe-detektorerna, blyskydd, elektronik och ibland även kombination med en aktiv muondetektor, medför att bakgrunden i γ-spektrometern kan reduceras ytterligare. Just det här området kallas ultra låg-nivå γ-spektrometri, ULGS (ultra low-level γ-ray spectrometry). Med ULGS-detektorer kan man idag detektera nivåer av radioaktivitet som tidigare var omöjliga att upptäcka samt reducera mättiden för vissa mätningar.

De senaste årens ökning av underjordiska laboratorier [Hult07] har förbättrat åtkomsten av ULGS-detektorer för såväl forskningsändamål som för privatindustrin. Många

forskningsgrupper och företag förbättrar kontinuerligt både tillverkningen och analysteknikerna för ett brett spektrum av tillämpningsområden. Ett av de mest spektakulära av de stora internationella forskningsprojekten i Europa [GERDA, GERDA06] och i USA [Majo, Majo05] inom det här området är sannolikt experimenten ämnade att detektera neutrinomassan.

I denna doktorsavhandling har et nytt γ-spektrometrisystem för mätningar av aktivitet i storleksordningen μBq utvecklats, karakteriserats och testats med prover från flera olika tillämpningsområden. Spektrometern är uppbyggd av två HPGe-detektorer inuti ett tjockt, graderat blyskydd, som är fodrat med koppar. Ovanpå blyskyddet är två plastscintillatorer placerade. De två plastscintillatorerna bildar tillsammans en aktiv muondetektor och signalen från den undre scintillatorn är filtrerad med koincidenssignalen från de två scintillatorerna för att på så sätt sålla fram muonpulserna. Alla signaler från HPGe-detektorerna samt signalen från den undre plastscintillatorn och tiden registreras. Pulserna från muondetektorn används som en vetofunktion vid datanalysen som sker offline med specialdesignad mjukvara. Spektrometern har använts för mätningar av mycket låga nivåer av radioaktivitet i prover från följande tillämpningar:

- Detektion av radionuklider aktiverade av laddade partiklar samt neutroner från fusionsplasma.
- Neutrondosimetri och spektrumbestämning av olika neutronflöden.
- Identifiering och karakterisering av ovanliga radioaktiva sönderfall samt förbättringar av existerande data.

I arbetet har en metod för neutronspektrometri vidareutvecklas och verifierats. Metoden består i princip av tre steg: (i) neutronaktivering av metalldiskar, (ii) detektion av de aktiverade radionukliderna med lågnivå γ-spektrometri, (iii) matematisk analys och beräkningar för bestämning av både neutronspektrumet och dosen. Den här metoden för neutrondetektion skulle i framtiden kunna användas som ett standardiserat, passivt monitorsystem kring alla typer installationer för kärnfysikaliska processer. Se vidare information i Paper V-VI.

En annan tillämpning kommer från den engelska fusionsforskningsanläggningen JET (Joint European Torus) där forskningsgrupper från hela EU arbetar tillsammans för att utveckla fusionstekniken. I detta experiment fördes en liten prob (cirka 15 cm) in i taket på tokamaken och proverna i proben aktiverades av de partiklar som spreds från fusionsplasmat. För första gången kunde laddade partiklar påvisas och kvantitativt mätas inuti en tokamak. Aktiveringen av neutroner beräknades också och jämfördes med flera andra netronflödesmätningar gjorda med annan utrustning vid JET. Neutronerna från fusionsplasmat kan ju enkelt detekteras med mätutrustning placerad

utanför själva tokamaken eftersom neutroner penetrerar väggarna, medan laddade partiklar måste detekteras inuti tokamaken då de knappt ens passerar proverna och aldrig väggarna. Se vidare information i Paper I-II.

I detta arbete har också ett nytt gränsvärde mätts för halveringstiden av det ovanliga sönderfallet i tantalum, dvs av isotopen ^{180m}Ta, se Paper IV. Ett av de mer spektakulära resultaten i doktorsavhandlingen är nog mätningarna av det ovanliga sönderfallet av ^{115}In till det första exciterade tillståndet i ^{115}Sn. Halveringstiden för sönderfallet bestämdes till $(4.1 \pm 0.6)\times 10^{20}$ år. Detta värde på halveringstiden och teoretiska beräkningar gjorda av forskare vid Jyväskylä Universitet resulterade i att ett värde på sönderfallsenergin (Q-värdet) kunde beräknas. Slutligen jämfördes resultaten från gammamätningarna med nya massmätningar av de ingående nukliderna, gjorda av IGISOL-gruppen vid Jyväskylä Universitet. Kombinationen av två separata mätningar och de teoretiska beräkningarna ledde till att vi tror oss möjligen ha funnit en av lägsta hittils kända sönderfallsenergierna för något radioaktivt sönderfall. Dessutom har det lett till ökad förståelse av den teoretiska modellen och vidareutveckling av de teoretiska beräkningarna inom teorigruppen.

De två sista artiklarna i den här avhandlingen handlar om det arbete som gjorts hittills (Paper VIIa) och det fortgående arbetet (Paper VIIb) för att lösa kvarstående frågor samt öka noggrannheten i mätningarna. Den första artikeln, Paper VIIa, är med sitt korta format avsedd för Physical Review Letters (PRL). Den är inkluderad här i ett utförande som förväntas förändras bara marginellt innan artikeln skickaas till PRL. Den längre artikeln, Paper VIIb, är bifogad som utkast eftersom arbete pågår för att inkludera alla detaljer kring mätningarna samt ytterligare mätdata med bättre noggrannhet och utökade lösningar till teorimodellen. Den artikeln kommer också att utförligare diskutera möjliga användningsområden för den här typen av mätningar och sammarbeten.

Publication list

Paper I
Low-level gamma-ray spectrometry for analysing fusion plasma conditions. **J.S.E. Wieslander**, M. Hult, G. Bonheure, D. Arnold, H. Dombrowski, J. Gasparro, M. Laubenstein, G. Marissens, P. Vermaercke. Nucl. Inst. Meth. A, 591 (2008) 383-393. (Performed measurements, all the data analysis & calculations and was the principal author of the paper.)

Paper II
Mega-electron-volt ion loss measurements in JET $D-^3He$ plasmas using activation technique. G. Bonheure, **E. Wieslander**, M. Hult, J. Gasparro, G. Marissens, D. Arnold, M. Laubenstein, S. Popovichev, A. Murari, I. Lengar and JET-EFDA contributors. FUSTE8 VOL 53(3) 806-815 (2008). (Contributed with the gamma-ray measurements, analysis and interpretation that are used in the paper and the calculations, which in turn lead to important conclusions for fusion research.)

Paper III
The Sandwich spectrometer for ultra low-level γ-ray spectrometry. **J.S.E. Wieslander**, M. Hult, J. Gasparro, G. Marissens, M. Misiaszek, W. Preuβe. Appl. Rad. Isot. (2009) DOI link: doi:10.1016/j.apradiso.2009.01.026. (The spectrometer is the principal work of my PhD. Contributed to the initial hardware design and built up the entire electronics. Performed all measurements, designed the software analysis system, carried out all data analysis & calculations, and wrote the paper.)

Paper IV
Search for the radioactivity of ^{180m}Ta using an underground HPGe Sandwich spectrometer. M. Hult, **J.S.E. Wieslander**, G. Marissens, J. Gasparro, U. Wätjen, M. Misiaszek. Appl. Rad. Isot. (2009) DOI link: doi.org/10.1016/j.apradiso.2009.01.057. (Performed measurements, all analysis of data from the Sandwich spectrometer and contributed to writing the paper.)

Paper V
Neutron fluence spectrometry using disk activation. G. Lövestam, M. Hult, A. Fessler, J. Gasparro, P. Kockerols, K. Okkinga, H. Tagziria, F. Vanhavere, **J.S.E. Wieslander**. Rad. Meas., 44(1) (2008), 72-79. (Constructed several of the neutron dosimeters, performed measurements, contributed to the data analysis and to writing the paper.)

Paper VI
A neutron dosimetry and spectrometry method using activation of thick metal discs. **J.S.E. Wieslander**, G. Lövestam, M. Hult, D. Arnold, A. Fessler, J. Gasparro, P. Kockerols, A. Zimbal, *to be submitted 2009 to Rad. Prot. Dos.*. (Performed the activations at PTB, carried out all measurements and data analysis from the measurements, parts of the calculations and was the principal author of the paper.)

Paper VIIa
The smallest known Q value of a nuclear decay: the rare β^- decay of $^{115}In(9/2^+) \rightarrow {}^{115}Sn(3/2^+)$ **J.S.E. Wieslander**, M. Hult, J. Suhonen, T. Eronen, M.T. Mustonen, V.-V. Elomaa, A. Jokinen, G. Marissens, M. Misiaszek, S. Rahaman, C. Weber, J. Äystö, *to be submitted 2009 to Phys. Rev. Lett.*. This is the short version of the "indium-paper" which will submitted to PRL. (Analysed the complete data from the γ-ray measurements on the Sandwich Spectrometer, carried out all calculations for that data including the final combined weighted values and uncertainties for all three spectrometers' data. Principal author of the article.)

Paper VIIb
Underground measurement of the rare β^- decay of the ^{115}In ground state to the first excited state of ^{115}Sn. **J.S.E. Wieslander**, M. Hult, J. Suhonen, T. Eronen, M.T. Mustonen, V.-V. Elomaa, A. Jokinen, G. Marissens, M. Misiaszek, S. Rahaman, C. Weber, J. Äystö, *to be submitted 2009 to Phys. Rev. C.* Included here is the first draft for a longer "indium-paper", which will include detailed information of the experiments, further theoretical work and updated data (of lower uncertainty). This longer paper will be submitted to Phys. Rev. C or similar journal during the early spring 2009.

Contents

1 Introduction

1.1 γ-ray measurements in today's society

In today's society there is an increasing need to establish standards and methods for control measurements of radionuclides in the environment. With time it has become interesting to develop ultra low-background detection systems, since the level of activity in the sample is often very low, there is a wide variety of radionuclides to be detected and the increasing demand for faster measurements requires lower detection limits.

The applications for radioactivity measurements best known to the public are those for radionuclides originating from nuclear bomb testing, nuclear fuel or plutonium proliferation, the manufacture of weapons and, finally, nuclear accidents as those at the Chernobyl power plant in 1986 and the JCO fuel plant in Japan in 1999 [Gasp04]. There are, however, many other applications for radionuclide detection that in several ways are part of our everyday life, such as measuring:

- Additives and contaminations in food and water.
- The doses given to patients during cancer treatment.
- The isotopic composition and radiopurity of materials.
- Narcotic substances, chemicals, industrial materials (scrap metal), typically at customs and airport controls.
- Neutrons around all nuclear installations.

It is important to develop reference materials and establish international standards and many international organisations are working continuously on development in this field. These measurement standards and references are particularly important in society as they form the basis of commercial transactions as well as many laws and ordinances. Without a reference material or an established and reliable measurement method, how would we be certain of what was detected and if the level of activity is reasonable or not?

To monitor bomb testing activities, the comprehensive nuclear-test-ban treaty organization (CTBTO) uses an international monitoring system that combines a wide network for sample collection with a series of laboratories for the analysis of radionuclides in aerosols [Mile09]. The criticality accident in Japan [Gasp04] showed the need for simple neutron dosimetry systems near to all nuclear installations and one example of such a detection system is presented in this work. For many applications it is appropriate to use low-background γ-ray spectrometry, which offers robust and sensitive detectors in combination with simple, non-destructive sample preparation. Another advantage is that since γ-rays can penetrate matter without any interaction, a sharp full energy peak can be detected even from thick samples, which is typically not the case in charged particle detection.

One of the detectors most widely used today for γ-ray spectrometry is the germanium detector. The first germanium detectors appeared in the early 1960s [Frec62], but at the time the crystals were very small and the detection efficiency low. With time, the detectors and γ-ray spectrometry techniques in general developed and today the high-purity germanium (HPGe) detectors are the workhorses in most γ-ray spectrometry laboratories around the world and range from general-purpose systems to custom designs for specific applications. One fast-growing field is ultra low-level γ-ray spectrometry (ULGS), which is performed underground. Moving a low-background HPGe detector to an underground laboratory greatly reduces the contribution to the spectrometer background from cosmic radiation. Combining this with careful design of the shielding, electronics, data collection system and even an active muon shield decreases the background further. These low-background spectrometers now detect levels of activity that were previously impossible to measure. It also turns out to be meaningful to reduce the detector background further, since this shortens the measurement time.

The increase in number of underground laboratories during recent years [Hult07] has contributed to an increased availability of ULGS measurements for both research groups and private industry. Many research groups and manufacturing companies are working on improving ULGS technology and analysis techniques in order to use expand the field of applications. Among the spectacular international research projects in fundamental physics are the experiments for the search of the neutrino mass that are set up both in Europe [GERDA, GERDA06] and the USA [Majo, Majo05].

In this work a new ultra low-level γ-ray spectrometer was developed, characterised and used for application measurements. The spectrometer has two HPGe detectors facing each other, a custom designed graded lead shield, an active muon shield and all data analysis is done off line. The spectrometer was used to detect radionuclides in low activity samples for the following applications:

- Charged particle activation by fusion plasma.
- Neutron dosimetry and spectrometry.
- Improvements of rare decay data of ^{180m}Ta.
- Rare decay data validation and characterization for ^{115}In.

During this work a new neutron dosimetry and spectrometry method was further developed and tested. The method was based on neutron activation of small, thick metal discs combined with ultra low-level γ-ray spectrometry and spectrum unfolding techniques to determine both the neutron energy spectrum and the dose from environmental neutron fields. This neutron spectrometry method and equipment could be used as a standard, passive monitoring system around any kind of nuclear installation, see Paper V-VI. In another application of ULGS, activation samples from JET (Joint European Torus fusion facility, UK) were measured and, for the first time, the charged particles leaking out from the fusion plasma could be quantitatively measured, see Paper I-II. Finally, among the more spectacular outcome of this work is probably the low-uncertainty measurement of the rare decay in ^{115}In to the first excited state in ^{115}Sn, for which the partial half-life was determined to $(4.1 \pm 0.6)\times10^{20}$ y. In the end it turned out that this partial half-life corresponds to a very low Q value, which could possibly be the lowest known Q value of any nuclear discovered so far, see Paper VIIa-b.

1.2 Synopsis

The general applications and usefulness of γ-ray spectrometry are briefly discussed in this chapter together with a short comment about the research in this work.

The basics of low-level γ-ray spectrometry are discussed in *Chapter 2* together with some important aspects in design of an ULGS system.

Chapter 3 briefly introduces the underground laboratory HADES and describes in detail the set-up of the new detector system, the Sandwich Spectrometer.

In *Chapter 4* the characteristics of the Sandwich Spectrometer and the overall system performance are presented together with other key system properties.

The applications included in this work are described in *Chapter 5* and, finally, the conclusion is found in *Chapter 6*.

2 Low-level γ-ray spectrometry

Reducing the levels of background radiation in a detection system improves the detection limits, thereby allowing lower levels of activity to be detected. The key to good performance, particularly of a low-level γ-ray spectrometry system is not to know only the background contributors but also to continuously work on reducing them, a process that starts as early as in the design phase and continues throughout the lifetime of every spectrometer.

The main background contributions are listed in Table 2.1. The major part of the background from the three first groups originate from the naturally-occurring decay chains ^{232}Th, ^{235}U and ^{238}U plus the activity from ^{40}K. A recently written overview of low-level γ-ray spectrometry [Hult07] discusses many aspects of low-background measurements and technology, as well as listing many interesting references, which investigate these in detail.

Contributor	**Description**
Environmental radioactivity	- Laboratory surroundings. - Unfiltered air, dust particles. - Airborne radioactivity from external sources.
Radon and its progeny	- Natural decay chains in the environment and the detector materials.
Radioactivity from spectrometer material & electronics	- Natural decay chains in lead and copper. - Impurities in: lead or copper shield, germanium crystal, endcap. - Solder and electronic components in the pre-amplifier and front-end electronics. - Glue or other adhesives used in the detector. - Activation products in lead, copper or the germanium crystal.
Cosmogenically-induced radiation	- Muons and neutrons.
Close geometry effects	- Coincidence summing effects. - Errors in measurements of the close geometry.

Table **2.1**: The background contributions and main issues in a low-background spectrometer.

A low-background spectrometer consists of the following main parts: the outer lead, inner lead, inner copper lining, high-purity germanium detector(s), signal electronics and data collection system. Each of these parts is subject to a series of considerations when designing a low-background spectrometry system.

The typical γ-ray interactions in a medium sized germanium detector and schematic drawings of the corresponding γ-ray spectra for both high and low photon energies are shown in Figure 2.1. Each incident photon can give rise to a series of interactions (one such sequence is referred to as a "history") and some of these interactions contribute to the background levels in a germanium detector, which will be discussed in this chapter.

2.1 Background radiation

A critical point in the design of a γ-ray spectrometer for very low levels of activity is to make sure that all parts of the spectrometer are radiopure. If the level of radiopurity is unknown the selected materials are screened and it should always be taken into consideration that the activity level can vary from batch to batch of industrially produced equipment, so radiopurity measurements cannot be generalised. The overall count-rate in the background can be reduced by a factor of almost 10 after careful selection of the materials [Hult06] and the major background reduction is achieved by selecting a good shield. Many of the issues that should be addressed when designing a low-background system are discussed in overview papers with extensive references [Hult06, Hult07] as well as in the information booklets from the manufacturers [Canb]. In the end, only materials selected and screened by the customers will be included in the state-of-the-art spectrometers for ultra low-level γ-ray spectrometry running in the world today [Heus06, GERDA, GERDA06, Majo, Majo05, Brod90]. In addition to the requirements on the hardware, the samples should be prepared in a clean environment in a way that ensures that no additional contaminants are added to the sample or the sample holder. This is necessary in order to avoid introducing background into the measurements or, at worst, contaminating the low-background spectrometer.

2.1.1 Cosmic rays and neutron induced background

The cosmic rays are mainly made up of protons (the majority), alpha particles and heavy ions [Knoll00, Grei01]. These particles have very high kinetic energies and when colliding with other particles upon entry into Earth's atmosphere they produce showers of secondary radiation such as muons, neutrons, electrons, protons, various mesons and photons. The particles in the secondary showers also have high energies and can

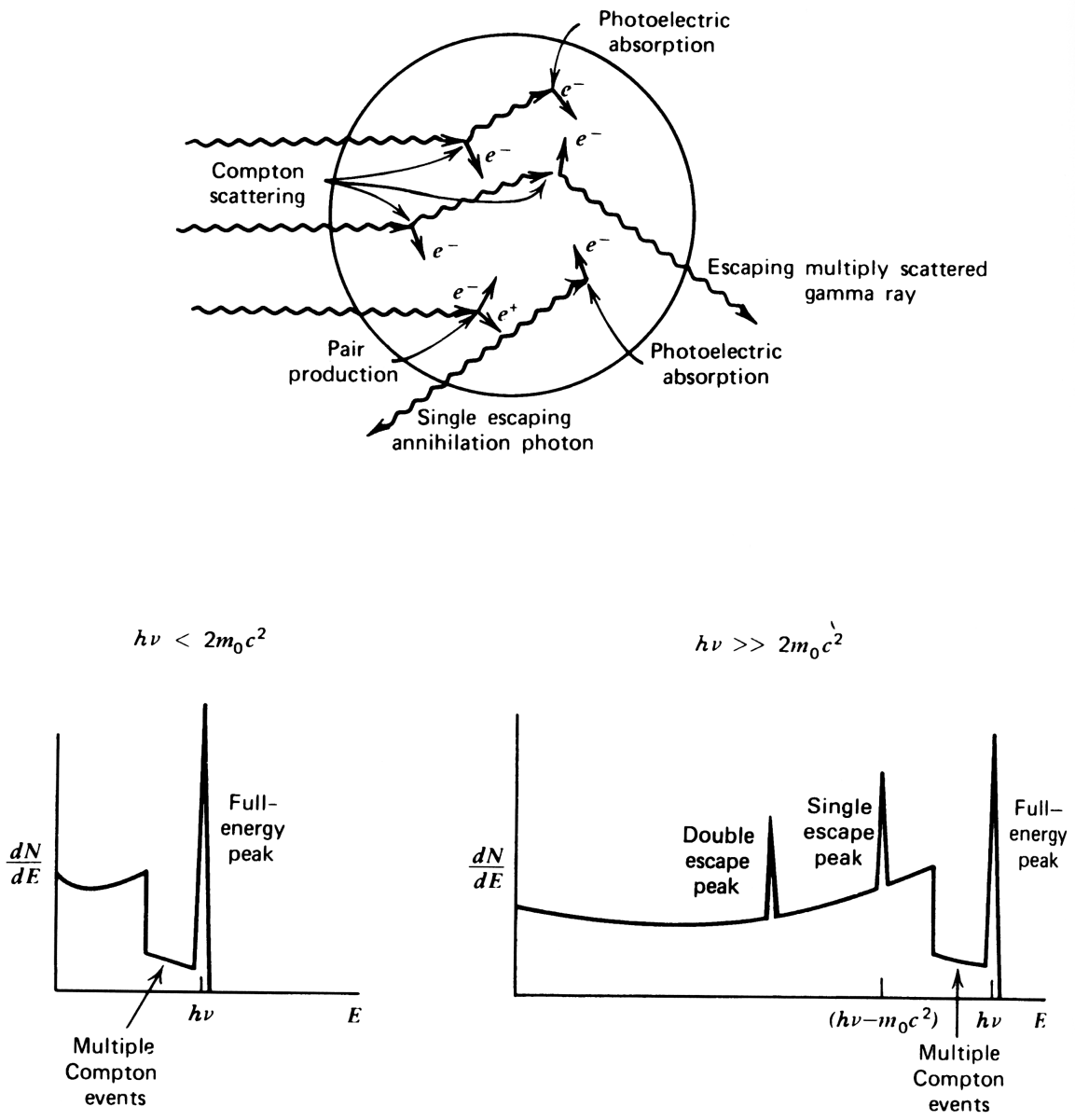

Figure **2.1**: The γ-ray interactions in a medium sized germanium detector and two schematic drawings of the resulting γ-ray spectra, which depend on the energy of the incident photon. (Figure 10.4 from *Radiation detection and measurement*, G.F. Knoll, third edition. Copyright 2000 by John Wiley & Sons, Inc. Reprinted with the permission of John Wiley & Sons, Inc).

travel long distances through the atmosphere. At ground level the main components left are electrons and photons (soft component) and the muons (hard component). In low-background γ-ray spectrometers the interactions of the secondary cosmic radiation with the shield and germanium detector lead to background contributions from bremsstrahlung, X-rays, neutrons and the annihilation lines.

Depth (m w.e.)	**Classification**	**Characteristics**
<10	Not underground or above ground	- The soft component from the cosmic background (e^-, e^+, photons) is greatly reduced. - Very little reduction of the muon flux and muon-induced neutrons. - Muon shields are useful. - The detector crystal and shield are still cosmogenically activated.
10-100	Shallow underground	- No soft component from the cosmic background. - The muon flux is reduced by a factor of 5-50. - The muon-induced neutron flux is reduced by a factor of 2-10. - Muon shields are useful. - The detector crystal and shield are still cosmogenically activated.
100-1000	Semi-deep underground	- Cosmogenic activation of the detector and shield can be neglected. - Slight improvements by discriminating against muons. - The neutron flux is dominated by (α,n) sources and not by cosmogenic neutrons.
>1000	Deep underground	- No cosmogenic activation. - The only neutron source is from (α,n) reactions.

Table **2.2**: Classification of underground laboratories for low-level γ-ray spectrometry after [Hult06]. The depth is given in metres water equivalent, m w.e.

The main reason to place a γ-ray spectrometer to an underground laboratory is to reduce the background from secondary cosmic radiation, and the soft component is removed even at shallow depths [Nies98]. An underground laboratory in combination with a veto detector for muon detection will greatly reduce the overall background contribution from the cosmic muons, which consitute approximately 80% of the secondary cosmic radiation of charged particles [Knoll00]. The classification of underground laboratories and the reduction of cosmically-induced background radiation as a function of depth are listed in Table 2.2 [Hult06].

The depth of an underground laboratory is commonly given in the unit of metres water equivalent, m w.e., which is useful when comparing underground laboratories such as those in references [Laub04, Neum00, Ways99, Arpe96, Mile91].

Energy (keV)	Reaction
68.2	^{73}Ge(n,n')^{73}Ge
562.9	^{76}Ge(n,n')^{76}Ge
569.7	^{207}Pb(n,n')^{207}Pb
595.9	^{74}Ge(n,n')^{74}Ge
669.6	^{63}Cu(n,n')^{63}Cu
691.3	^{72}Ge(n,n')^{72}Ge
803.1	^{206}Pb(n,n')^{206}Pb
846.8	^{56}Fe(n,n')^{56}Fe
962.1	^{63}Cu(n,n')^{63}Cu
1115.5	^{65}Cu(n,n')^{65}Cu
2624.6	^{208}Pb(n,n')^{208}Pb

Table **2.3**: Background γ-lines originating from inelastic scattering of fast neutrons leading to prompt γ-rays (i.e. not activation) [Canb].

Energy (keV)	Reaction
23.4	^{70}Ge(n,γ)^{70}Ge
53.4, 66.7	^{72}Ge(n,γ)^{73m}Ge
139.7	^{74}Ge(n,γ)^{74m}Ge
159.5	^{76}Ge(n,γ)^{77m}Ge
174.9, 198.9	^{70}Ge(n,γ)^{71m}Ge
203.1	Cu(n,γ)Cu
278.3	^{63}Cu(n,γ)^{64}Cu

Table **2.4**: Background γ-ray lines from absorption of thermal neutrons leading to activation of the material [Canb].

Fast and thermal neutrons also contribute to the spectrometer background and these neutrons originate from both cosmic radiation and nearby nuclear installations. The typical γ-ray lines in the background due to neutron interactions with the detector materials are listed in Table 2.3-2.4 [Canb]. The inside of a low-background spectrometer located underground is usually lined with radiopure electrolytic copper, which efficiently shields off the background from the lead shield (^{210}Pb, see section *2.1.3*). Since copper has a very high cross-section for the capture of thermal neutrons it is activated by the thermal neutrons produced from interactions of the secondary cosmic showers with matter through the reactions listed in Table 2.4. Consequently, a copper lining is only suitable in underground laboratories and it is crucial that it does not

spend time above ground prior to its installation in the underground facility. None of the γ-rays from the reactions listed in Table 2.3-2.4 have been identified in the background spectra of the present work, mainly because the materials used in the spectrometer were stored underground.

2.1.2 Radon

Since traces of the natural decay chains are present in several of the construction materials used for detector shielding as well as in the environmental background, small amounts of ^{222}Rn (radon) and ^{220}Rn (thoron), see Figure 2.2, are always present. Radon is a noble gas and migrates through the system before it finally decays. When radon decays to polonium it is ionised and has great affinity to surfaces, which leads to higher concentrations on the walls of the sample volume inside the spectrometer. The sequence of beta decays of radon and thoron will contribute to the detector background with bremsstrahlung and individual γ-ray lines. The dominant contributions from radon are the ^{222}Rn daughters ^{214}Pb and ^{214}Bi that result in a few easily identified γ-ray peaks in the background spectra of the present work. A small background contribution originates from thoron that is identified by the γ-ray lines from ^{212}Pb and ^{208}Tl.

Flushing the sample volume inside the detector with the boil-off nitrogen gas from the liquid nitrogen (LN2) used to cool the germanium crystals efficiently reduces the radon concentration. However, the LN2 can be contaminated if the tank or Dewar used for storage is made of steel with a high ^{226}Ra concentration. Additionally, the concentration of ^{226}Ra is higher in the last portion of LN2 in the tank, so a tank should not be run empty.

2.1.3 Shielding materials

Lead

Lead is a commonly used shielding material since it is an efficient absorber of radiation with its high density and large Z, it has suitable mechanical properties, it has low neutron cross-section, low interaction probability with secondary cosmic radiation and is of reasonable cost. However, lead has an intrinsic activity of ^{210}Pb that is not negligible and the precence of that as well as other contaminants were discussed in references [Heus95, Theo97]. ^{210}Pb is the isotope with the longest half-life (22 y) in the deay chain of radon from the ^{238}U series, see Figure 2.2. The major sources of ^{210}Pb are the minerals in the lead ores. The small concentrations of uranium and

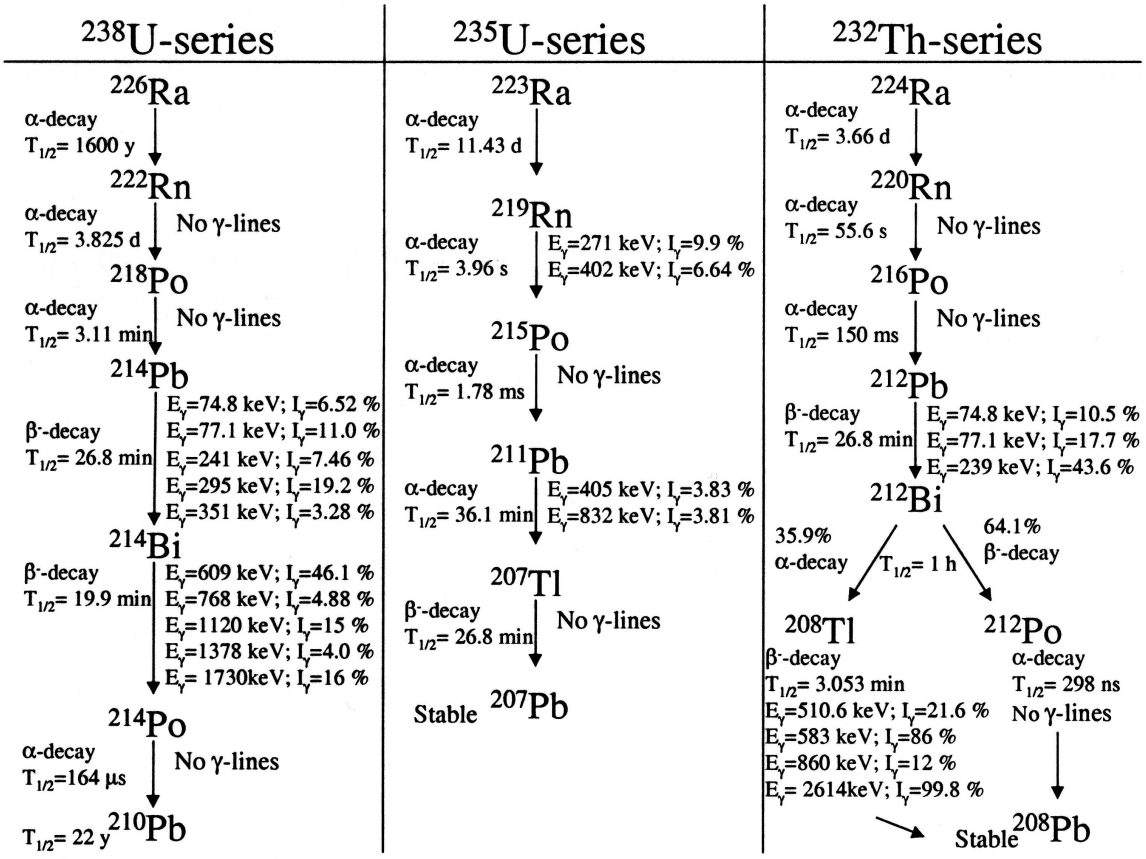

Figure **2.2**: The simplified structure of three natural decay chains, showing the part in which radium decays to the main background contributors: radon (^{222}Rn) and thoron (^{220}Rn) [Ellm02].

thorium are usually efficiently separated during the start of the smelting and refining processes. However, the ^{210}Pb that is already present can not be separated from the other lead isotopes and will continue through the process with the rest of the lead. If coal/coke is used in the smelting process this can increase the transfer of ^{210}Pb to the smelted lead since coal and coke contains quite high levels of uranium.

Today certified lead produced with low levels of contamination is readily available, although the price increases with the radiopurity. However, an alternative to using modern certified lead is the so-called "old lead" . The lead is labeled "old" because of its ancient origin and the advantage is that many half-lives of ^{210}Pb have passed since it was produced. Since lead is toxic, today it is replaced with less polluting materials and in those cases the removed lead becomes available for research groups. However, the sources of old lead are somewhat limited to roof tiles of historical buildings, old water pipes and a few exeptional discoveries such as that of a large quantity of antique Roman lead on a sunken ship near Sardinia [Ales91]. By using old lead, not only is the metal itself recycled but advantage is also taken of the very low levels of activity

that is a result of undisturbed decay during hundreds of years. After 200 years only 0.2% of the original activity of ^{210}Pb remains.

The level of radiopurity of lead is commonly given as the activity of ^{210}Pb. The main contributions from ^{210}Pb to the background in a germanium detector stems from individual γ-ray lines, see examples in Table 4.2 in *Chapter 4*, and the bremsstrahlung from the daughters' subsequent beta decays. The lead shield in low-level γ-ray spectrometry is usually split into two parts, with an outer part of 10-20 cm thickness made of lead with an activity of $<$20 Bq/kg (^{210}Pb). The inner part is $<$10 cm thick with an activity of $<$1-3 Bq/kg (^{210}Pb).

Copper

The inner part of the lead shield is lined with radiopure electrolytic copper to protect the measurement volume from the background contributions of lead. Copper can be produced with very high levels of radiopurity and that makes it suitable as lining material. This type of graded shields, i.e. shields with several layers of different materials shielding off the background from each other, are commonly used in low-level γ-ray spectrometry although the materials used depend on the application. Copper is, for example, an excellent lining material in an underground laboratory but above ground interactions and activation by the high level of cosmic secondary radiation (see Tables 2.3-2.4) may increase the background instead of reducing it. Hence the copper layer must be very thin or replaced with a radiopure lining material that is suitable above ground.

Other materials

Mercury is a good absorber that can be produced with very high radiopurity and could as such be a suitable shielding material, which was discussed in Ref. [Hult08]. Hg is activated by high energy neutrons producing ^{194}Hg with a half-life of 520 years, which makes it suitable mainly for underground laboratories where the background contribution from secondary cosmic radiation is reduced. However, since Hg is fluid at room temperature it has to be in a container and it is more difficult to ensure the radiopurity of the container than of Hg itself, which in combination with the higher cost of radiopure Hg makes it less interesting as a shielding material. Old Fe is an alternative for shielding, but due the modern prodction processes the Fe produced today is usually contaminated with ^{60}Co from the furnace lining or added scrap metal.

2.1.4 Other radionuclides

Some radionuclides present in the environment are a part of the materials of the detector itself and can contribute to the background. The main contributors are ^{137}Cs from bomb testing and the Chernobyl accident, ^{134}Cs from the Chernobyl accident and finally ^{60}Co that is a common impurity in metals such as steel and iron and originates from the production processes. ^{40}K is a common naturally occuring radioactive isotope and its 1460 keV γ-ray is readily visible in all background spectra. Since potassium is one of the most abundant elements on earth it is rather difficult to avoid in the construction materials of the detector as well as in the laboratory and therefore the ^{40}K isotope will be present.

2.1.5 Compton scattering and cross talk

Compton scattering is the process of γ-rays scattering on free or nearly free electrons, in which the incident photon transfers a part of its energy to the electron. The probability for Compton scattering increases linearly with Z of the material and depends on the scattering angle. At angles near 0° very little energy is transferred to the recoil electron. The opposite occurs when the scattering angle is 180° and the recoil electron is given the maximum energy [Knoll00]

$$E_{max-e^-} = h\nu \, \frac{2\,\gamma}{1+2\gamma} \tag{2.1}$$

$$E_\gamma = \frac{h\nu}{1+\gamma} \tag{2.2}$$

where

$$\gamma = \frac{h\nu}{m_e\, c^2} \tag{2.3}$$

and $h\nu$ is the incident photon energy, E_γ is the scattered photon energy, E_{max-e^-} is the maximum energy given to the electron and $m_e c^2$ is the electron rest mass energy.

When detecting γ-rays with a detector, partial absorption of γ-rays due to escaped Compton scattered γ-rays results in a continous background (Compton tail), which extends up to this maximum energy, called the Compton edge. For some typical radionuclides used for calibration purposes the Compton edge is at (incident photon

energy in brackets): 963/1118 keV for ^{60}Co (1173/1332 keV), 476 keV for ^{137}Cs (661 keV) and 11 keV for ^{241}Am (59 keV). For the germanium detectors used in the present work, the probability for partial absorption of 661 keV γ-rays is more than twice that of total absorption.

The **backscatter peak** appears in the spectrum when γ-rays from the radioactive source are Compton scattered by the surrounding material to the germanium detector where they are absorbed. The backscattering depends on the original photon energy and scattering angle. A maximum energy of 0.25 MeV is obtained when the incident photon energy can be assumed to be very large, $h\nu >> m_e c^2/2$ [Knoll00]. Consequently, the backscatter peak is visible in the γ-ray spectrum up to 0.25 MeV with typical values around 0.20-0.25 MeV. By using low Z materials such as copper as inner lining, the backscattering from the shielding material to the germanium detectors is minimised.

Cross talk between two detectors located close to each other occurs when a γ-ray is Compton scattered from one detector to the other. The recoil electron will result in an event in the background continuum in the first detector, while the photon will interact in the second detector either through photo absorption or Compton scattering. The probability for cross talk increases with decreasing distance between the detectors. The events in the two detectors will be in coincidence and by recording detector coincidences the cross talk can be eliminated. When measuring samples, the attenuation in the sample will reduce the probability for cross talk, which was seen experimentally during this work.

2.1.6 Bremsstrahlung

Bremsstrahlung is produced in the detector and the surrounding material when electrons lose parts of their energy by radiation. Bremsstrahlung varies with Z^2 and the generated spectrum is continuous, even if it may be generated by monoenergetic electrons. These electrons originate from beta decays in the samples or shielding and from interactions of secondary cosmic radiation in the detector (typically ionisation of muons). An approximation of the average fraction of energy released from an electron as bremsstrahlung when the electron is completely stopped by the absorber, is given by the radiation yield [Canb]

$$Y = \frac{S}{S+1} \tag{2.4}$$

where $S = 0.00061 Z E_k$, Z is the atomic number and E_k is the kinetic energy (MeV) of the incident electron. The resulting radiation yield for an electron with an energy

of 2 MeV is 1.6% (Z=13) in aluminium , 3.4% (Z=29) in copper and 9.1% (Z=82) in lead. To avoid bremsstrahlung, radiopure low Z materials should be used close to the measurement volume.

2.1.7 Pair production and the escape peaks

A γ-ray energy above 2 $m_e c^2$ (1022 keV) can create an $e^+ - e^-$ pair in the germanium crystal. The probability of pair production increases with the photon energy. The resulting e^+ will be annihilated and one or both of the two resulting 511 keV gamma quanta may excape from the germanium crystal and generate single and double escape peaks, 511 keV and 1022 keV below the total absoption peak respectively. Pair production outside the germanium crystal can generate a 511 keV peak in the spectrum as well as contribute to the continuous bremsstrahlung background.

2.2 Dimensions of the shield

The dimensions of the lead shield's outer and inner parts as well as the copper lining depend on the overall background in the laboratory and on the targeted background level inside the final shield. The research group strives for lead shields of 20 cm thickness for the spectrometers in the underground laboratory, i.e. a background reduction of a factor of 10 000, but is often limited by funding or available space. Above ground the lead shield should be thinner in order to avoid excessive activation by the secondary cosmic radiation.

The fraction of γ-rays that are left after passing a distance x (cm) in an absorber is estimated by [Leo87] (p 62-63)

$$\frac{I}{I_0} = e^{-\mu x} \tag{2.5}$$

where μ is the total absorption coefficient (probability per unit length for an interaction) and

$$\mu = \sigma N = \frac{\sigma \ \rho \ N_A}{A} \tag{2.6}$$

where σ is the cross-section, N_A is Avogadro's Number, ρ is the density and A is the atomic mass. A commonly used quantity is the *half thickness* denoting the thickness

at which the γ-ray intensity has been reduced to half, i.e. $ln2/\mu$. For the 2614 keV γ-ray line from ^{208}Tl, which is present in the environmental background, the half thickness in lead is approximately 1.5 cm (ρ 11.34 g cm^{-3}, A 207.2 g mol^{-1} and σ 14 barns atom^{-1}). The lead shield in this work is 18.5 cm thick, which corresponds to 12 times the half thickness resulting in about 0.01% of the 2614 keV γ-rays passing through the lead.

The copper lining on the inside of the lead shield protects the measurements from β and γ-rays from the lead shield. The electrons from the β decay of ^{214}Bi with an endpoint energy of approximately 1.2 MeV can be used as an example. At this energy the *range* [Lill01, Leo87] of e^- in the copper is approximately 0.5 g cm^{-2} and with a density of copper of 8.96 g cm^{-3}, the electron will have stopped after only 0.06 cm. The total absorption coefficient for the 2.6 MeV γ-ray from ^{208}Tl is approximately 0.04 cm^2 g^{-1} in copper, leading to a half thickness of 1.9 cm.

2.3 The germanium crystal

The lithium-drifted germanium crystal for γ-ray spectrometry was first mentioned in a paper by Freck and Wakefield in *Nature* in February 1962 [Frec62]. The lithium drifted germanium detectors must be continuously cooled in order to avoid a complete redistribution of the drifted lithium, which would occur rapidly at room temperature [Knoll00]. The lithium drifted germanium detectors were used for a couple of decades, but since then the technology has rapidly improved and the high-purity germanium (HPGe) detectors used today can be heated to room temperature without being damaged. The germanium crystal is a semiconductor and needs cooling with liquid nitrogen (LN2) since at higher temperatures the electrons can easily cross the band gap, which results in levels of thermally-induced leakage current that are too high for the detector to be useful. Since it is common in low-level γ-ray spectrometry to use the boil-off nitrogen gas from the LN2 Dewars to flush away radon and its progenies from the spectrometer sample volume, it is important that the LN2 is not contaminated.

The HPGe crystals are today produced in many shapes and sizes; the background from radioimpurities in the detector crystal itself is reduced due to the use of high-purity germanium. Extensive work is done on creating extremely pure germanium as well as methods of crystal production that are contamination-free [GERDA, Majo, Brod90]. To achieve a high full energy peak (FEP) detection efficiency and a good peak-to-total ratio it is an advantage to select a big crystal, but doing so also increases the full width at half maximum (FWHM) and the inherent background from the crystal itself - as well as the price. The larger FWHM the worse γ-ray energy resolution. It can be useful to remember that the FEP detection efficiency depends on the γ-ray energy, so if the targeted energy range is in the low part of the energy spectrum (for

which germanium is a strong attenuator) it may be wiser to choose a smaller crystal since the background would then automatically be lower and the resolution better. The bigger the crystal is, the more important it becomes to work on the general background reduction to achieve good system performance. The section *2.7 Figure of merit* contains a brief discussion of the figure of merit of a γ-ray spectrometer and how the crystal size is related to the performance of the spectrometer.

2.4 Close geometry problems

The samples in low-background applications are very close to the detector and are usually placed directly on the endcap. The close geometry together with the increasing size of the germanium crystals lead to two issues that must be addressed (i) the strong coincidence summing effects for radionuclides with cascading γ-rays and X-rays and (ii) the small errors in measurements of the geometry and lack of homogeniety that can result in rather large errors in the FEP efficiency calculations. These problems are well known to the low-level γ-ray spectrometry community and major efforts are continuously undertaken to improve the techniques to deal with these issues. An example of a method performed in the HADES laboratory of how to calibrate a detector and then accurately calculate the FEP detection efficiency for a sample with cascading γ-rays was presented by Johnston et al. [John06]. In that paper the combined uncertainty of the FEP detection efficiency was determined by using the Monte Carlo technique and the EGS4 simulation software together with the geometrical model of the detector and the complete decay scheme of the measured radionuclide. The results indicated a typical combined uncertainty value of 4% for the FEP detection efficiency calibration, a value that last year was updated to $<$3% for the HADES laboratory [Gasp08].

2.4.1 Determining the geometry

The geometrical model on which the whole calibration process is based, is built from information that originates from the detector supplier, radiographs of the detector (see *Appendix A*) and measurements of the detector, shield, sample and sample holder. It is crucial that these geometrical values are determined with the lowest uncertainties possible, although in some cases it can be difficult to do so accurately due to the rounded edges (bulletising) of the germanium crystal and the fact that the tilting affects the visibility in the radiographs. The radiographs will reveal the distance between the endcap and the crystal front surface and if the crystal is tilted inside the endcap. The tilting of the crystal can be generally overlooked, since it was shown by Gasparro et al. [Gasp08] that the effect on the calculations of the absolute FEP

detection efficiency is very small. The thickness of the dead layers of the germanium crystal are determined during the calibration iterations (starting with the values given by the manufacturer) and are a vital part of the geometrical model since they directly affect the calculated detection efficiencies, see further details in section *2.5*.

2.4.2 Summing effects

Cascading γ-rays and X-rays will give rise to summing effects in the detector and the evaluation of this is rather complex, as described in reference [John06]. The summing effects increase proportionally to the square of the solid angle [Knoll00] and are a real issue in low-level γ-ray spectrometry since measurements are typically performed with samples of weak activity very close to large detectors. True summed total absorption shows up as a sum peak and the Compton events show up as a continuous background in the spectrum. The main problem with summing effects is that events that should have been registered in the full energy peaks are moved to the sum spectrum.

The uncertainties due to summing effects can be reduced by including the full decay scheme of the measured source in the Monte Carlo code used for the FEP detection efficiency calculations, see section *2.5*. In addition, the Monte Carlo code includes the full sequence of interactions, i.e. histories (see Figure 2.1), in the germanium crystal.

High count-rate from a strong radiation source may result in random piling up of the linear amplifier signals generated by γ-rays originating from different nuclear decays. This effect, called random or chance summing events [Knoll00] or random pile-up, can be neglected in the low count-rate measurements in the present work.

2.5 Detection efficiency calibration

The efficiency of a germanium detector can be given in several different ways. The relative efficiency, $\varepsilon_{Rel}(E)$, refers to the full energy peak (FEP) detection efficiency for a ^{60}Co source (total absorption peak of the 1332 keV γ-ray energy) at a distance of 25 cm from the germanium detector endcap relative to a 3"$\times$ 3" NaI detector. The HADES underground laboratory has detectors with a relative efficiency in the range of 20-110% and the two detectors included in this work are 80% (Ge-6) and 90% (Ge-7) respectively.

The full energy peak (FEP) detection efficiency of a germanium detector corresponds to the detector's efficiency for totally absorbing a γ-ray. The γ-ray can interact with the detector in the various ways shown in Figure 2.1 and the probability of a

full absorption depends on the γ-ray energy as well as the complete measurement geometry.

The FEP detection efficiency is largely governed by the geometry [Gasp08] and the source to be measured and is thus different for each measurement. The FEP detection efficiency calibration in the HADES laboratory is performed by matching measurements of reference point sources placed at three different distances, in the range 2-15 cm from the detector, to calculated FEP detection efficiency values. A complete geometrical model is set up, which includes: the germanium detector, the cryostat, the sample, the sample holder (for each individual measurement) and the nearby shielding. The Monte Carlo technique is employed by using the EGS4 software [Nels85] to calculate the theoretical FEP detection efficiency values. However, the Monte Carlo code simulations can be carried out using a variety of software for γ-ray spectrometry, which are described in the litterature [Nels85, Sima01, Arno03, Agos03, Alli06] and many of these were recently compared in an intercomparison exercise [Vidm08]. Together with the complete decay scheme of the studied radionuclide the geometrical model is used to write the Monte Carlo code in MORTRAN, which is compiled to FORTRAN by the EGS4 software. During the EGS4 simulation iterations, the thicknesses of the dead layers (of the germanium crystal) on the front, side and back of the germanium crystal are varied until an agreement between the calculated and measured value is within the given uncertainty of the reference source. The simulations are is typically run with 10^6 to 10^8 histories.

The decay scheme of each measured radionuclide is compiled from the most recent data found on the DDEP website [DDEP]. The reference point sources are from PTB (Physikalisch-Technische Bundesanstalt), Germany, and the absolute level of activity is known with an uncertainty of 1-2% at a given reference date. The following range of typical point sources were measured to cover both the energy range and the effect from cascading γ-rays in this work: ^{60}Co, ^{22}Na, ^{88}Sr, ^{88}Y, ^{109}Cd, ^{133}Ba, ^{134}Cs, ^{137}Cs, ^{152}Eu, ^{241}Am. Cascading γ-rays are found in for example ^{60}Co, ^{88}Y, ^{133}Ba and ^{152}Eu. The uncertainty requirement connected to the counting statictics of a point source measurement to be used for the FEP detection efficiency calibration is 1%, which means at least 10 000 counts ($unc = \sqrt{counts}$) must be collected. When true summing from cascading γ-rays is expected, the number of summing events will increase the closer the source is to the detector.

The relative difference, D, between the calculated and measured detection efficiencies was then determined for each full peak energy

$$D = \frac{\varepsilon_{MC} - \varepsilon_{measured}}{\varepsilon_{measured}} \tag{2.7}$$

Changes in the front dead layer have greater effect on the FEP detection efficiency

in the low part of the energy spectrum, while the side dead layer contributes more in the high-energy range. The relative difference, D, also depends on:

- Uncertainties in the experimentally determined values.
- Uncertainties in the decay scheme.
- Uncertainties in the geometrical model, especially the source-to-crystal distance.

The uncertainties in MC modelling are further discussed in a recent paper by Gasparro et al. [Gasp08] in which it is reported that the effect of a tilted germanium crystal is negligible while a bulletised germanium crystal can not be approximated with straight edges without greatly overestimating the FEP detection efficiency, especially for close geometries and low γ-ray energies. The paper also discusses why the dead layers in the geometrical models are not necessarily the real-life values since the model cannot compensate for effects such as the graded response of the dead layers. The calibration model fit to the measured values, i.e. the contribution to the uncertainty from the calibration procedure, is typically in the HADES laboratory:

- 5%: a normal calibration model fit.
- 3%: well-fitted calibration model fit.
- $<$3%: extremely good fit to the calibration model (requires considerable effort to achieve).

By participation in several international proficiency tests and intercomparison exercises it has been confirmed that the calibration approach with the Monte Carlo technique and reference sources in the HADES laboratory is accurate within an uncertainty of $<$3%.

Three different measurements of rare decay events were performed in this work. The samples were metal discs of tantalum, indium and tin for which both the material and the geometry were different:

- **tantalum**: 6 discs, diameter 100 mm, total thickness 11.5 mm, mass 1500 g.
- **indium**: 1 disc, diameter 106 mm, thickness 40 mm, mass 2566 g.
- **tin**: 1 disc, diameter 100 mm, thickness 25 mm, mass 1465 g.

A photo of the stacked tantalum discs is shown in Figure 2.3. The calculated FEP detection efficiencies of the Sandwich Spectrometer for these three measurements are shown as a function of energy in Figure 2.4. As can be seen in Figure 2.4 the absolute FEP detection efficiency was <5% for γ-ray energies up to 2400 keV; below 200 keV the FEP detection efficiency rapidly decreases.

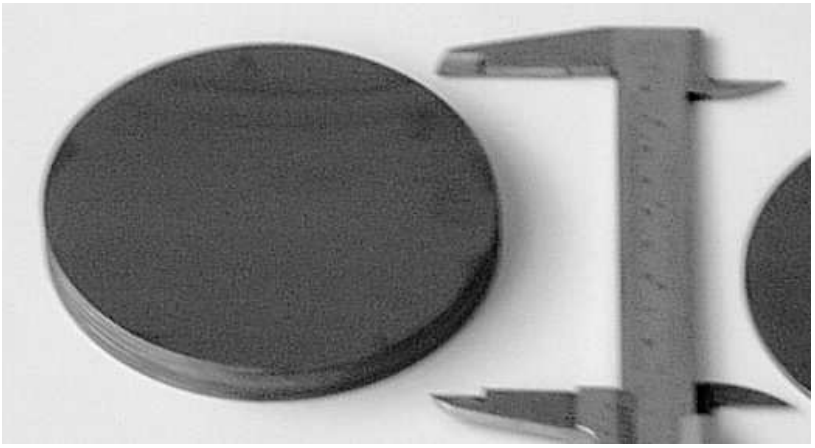

Figure **2.3**: The stacked tantalum discs with a diameter 100 mm and total thickness of 11.5 mm.

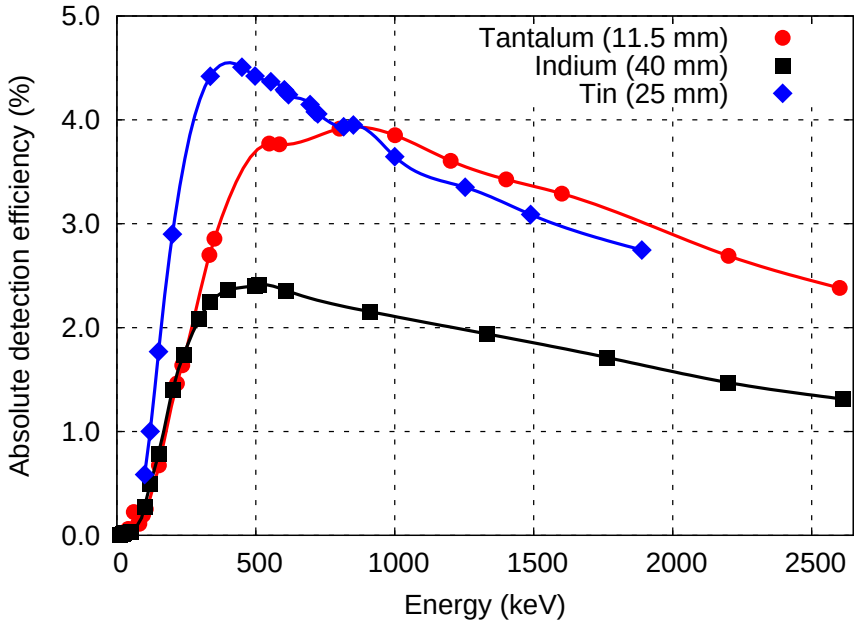

Figure **2.4**: Calculated absolute FEP detection efficiencies as a function of energy of the Sandwich Spectrometer for the measurement geometries of tantalum, indium and tin. These values are compared to measurements of calibration reference point sources and agree within an uncertainty of <3%. The values in brackets correspond to the thickness of each the metal disc(s), the diameter is in all three cases ≈10 cm.

A simple experimental determination of the peak-to-total (P/T) ratio was carried out by dividing the counts in the full energy peak by the total number of counts in the spectrum in a calibration measurement of ^{137}Cs. For the detectors employed in this work, the P/T ratio is from this determined to ≈0.3.

2.6 Detection limit and decision threshold

By reducing the background, lower detection limits can be achieved. The **detection limit** [Hult07] is the *a priori* minimum detectable activity determining the performance of an instrument or measurement, and is typically calculated when analysing the *background measurements* from a spectrometer. The **decision threshold**, on the other hand, is defined as the *a posteriori* minimum detectable activity determining the performance of a specific measurement and as such it is mainly calculated for *application measurements*. Low detection limits open the possibility of measuring samples

- of smaller volume and mass
- with very low levels of activity
- for a shorter time, i.e. better temporal resolution

Along with the reduced background there will be extra work to identify the additional peaks in the γ-ray spectra that were previously obscured by the higher levels of background radiation. The detection limits and decision thresholds in this work are calculated according to the ISO report *Determination of the detection limit and decision threshold for ionising radiation measurements* [ISO00] and for simplicity they are given in the formulae below, although here in the unit of *counts* and not *count-rates*. The basic assumptions are [ISO00]: (i) the radioactive decay and pulse counting is random, (ii) the distance between two peaks is >4 FWHM, (iii) the background is a nearly straight line, (iv) the duration of the measurement is small in relation to the half-life, (v) the system dead time is negligible and (vi) the conversion of pulse rate into activity is so well determined that the influence of its uncertainty can be ignored. The simplified decision threshold derived from reference [ISO00] is

$$DT = k_{1-\alpha}\ \sqrt{2\ C(E_{DT})} \tag{2.8}$$

where $k_{1-\alpha}$ is a constant related to the error of probability α, given in Table 2 in ref. [ISO00], and $C(E_{DT})$ is the total background counts in an energy interval defined by

$$E_{DT} = k_{1-\frac{\gamma}{2}}\ R(E_{peak}) \tag{2.9}$$

where $k_{1-\frac{\gamma}{2}}$ is a constant related to the confidence interval $(1-\gamma)$ from ref. [ISO00] and $R(E_{peak})$ is the FWHM in keV at the expected peak energy (for the relation to the resolution see section *2.3 The germanium crystal*).

Finally, the detection limit is the smallest expectation of the net counts for which a wrong decision occurs with a probability of β, where β is an error of probability. The simplified explicit expression for the detection limit is

$$DL = (k_{1-\alpha} + k_{1-\beta})\ \sqrt{2\ C(E_{DT})} \tag{2.10}$$

where $C(E_{DT})$ is the total background counts in the energy interval given in equation (2.9). The constants and confidence intervals $(1-\gamma)$ chosen from reference [ISO00] in the present work are generally

$$\alpha = \beta = 0.0500 \iff k_{1-\alpha} = k_{1-\beta} = 1.645 \iff (1-\gamma) = 90\%$$

The energy interval E_{DT} is centralised around the main peak energy E_{peak}. The given expressions ensure a 90% probability that the background will not exceed the detection limit. The detection limits (in Bq) in the background spectra in this work are given in Table 4.2 in *Chapter 4*. At the start in 1963 the detection limit for germanium detectors was in the range of a few Bq, but over the past decades has been reduced to just fractions of mBq. For the most advanced γ-ray detection systems in the world, in which measurements of several years can be performed, the detection limits are in the order of a μBq [GERDA, GERDA06].

2.7 Figure of merit

In order to reach low detection limits not only the background but also other properties of the detector, such as the resolution, peak-to-Compton ratio and crystal size, are important. An interesting figure of merit (FoM) has been introduced for low level γ-ray spectrometry by Hult et al. [Hult06]

$$FoM = \frac{\varepsilon_{Rel}(E)}{\sqrt{R(E)B(E)}} \tag{2.11}$$

where $\varepsilon_{Rel}(E)$ is the relative efficiency (see section *2.5 Detection efficiency calibration*), $R(E)$ is the FWHM in keV and $B(E)$ is the background count-rate per keV (keV^{-1}), all given at the selected energy E. From the expression of FoM it is clear that by increasing the crystal size the FoM does not necessarily improve since both the FWHM (R(E)) and the background (B(E)) will increase as well. It therefore makes good sense to work on the overall background reduction independently from changes in the crystal size.

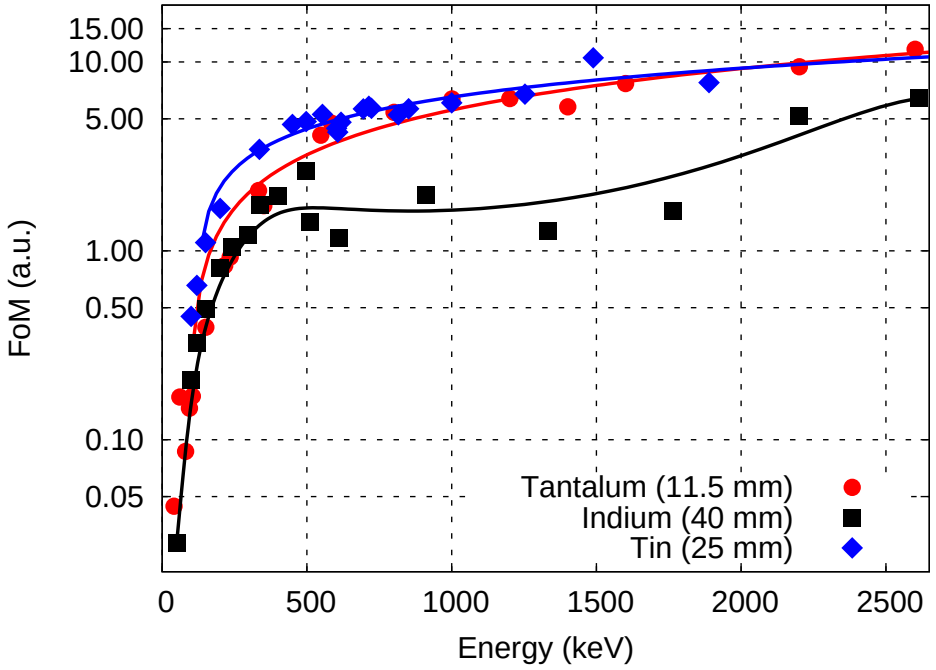

Figure **2.5**: A simple approximation of the figure of merit (FoM) for the Sandwich Spectrometer, for three different sample measurements of tantalum, indium and tin. The absolute FEP detection efficiencies from Figure 2.4 are used instead of the relative efficiencies, the FWHM is averaged from Figure 4.7.

Figure 2.5 shows a simple approximation of the FoM of the two germanium detectors in this work, but note that the absolute FEP detection efficiency, see Figure 2.4, was used instead of the relative efficiency for all the three samples (indium, tantalum and tin). The FWHM for the two germanium detectors was taken from Figure 4.7 in *Chapter 4* and averaged to calculate the FoM. Below 200 keV the FEP detection efficiency decreases rapidly and thus so does the FoM.

A common way to compare detectors between low-background γ-ray spectrometry laboratories is to state the integrated count-rate in the background for a certain energy interval and normalise this with the germanium crystal mass (day^{-1} kg^{-1}).

2.8 Calculations of weighted mean activity and combined uncertainties

The major source of uncertainty in low-level γ-ray spectrometry is from counting statistics due to the low activity in the samples. In order to reach reasonable uncertainties some measurements may take years to complete, such as the continuously running measurements of samples from Hiroshima [Hult04] or the future high-profile $\beta\beta$ decay experiments in Europe [GERDA, GERDA06] and the USA [Majo05, Majo], which in the long run aim to determine the neutrino mass. However, common application samples usually occupy a detector for a couple of days (see Paper I) or weeks [Gasp04], up to a few months as in Paper IV and Paper VIIa-b. Other contributions to the uncertainty originate from:

- Geometry measurements of the detector and sample
- True summing effects
- Decay data uncertainties
- FEP detection efficiency calculations >2-3%
- Mass measurements ≈0.05 g
- Time measurements ≈1 s

All information concerning half-lives and decay schemes of the radionuclides in this thesis were collected from the DDEP website [DDEP] and, when not available there, the information was taken from the table of isotopes. The combined standard uncertainties in this work are expressed as standard uncertainties following the *Guide to the Expression of Uncertainty in Measurement* [ISO95] given in brackets after each measurement value and the last digit(s) of their numerical value correspond(s) to the last digit(s) of the quoted result. Below is a condensed description of the equations used for the calculations.

The net counts in a γ-ray peak in a measurement spectrum are given by

$$C_{net} = C_{peak} - C_{conti} \tag{2.12}$$

$$C_{conti} = \frac{Nb_{peak}}{2} \left(\frac{C_{left}}{Nb_{left}} + \frac{C_{right}}{Nb_{right}}\right) \tag{2.13}$$

Where C_{peak} is the number of counts in the peak, C_{conti} is the number of counts in the continuum given by the second equation above in which C is the counts and Nb is the number of bins for the *peak*, *left* and *right*. The uncertainty of the measurement, u_C, i.e. the uncertainty in the counting statistics is

$$u_C = \sqrt{C_{peak} + C_{left}\ (\frac{Nb_{peak}}{2\ Nb_{left}})^2 + C_{right}\ (\frac{Nb_{peak}}{2\ Nb_{right}})^2} \tag{2.14}$$

The activity of an individual measurement, A_{ind}, is calculated as

$$A_{ind} = \frac{C_{net}}{\varepsilon\ t\ P_\gamma} \tag{2.15}$$

Where C_{net} is the net peak counts in the selected peak, ε is the FEP detection efficiency of the germanium detector at that γ-ray energy, t is the measurement time and P_γ is the γ-ray emission probability. The combined uncertainty of an individual measurement, u_i, is normally calculated as

$$u_i = A_{ind}\ \sqrt{(\frac{u_\varepsilon}{\varepsilon})^2 + (\frac{u_C}{C})^2 + (\frac{u_t}{t})^2 + (\frac{u_m}{m})^2 + (\frac{u_{P_\gamma}}{P_\gamma})^2} \tag{2.16}$$

Where i is the number of measurements and m is the total mass of the sample. However, if several measurements are combined, the ε and P_γ are usually not included in the combined uncertainty calculated for each measurement, since their weight in the final value would then be overestimated. Instead, the weighted mean activity, A_{mean}, and corresponding weighted mean uncertainty, u_{mean}, are calculated for the series of measurements without the contribution of ε and P_γ in the mean uncertainty

$$u_{mean} = \sum_i (\frac{1}{u_i^2}) \tag{2.17}$$

$$A_{mean} = \frac{\sum_i (\frac{A_i}{u_i^2})}{u_{mean}} \tag{2.18}$$

where A_i is the activity (in Bq) from each individual measurement i. The final total uncertainty is then calculated in which the contribution from ε and P_γ are added in quadrature

$$u_{tot} = A_{mean} \sqrt{(\frac{u_{mean}}{A_{mean}})^2 + (\frac{u_{P_\gamma}}{P_\gamma})^2 + (\frac{u_\varepsilon}{\varepsilon})^2} \tag{2.19}$$

The half-life can be calculated by using the weighted mean activity, A_{mean},

$$t_{1/2} = ln2 \ (\frac{m \ \theta \ N_A}{A_{mean} \ M}) \tag{2.20}$$

where $t_{1/2}$ is the half-life, M is the atomic mass, m is the total mass of the sample, θ is the isotopic abundance and N_A is the Avogadro number. The number of a particular atom in a sample is given by $(m \ \theta \ N_A/M)$. It is important that θ is accurately determined and this can be done using various mass spectrometry methods such as secondary ion mass spectrometry (SIMS) or thermal ionisation mass spectrometry (TIMS).

For some application measurements it is interesting to determine the branching ratio, BR, for a particular decay, see Paper IV and Paper VIIa-b. By using the half-life of the dominating decay branch (d) together with the partial half-life that is calculated from the experiment (r, rare decay) the branching ratio is given by the expression

$$BR = \frac{t_{1/2}(r)}{t_{1/2}(d) + t_{1/2}(r)} \tag{2.21}$$

In order to achieve a low uncertainty for the calculation of a branching ratio for a rare decay it is also necessary that the reference value of the half-life of the main branch has a low uncertainty, which is not always the case.

3 The Sandwich Spectrometer and the underground laboratory

3.1 The underground laboratory HADES

The Belgian research programme for the disposal of radioactive waste started as early as in 1974 at the Belgian nuclear research centre SCK•CEN (studiecentrum voor kernenergie • centre d'étude de l'énergie nucléaire), located in Mol, Belgium [Sck]. The construction of the high-activity disposal experimental site (HADES), in Figure 3.1, began in 1980 and this underground laboratory is dedicated to experimental research on deep geological disposal of radioactive waste from the Belgian nuclear power programme. The HADES laboratory is run by the economic interest group EURIDICE (European underground research infrastructure for disposal of nuclear waste in clay environment). During the past 28 years three parts of the gallery have been completed, the last of which was finished during 2008 for storage tests of heat-producing nuclear waste. HADES is located in the Boom clay layer at a depth of 223 metres, which for the low-level γ-ray measurements corresponds to 500 metres water equivalent (m w.e.). The Boom clay layer is about 100 metres thick and the HADES gallery is drilled through the centre of it, leaving approximately 50 metres of clay above as well as below the tunnel. What makes this clay layer exceptionally interesting for storing nuclear waste is that the plasticity of the clay ensures that no extreme pressure or grinding movements destroy containers placed within it - the containers are simply incorporated into the clay. Also, the clay has very low permeability for water, which reduces the risk of corrosion and, finally, the research done by SCK•CEN shows that radionuclides travel very slowly through the clay. Many different kinds of geological experiments and research have been performed in HADES over the past years and both new and old experiments are continuously running there.

Located in a small section of HADES is an ultra low-level gamma spectrometry laboratory run by the European Commission - JRC - IRMM (Joint Research Centre - Institute for Reference Materials and Measurements), see Figure 3.2. The γ-ray measurement facility was started in 1992 with one high-purity germanium (HPGe) detector and after continuous expansions [Hult00, Hult06] the laboratory today has seven γ-ray spectrometers running. The latest detector, the Sandwich Spectrometer described in Paper III, is the main part of this work.

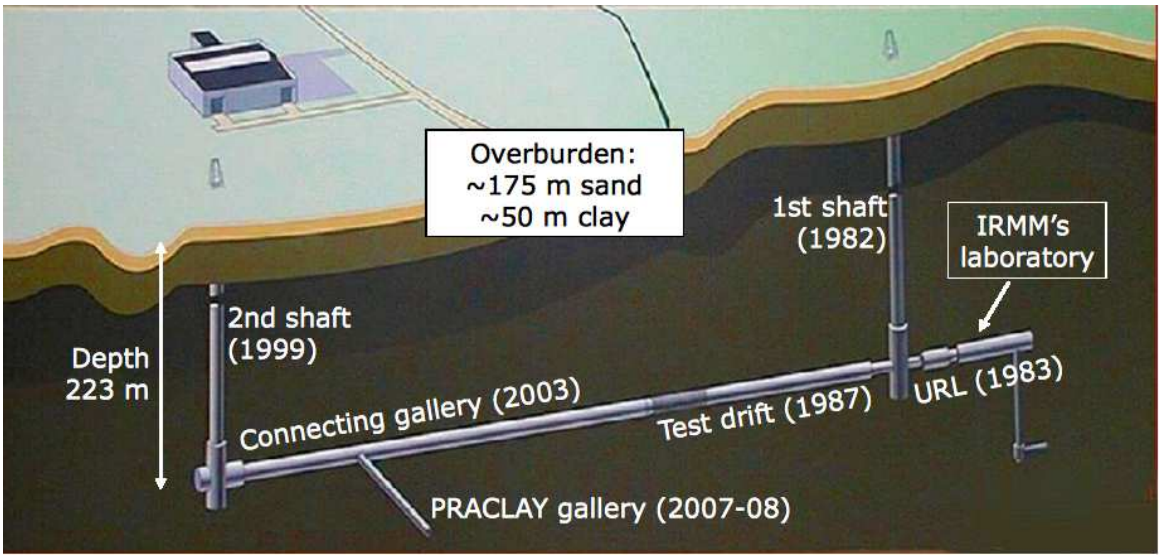

Figure **3.1**: A schematic drawing of the HADES underground laboratory.

Generally, the measurements performed in this laboratory are support measurements for EU policies and the work of the European Commission in fields such as nuclear safety, the environment and harmonisation of measurements. Additionally, measurements for fundamental research and industry can be performed, such as very accurate measurements of nuclear decay data and radiopurity measurements. Due to the diversity of samples and required measurements, IRMM's ultra low-level γ-ray spectrometry (ULGS) laboratory is equipped with general-purpose spectrometers. This diversity also leads to extra requirements on the method and accuracy of the absolute FEP detection efficiency calibration, which is calculated for each individual measurement using the Monte Carlo code EGS4 [Nels85, Hult06]. The calculations are compared to measurements of reference sources with a matrix and composition of radionuclides similar to that of the sample to be measured, see section *2.5*.

The major benefit of locating a ULGS laboratory underground is that the contribution from cosmic radiation is diminished. It might, however, be thought paradoxal that a low-background measurement laboratory is placed in the same underground facility as high-activity nuclear waste experiments. Geological experiments on nuclear waste have shown that the radionuclides from the high-activity samples do not travel far in the clay over time. That, in combination with the radioactivity's inverse dependence on the distance, r^{-2}, has to date spared the ULGS laboratory from contaminations from the high-activity experiments. HADES will remain a laboratory in the future so there are no plans for high-activity waste to be stored there.

Figure **3.2**: On the left is IRMM's ultra low-level γ-ray spectrometry laboratory in HADES and on the right a view down the elevator shaft, 223 metres deep. The Research Group Leader, Mikael Hult, is working on the left in the photo of the HADES γ-ray spectrometry laboratory.

3.2 The Sandwich Spectrometer set-up

The Sandwich detector hardware is described in an overview paper Paper III and in this section additional information about the spectrometer is presented and discussed.

3.2.1 The lead and copper shield

The final check of the drawings of the shield and detectors, see Figure 3.3 and 3.4, was the starting point for this thesis work, although the equipment had been designed and ordered beforehand due to the long lead times on such hardware. During 2006 the manufacturer Von Gahlen [Gahl] cast the lead into shape, delivered and put the shield into place in the HADES underground laboratory together with the HADES research group. The outer part of the shield is 14.5 cm thick with an activity of 20 Bq/kg (^{210}Pb). The inner lead is 4.0 cm thick and was produced by the Polish company Plombum FL [Plom], which entered the market in 1991, and in spite of being new lead it has an activity of only 2.5 Bq/kg (^{210}Pb). The specific lead ore that Plombum use in combination with their specific and well controlled smelting and refining process ensures the low activity of their lead. The 3.5 cm-thick inner lining of radiopure electrolytic copper has an estimated activity of $<$15 μBq/kg (^{60}Co) [Laub09].

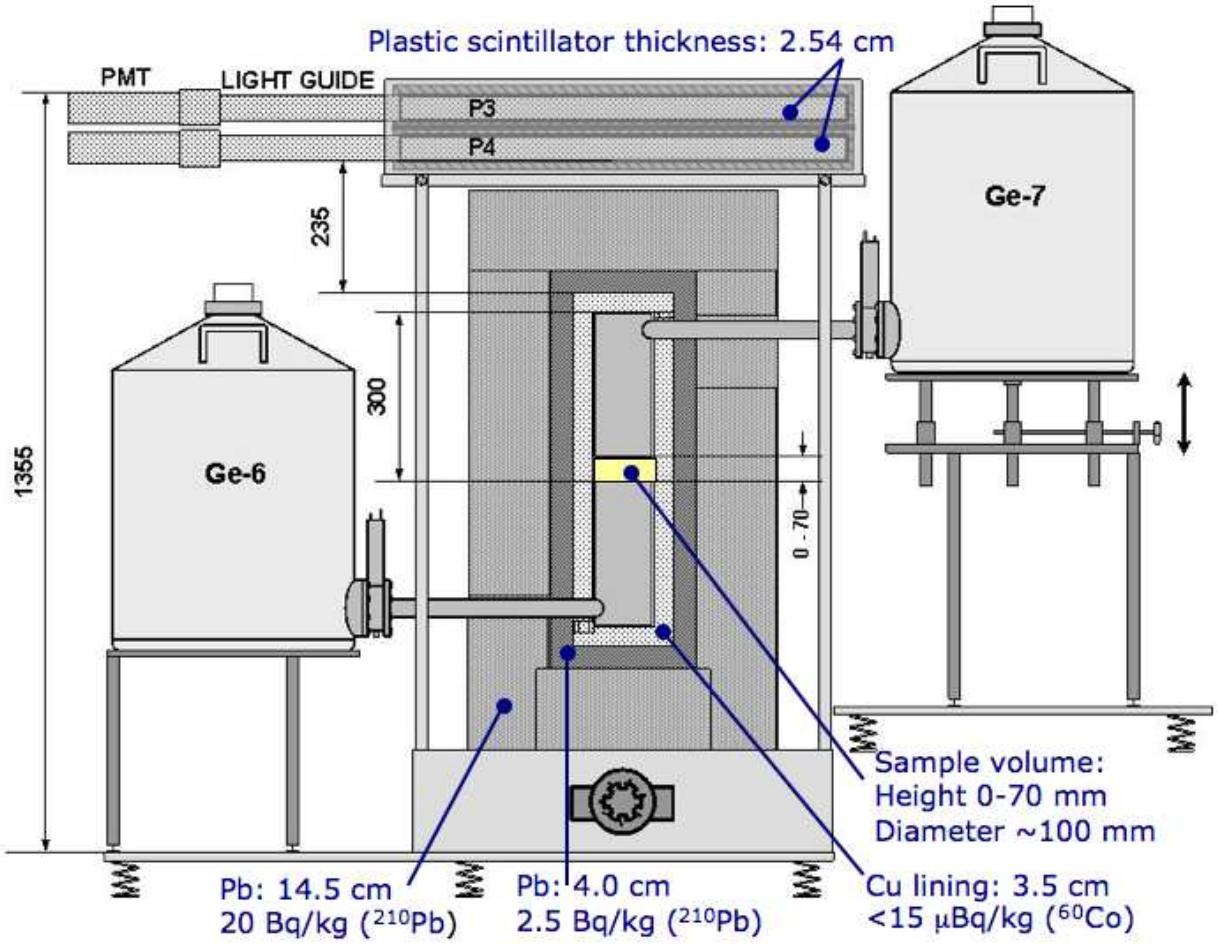

Figure **3.3**: The Sandwich Spectrometer detectors and lead shield. Two germanium detectors, Ge-6 and Ge-7, combined with an active muon shield of two plastic scintillators, P3 and P4.

In Figure 3.4 a blue bag is rolled up on top of the Sandwich Spectrometer. The blue bag is a thick, custom-made plastic cover that is made for each spectrometer in HADES. The cover reduces the possibility for radon and its progenies, ^{41}Ar from the nearby nuclear installation and other airborne radionuclides to enter the spectrometer. When the spectrometers are closed and covered, ^{41}Ar (1294 keV) is not detected in the measurements. The cover also protects the spectrometer from dust produced during heavy construction work in the HADES gallery, such as drilling new galleries or installing new geological experiments.

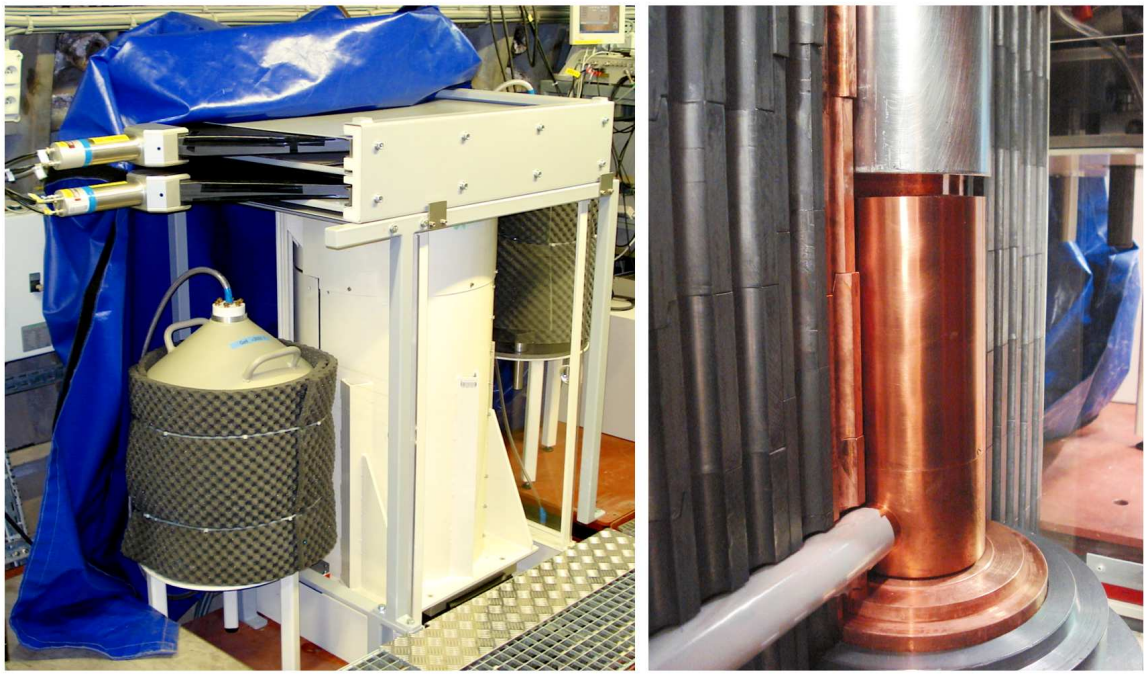

Figure **3.4**: The Sandwich Spectrometer photographed in HADES 2008. a) The plastic scintillators on top of the lead shield. b) The two germanium detectors placed face to face inside the lead shield with Ge-6 (copper endcap) as the lower and Ge-7 (aluminium endcap) on the top.

3.2.2 The germanium detectors

The two high-purity germanium (HPGe) detectors are labeled Ge-6 and Ge-7. The detectors are placed face-to-face inside the lead shield as shown in Figures 3.3-3.4. Both detectors are p-type, closed-ended coaxial detectors from Canberra [Canbw]. Ge-6 has a thick front dead layer, copper endcap and a relative efficiency of 80% [Canb6]. Ge-7 is an extended range (XtRa) detector with a thin front dead layer, aluminium endcap and a relative efficiency of 90% [Canb7]. Details of the germanium detectors are listed in Table 3.1.

A schematic drawing of a germanium crystal is given in Figure 3.5. The outer n^+ contact is typically made of diffused lithium of about 0.5 mm thickness, while the inner p^+ contact is usually made of implanted boron of approximately 0.3 mm thickness. However, the dead layers can be both thicker and thinner, even in the μm range for some custom-made crystals. In the present work the inner boron implanted contact is <1 μm thick for both germanium detectors.

The p^+ and n^+ contacts are commonly called dead layers because they are not an active part of the detector crystal. The thicknesses of the dead layers are varied during the Monte Carlo simulations that are performed to obtain the correct efficiency

calibration, see section *2.5 Detection efficiency calibration*. The dead layers that are used in the geometrical model are not necessarily the real life values, because the goal of the model is to achieve an FEP detection efficiency calibration that agrees with the measurement data and in that process some effects are not included, such as the graded response of the dead layers.

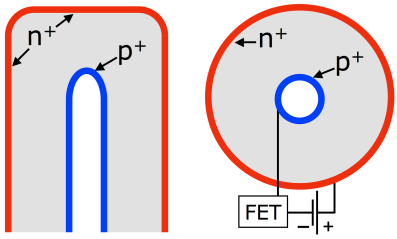

Figure **3.5**: A cross section through a closed ended, coaxial, HPGe detector. The outside n^+ contact (red) is made of diffused Li (lithium), the inner contact p^+ (blue) is made of implanted B (boron) and the active volume is grey.

To obtain the exact internal dimensions and position of the crystal a radiograph is made of each germanium detector, see *Appendix A*, from which the distances are determined. The uncertainty in the measurements from the radiograph are due to the fact that the edges of the crystal are sometimes rounded and the crystal is not always exactly vertically positioned, but slightly tilted.

The germanium detectors are normally cooled with liquid nitrogen (LN2) and only heated up to room temperature in special cases. A short period at room temperature does not affect the dead layers of HPGe crystals in comparison to the older Ge(Li) detectors, but for ultra low-level γ-ray systems it is crucial to make sure that the geometrical model used for calibration simulations is still valid after a "warm period" in order to maintain the low measurement uncertainties.

Details	**Ge-6**	**Ge-7**
Crystal diameter × thickness	78.0 × 84.0 mm	80.5 × 66.5 mm
Dead layer front / side	0.9 mm/3.0 mm	0.3 μm/0.7 mm
Distance endcap top to crystal surface	8.3 mm	6.0 mm
Distance endcap side to crystal side	11.5 mm	9.75 mm
Endcap material	Cu	Al
Endcap diameter	10 cm	10 cm
Bias voltage	+ 3000 Volt	+ 4500 Volt
Relative efficiency	80 %	90 %
Year of manufacture/refurbishment	2004	2004/2007

Table **3.1**: General information for the two germanium detectors Ge-6 and Ge-7. Radiographs are in *Appendix A*.

The pre-amplifiers for Ge-6 and Ge-7 are both placed on their respective LN2 Dewar, see Figure 3.3, which results in the amplifier being at the other end of the cooling arm as well as outside the lead shield. This is a mandatory design for low-background measurements in order to avoid background radiation from the electronics.

3.3 Solid angle

The solid angle is calculated for an infinitely thin sample that is 1 cm in diameter, which is a good approximation for the smallest samples. The sample was placed directly on the endcap of the lower detector (Ge-6, not visible in Figure 3.6) and it is assumed that the top detector (Ge-7) will be so close that the two endcaps touch each other. For simplicity the edges of the germanium crystal are assumed to be straight. The geometry used for the calculation is shown in Figure 3.6, in which h is the distance between the endcap and the germanium crystal surface, a is the radius of the germanium crystal and b is the radius of the sample. The total solid angle is the sum of the two individual solid angles for the two germanium detectors and, thus, this is the maximum total solid angle under optimal conditions.

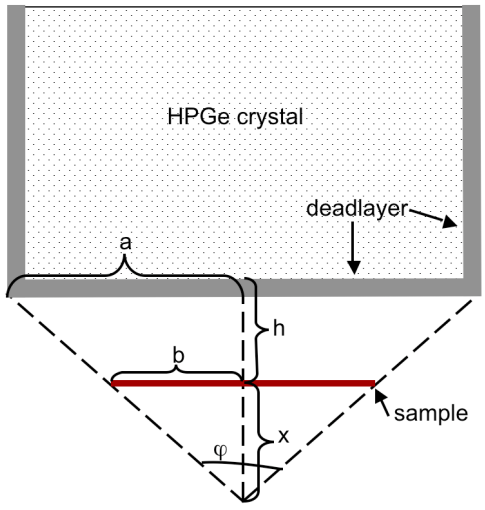

Figure **3.6**: The schematic drawing of the geometry used for the calculations of the solid angle for one germanium detector. The germanium crystal (without endcap) with dead layers (grey) and the sample (red) are shown in the figure. The sample is placed on the (here imagined) surface of the endcap at the distance h (measured in a radiograph) from the germanium crystal.

The total solid angle for the Sandwich Spectrometer under optimal conditions for a small sample was determined to ≈24% of 4π (3.0 sr) without dead layers. This is increased by 3% if the dead layers are included. The solid angle decreases with larger distances between the two germanium detectors.

3.4 The active muon shield

At the surface of the earth the muons represent the larger part of the background contribution from secondary cosmic radiation. The muon is a negatively charged particle and with a mass about 200 times that of the electron. The muons are relativistic particles and therefore highly penetrative through matter, which results in a large fraction of muons also travelling to the HADES laboratory. In an underground laboratory the background is dominated by muons and the showers of radiation and particles from their interraction with matter. The main part of the muon flux in the underground laboratory comes from the vertical direction since the mass of overburden is thinnest in this direction. With increasing horizontal angles the thickness of the overburden that the muons must penetrate increases and consequently the muon contribution from these directions is reduced. The muon flux is here approximated to be vertical while the horizontal contribution is assumed to be negligible, hence an active muon shield is positioned on top of the lead shield of the germanium detectors and the sides of the set-up are omitted.

The muon flux at ground level was measured to approximately 160 m^{-2} s^{-1} during a previous experiment in the HADES research group, although it is believed that this value also contains contributions from the soft background. In this work the muon flux in HADES was determined to 0.138 m^{-2} s^{-1}, see section *4.2*. From muon flux measurements at several depths in the Pyhäsalmi underground laboratory [Enqv05] the muon flux can be approximated from Figure 3 in [Enqv05] to 110 m^{-2} s^{-1} at ground level and 0.2 m^{-2} s^{-1} at 500 m w.e. (meter water equivalent), which is comparable to the measurements in HADES.

A theoretical model of the muon distribution in the HADES laboratory was set up and the preliminary computer simulations show that the energy of the largest fraction of muons that can be expected in HADES should have energies up to several hundred GeV. The energy loss experienced by a particle in an absorbing material depends on the Z of the absorber and Table 3.2 lists the information about the muon detector material as well as the muon interaction. The plastic scintillator material is polyvinyltoluene (Scionix: EJ-200, PVT), which is a commonly-used material for muon detectors. Particles producing Cherenkov radiation can also be detected by the active muon shield, but their contribution can be neglected at these low energies and in any case the events detected in the muon shield are primarily used to remove background events from the germanium detectors.

The active muon shield includes the two plastic scintillators placed on top of the lead shield, see Figures 3.3-3.4, and the coincidence circuit shown in Figure 3.7. The coincidence signal between the two plastic scintillators is used as a gate pulse for ADC 1. This coincidence pulse ensures that only events occurring in both plastic

scintillators are collected, i.e. mainly high-energy charged particles such as muons, while other background events are discarded. By using the coincidence pulse as a gate, the typical muon energy spectrum is collected from the lower plastic scintillator.

Quantity	**Value**	**Unit**
Detector model	Scionix: R25 × 800 B 800, 2M-X+VD14-E2, built-in voltage divider/preamplifier.	
Photomultiplier tube	Type 2" ETL 9266, 14 pins connector, diameter 51 mm, Al housing.	
PM voltage	+1000	Volt
Plastic type	EJ-200: Polyvinyltoluene	
Chemical composition	$[2\text{-}CH_3C_6H_4CHCH_22]_n$	
Refractive index	1.58	
Rise / Decay time	0.9 / 2.1	ms
Maximum signal height	±10	Volt
Detector dimensions	800 × 800 × 25.4	mm
Density	1.032	g cm^{-3}
Minimum ionisation $(-\frac{dE}{dx})_{min}$	1.956	MeV cm^2 g^{-1}
Critical energy E_c	1194	GeV
Radiation length	43.90	g cm^{-2}

Table **3.2**: Details of the plastic scintillators used in this work for muon detection. Information collected from the manufacturer *Scionix* and references [Groo01, Infn].

The mean stopping power of muons in matter can be divided into two parts, the electronic stopping power and the radiation losses [Groo01]. The radiation losses are bremsstrahlung, pair production and photonuclear interactions, which become more important at higher muon energies. The muon critical energy can be defined as the energy at which the electronic and radiation losses are equal, and above this energy the stopping power will rapidly increase as a function of muon energy. The energy loss of the muons in the detector is approximately constant between the minimum ionisation energy up to the critical energy. For the muon detectors in this work, the critical energy is 1.2 TeV, which is well above the energy of most muons expected in HADES. The deposited energy in a muon detector of a thickness x and a density ρ can thus be approximated by using the values for minimum ionisation stopping force given in Table 3.2

$$E_{min} = (-\frac{dE}{dx})_{min}\ \rho\ x = 5.1\ MeV \tag{3.1}$$

The minimum energy E_{min} is well above the noise level in the plastic scintillator and the selected thickness of 2.54 cm is determined to give a sufficient muon signal that should show up as a broad peak or hump in the spectrum from the active muon shield. The preliminary results from the computer simulations confirm that the main peak in the muon spectrum is to be expected at about 5 MeV.

3.5 Signal electronics and data collection system

The electronics used to detect the signal from Ge-6 and Ge-7 and the active muon shield are shown in Figure 3.7 with details listed in Table 3.3. The data acquisition system, DAQ2000, used in the Sandwich Spectrometer set-up is designed and manufactured by IRMM. The DAQ2000 records up to four channels of data simultaneously and saves it in binary format. The step of the time stamp is 0.100 μs. For each measurement a report file is also stored with information about the hardware settings as well as the measurement dates and times.

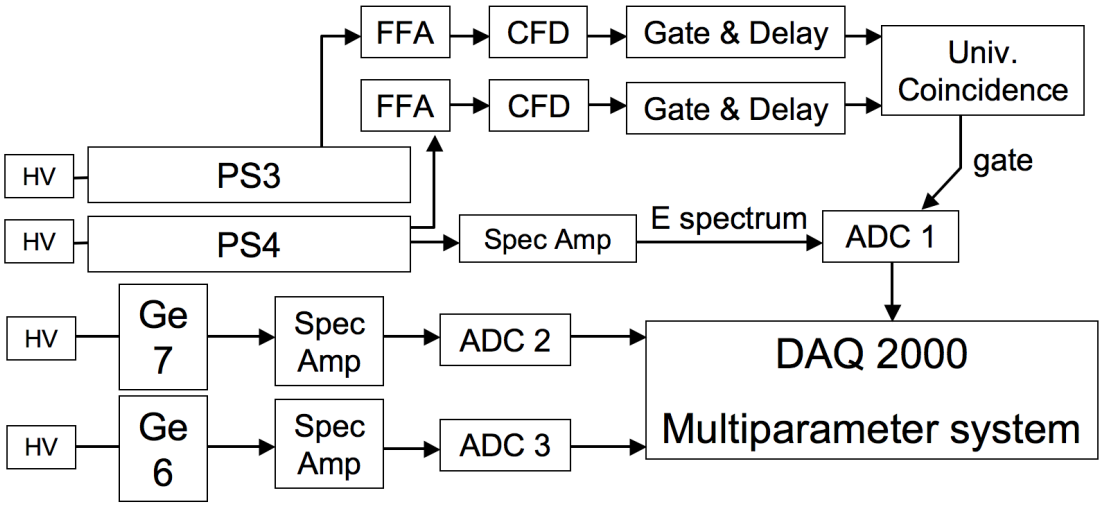

Figure **3.7**: The Sandwich spectrometer electronics.

All data is collected from Ge-6 and Ge-7, but only the spectrum from the lower of the two plastic scintillators in the muon shield is collected (gated with the coincidence pulse), see section *3.4 The active muon shield*. By not using the coincidence circuit as a hardware gate for the germanium detectors no events in Ge-6 and Ge-7 are lost,

which could otherwise be the case. All data, including the muon-induced events, are analysed in detail with the custom-made, offline software that was designed by J.S.E. Wieslander and implemented by M. Misiaszek (M. Smoluchowski Institute of Physics, Jagiellonian University, Krakow, Poland).

NIM Module	**Value**	**Unit**
MMPM time out	2.4	μs
MMPM coincidence time	1.6	μs
MMPM coincidence mode	Non overlap mode	
MMPM step of the time stamp	0.100	μs
PS4 Spec Amp shaping time	1	μs
PS4 Spec Amp amplitude/FWHM	4/3.5	V/μs
FFA output amplitude/time	0.5-1/0.25	V/μs
CFD amplitude/time	5/0.5	V/μs
Gate & delay amplitude/time	8/10	V/μs
Univ. Coincidence amplitude/time	8/10	V/μs
ADC1 Gate input pulse	Overlap mode	
Ge-6, Ge-7 Spec Amp shaping time	4 and 6	μs

Table **3.3**: Details of the electronic equipment in Figure 3.7.

The time stamp is tracked using a continuous clock that starts over every 215 seconds. When an event is registered in one channel on the MMPM (modular multi-parameter multiplexer), that is connected to the DAQ2000 system, all 3 channels are read out and time-stamped. The most frequent pulses originate from the muon detectors, with 3 events in 20 seconds (0.138 $m^{-2}s^{-1}$), while the germanium detectors have a background count-rate of about 450-550 d^{-1} (0.005 s^{-1}). The count-rate with real samples in the spectrometer is usually $<$1000 d^{-1}, so in all normal cases it is sufficient for the Sandwich Spectrometer to have a rather long resolving time.

The **resolving time** of the Sandwich Spectrometer, which is the precision with which two pulses can be determined to occur simultaneously in two detectors, is given by the expression

$$t_{res} \approx \sqrt{t_{clock}^2 + t_{rise-P4}^2 + t_{rise-Ge6}^2 + t_{rise-Ge7}^2} \tag{3.2}$$

where, as leading edge discriminators are used, the uncertainty is approximately the peaking time of the pulses. The t_{clock} is the step of the time stamp clock. For the plastic scintillator the peaking time, t_{rise}, was measured to 0.41 μs, while for the germanium detectors $t_{rise-Ge6}$ and $t_{rise-Ge7}$ are estimated as the *shaping time*/2.2 = 1.8-2.7 μs. Since the pulses are roughly Gaussian this represents an upper limit to the resolution. The Sandwich Spectrometer resolving time was determined to $\approx$**3.7** μ**s**.

3.6 The sample volume and radon removal

The dimensions of the sample volume in the Sandwich Spectrometer can be adjusted by changing the distance between the two germanium detectors in an interval of 0-70 mm by changing the vertical position of Ge-7. The distance should be adjusted for each sample to position the two detectors as close to the sample as possible, which maximises the FEP detection efficiency of the spectrometer. The diameter of the endcaps is 10 cm and since the lead shield is tightly fitted to the germanium detectors, this also limits the sample diameter.

The measurement volume inside the spectrometer is flushed with the boil-off nitrogen gas from the LN2 Dewars used to cool the germanium crystals. ^{41}Ar (1294 keV) from the nearby nuclear test reactor is visible in the sample spectra only if the Sandwich Spectrometer was open when ^{41}Ar was present. The peak in the γ-ray spectrum is significant for several hours after the spectrometer has been closed, but is completely removed after 24 hours of measurement. Spectra with ^{41}Ar are usually omitted.

3.7 Sample preparation

Generally speaking, the sample preparation for ultra low-level γ-ray spectrometry is very simple and non-destructive. That said, for successful low-background measurements the samples should be prepared with care because when it comes to very low levels of activity the problem is quite the opposite of that with high levels of activity: the sample must be protected from contamination by people, surrounding air and

equipment. The activity of the samples to be measured in the HADES laboratory should be in the μBq range, up to a few mBq, while higher levels of activity do not require access to an underground laboratory: it is sufficient to use low-background spectrometers at ground level. If the level of activity is unknown, the sample is first screened on a spectrometer in the ground level laboratory.

All samples going to the HADES laboratory are prepared in a clean room, which is equipped with a fume hood and an air-conditioning system providing a constant, laminar flow of cleaned air (to decrease the presence of radon, thoron and dust particles). Extra care is taken by the staff not to introduce any contaminants into the clean room, by using lab coats and plastic gloves and not bringing in unnecessary equipment or high-activity samples. All tools used in the clean room are routinely cleaned. The Sandwich Spectrometer is suitable for small samples fitting into the sample cavity of 10 cm in diameter and 7.0 cm in height, which means that some larger samples may need additional preparation to be reduced in size before they are measured. Typical sample preparation of larger samples includes grinding or some kind of cutting, but it is very uncommon to use chemical preparation. In some cases the samples are cleaned with strong acids or immersed in isopropanol for a longer time to remove difficult surface contaminants. Samples that have low activity but could be tritium-contaminated are cleaned with the necessary equipment in the pre-room before they are allowed into the main clean room for further sample preparation. All sample holders are routinely cleaned with isopropanol before each measurement and the samples and sample holders are kept in sealed plastic bags after cleaning until they are placed on a detector. Finally, the spectrometers in HADES are always cleaned with isopropanol before a sample is placed on the detector and the measurement started.

Over time the extensive cleaning procedures have turned out to be a successful way to decrease the overall level of background radioactivity from external contaminants in the ULGS detectors, and today they are standard procedure in the HADES laboratory.

3.7.1 Spectrometer contamination from samples

Contamination from samples can be problematic and in our case a $\approx$1Bq contaminating activity could be traced to a build-up of contamination at a corroded screw. The contamination of ^{176}Lu was removed from the top detector, Ge-7, after cleaning it with 0.1 M HNO_3 acid. In this case the vapours from the liquid ^{176}Lu source were not so aggressive, but it is not certain that a contamination from more aggressive sources would have been removed so easily. It is therefore of serious importance to take all possible precautions to avoid contaminating a low-background spectrometer.

3.8 Energy drift and other artefacts

The problem with malfunctioning equipment is that sometimes the issues are not seen until after very long measurements and detailed analysis of the data, while in other cases the output signal is lost and a broken part easily identified. It is clear that one of the most important things to which daily attention should be paid is energy drift in the spectra and ensuring that the count-rate is as expected in each detector. Unfortunately, in many cases it is problematic to find the origin of the energy drift. Generally speaking, it is crucial to ensure that the power supply to the pre-amplifier and the germanium detector is stable, since fluctuations will immediately affect the energy calibration.

Since the count-rate in the Sandwich Spectrometer is very low, as in all low-background systems, it is rather difficult to adjust the calibration of individual spectra since peaks from the background, which could be used as approximate points of reference, are so few in number that they are only visible after several days of measurements. Consequently, it may be impossible to adjust the energy calibration if the system experiences considerable energy drift over a 24-48 hour measurement.

4 Performance of the Sandwich Spectrometer

4.1 Calibration

4.1.1 Energy calibration

The energy calibration measurements were regularly performed with a custom-made point source with the γ-ray lines listed in Table 4.1, which cover a large part of the energy spectrum. The energy calibration source was always placed in the dedicated sample holder to ensure a constant detector-to-sample distance over time. Figure 4.1 shows a typical energy calibration spectrum for the Ge-7 detector. For the characterisation of the spectrometer also other reference point sources with different energies and γ-ray level scheme were used, but these were only measured at specific occasions and not regularly. The laboratory have reference sources covering the energy spectrum of the Sandwich Spectrometer, i.e. 40-2400 keV.

Source	**γ-ray energy (keV)**
^{241}Am	59.54
^{137}Cs	661.66
^{60}Co	1173.230, 1332.508

Table **4.1**: The radionuclides and γ-ray lines of the calibration reference source.

A linear fit was used to calibrate the energy scale. This calibration is a system energy calibration, i.e. a calibration of the whole chain of germanium detectors and electronics since it is done on the output spectra. The germanium detectors and the electronics are not entirely linear in their energy response, but the HADES group have in the past determined the nonlinearities in these energy calibrations for the interval 40-2700 keV to be negligible for the detectors used in the HADES laboratory.

The energy drift due to hardware issues during this work made it necessary for every single spectrum to be individually checked and in many cases also calibrated separately. For sample spectra a calibration is rather simple due to the often clear and

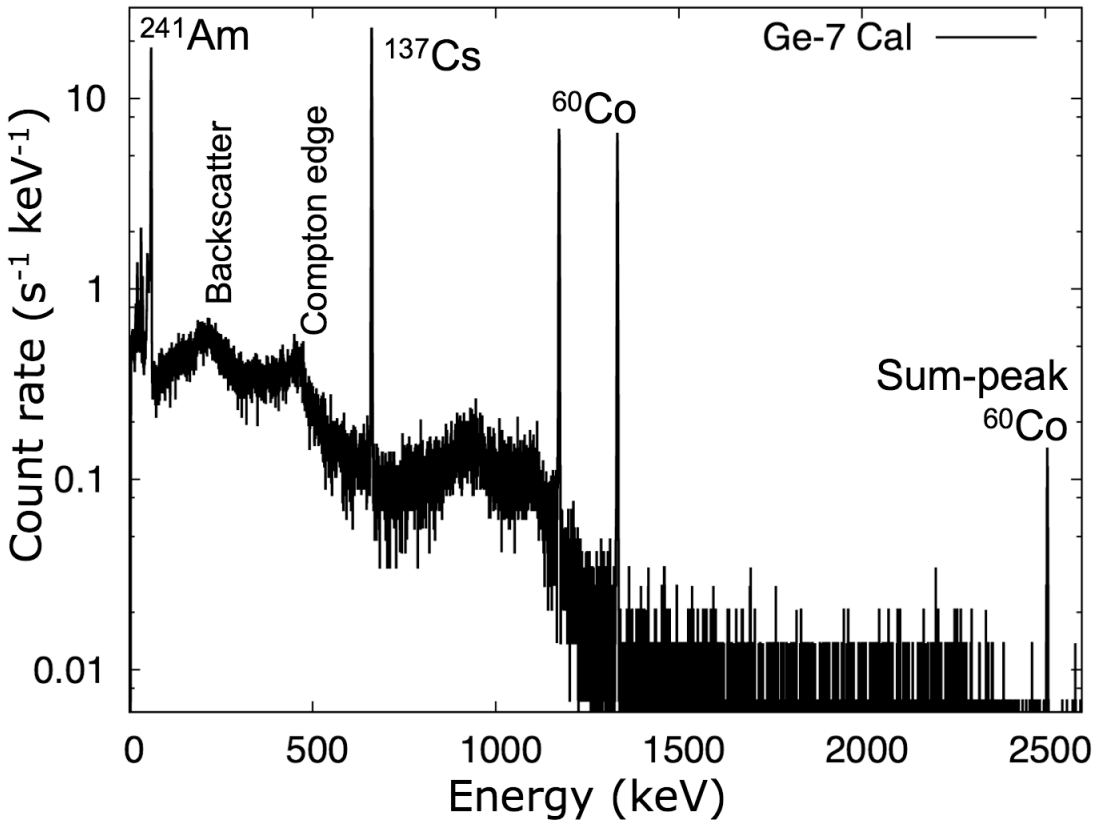

Figure **4.1**: The energy calibration spectrum for Ge-7.

easily identified γ-ray lines from the radionuclide to be detected, but the background spectra are more difficult due to the low count-rate. A new calibration was used only if it was absolutely certain that the new calibration was correct. If a new calibration was not possible to find and the existing calibration was not sufficiently accurate, the spectrum was omitted. Work was continuously done to solve the energy drift and at the end of this work, the energy drift stopped and the energy scale of the Sandwich Spectrometer became stable.

4.1.2 FEP detection efficiency calibration

The full energy peak (FEP) detection efficiency calibration was performed according to the procedure in section *2.5 Detection efficiency calibration*. However, in some cases the calibration with point sources does not give enough accuracy and the absolute FEP detection efficiency is also calibrated with volume sources, which are described in the next section.

4.1.3 Volume sources

Volume sources are needed for accurate FEP efficiency calibrations because they take geometrical effects, such as self-shielding and self-absorption into account and this is especially important for measurements of thick sources, very low levels of activity and from sources with cascading γ-rays. The Sandwich Spectrometer was during this work validated with a ^{176}Lu volume source in liquid form and the γ-ray spectrum from that measurement is shown in Figure 4.2. The volume source described in Paper IV was used as a volume calibration source for the measurements of tantalum that will be measured for seveal years. The half-life of ^{176}Lu is long, 3.6×10^{10} years, and the decay scheme for the β^- decay is similar to that of ^{180m}Ta, which is the radionuclide to be measured.

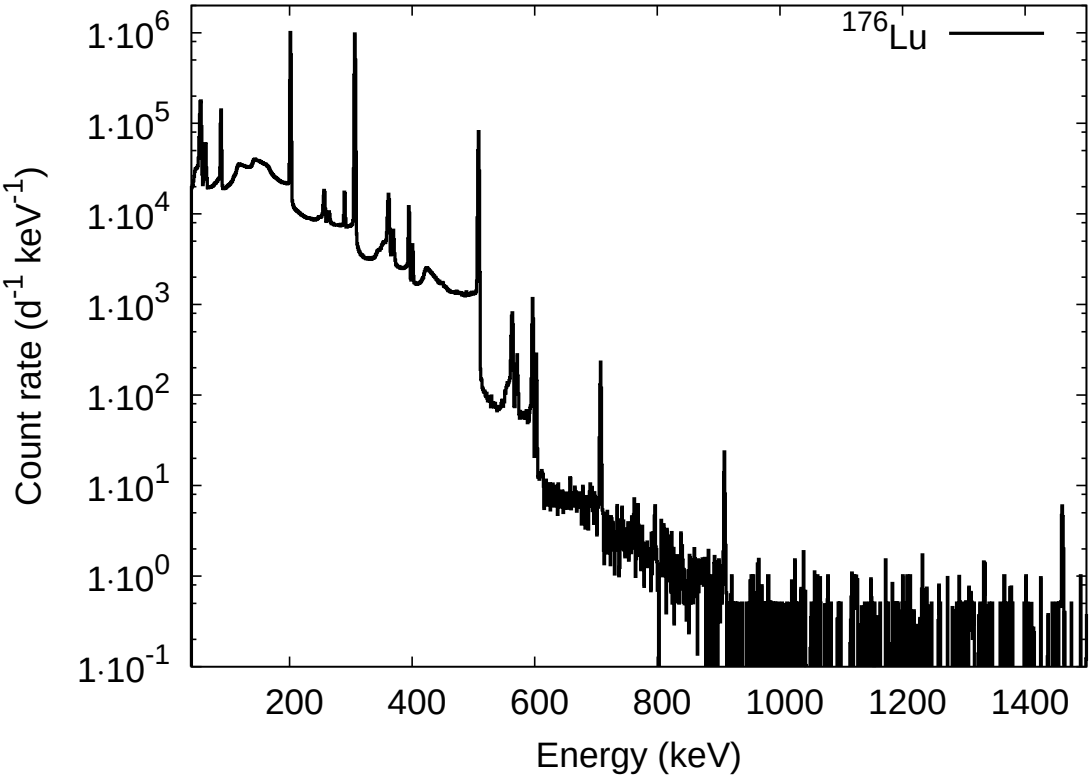

Figure **4.2**: The gamma-ray spectrum of the ^{176}Lu volume source on the Sandwich Spectrometer.

4.2 Muon background contribution in HADES

The muon background discussed in section *2.1.1 Cosmic rays and neutron induced background* gives rise to spectra such as those shown in Figures 4.3-4.4. In Figure 4.3 the coincidence circuit (see section *3.4-3.5*) is disconnected, while in Figure 4.4 the spectrum is gated with the coincidence signal, and these two figures show the necessity of an active muon shield for efficient muon detection in HADES. At ground level, the muon flux is much higher than underground and consequently the muon peak is clearly visible in a spectrum even without an active muon shield.

The muon events are defined as the events above the "valley" in Figures 4.3-4.4, a valley that is difficult to determine unless the muon energy signal is gated with the coincidence circuit. In Figure 4.4 the muon events are those above channel 840. The high count-rates to the left in the spectrum (below the "valley") originates from the γ-ray background. Since the majority of the muons pass the muon shield in the vertical direction, the most probable deposited energy corresponds to the 5 MeV that was calculated in section *3.4 The active muon shield* and this results in a peak or "hump" that is visible in the spectra in Figure 4.3 (channel 4000, hardly visible since it is obscured by the γ-ray background) and 4.4 (approximately at channel 2000).

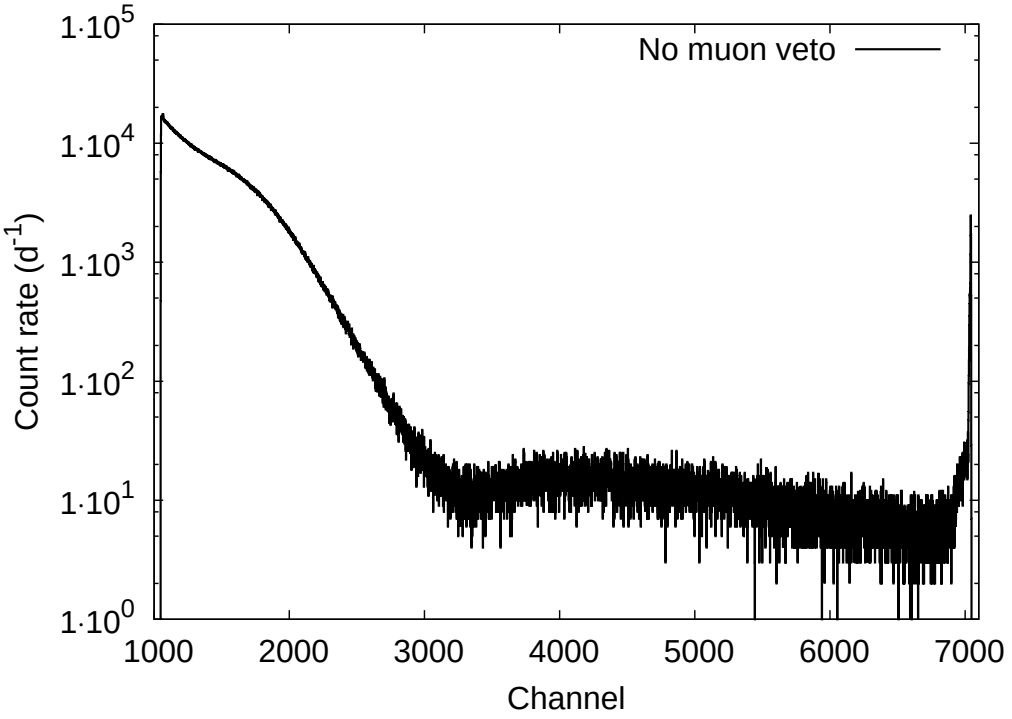

Figure **4.3**: The muon spectrum from the active muon shield's lower plastic scintillator with the coincidence signal disconnected. To be compared with Figure 4.4. The energy scale is in channels.

The muon count-rate in HADES was in this work determined to 0.138 m^{-2} s^{-1}. This value should be compared to a previous measurement of the muon count-rate at ground level at IRMM of 160 m^{-2} s^{-1}. The muon flux is thus reduced by three orders of magnitude by bringing the spectrometer underground. It should, however, be borne in mind that measurements with this kind of set-up at ground level not only contain contributions from muons but also from other components of the secondary cosmic radiation that are not present in the underground measurements.

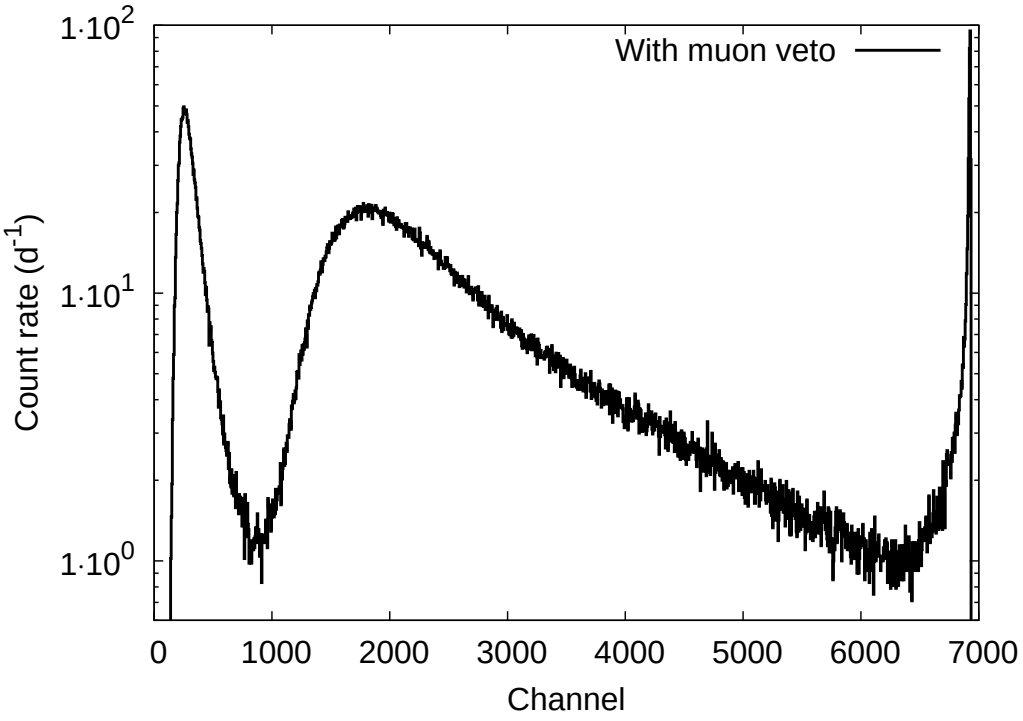

Figure **4.4**: The muon spectrum from the active muon shield's lower plastic scintillator with the coincidence signal connected as a gating pulse to the ADC. The lower threshold of the ADC was altered between this measurements and the one in Figure 4.3, leading to an energy shift of the "valley". All pulses above channel 840, i.e. the "valley", are defined as muon events. Below channel 840 the γ-ray background is visible. The energy scale is in channels.

4.3 Background spectra, count-rates and detection limits

The muon-induced events in the germanium detectors were identified and removed from the γ-ray background spectrum, see Figures 4.5-4.6, using the offline analysis software. Table 4.2 lists the count-rate in different γ-ray peaks present in the background, while Table 4.3 lists the background reduction from muon anti-coincidences in different energy ranges. A detection limit is given when a background peak is not visible at the expected energy range in the background spectrum. In Table 4.2 the uncertainty is given within brackets and correspond to the last digit of the given value. The background count-rate in one germanium detector is approximately 450-550 d^{-1} and typically not more than twice as much in a measurement spectrum from a sample.

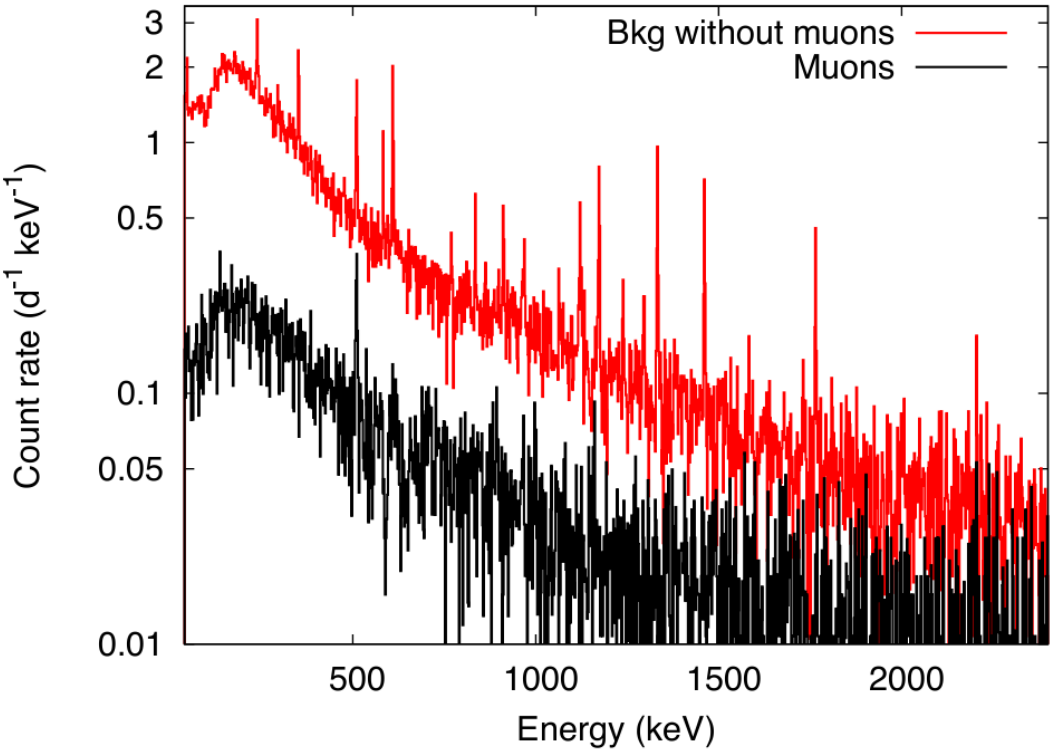

Figure **4.5**: The background γ-ray spectrum from the Sandwich Spectrometer, showing the count-rate (d^{-1} keV^{-1}) as a function of energy (keV). The red line (Bkg without muons) shows the background spectrum with the muon-induced events removed. The black line (Muons) shows the muon-induced events that were removed from the original background spectrum.

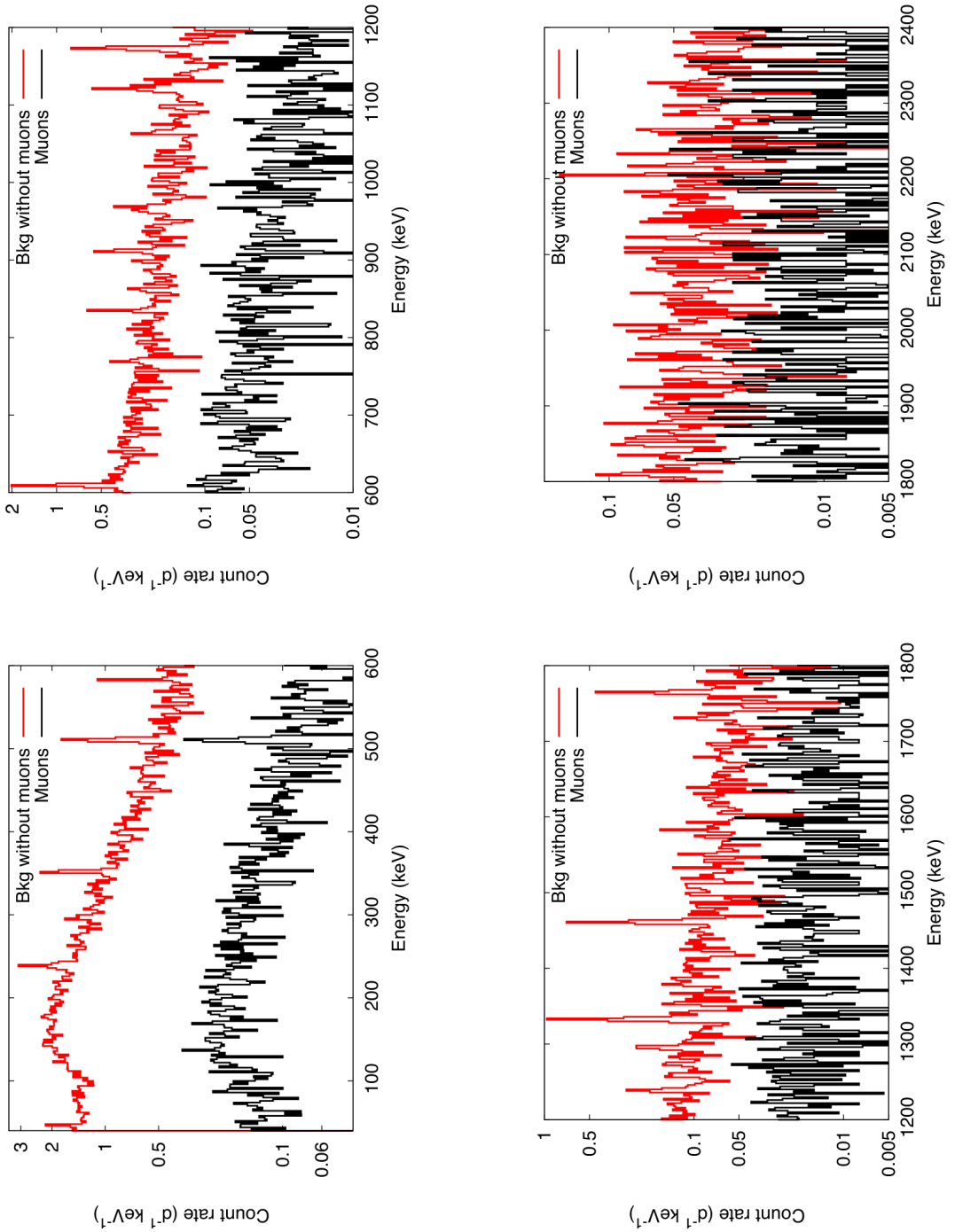

Figure **4.6**: The background spectra in Figure 4.5 in detail, showing the count-rate (d^{-1} keV^{-1}) as a function of energy (keV). The red line (Bkg without muons) shows the background spectrum with the muon-induced events removed. The black line (Muons) shows the muon-induced events that were removed from the original background spectrum. The scale on the y-axis is generally logarithmic but for the highest energy range here it is displayed in linear scale. The 511 keV peak comes from annihilation events.

E_γ (keV)	Radionuclide	Ge-7 (counts d^{-1})	Ge-6 (counts d^{-1})
46	^{210}Pb	2.1 (3)	<0.5
63	^{234}Th	<0.6	<0.6
93	^{234}Th	<0.6	<0.6
186	^{226}Ra + ^{235}U	<0.7	<0.7
238	^{212}Pb	2.2 (3)	2.1 (4)
242	^{214}Pb	0.34 (25)	<0.8
295	^{214}Pb	0.70 (29)	0.56 (26)
338	^{228}Ac	0.28 (17)	<0.6
351	^{214}Pb	2.1 (3)	2.3 (3)
511	Annihilation	2.51 (28)	2.9 (4)
583	^{208}Tl	1.05 (19)	0.61 (19)
609	^{214}Bi	2.37 (25)	2.5 (0.3)
661	^{137}Cs	<0.3	<0.4
911	^{228}Ac	0.48 (14)	0.7 (20)
969	^{228}Ac	0.22 (11)	0.26 (14)
1120	^{214}Bi	0.50 (13)	0.86 (19)
1173	^{60}Co	1.44 (17)	0.85 (18)
1332	^{60}Co	1.24 (16)	1.32 (20)
1460	^{40}K	1.31 (16)	0.84 (17)
1764	^{214}Bi	0.41 (10)	0.72 (14)

Table **4.2**: The count-rate in the detected background peaks and the detection limits in the ranges where a common background peak could have been expected. The unit is counts d^{-1}. The uncertainty is given in brackets and correspond to the last digit(s) in the given value.

The reason for the difference in measurement time between the two germanium detectors, see Table 4.3, is that some spectra were not possible to calibrate due to energy drift during this work and such spectra were omitted. Table 4.2-4.3 also show the difference between the two germanium detectors, which could depend on for example differences in the geometry and materials, see table 3.1.

4.4 $\gamma\gamma$-coincidences

The prompt coincidences between Ge-6 and Ge-7 in 38.5 days of background measurement were investigated in the energy interval 0-2400 keV. The coincidences were 77 in total, which corresponds to approximately 0.2% of the total counts per day ($\approx$900 counts d^{-1}) in the Sandwich Spectrometer. This verifies that background coincidences between the germanium detectors in the Sandwich Spectrometer can be neglected.

Energy range (keV)	Ge-6+Ge-7	Ge-6	Ge-7	Unit
Background reduction by anticoincidence with muons				
0-600	11	10	13	%
600-1200	15	12	18	%
1200-1800	16	12	21	%
1800-2400	22	18	26	%
Background events without muons / deleted muon-induced events				
40-2400 keV	869 / 124	441 / 52	428 / 72	counts d^{-1}
40-400 keV	532 / 74	268 / 39	264 / 35	counts d^{-1}
400-1400 keV	281 / 47	145 / 19	136 / 28	counts d^{-1}
1400-2400 keV	56 / 14	28 / 5	28 / 9	counts d^{-1}
Measurement time	-	63.4	46.4	days

Table **4.3**: The reduction of the muon-induced background events from the total background in the germanium spectra in Figure 4.5-4.6 in different energy ranges. In the top part the reduction is given in % and calculated as the number of muon-induced events divided by the total number of events in the respective energy interval. In the lower part the count-rate is given in counts d^{-1} in respective energy interval with the muons after the dash

.

4.5 Sample thickness and self-absorption

Since the level of activity is very low in samples measured in a low-background spectrometer, a substantial mass of the sample is needed. However, by increasing the thickness of the sample the self-absorption becomes dominant. The trade-off between the requirement for sufficient mass (i.e. number of isotopes of the targeted type) and the effect of self-absorption in the sample requires the samples to be carefully designed, especially in the case of measurements of rare decays such as those in tin, tantalum (see Paper IV) and indium (see Paper VIIa-b). These samples are always made of ultra pure material which results in the price of the material being a factor in the design.

The design starts with Monte Carlo simulations of the decay that is to be studied. The FEP detection efficiency increases almost linearly with the number of atoms in the sample, while it decreases approximately with the $\sqrt{thickness}$ of the sample. By plotting the ($FEP\ detection\ efficiency \times thickness$) on the y-axis against the thickness on the x-axis, the values on the y-axis will reach a plateau after which an increase in thickness will not have any effect. The beginning of this plateau indicates a suitable sample thickness for the detectors for which the Monte Carlo simulations have been

carried out. The dimensions of the metal discs specifically designed for measurements of rare decays in the Sandwich Spectrometer during this work were listed in the end of section *2.5 Detection efficiency calibration* and these are: a stack of six tantalum discs (that are also shown in Figure 2.3) and one tin disc. The indium disc was made of radiopure indium that was already available in the resarch group and it was used in its entirety (see Paper VIIa-b).

4.6 Energy resolution

The energy resolution depends on the full width at half maximum (FWHM) and the larger FWHM, the worse γ-ray energy resolution. The FWHM as a function of the γ-ray energy is shown in Figure 4.7. The FWHM was extracted from measurements of the standard calibration source, see Table 4.1. Due to hardware issues the FWHM have fluctuated over time, but continuous development is undergoing to minimise this. The curves in Figure 4.7 show the best performance for each detector.

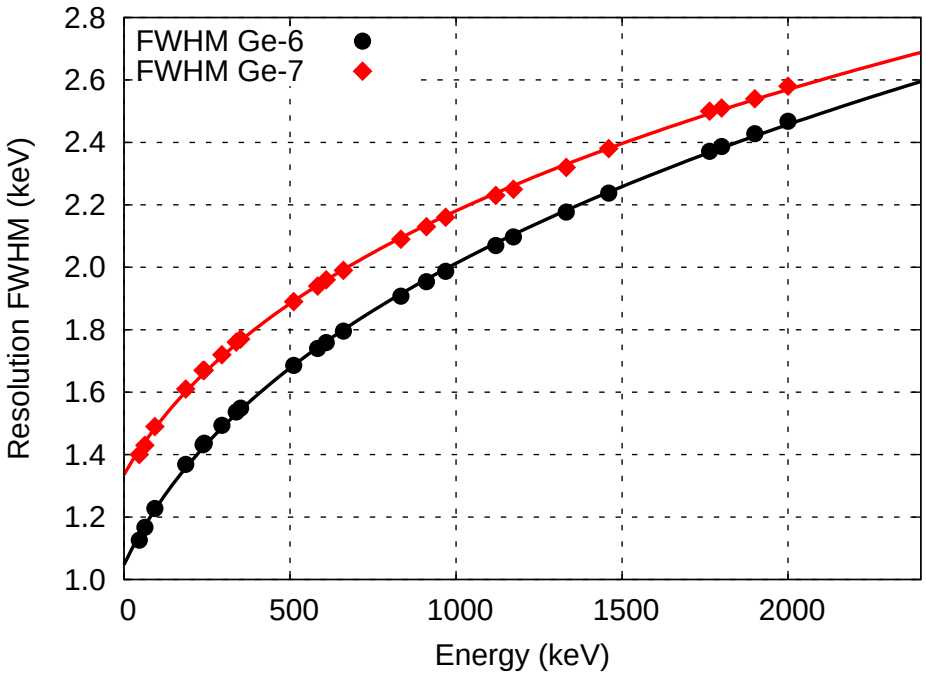

Figure **4.7**: The FWHM (keV), during best performance of detectors Ge-6 and Ge-7 as a function of energy (keV).

4.7 Timing performance

Figure 4.8 shows the time distribution of the muon-induced events in the germanium detectors in background measurements of 38.5 days. The time distribution is calculated as the time elapsed from the detection of a muon event until an event is detected in the germanium detector. The FWHM is ≈1.1μs, which is an approximation of the coincidence resolving time and in the same order of magnitude as the system resolving time calculated in section *3.5*. The speed of the resolving time is limited by the germanium detectors, which is to be expected since they are slower in their response compared to the plastic scintillators and the system electronics.

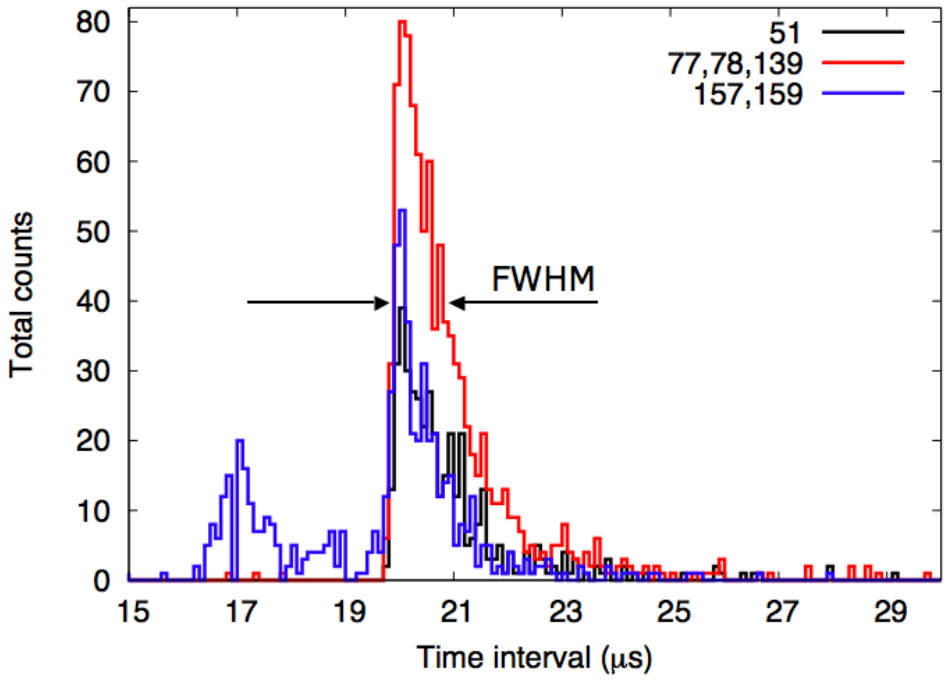

Figure **4.8**: Time distribution of the muon-induced events in Ge-6, i.e. the time it takes for an event to occur in the germanium detectors after an event in the active muon shield. The FWHM is ≈1.1 μs and is an approximation of the resolving time of the Sandwich Spectrometer. Background measurement (38.5 days). The numbers 51-159 correspond to measurement files.

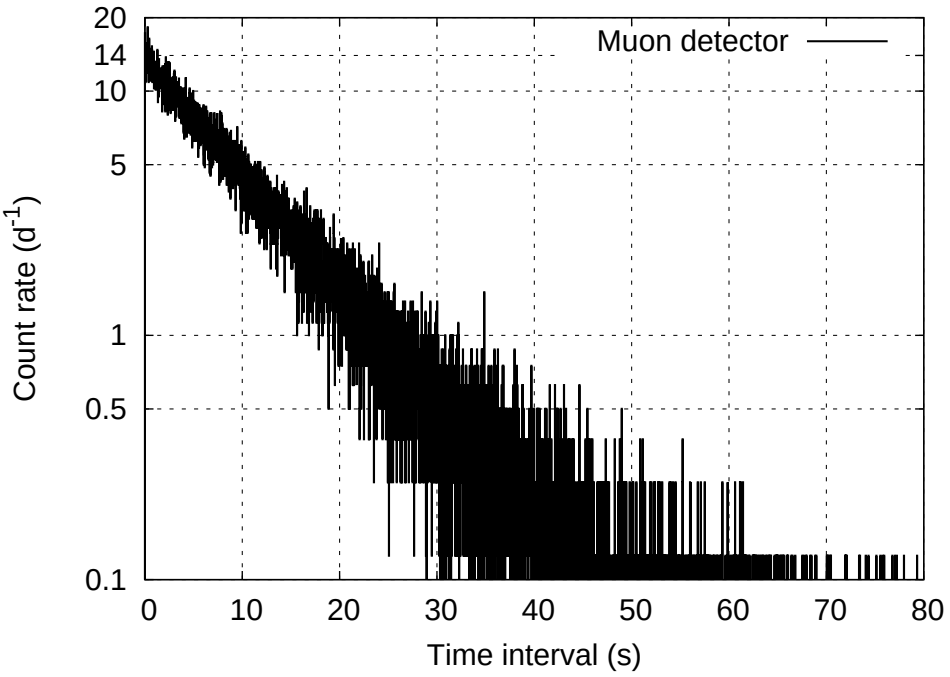

Figure **4.9**: The time intervals between events in the active muon shield.

The time intervals between events occurring in each individual detector are shown in Figure 4.9 and 4.10, with count-rate as a function of the time interval. The function for each detector was determined to

$$C_{muons}(t) = 13.8 \times 10^{-0.048t} \tag{4.1}$$

$$C_{Ge6}(t) = 2.5 \times 10^{-2.2 \times 10^{-3}t} \tag{4.2}$$

$$C_{Ge7}(t) = 5.8 \times 10^{-2.8 \times 10^{-3}t} \tag{4.3}$$

where t is the measurement time. The dead time is short compared to the time between the pulses in the detectors. Any problems with the dead time would have shown up as abnormalities in the timing spectra.

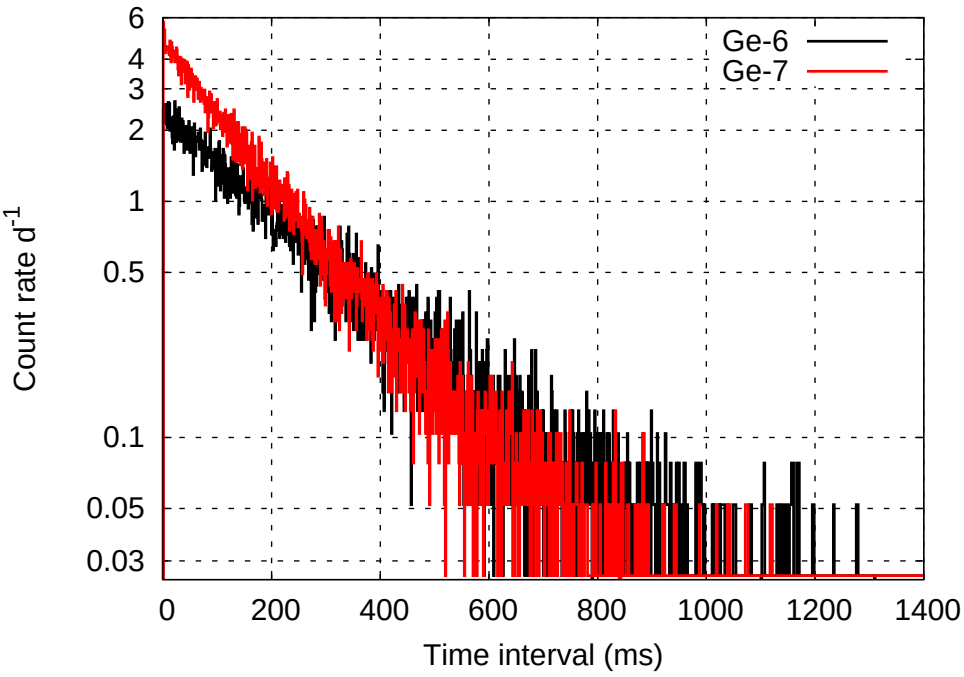

Figure **4.10**: The time intervals between background events in each individual germanium detector, Ge-6 (black) and Ge-7 (red).

4.8 Comparison with other underground laboratories

In Figure 4.11, the line corresponding to the letter *D* put the detection levels in the HADES laboratory into perspective in comparison with other laboratories. The red line shows the Sandwich Spectrometer and the superposed grey line is the previous best detector in HADES. By decreasing the background radiation in the spectrometer, peaks that were previously obscured are now visible. All peaks were identified and are listed in Table 4.2. There is no activation of germanium or copper and all environmental background is strongly reduced. The integrated count-rate normalised to the germanium crystal mass for the Sandwich Spectrometer is 220 day^{-1} kg$_{Ge}^{-1}$ (in the energy range 40-2700 keV), which is the lowest in the HADES laboratory. This value for the Sandwich Spectrometer can be compared with the two other detectors in HADES closest in range that are slightly less than 300 day^{-1} kg$_{Ge}^{-1}$.

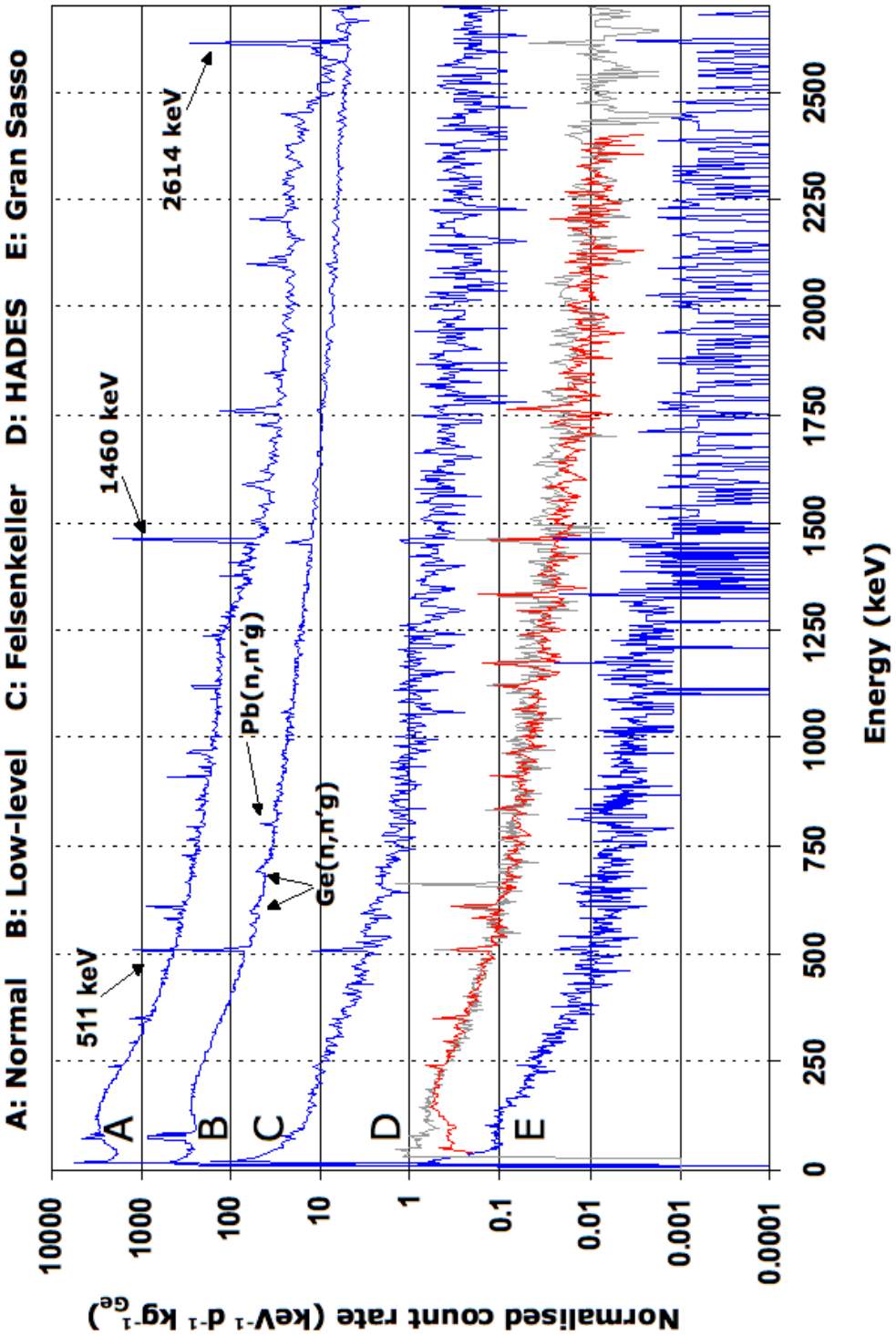

Figure **4.11**: A comparison between different underground laboratories. A) A ground-level laboratory, B) a low-level laboratory at ground level, C) Felsenkeller at 125 *m w.e.*, D) Hades at 500 *m w.e.*, E) Gran Sasso at 3800 *m w.e.*.

5 Achievements with the Sandwich Spectrometer

This chapter is an introduction to the applications included in this work, while further details are found in Paper I-VII. Paper III is a short instrumental paper with an overview description of the Sandwich Spectrometer and that will not be discussed here since all the details are found in *Chapter 2-4*. The Sandwich Spectrometer can be used for a wide range of applications in many different fields, such as environmental measurements, medicine, fundamental research, nuclear dosimetry, materials science and industrial applications. The common denominator for the measurements in these fields performed with the Sandwich Spectrometer during this work was the need for ultra low-level γ-ray spectrometry to detect the low levels of activity in the samples.

5.1 Particle detection from a fusion plasma

This is an introduction to the work described in further detail in Paper I-II.

Many different diagnostic techniques for particle losses from fusion plasma (i.e. escaping neutrons and charged particles) are continuously developed. The measurements done with these diagnostic tools are compared to the theoretical models of the fusion reactions inside the tokamak. One of the long term goals of fusion research is to understand, describe and control the fusion process in a way that it will be possible to build fusion energy power plants in the future.

The fusion reactions produce neutrons and protons as well as α particles, depending on which fuel is used, and if the quantity and energy spectrum of these could be accurately determined this could be used to confirm the developed models for the fusion tokamak. So far in fusion technology, mainly neutron diagnostic tools have been successfully developed since neutrons penetrate the walls of the tokamak and the equipment can thus be placed outside the tokamak. One of the largest neutron detectors is a neutron camera [Adam93] in use at JET (the Joint European Torus, UK). However, it is difficult to detect the protons and other charged particles since they can not penetrate the walls of the tokamak and thus must be detected within the tokamak itself. Due to the extreme conditions in the tokamak, with high temperatures and intense radiation, the instrument options are very limited.

In this work, a new method for detection and quantitative determination of the charged particle fluxes and angular distribution with respect to the magnetic field inside the fusion tokamak at JET was studied. A probe, see Figure 1 in Paper II, with carefully selected samples of different materials was inserted into the ceiling of the fusion tokamak at JET. Due to the conditions inside the tokamak the samples were small (1×1 cm, 1 mm thick) and thus the total induced radioactivity in the majority of samples was very low. The levels of activity are listed in Paper I and the lowest was ≈40 μBq. The only way to detect the activated radionuclides was to use underground ultra low-level γ-ray spectrometry (ULGS). The start of the γ-ray measurements as well as the total measurement time was limited by the half-life in combination with the low levels of activity, and several ULGS detectors therefore had to be used simultaneously. Detailed analysis of all possible activation reactions, thresholds, cross sections, levels of impurities and possible interferences of impurities were investigated for all activated sample materials, see Paper I.

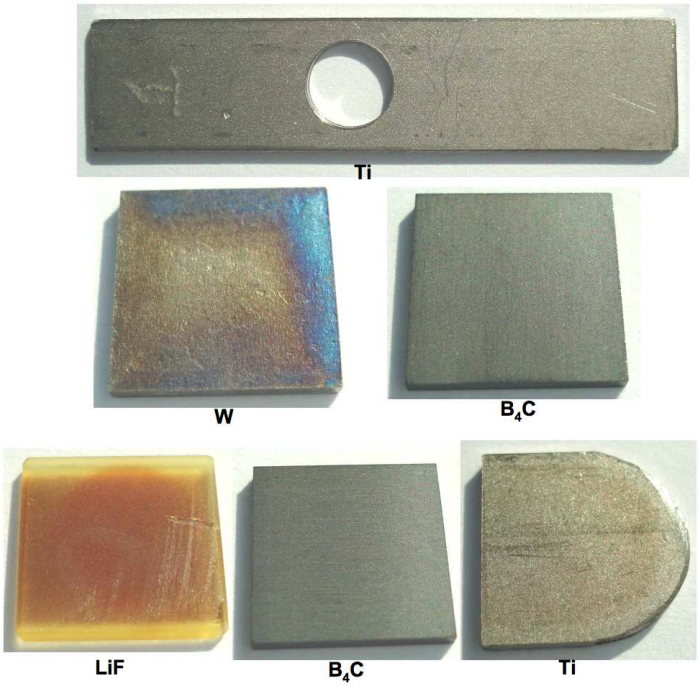

Figure **5.1**: Samples from the probe activated at JET. Square samples are: 1×1 cm, 1 mm thick. Materials are: titanium (Ti), tungsten (W), boroncarbide (B_4C) and lithiumfluoride (LiF).

By using ULGS detectors, the radionuclides from charged particle activation by the fusion plasma inside a tokamak were detected and quantified for the first time in this work, see Paper I. Additionally, the low uncertainties in the ULGS measurements made it possible to identify an angular distribution, which after detailed analysis was attributed the angular dependence of the charged particles on the magnetic field inside the tokamak. The measurement results correlated with computer simulations of charged particle escape from the fusion plasma, see Paper II.

5.2 Neutron spectrometry and dosimetry

This is an introduction to the work described in further detail in Paper V-VI. In this work a new dosimetry and spectrometry method for environmental neutrons was further developed from an initial study. The spectrometry method was tested with several different neutron fields at IRMM in Paper V, then characterised with a calibrated neutron source and finally tested in a *real life* experiment with MOX nuclear fuel (mixed oxide/plutonium fuel) in Paper VI. In principle the neutron detection method includes only three steps (i) activation of thick metal discs, (ii) low-level γ-ray spectrometry measurements and (iii) spectrum unfolding and analysis. The advantage with this method is that in addition to the neutron dose also the energy spectrum is obtained, which is usually not the case with common dosimeters.

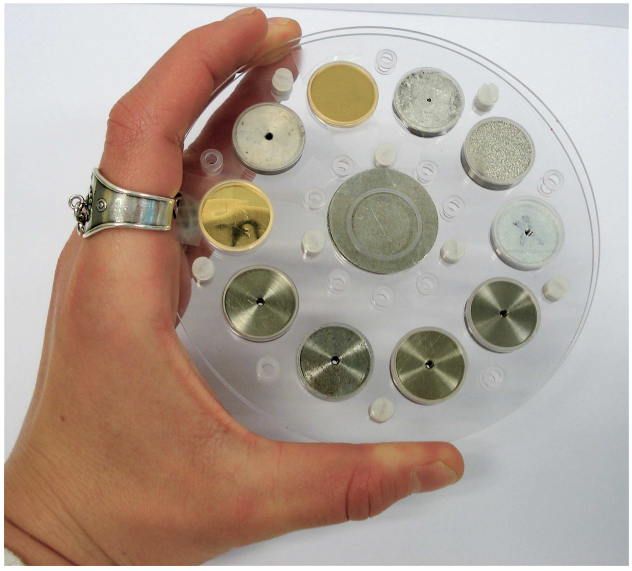

Figure **5.2**: The neutron detector unit 2007.

It is an advantage to use small metal discs since the neutron spectrometry unit (12 cm diameter) then can basically be placed in any environment and a wide variety of radiopure metals can be used. From the very low neutron fluxes in some of the irradiations, the levels of induced activity in the small discs was so low that it could only be detected by a low-level γ-ray spectrometer. In this application the activity is normally given as Bq atom^{-1} of the measured isotope, however, here it makes more sence to give it in Bq g^{-1} of the disc material. The induced activity from the stronger fields were typically ranging from several Bq g^{-1} down to a few mBq g^{-1}, while the lowest fields were usually just a few mBq g^{-1}. After an activation irradiation both the order in which the metal discs are measured as well as the measurement time is determined by the half-life of the radionuclides produced, level of activity and the number of available low-background γ-ray spectrometers. The level of activity

is determined by the threshold and cross-section of the activation reaction as well as the neutron flux of the irradiation source. All these factors must be investigated beforehand in order to select appropriate metals that will produce radionuclides of activity levels that are detectable on the intended γ-ray spectrometers within the time frames given for the measurements.

For the experiments included here a range of metals were selected, a disc holder was designed and manufactured and the neutron spectrometry method was tested in the well determined neutron fields in Paper V-VI. Finally, the method was successfully tested in a *real-life* experiment, see Paper VI, to detect the neutron spectrum and the dose from a MOX (mixed oxide/plutonium) nuclear fuel storage box. All γ-ray measurements were carried out using ULGS detectors. This simple dosimetry and spectrometry method using activation of thick metal discs to detect environmental neutrons was determined to work well and the difference between the measured results and reference values was only $\approx$8% in the latest experiments.

5.3 Decay data and fundamental research

This is an introduction to the work described in further detail in Paper IV (tantalum) and Paper VIa-VIb (indium, of which the first is a short paper and the second is a draft for a longer paper to be published later).

Basic data on materials and phenomena are of essential importance in many aspects of society and this information is collected in databases, which are used for design and interpretation of natural phenomena. Some materials and processes are well understood and reliably documented, while for others there are gaps in knowledge. Uncertain basic data leads to uncertain behaviour and can result in unwanted surprises in applications ranging from nuclear power engineering to electronics design for consumer products and medical equipment. For this reason it is important to perform fundamental research and reference measurements to quantify the properties of materials for future use.

There are many examples and I will here mention just a few to shed some light on this topic. The first example concerns indium that was included in soldering of electronic contacts. Since indium is a very strong β emitter it really increases the background of a low-background measurement system and should be avoided in any electronics used for such applications. Hence the manufacturer of the electronics must be aware of this unwanted effect. Another example is the germanium and silicon used for chip components. Here the industry demands for low defect centre contaminations lead to the production of more radiopure silicon and germanium, of which the latter is nowadays used also in low-background γ-ray detectors since it is very radiopure.

The low detection limits of the Sandwich Spectrometer makes it especially suitable for measurements of rare decay events and radiopurity measurements, for which it was specifically designed. In the present work, the Sandwich Spectrometer has been used in low-uncertainty ULGS measurements of rare radioactive decay data. This rare decay data not only adds information to the materials databases but also, in some particular cases, contributes to further understanding of fundamental nuclear physics by confirming the present theories or pointing out where further research is needed - which in the long run will affect the way materials and processes are used and interpreted in society.

5.3.1 Tantalum

The decay of ^{180m}Ta, the world's rarest primordial isotope, is a 3^{rd}-forbidden unique transition with a very long half-life that has not yet been determined. In this work, the lower limit of the half-life was determined by measuring the emitted γ-rays from discs of radiopure tantalum on the Sandwich Spectrometer, see Paper IV. Since the decay is not detected during this short measurement, the detection limits are determined in the energy regions where the peaks are expected. The combined lower bound of the half-life of ^{180m}Ta was determined to 2.0×10^{16} y and the research group will continue to measure the rare decay on the Sandwich Spectrometer with the goal to increase the lower bound of the half-life to 10^{17} y after 3.7 years of further measurements.

5.3.2 Indium

The last measurement included in this work was that of the rare β^- decay of ^{115}In to the first excited state of ^{115}Sn, see Paper VIIa (short paper prepared for Physical Review Letters and to be submitted during February 2009) and VIIb (longer draft version to be updated with further data and analysis, to be published later). The 497.334 keV γ-ray that is emitted from the first excited state of ^{115}Sn was detected during three individual measurements of one thick disc (40 mm thick, 106 mm diameter) of radiopure indium. The disc was measured on the Sandwich Spectrometer and on one other detector in HADES (Ge-4). The combined level of activity of the individual measurements was 0.69(9) mBq. The first low-uncertainty value of the half-life and branching ratio of the rare β^- decay in indium was determined to $4.1(6)\times10^{20}$ y and $1.07(17)\times10^{-6}$, which were in agreement with the only previously published values [Catt05].

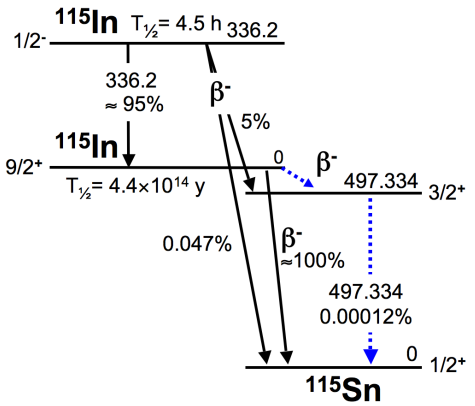

Figure **5.3**: The decay scheme of ^{115}In.

The determination of the partial half-life was combined with theoretical calculations done by a research group at Jyväskylä University in Finland. The conclusion from the advanced computer models of this 2^{nd}-forbidden unique transition in indium was that the Q value was only 0.057(3) keV. However, when comparing that Q value with the one obtained from high-precision mass measurements done by the IGISOL group at Jyväskylä University (with their Penning trap equipment), the conclusion was that further work is needed! The Q value from the mass measurements was 0.35(17) keV and hence quite a lot higher than the value obtained via the determination of the partial half-life from the γ-ray measurements.

The theoretical model of this β decay with such ultra-low Q value is not yet complete, but work is ongoing. At the same time further measurements of the partial half-life are underway to decrease the uncertainty as much as possible. A major source of uncertainty in the determination of the partial half-life is the high uncertainty of the half-life of the main decay branch of indium. To achieve an extremely low-uncertainty value of the partial half-life and branching ratio of the rare β^- decay of ^{115}In it is required that the uncertainty of the main branch is reduced.

The combined efforts of the two measurements and the theoretical calulations of the rare β^- decay of ^{115}In, see Paper VIIa-b, lead thus to the fundamental discovery that this transition may have one of the lowest known Q values of any nuclear decay discovered so far, about one order of magnitude lower than that of ^{187}Re. The measurements also indicate where more work on the theoretical model is needed, which in turn will demand further measurements.

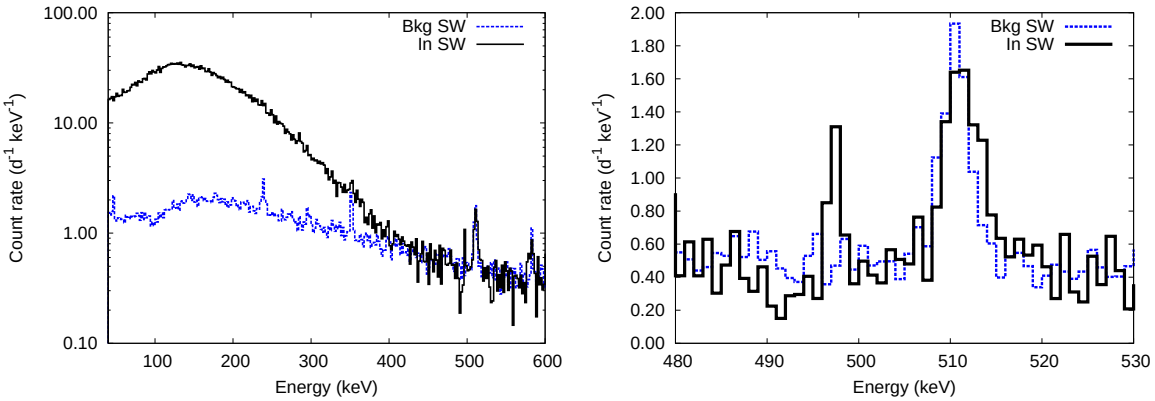

Figure **5.4**: The γ-ray spectrum from measurements of idium (black solid line) and the background (blue dotted line) on the Sandwich Spectrometer. The interesting peak is at 497.334 keV.

One topic that lies outside the scope of this thesis is to use the extreme sensitivity that can be achieved with ULGS to study the double beta decay in the future. Additionally, the continuing characterisation of very low transition energies in nuclear decays may contribute to the future detection of the neutrino mass.

6 Conclusion

The Sandwich Spectrometer is an ultra low-level γ-ray spectrometer that was set up, characterised and used in a series of applications to measure activity in the range of mBq down to μBq. The detection limits in the background measurements in this work are in the order of a few hundred μBq. The most important benefits of low detection limits are that lower levels of activity can be measured and that time spent on each measurement is reduced. The main uncertainty in low-background measurements originates from the counting statistics: increasing the full energy peak (FEP) detection efficiency by using bigger germanium crystals and decreasing the detection limits of the spectrometry system means that the uncertainty from the counting statistics is reduced as long as the measurement time is sufficient. In addition, an advantage of γ-ray spectrometry with germanium detectors that is not always commented on is that the sample preparation is very simple and in almost all cases non-invasive and non-destructive in comparison to for example radiochemical preparation of samples. However, it is important to keep the sample preparation clean from contaminants.

The ultra low-level γ-ray spectrometer presented here achieved low detection limits by:

- Using two germanium detectors facing each other, which essentially doubles the absolute FEP detection efficiency.
- Locating the spectrometer underground which removes the majority of the cosmic background radiation.
- Using an active muon shield to further decrease the muon-induced background in the germanium detectors.
- Careful selection of all materials used in the shield and detectors.
- Placing the electronics outside the shield.
- Accurate measurements of well defined calibration sources.
- Using well determined geometrical models and the Monte Carlo technique for accurate calibration of the spectrometer's FEP detection efficiency.
- Detailed analysis and calibration of individual measurement spectra.

Low levels of activity can be found in samples from for example the environment, customs controls, additives in food, contaminants in water, accelerator or nuclear power installations, radiopurity screening and medical applications. The application measurements included in this work are on samples from:

- Detection and quantification of escaping neutron and charged particles from fusion plasma inside a fusion tokamak.
- Further development of a small detector for neutron dosimetry and spectrometry using thick metal discs.
- Fundamental research such as the determination of rare decay data for tantalum and indium.

The charged particles escaping the fusion plasma were in this work detected and quantified for the first time inside the tokamak at JET, since no diagnostic tool has been able to do this previously. It will be interesting to see if the approach and the results from these experiments will bring new ideas for the further development of fusion diagnostic tools for charged particles.

The Sandwich Spectrometer was originally designed to meet the additional requirements for measurements in fundamental reasearch, such as the mentioned measurements of rare decay events that are not yet measured or for which today's values have excessive uncertainties. In this area the spectrometer has contributed to several improvements and the probably greatest achievement of this work was the low-uncertainty determination of the partial half-life of the rare decay in indium. The partial half-life and the branching ratio were determined from γ-ray measurements of the 497.334 keV γ-ray from a thick indium disc. Furthermore, when these results were combined with theoretical calculations of the rare β^- decay, the lower bound of a previously undetermined transition energy, Q value, could be calculated. Finally, this value was compared to the Q value determined from new mass measurements of the nuclei participating in the transition. One conclusion from the combination of these two measurements and the theoretical work was that further work is needed to accurately characterise this rare decay in indium - a work that is now ongoing. However, the main outcome of the work on indium presented here was that the combination of results strongly indicate that the β^- decay of ^{115}In to the first excited state of ^{115}Sn could have the lowest known transition energy of any nuclear decay so far, with a Q value about one order of magnitude lower than the previously lowest.

A Radiographs

Radiographs of the two germanium detectors in the Sandwich Spectometer, Ge-6 [Canb6] and Ge-7 [Canb7]. The radiographs are reproduced with the permission of Jan Verplancke, Managing Director of Canberra Semiconductor n.v.[Canbw].

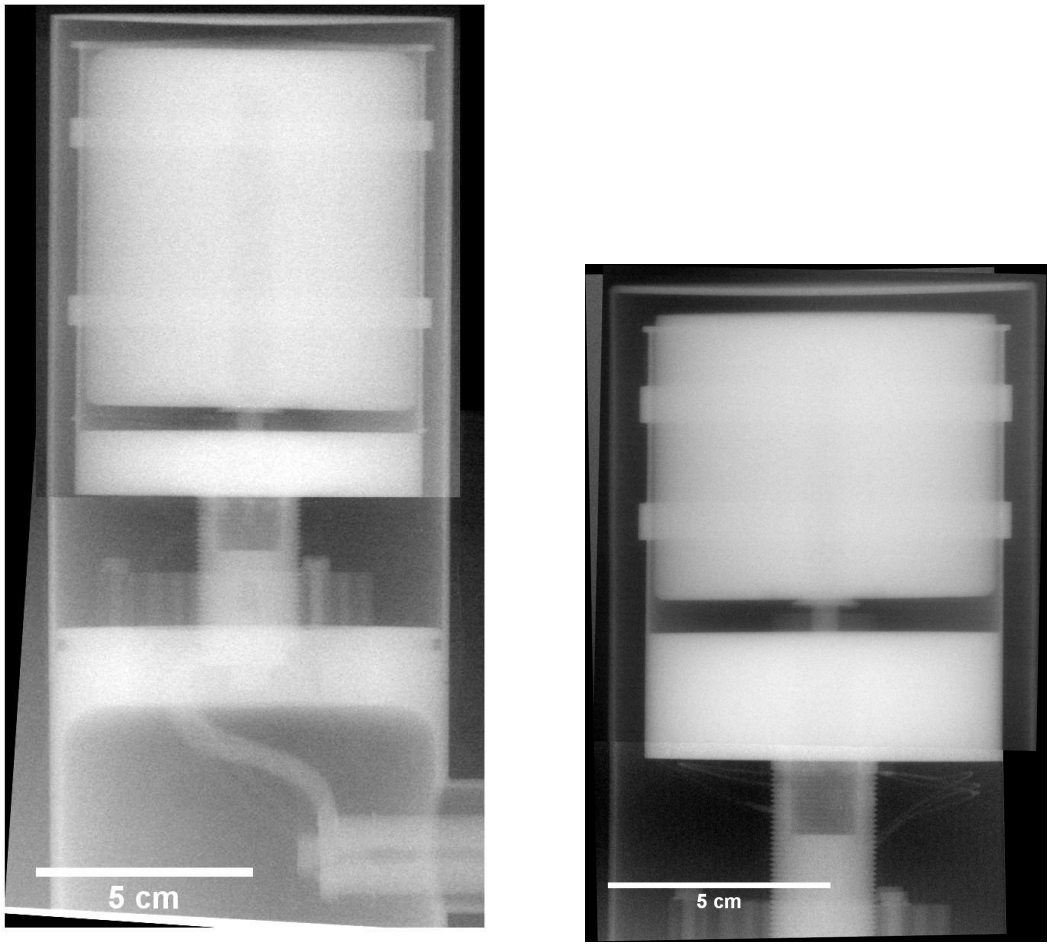

Figure **A.1**: Radiographs of Ge-6 to the left (diameter 7.80 cm, thickness 8.40 cm) and Ge-7 to the right (diameter 8.05 cm and thickness 6.65 cm).

B Other publications by the author

The search for the decay of nature's rarest primordial isotope, Ta-180m. M. Hult, J. Gasparro G. Marissens, U. Wätjen, P.N. Johnston, W. Preuβe, C. Wagemans, P. Lindahl, **E. Wieslander**. EC-JRC-IRMM GE/R/IM/22/06 (2006).

Calibration of detector T4 in Lab-8. **E. Wieslander**. EC-JRC-IRMM GE/R/IM/10/06 (2006).

Validation of detector T4 in Lab-8 with NPL samples. **E. Wieslander**. EC-JRC-IRMM GE/R/IM/11/06 (2006).

DONA detector: Further improvements and evaluation for field applications. G. Lövestam, A. Fessler, J. Gasparro, M. Hult, P. Kockerols, G. Marissens, K. Okkinga, **J.S.E. Wieslander**. JRC Scientific and Technical Reports EUR 23305, EN - 2007, ISBN 978-92-79-08813-1, ISSN1018-5593.

MeV ion losses measurements in JET using activation technique. G.Bonheure, **E. Wieslander**, M. Hult, J. Gasparro, G. Marissens, D. Arnold, M. Laubenstein, S. Popovichev, A. Murari and JET-EFDA contributors. 34th European Physical Society Conference on Plasma Physics, Warsaw, Poland, P5.095 (2007).

Fast neutron environmental spectrometry using disk activation G. Lövestam, M. Hult, J. Gasparro, H. Tagziria, F. Vanhavere, **J.S.E. Wieslander**. Conference Proceedings ISRD 13, The Netherlands (2008).

In-vessel Activation Monitors in JET: progress in modelling. G. Bonheure, I. Lengar, B. Syme, **E. Wieslander**, M. Hult, J. Gasparro, G. Marissens, D. Arnold, M. Laubenstein, S. Popovichev. Proceedings of 17th Topical conference on High-Temperature Plasmas Diagnostics, Albuquerque, USA. Review of Scientific Instruments 79 (2008) E504-1.

Bibliography

[Adam93] J.M. Adams, O.N. Jarvis, G.J. Sadler, D.B. Syme and N. Watkins, Nucl. Instr. Meth. A **329**, 277-290 (1993). The JET neturon emission profile monitor.

[Agos03] S. Agostinelli et al., Nucl. Instr. Meth. A **506**, 250-303 (2003). $G_{EANT}4$ a simulation toolkit.

[Ales91] A. Alessandrello, C. Cattadori, G. Fiorentini, E. Fiorini, G. Gervasio, G. Heusser, G. Mezzorani, E. Pernicka, P. Quarati, D. Salvi, P. Sverzellati and L. Zanottic. Nucl. Instr. Meth. B **61**, 106-117 (1991). Measurements on radioactivity of ancient roman lead to be used as shield in searches for rare events

[Alli06] J. Allison et al., IEEE Transactions on Nuclear Science **53**, 270-278 (2006). Geant4 developments and applications.

[Arno03] D. Arnold, O. Sima, App. Rad. Isot. **60**, 167-172 (2003). Application of GESPECOR software for the calculation of coincidence summing effects in special cases.

[Arpe96] S. Arpesella, App. Rad. Isot. **47**, 991-996 (1996). A low background counting facility at laboratori nazionali del Gran Sasso.

[Brod90] R.L. Brodzinski, H.S. Miley, J.H. Reeves, F.T. Avignone III, Nucl. Inst. Meth. A **292**, 337-342 (1990). Further reduction of radioactive backgrounds in ultrasensitive germanium spectrometers.

[Canb] Canberra reference **2**, Low Level Gamma Spectroscopy.

[Canb6] http://www.canberra.com/products/486.asp

[Canb7] http://www.canberra.com/products/496.asp

[Canbw] http://www.canberra.com/be/

[Catt05] C.M. Cattadori, M. De Deo, M. Laubenstein, L. Pandola and V.I. Tretyak, Nucl. Phys. A **748**, 333-347 (2005). Observation of β decay of ^{115}In to the first excited level of ^{115}Sn.

[DDEP] http://www.nucleide.org/DDEP_WG/DDEPdata.htm

[Enqv05] T. Enqvist, , A. Mattila, V. Föhr, T. Jämsen, M. Lehtola, J. Narkilahti, J. Joutsenvaara, S. Nurmenniemi, J. Peltoniemi, H. Remes, J. Sarkamo, C. Shen, I. Usoskin, Nucl. Instr. Meth. A **554** 286-290 (2005). Measurements of muon flux in the Pyhäsalmi underground laboratory.

[Ellm02] C. Ellmark. Thesis at Lund University / IRMM internal report (2002). Installation and calibration of a HPGe-detector in an ultra low-level background environment.

[Frec62] D.V. Freck, J. Wakefield, Nature **4816**, 669 (1962, February 17). Gamma-Ray Spectrum obtained with a Lithium-drifted p-i-n Junction in Germanium.

[Gahl] http://www.vongahlen.nl/

[Gasp04] J. Gasparro, M. Hult, K. Komura, D. Arnold, L. Holmes, P.N. Johnston, M. Laubenstein, S. Neumaier, J.-L. Reyss, P. Schillebeeckx, H. Tagziria, G. Van Britsom, R. Vasselli, J. Env. Radioactivity. **73**, 307-321(2004). Measurements of ^{60}Co in spoons activated by neutrons during the JCO criticality accident at Tokai-mura in 1999.

[Gasp08] J. Gasparro, M. Hult, P.N. Johnston, H. Tagziria, Nucl. Inst. Meth. Phys. A **594**, 196-201 (2008). Monte Carlo modelling of germanium crystals that are tilted and have rounded front edges.

[GERDA] http://www.mpi-hd.mpg.de/gerda/

[GERDA06] S. Schönert, I. Abt, M. Altmann, A.M. Bakalyarov, I. Barabanov, C. Bauer, M. Bauer, E. Bellotti, S. Belogurov,S.T. Belyaev, A. Bettini, L. Bezrukov, V. Brudanin, V.P. Bolotsky, A. Caldwell, C. Cattadori, M.V. Chirchenko, O. Chkvorets, E. Demidova, A. Di Vacri, J. Eberth, V. Egorov, E. Farnea, A. Gangapshev, J. Gasparro, P. Grabmayr, G.Y. Grigoriev, V. Gurentsov, K. Gusev, W. Hampel, G. Heusser, M. Heisel, W. Hofmann, M. Hult, L.V. Inzhechik, J. Jochum, M. Junker, S. Katulina, J. Kiko, I.V. Kirpichnikov, A. Klimenko, M. Knapp, K.T. Knopfle, O. Kochetov, V.N. Kornoukhov, K. Kroninger, V.V. Kuzminov, M. Laubenstein, V.I. Lebedev, X. Liu, B. Majorovits, G. Marissens, I. Nemchenok, L. Pandola, P. Peiffer, A. Pullia, C.R. Alvarez, V. Sandukovsky, S. Scholl, J. Schreiner, U. Schwan, B. Schwingenheuer, H. Simgen, A. Smolnikov, F. Stelzer, A.V. Tikhomirov, C. Tomei, C.A. Ur, A.A. Vasenko, S. Vasiliev, D. WeiBhaar, M. Wojcik, E. Yanovich, J. Yurkowski, S.V. Zhukov, F. Zocca, and G. Zuzel. Phys. Atom. Nucl. **69**, 2101 (2006). Status of the Germanium detector array (GERDA) in the search of neutrinoless $\beta\beta$ decays of ^{76}Ge at LNGS.

[Grei01] Peter K. F. Greider, Cosmic rays at earth : researcher's reference manual and data book, 1st edition, Elsevier Science B.V., The Netherlands (2001).

[Groo01] D.E. Groom, N.V. Mokhov, S. Striganov, Atomic Data and Nuclear Data tables **76**(No 2), LBNL-44742 (2001). http://pdg.lbl.gov/AtomicNuclearProperties/adndt.pdf. Muon stopping power and range tables 10 MeV - 100 TeV.

[Heus95] G. Heusser, Annu. Rev. Nucl. Part. Sci. **45**, 543-90 (1995). Low-radioactivity background techniques.

[Heus06] G. Heusser, M. Laubenstein, H. Neder, International coneference on isotopes and environmental studies, 8 - Aquatic Forum 2004, ed. P. Povinec and J.A. Sanchez-Cabeza (Elsevier, Amsterdam) (2006).

[Hult00] M. Hult, M. J. Martinez Canet, M. Köhler, J. das Neves, P.N. Johnston, Appl. Rad. Isot. bf 53, 225-229 (2000).

[Hult04] M. Hult, J. Gasparro, R. Vasselli, K. Shizuma, M. Hoshi, D. Arnold, S. Neumaier, Appl. Radiat. Isot. **61**, 173-177 (2004). Deep underground measurments of ^{60}Co in steel exposed to the Hiroshima atomic bomb explosion.

[Hult06] M. Hult, W. Preuβe, J. Gasparro, M. Köhler, Acta Chim. Slov. **53**, 1-7 (2006). Underground Gamma-Ray Spectrometry.

[Hult07] M. Hult, Metrologia **44**(4), S87-S94 (2007). (Erratum Metrologia **44**(5), 435 (2007). Low-level gamma-ray spectrometry using Ge-detectors.

[Hult08] M. Hult, J. Gasparro, P. Lindahl, G. Marissens, A. Fessler, Peter N. Johnston, Appl. Rad. Isot. **66**, 829-834 (2008). On the use of mercury as a means of locating background sources in ultra low-background HPGe-detector systems.

[Infn] The particle data group, http://pdg.ge.infn.it/2007/AtomicNuclearProperties/substances/216.html (2007). Atomic and nuclear properties of materials: Polyvinyltoluene.

[ISO95] ISO/IEC/OIML/BIPM, Guide to the Expression of Uncertainty in Measurement, 1st corrected edition, International Organization for Standardization, Geneva, Switzerland (1995).

[ISO00] ISO 11929-3, Determination of the detection limit and decision threshold for ionising radiation radiation measurements - Part 3, 1st edition, International Organization for Standardization, Geneva, Switzerland (2000).

[John06] P.N. Johnston, M. Hult, J. Gasparro, App. Rad. Isot. **64**, 1323-1328 (2006). Cascade summing effects in close geometry gamma-ray spectrometry.

[Knoll00] Glenn F. Knoll, Radiation Detection and Measurement, 3rd edition, John Wiley and Sons Inc. USA, (2000).

[Laub04] M. Laubenstein, M. Hult, J. Gasparro, D. Arnold, S. Neumaier, G. Heusser, M. Köhler, P. Povinec, J.-L. Reyss, M. Schwaiger, P. Theodorsson, App. Rad. Isot. **61**, 167-172 (2004). Underground measurements of radioactivity.

[Laub09] M. Laubenstein, G. Heusser, App. Rad. Isot. *accepted* (2009). Cosmogenic radionuclides in metals as indicator for sea level exposure.

[Leo87] W.R. Leo, Techniques for Nuclear and Particle Physics Experiments, A How-to Approach, 2nd edition, Springer-Verlag, Germany (1987).

[Lill01] John Lilley, Nuclear Physics, Principles and Applications, John Wiley and Sons Ltd. England, (2001).

[Majo] http://majorana.pnl.gov/

[Majo05] C. E. Aalseth, D. Anderson, R. Arthur, F.T. Avignone III, C. Baktash, T. Ball, A. S. Barabash, F. Bertrand, R. L. Brodzinski, V. Brudanin, W. Bugg, A. E. Champagne, Y-D. Chan, T. V. Cianciolo, J. I. Collar, R. W. Creswick, M. Descovich, M. Di Marco, P. J. Doe, G. Dunham, Yu. Efremenko, V. Egerov, H. Ejiri, S. R. Elliott, A. Emanuel, P. Fallon, H. A. Farach, R. J. Gaitskell, V. Gehman, R. Grzywacz, A. Hallin, R. Hazma, R. Henning, A. Hime, T. Hossbach, D. Jordan, K. Kazkaz, J. Kephart, G. S. King III, O. Kochetov, S. Konovalov, R. T. Kouzes, K. T. Lesko, P. Luke, M. Luzum, A. O. Macchiavelli, A. McDonald, D. Mei, H. S. Miley, G. B. Mills, A. Mokhtarani, M. Nomachi, J. L. Orrell, J. M. Palms, A. W. P. Poon, D. C. Radford, J. H. Reeves, R. G. H. Robertson, R. Runkle, K. Rykaczewski, K. Saburov, Y. Sandukovsky, A. Sonnenschein, W. Tornow, C. Tull, R. G. van de Water, I. Vanushin, K. Vetter, R. A. Warner, J. F. Wilkerson, J. M. Wouters, A. R. Young, and V. Yumatov. Nucl. Phys. B (Proc. Suppl.) **138**, 217-220 (2005). The proposed Majorana ^{76}Ge double-beta decay experiment.

[Mile91] H.S. Miley, R.L. Brodzinski, J.H. Reeves, J. Radioanalytical and Nuclear Chemistry **160**(No 2), 371-385 (1991).

[Mile09] H.S. Miley, C.E. Aalseth, T.W. Bowyer, J.E. Fast, J.C. Hayes, E.W. Hoppe, T.W. Hossbach, M.E. Keillor, J.D. Kephart, J.I. McIntyre, A. Seifert, Appl. Rad. Isot. *accepted* (2009).

[Nels85] W.R. Nelson, H. Hirayama, D.W.O. Rogers, The EGS4 code system, SLAC Report (1985).

[Neum00] S. Neumaier, D. Arnold, J. Böhm, E. Funck, App. Rad. Isot. **53**, 173-178 (2000). The PTB underground laboratory for dosimetry and spectrometry.

[Nies98] S. Niese, M Köhler, B. Gleisberg, J. Radioanalytical and Nuclear Chemistry **233**(No 1-2), 167-172 (1998). Low-level counting techniques in the underground laboratory "Felsenkeller" in Dresden.

[Plom] http://plombum.republika.pl/

[Sck] www.sckcen.be: the Belgian nuclear research centre SCK•CEN (studiecentrum voor kernenergie • centre d'étude de l'énergie nucléaire).

[Sima01] O. Sima, D. Arnold, C. Dovlete, J. Radioanalytical and Nuclear Chemistry **248**(No 2), 359-364 (2001). GESPECOR: A versatile tool in gamma-ray spectrometry.

[Theo97] P. Theodorsson, Measurement of weak radioactivity (1997). World Scientific Publishing Co Pte Ltd.

[Vidm08] T. Vidmar, I. Aubineau-Laniece, M.J. Anagnostakis, D. Arnold, R. Brettner-Messler, D. Budjas, M. Capogni, M.S. Diash, L-E. De Geer, A. Fazio, J. Gasparro, M. Hult, S. Hurtado, M. Jurado Vargas, M. Laubenstein, K.B. Lee, Y-K. Lee, M-C. Lepy, F-J. Maringer, V. Medina Peyres, M. Mille, M. Moralles, S. Nour, R. Plenteda, M.P. Rubio Montero, O. Sima, C. Tomei, G. Vidmar, App. Rad. Isot. **66**, 764-768 (2008). An intercomparison of Monte Carlo codes used in gamma-ray spectrometry.

[Ways99] G. Waysand, D. Bloyet, J.P. Bongiraud, J.I. Collar, D. Dolabdjian, Ph. Le Thiec, Nucl. Inst. Meth. Phys. A **444**, 336-339 (2000). First characterization of the ultra-shielded chamber in the low-noise underground laboratory (LSBB) of Rustrel-Pays d'Apt.

Paper I

This article **was published** in Nuclear Instruments and Methods A, volume 591, 383-393.

Available online at www.sciencedirect.com
ScienceDirect
Nuclear Instruments and Methods in Physics Research A 591 (2008) 383–393
NUCLEAR INSTRUMENTS & METHODS IN PHYSICS RESEARCH Section A
www.elsevier.com/locate/nima

Low-level gamma-ray spectrometry for analysing fusion plasma conditions

J.S. Elisabeth Wieslander[a,f], Mikael Hult[a,*], Georges Bonheure[b], Dirk Arnold[c], Harald Dombrowski[c], Joël Gasparro[a], Matthias Laubenstein[d], Gerd Marissens[a], Peter Vermaercke[e]

[a]*EU Commission – JRC – IRMM, Institute for Reference Materials and Measurements, Retieseweg 111, B-2440 Geel, Belgium*
[b]*Laboratory for Plasma Physics, Association "Euratom-Belgian State", Royal Military Academy, Avenue de la Renaissance, 30 Kunstherlevinglaan, B-1000 Brussels, Belgium*
[c]*Physikalisch-Technische Bundesanstalt, Bundesallee 100, D-38116 Braunschweig, Germany*
[d]*Laboratori Nazionali del Gran Sasso, S.S. 17/bis, km 18+910, I-67010 Assergi (AQ), Italy*
[e]*SCK•CEN, Boeretang, B-2400 Mol, Belgium*
[f]*Department of Physics, P.O. Box 35 (YFL), FIN-40014 University of Jyväskylä, Finland*

Received 19 November 2007; received in revised form 25 January 2008; accepted 13 February 2008
Available online 4 March 2008

Abstract

A new method, combining activation by neutrons and charged particles with ultra low-level gamma-ray spectrometry, aimed at obtaining a better understanding and more adequate measurements of MeV particle leaks in magnetic fusion devices was studied here. A total of 36 samples containing Ti, LiF, B_4C and W were placed in a boron-nitride holder mounted on the ceiling of the JET Tokamak. The samples were activated by 63 pulses from a D–^{3}He plasma and were later measured using underground gamma-ray spectrometry. The radionuclides ^{7}Be, ^{46}Sc, ^{54}Mn, ^{56}Co, ^{57}Co, ^{58}Co, ^{124}Sb, ^{181}Hf, ^{182}Ta, ^{181}W and ^{185}W were detected in several of the samples, with very low levels of activity of ^{47}Sc and ^{48}V found in a few of the samples. The various production channels for the radionuclides in question are discussed.

PACS: 52.55.Fa; 52.70.Nc; 29.30.Kv; 29.40.Wk

Keywords: Ultra low-level gamma-ray spectrometry; Thermonuclear fusion; Underground laboratory; Charged particles; Activation

1. Introduction

Efforts to improve the confinement of a fusion plasma are usually aided by measurements of charged particle and neutron emission as close to the plasma as possible. Neutron emission is presently being studied at Joint European Torus (JET) using several neutron flux monitors and large neutron spectrometers located outside the vacuum chamber [1,2]. Until recently there was no way of measuring the emission of charged particles inside the Tokamak directly [3]. In 2004 a study of a ^{4}He plasma in which the concentration of residual D was raised to 50% was conducted at JET using an activation technique to investigate the flux of neutrons and charged particles inside the Tokamak [4,5]. A boron-nitride (BN) sample holder containing 18 small samples ($1 \times 1\,cm^2$) of three types, Ti, MgF_2 and TiVAl, was placed in one of the experimental ports in the vacuum chamber and irradiated by 49 plasma pulses. Many of the radionuclides produced had a very low level of activity due to (i) the small size of the samples, (ii) the small cross-section of some of the reactions, (iii) the low isotopic abundance of certain of the target isotopes and (iv) the limited time the samples were exposed to the plasma. In order to quantify these radionuclides, ultra

*Corresponding author. Tel.: +32 14 571 269; fax: +32 14 584 273.
E-mail addresses: elisabeth.wieslander@gmail.com (J.S.E. Wieslander), mikael.hult@ec.europa.eu (M. Hult).

0168-9002/$ - see front matter © 2008 Elsevier B.V. All rights reserved.
doi:10.1016/j.nima.2008.02.052

low-level gamma-ray spectrometry (ULGS) was carried out in an underground laboratory [4].

A similar approach is used in the experiment described here, aimed at measuring the emission of neutrons and charged particles inside the Tokamak. Compared with previous measurements, the main differences are that in the present experiment a D–^{3}He plasma with a ^{3}He concentration of 8–20% was studied and the sample holder held 36 samples of the different materials Ti, LiF, B_4C and W. The samples were irradiated with 63 plasma pulses. Because of the greater number of samples and the time it would take to measure them successively, the measurements were carried out simultaneously in three underground laboratories, using a total of six ultra low-background HPGe-detectors.

2. Materials and methods

2.1. Sample materials and holder

The activation samples were mounted on a 10 cm long probe with a hexagonal cross-section (see Fig. 1). The probe was fixed to the ceiling of the JET vacuum chamber at experimental point 1, as shown in Fig. 2. The probe was made of BN since experience has shown that this material is well suited to the harsh environment inside the JET Tokamak [4,5]. The extreme conditions in the JET vacuum chamber place severe restrictions on the materials that can be used for the experiments. A material must be neither fragile nor brittle, and able to withstand a strong magnetic field and temperatures as high as 300 °C.

There were 12 samples of titanium (Ti), 12 samples of boron carbide (B_4C), six samples of lithium fluoride (LiF) and six samples of tungsten (W) used in the experiment (see Table 1). Each sample was of natural isotopic composition, meaning that in total the samples contained 17 different

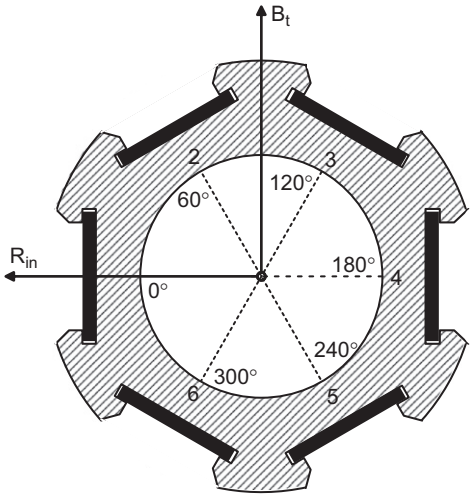

Fig. 1. A horizontal cross-section of the boron-nitride probe in which all the samples were held. B_t is the standard direction of the toroidal magnetic field and R_{in} is the direction along the major radius of the Tokamak and pointing radially inward. The numbers indicate the six sample positions.

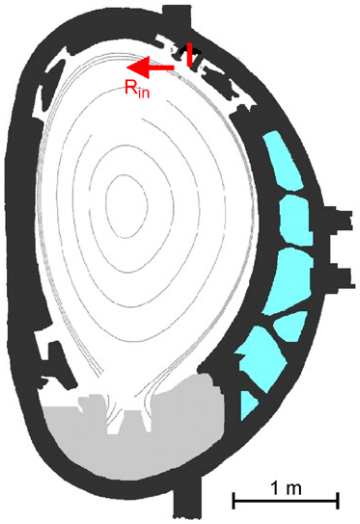

Fig. 2. A schematic drawing of the boron-nitride probe attached to the ceiling of the JET Tokamak.

Table 1
Details of the samples contained in the test probe, listed in the same vertical order as when they are mounted in the sample holder

Material	No. of samples	Name	Exposed area (cm^2)	Mass (g)
Ti	6	TiTop1–6	3.52	1.90
W	6	W1–6	0.825	1.95
B_4C	6	B_4C7–12	0.825	0.26
LiF	6	LiF1–6	0.825	0.33
B_4C	6	B_4C1–6	0.825	0.26
Ti	6	Ti1–6	0.680	0.39

naturally occurring isotopes of titanium, lithium, boron, carbon, fluorine and tungsten (see Table 2). One non-irradiated sample of each type was analysed at StudieCentrum voor Kernenergie•Centre d'Etude de l'energie Nucleaire (SCK•CEN) in Mol, Belgium [6], by means of k_0-neutron activation analysis (k_0-NAA). This analysis procedure showed that there were relatively high concentrations of certain impurities in some of the samples (see Table 3). All the samples in one series were from the same batch, so it was assumed that their impurity levels would be approximately the same.

Each sample was 1 mm thick and had a surface area of 1×1 cm^2, except for the 12 Ti samples which had different surface dimensions. As shown in Fig. 3, the Ti samples located in the lower portion of the sample holder were rounded at the lower end, whereas the Ti samples at the top were each approximately 44 mm long, some of them with a hole in them in which a stainless steel screw was affixed. The materials were placed in the positions indicated in Figs. 1 and 2. The samples were placed in their slots by sliding them along the holder. Consequently, a portion of the sample about 8.25 mm in width was uncovered, whereas the remainder of the width was covered by the edges of the slot. The angled edges (see Fig. 1) were 1–2 mm

Table 2
The relative isotopic abundance of the stable isotopes contained in the samples used in the experiment

Isotope	Relative abundance (%)
^{6}Li	7.59
^{7}Li	92.41
^{10}B	19.9
^{11}B	80.1
^{12}C	98.93
^{13}C	1.07
^{19}F	100
^{46}Ti	8.25
^{47}Ti	7.44
^{48}Ti	73.7
^{49}Ti	5.5
^{50}Ti	5.2
^{180}W	0.12
^{182}W	26.5
^{183}W	14.3
^{184}W	30.6
^{186}W	28.4

Table 3
Trace element concentrations in μg/g as measured using k_0-neutron activation analysis (k_0-NAA)

Impurity	Ti	W	LiF	B_4C
Cr	146 (6)	0.53 (10)	<0.3	10 (3)
Fe	734 (35)	5.33 (8)	27 (10)	600 (180)
Co	0.71 (4)	0.019 (3)	<0.05	0.23 (7)
Ni	135 (14)	<10	<15	<100
Sb	9.9 (4)	<0.004	0.011 (5)	<0.015

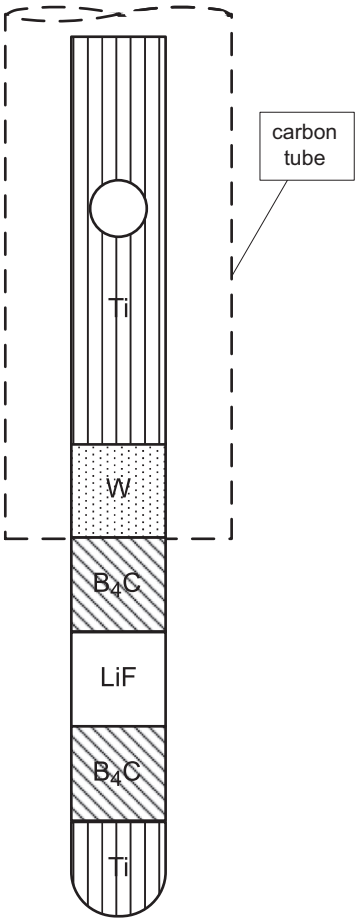

Fig. 3. The vertical arrangement of the samples in one slot of the boron-nitride probe. The carbon tube that shielded a part of the probe is also indicated.

thick and thus could not completely stop the neutrons, high-energy protons or deuterons.

Fig. 2 shows the direction of sample 1 (the normal vector to the surface of sample 1) perpendicular to the toroidal field (B_t) and pointed inwards along the major radius (R_{in}) of the Tokamak. The activation samples were placed in the six slots of the probe. There was a 60° angle between any two adjacent slots, which meant that each slot had a different orientation with respect to the magnetic field. The six slots of the probe contained six samples each, resulting in a total of 36 samples. Two of the sample series were numbered from 1 to 6: LiF1–6 and W1–6. The B_4C samples were numbered from 1 to 12 (B_4C1–12). The titanium samples at the bottom of the probe were labelled Ti1–6, and the larger samples closest to the ceiling were labelled TiTop1–6 (see Fig. 3). For each of the samples, the number indicates the slot. The B_4C samples numbered 1–6 were located second from the bottom in the holder, whereas those numbered 7–12 were located third from the top, with samples numbers 1 and 7 in the same slot (see Fig. 3).

As indicated in Fig. 3 the upper part of the sample holder was covered by a carbon tube, which shielded the TiTop and W samples from the plasma to some extent.

Before the samples left JET for transport to the Institute for Reference Materials and Measurements (IRMM), smear tests taken from them were analysed in order to rule out tritium contamination. At IRMM, the samples were cleaned by immersing them in isopropanol for 10 min. After cleaning, 23 of the samples were dispatched to the other two underground laboratories, while 13 of them were kept at IRMM for measurements.

2.2. The plasma

Activation took place between 15 and 18 May 2006, and the total neutron fluence was approximately 62 times higher than in the previous experiment [4,5]. The total number of neutrons produced during the experiment as a whole was $(5.1 \pm 0.5) \times 10^{17}$, with 10^{12} of the neutrons estimated to reach the sample probe. The main reactions that occurred in this thermonuclear plasma were the following:

$$D + {}^{3}He \rightarrow p(14.7\,MeV) + \alpha(3.7\,MeV)$$
$$D + D \rightarrow p(3.0\,MeV) + T(1.0\,MeV)$$
$$D + D \rightarrow n(2.5\,MeV) + {}^{3}He(0.8\,MeV)$$
$$D + T \rightarrow n(14.1\,MeV) + \alpha(3.6\,MeV)$$

Since the fuel was D–^{3}He, the first three of these — the D–^{3}He reaction and the two D–D reactions — were the dominating production channels. Most of the T produced in either of the D–D reactions remained confined to the plasma and reacted with D to produce 14.1 MeV neutrons. Measurements made by the 14 MeV neutron yield monitor [1] showed that approximately 1% of the total neutron emission originated from the D–T reaction.

The sample holder was inserted into the JET Tokamak vacuum chamber near the edge of the plasma at a position 1790 mm above the mid-plane of the Tokamak. The samples were exposed for 4 days and were irradiated by 63 JET plasma pulses in total. Further exposure was planned but was not carried out because of difficulties connected with the plasma operation. The sample holder was removed from the Tokamak after a cooling period of 20 days, and a preliminary gamma-ray spectrometry analysis of the sample holder assembly in its entirety was then performed at JET.

2.3. Gamma-ray measurements conducted in underground laboratories

In order to achieve low detection limits, the samples were measured underground in ULGS laboratories in which the background stemming from cosmic-ray induced reactions was low [7]. The main drawback of ULGS measurements is the long measurement time required when radionuclide activity in the order of mBq is to be detected. To speed up the measurement process, the ULGS measurements were performed simultaneously by three institutes within the Collaboration of European Low-level underground LaboRatories (CELLAR) network, namely IRMM, Physikalisch-Technische Bundesanstalt (PTB) and Laboratori Nazionali del Gran Sasso (LNGS). Various characteristics of the three underground laboratories and of the detectors are presented below and additional information is provided in Table 4.

IRMM operates seven HPGe-detectors in the underground laboratory HADES, located 225 m underground in the middle of a 100 m thick clay layer, corresponding to a 500 m water equivalent. It is operated by European Underground Research Infrastructure for Disposal of nuclear waste In Clay Environment (EURIDICE) and located at the Belgian nuclear centre SCK•CEN [7–9]. The detectors are shielded by a layer of 15 cm of low-background lead and lined with a 3–10 cm layer of electrolytic copper.

PTB operates two HPGe-detectors in the underground laboratory UDO, located at a depth of 490 m in the ASSE salt mine near Braunschweig, Germany [10]. The two HPGe-detectors are shielded by a 15–20 cm layer of low-background lead lined with a 1 cm and a 10 cm layer of electrolytic copper respectively.

LNGS is located in central Italy alongside the Gran Sasso highway tunnel connecting Teramo and Rome, about 6 km from the west entrance, near the small village of Assergi. The underground laboratories are located 963 m above sea level and have a maximum rock overburden of 1400 m, corresponding to a 3800 m water equivalent [11,12]. The facility operates 12 HPGe-detectors, shielded by a 20–25 cm layer of low-background lead and a 5 cm layer of electrolytic copper.

As Table 4 indicates, six detectors were employed, providing a separate detector for each sample series except for sample LiF-1. Such an approach minimised uncertainties concerning the shape of the graphs describing the angular distribution of activity within a given sample series. Each sample was measured for a week. The radionuclides ^{48}V and ^{47}Sc, which have short half-lives, had thus decayed significantly by the time the last measurements were taken.

The methods of calculating the full energy peak efficiencies (FEP) using Monte Carlo techniques were similar in each of the laboratories, although the computer codes employed differed: EGS4 (at IRMM) [13], GEANT4 (at LNGS) [14,15] and GESPECOR (at PTB) [16]. The codes included models of the detector, cryostat, crystal-holder, shield and the samples. The computer models of the detectors were optimised by comparing the measured and the calculated efficiencies of the reference sources and varying the dead-layer thicknesses (at the front, side and back) iteratively until there was a match within the uncertainty of the reference sources.

Obtaining exact geometric measurements required the use of careful coincidence summing corrections. The

Table 4
Selected characteristics of the three underground laboratories and the six HPGe-detectors used for the measurements

Institute	IRMM		PTB		INFN-LNGS	
Laboratory	HADES		ASSE/UDO		Gran Sasso	
Depth (m.w.e.)	500		1100		3800	
Detector relative efficiency (%)	60	50	88 (a)	94 (b)	113	120
Crystal configuration	Coaxial	Planar	Coaxial	Coaxial	Coaxial	Coaxial
Front deadlayer thickness	0.7 mm	0.3 μm	0.3 μm	0.3 μm	0.3 mm	0.5 mm
Radon removal	Flushing with boil-off LN2 + minimising empty space.		(a) Flushing with boil-off LN2. (b) Flushing with boil-off LN2 + air-lock.		Flushing with boil-off LN2 + sealed PMMA housing.	

PMMA is polymethyl methacrylate and LN2 is liquid nitrogen.

computer codes included the complete decay schemes for the coincidence summing calculations, obtained from the DDEP website [17] and the Table of Radioactive Isotopes website (LNGS) [18]. The distribution of radionuclides in the samples is not evident. As in the previous study (see Fig. 2 in Ref. [4]), the gamma-ray efficiency was determined as a function of the range of the distribution of the radionuclide in question. For the proton- and deuteron-induced reactions, the additional systematic uncertainty of the range distribution was limited to 1–2%.

3. Results

The analysis of the measurements is very complex, taking into account many aspects of the experiment set-up, the production channels for the radionuclides and their properties. The radionuclides were produced in various ways; some were produced by neutrons and others by protons or deuterons, while the contribution of photo-nuclear reactions here was assumed to be very small. The range of such charged particles as protons and deuterons in the samples depended on the energy they possessed, whereas the samples were basically transparent for neutrons. The high-energy neutrons could be moderated slightly by the mass of the BN sample holder, which would explain the small angular dependence observed for the high-energy neutron reactions. There was no visible angular dependence in the case of low-energy reactions with neutrons. This could be explained in terms of scattered neutrons hitting the sample probe from all possible directions.

In order to avoid any assumptions regarding the distribution of radionuclides in the samples, all the results are presented in terms of mBq per sample instead of massic or surface activities.

All the major data, including the uncertainties, are listed in Table 7. The measured values are shown in Figs. 4–6. The data points without uncertainty bars or connections represent decision thresholds used as upper limits in the analysis of the neutron and charged particle activation of the samples.

3.1. Uncertainties, decision thresholds and reference date

Uncertainties in the activity measurements are expressed as combined standard uncertainties, following the *Guide to the* Expression *of Uncertainty in Measurement* [19]. The uncertainties are given in brackets after each measurement value presented, the last digit(s) corresponding to the last digit(s) of the quoted result (see Tables 5 and 7).

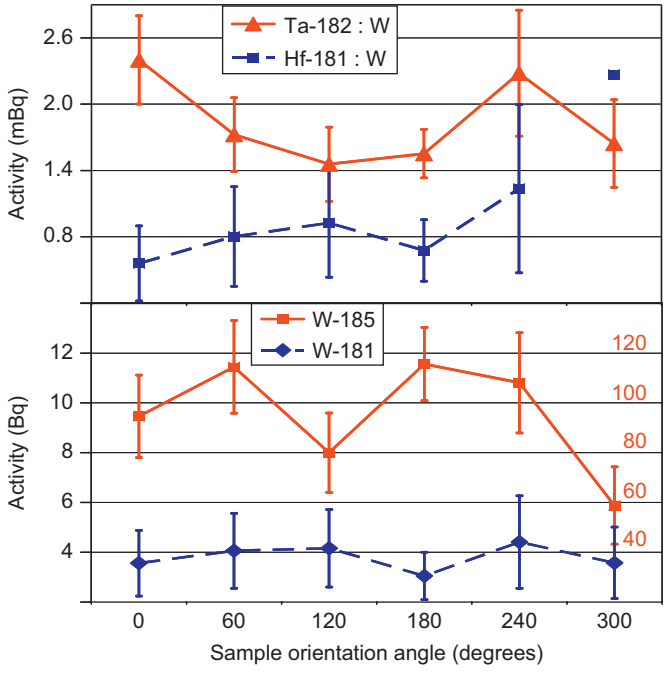

Fig. 4. The level of activity of ^{181}Hf, ^{182}Ta, ^{181}W and ^{185}W in mBq or Bq per sample as a function of the sample position, defined in Fig. 1, and measured in the W samples. The values without uncertainty bars and connections to other points are decision thresholds, i.e. upper limits. The scale to the right refers to ^{185}W.

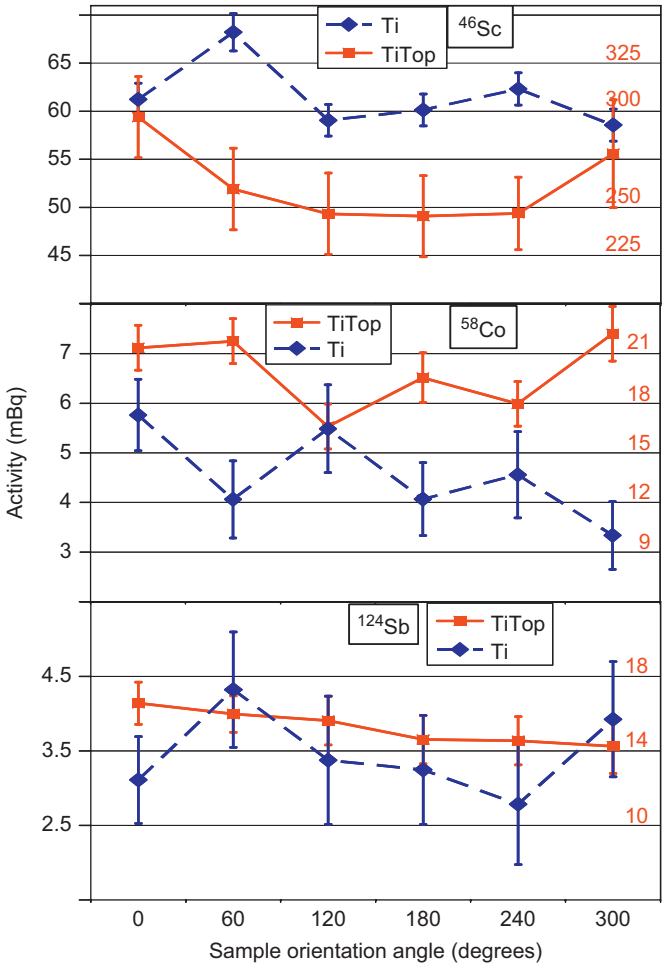

Fig. 5. The level of activity of ^{46}Sc, ^{58}Co and ^{124}Sb in mBq per sample as a function of the sample position, defined in Fig. 1, and measured in the Ti and TiTop samples. The scale to the right refers to TiTop.

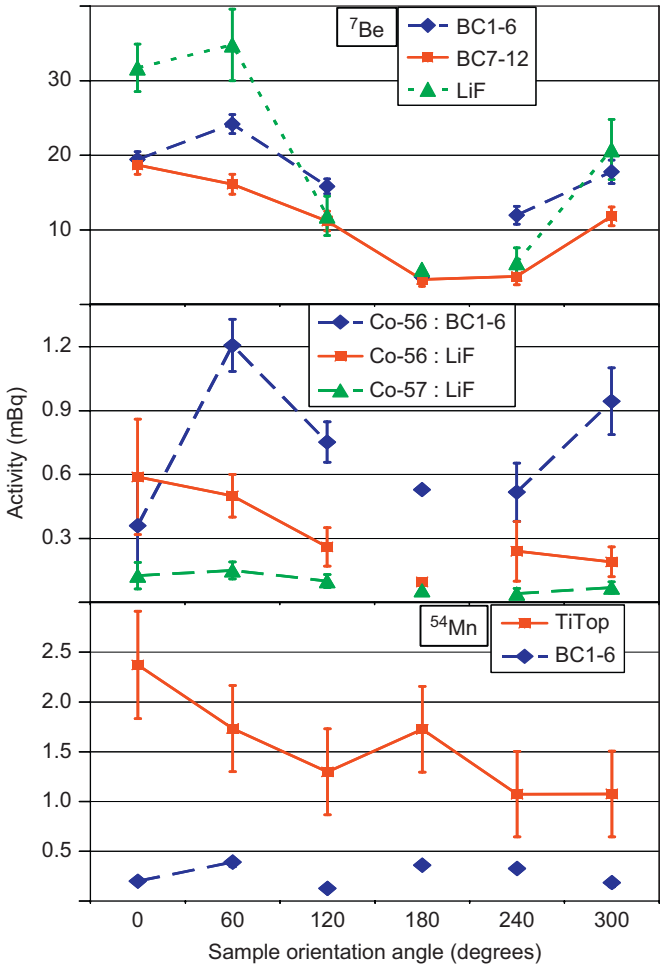

Fig. 6. The level of activity of ^{7}Be, ^{56,57}Co and ^{54}Mn in mBq per sample as a function of the sample position, defined in Fig. 1, and measured in the B_4C, LiF and TiTop samples. The values without uncertainty bars and connections to other points are decision thresholds, i.e. upper limits.

Table 5
Uncertainty budget for the activity of two different radionuclides detected in sample 2 of the W and B_4C sample series (in the 60° position)

Uncertainty contribution	Relative uncertainty contribution (%)	
	^{181}Hf	^{7}Be
Counting statistics	79	59
Gamma-ray emission probability	3.2	2.3
Correction for decay during cooling	0.3	1.7
Correction for decay during measurement	0	0.3
Efficiency—from counting statistics	0.2	0.7
Efficiency—from electron & photon transport	4.3	12.5
Efficiency—from geometry	6	12.5
Efficiency—precision of calibration sources	6	9.5
Efficiency—range distribution	1	1.5
Total	100	100

The major contribution to the uncertainty budget is made by the counting statistics. Other major contributions stem from the calculation of the gamma-ray efficiency, since the characterisation of the geometry involved creates uncertainties due to the short distance between the detector and the sample. Details of the uncertainty budget of two different samples are shown in Table 5.

All the results are compared with the decision threshold, using $\alpha = 0.01$ [20]. The reference date for each of the results is 18 May 2006, which is the day activation inside the JET Tokamak ceased.

3.2. Radionuclides detected

The 36 samples from JET consist of six series of six samples each. The following radionuclides were detected in at least 3 of the samples in a given series: ^{7}Be, ^{54}Mn, ^{46}Sc, ^{56}Co, ^{57}Co, ^{58}Co, ^{124}Sb, ^{181}Hf, ^{181}W, ^{182}Ta and ^{185}W (see Table 6 for an overview). Furthermore, very low levels of activity were found for ^{47}Sc and ^{48}V in some of the samples. Due to their short half-lives of 3.35 days (for ^{47}Sc) and 16 days (for ^{48}V), it was difficult to detect these since the shortest cooling time before any measurement could be made was 20 days.

Fig. 4 shows the level of activity as a function of sample position for the radionuclides detected in the W samples, whereas Fig. 5 shows the level of activity in the Ti and TiTop samples. Fig. 6 shows the level of activity as a function of sample position for the radionuclides detected in the B_4C and LiF samples, with the addition of the ^{54}Mn detected in the TiTop samples.

4. Production of the radionuclides detected

In general, a radionuclide can have several different production channels. Taking account of the production cross-sections (σ), the isotopic abundances (θ) and the materials the Tokamak vacuum chamber is made of allows the dominant production channels to be assessed. A discussion of the possible production channels for the different radionuclides follows. Five production channels were considered: (i) neutron activation of the bulk material of the sample, (ii) charged particle activation of the bulk materials, (iii) neutron activation of trace impurities in the samples, (iv) charged particle activation of trace impurities in the samples and (v) surface deposition of radionuclides sputtered from activated parts of the inner walls of the Tokamak or the sample holder. The possibility of photo-nuclear activation of the samples was ruled out due to the low yield. Contrary to the conclusions suggested in the previous study [3], no significant deposition of radio-nuclides sputtered from other parts of the Tokamak was found on the sample surfaces. In the present study, the same radionuclides were not found in all the samples. It could also be shown that certain radionuclides originated from the activation of impurities, which was not considered in the previous study.

Approximately 100 activation reactions were identified as representing possible production channels. These included activation reactions for the sample materials Ti,

Table 6
Overview of the six series of samples in which the various radionuclides were detected

Sample notation	^{7}Be	^{46}Sc	^{47}Sc	^{48}V	^{54}Mn	^{56}Co	^{57}Co	^{58}Co	^{124}Sb	^{181}Hf	^{182}Ta	^{181}W	^{185}W
TiTop1–6		X	O		X			X	X				
W1–6										X	X	X	X
B_4C7–12	X				O	O		O					
LiF1–6	X				O	X	X	O					
B_4C1–6	X				X	X		O					
Ti1–6	O[a]	X		O	O			X	X				
$t_{1/2}$ (days)	53	84	3.4	16	312	77	272	71	60	42	114	121	75
Suggested reactions	p,α p,n	d,α n,p	n,p n,np	p,n d,n	n,p d,α	d,2n p,n	d,n n,np α,p	n,2n n,p d,2p	n,γ	n,α	d,α n,p	n,2n	n,2n n,γ
$\theta\sigma$-product (a.u.)	76 508	30 22	5–9 3.7	1–11 5–10	43 6.5	204 34–106	<237 30 25	0.8 21–27 0.4–14	21	0.3	20 1.1	583	682 31
Threshold (MeV)	0.5 1.5	7.7 3	1 11	5 2	0.4 3.7	8 4.8	5 10 5.8	10.5 1 4.1	N	10	9 9.5	8	7.2 N

X: found in three to six of the samples in the series in question; O: found in one or two of the samples in the series. N: not a threshold reaction.
[a]Produced in the sample holder and deposited on the sample surface.

W, B_4C and LiF, and the impurities Fe, Cr, Co, Ni and Sb, found using the k_0-NAA (see Section 2.1). The product of the cross-section σ (b) (up to 14.7 MeV for protons and 14.1 MeV for neutrons, see Section 2.2) [21,22] and the isotopic abundance θ (%) for each of the target materials (see Tables 2 and 3) was calculated for all of the reactions listed and is henceforth referred to as the $\sigma\theta$-product. The reactions with the highest $\sigma\theta$-product values were studied more carefully and will be discussed below. It was suggested that stainless steel could possibly have influenced the results, since it could conceivably have been sputtered and deposited onto the samples after its activation in other parts of the Tokamak. This idea was later deemed improbable, in particular because the activation analysis (k_0-NAA) did show significant levels of Fe-impurities in the samples, which could explain the presence of some of the detected radionuclides.

4.1. ^{181}Hf, ^{181}W, ^{185}W and ^{182}Ta in the W samples

The most probable activation reaction for the ^{181}Hf found in the W samples is ^{184}W(n,α) ^{181}Hf, which has the highest $\theta\sigma$-product and a threshold of about 11 MeV. The modest variation in activity evident in Fig. 4a can be interpreted as a nearly constant activity level of about 0.8 mBq. Preliminary results from computer simulations [21] indicated that the variation can be explained by moderation of the neutrons while they pass through the sample holder.

There are several possible ways for ^{182}Ta to be produced in the W samples, such as ^{184}W(d,α)^{182}Ta, ^{182}W(n,p)^{182}Ta, ^{183}W(n,pn)^{182}Ta, ^{183}W(n,d)^{182}Ta and ^{183}W(γ,p)^{182}Ta. Since a carbon tube shielded the W samples, charged particle activation can be ruled out and the neutron reaction with highest $\sigma\theta$-product was ^{182}W(n,p)^{182}Ta. The angular distribution evident in Fig. 4a indicates a change in cross-section with the increase of energy as neutrons are moderated in passing through the sample holder to reach samples on the opposite side. The yield of ^{182}Ta is roughly twice that of ^{181}Hf, which also correlates with the preliminary results from computer simulations of the neutron activation of tungsten [21].

^{181}W and ^{185}W in Fig. 4b are mainly produced by ^{182}W(n,2n)^{181}W, ^{186}W(n,2n)^{185}W and ^{184}W(n,γ)^{185}W. The activity is in the order of Bq rather than mBq, since the reactions have high cross-sections over an extended energy range. The yield of the two radionuclides compares well with the preliminary computer simulations when neutron activation involving neutrons from the entire energy spectrum available is assumed.

4.2. ^{46}Sc, ^{47}Sc ^{48}V and ^{124}Sb in the Ti samples

^{46}Sc was detected in all of the Ti samples, i.e. all of the six samples at the bottom (Ti1–6) and the six larger ones at the top (TiTop1–6). The following reactions are possible: ^{46}Ti(n,p)^{46}Sc, ^{46}Ti(d,2p)^{46}Sc, ^{47}Ti(n,np)^{46}Sc, ^{47}Ti(n,d)^{46}Sc, ^{48}Ti(d,α)^{46}Sc, ^{48}Ti(d,nα)^{46}Sc and ^{48}Ti(p,α)^{46}Sc. Two reactions were similar in terms of the high $\theta\sigma$-product values, namely ^{48}Ti(d,α)^{46}Sc and ^{46}Ti(n,p)^{46}Sc. The activity distribution of ^{46}Sc in the TiTop samples (see Fig. 5a) is similar to that of ^{182}Ta in the W samples. This can be explained by assuming that both radionuclides were produced by neutrons. The long pathway inside the BN-holder to reach sample 4 (180°) after passing sample 1 (0°) results in lower activation of that particular sample because the neutron cross-section decreases at lower energy (Table 7). Moreover, the two sample series W and TiTop

Table 7a
The total activity level per sample (mBq) as a function of sample position

Radionuclide	^{7}Be (mBq)			^{46}Sc (mBq)		^{48}V (mBq)
Series	B_4C1–6	B_4C7–12	LiF	Ti	TiTop	Ti
0°	19.4 (1.0)	18.7 (1.2)	32 (3)	61.2 (1.7)	270 (4)	79 (12)
60°	24.2 (1.3)	16.1 (1.3)	35 (5)	68.2 (2.0)	260 (4)	47 (10)
120°	15.8 (1.0)	11.2 (1.3)	12 (3)	59.1 (1.7)	247 (4)	<199
180°	<3.7	3.3 (0.9)	<5	60.1 (1.7)	223 (4)	<98
240°	12.0 (1.2)	3.7 (1.1)	5.6 (2.0)	62.3 (1.7)	247 (4)	<224
300°	17.8 (1.6)	11.8 (1.3)	21 (4)	58.6 (1.7)	278 (6)	<124

The radionuclides are listed in the order of increasing mass.

Table 7b
The total activity level per sample (mBq) as a function of sample position

Radionuclide	^{54}Mn (mBq)		^{56}Co (mBq)		^{57}Co (mBq)	^{58}Co (mBq)	
Series	B_4C1–6	TiTop	B_4C1–6	LiF	LiF	Ti	TiTop
0°	0.20 (0.03)	2.2 (0.5)	0.36 (0.24)	0.59 (0.27)	0.13 (0.06)	5.8 (0.7)	19.4 (1.2)
60°	0.39 (0.05)	1.7 (0.4)	1.21 (0.12)	0.50 (0.10)	0.15 (0.04)	4.1 (0.8)	21.8 (1.4)
120°	<0.13	1.3 (0.4)	0.75 (0.09)	0.26 (0.09)	0.10 (0.03)	5.5 (0.9)	16.6 (1.4)
180°	<0.36	1.6 (0.4)	<0.53	<0.10	<0.06	4.1 (0.7)	17.7 (1.4)
240°	<0.33	1.1 (0.4)	0.52 (0.14)	0.24 (0.14)	0.041 (0.024)	4.6 (0.9)	18.0 (1.4)
300°	0.19 (0.04)	1.1 (0.4)	0.94 (0.16)	0.19 (0.07)	0.07 (0.03)	3.3 (0.7)	22.2 (1.7)

The radionuclides are listed in the order of increasing mass.

Table 7c
The total activity level per sample (mBq) as a function of sample position

Radionuclide	^{124}Sb (mBq)		^{181}Hf (mBq)	^{182}Ta (mBq)	^{181}W (Bq)	^{185}W (Bq)
Series	Ti	TiTop	W	W	W	W
0°	3.1 (0.6)	15.0 (1.0)	0.6 (0.3)	2.4 (0.4)	3.6 (1.3)	95 (17)
60°	4.3 (0.8)	16.0 (1.0)	0.8 (0.5)	1.7 (0.3)	4.1 (1.5)	114 (19)
120°	3.4 (0.9)	15.6 (1.3)	0.9 (0.5)	1.5 (0.3)	4.2 (1.6)	80 (16)
180°	3.2 (0.7)	13.2 (1.2)	0.7 (0.3)	1.55 (0.22)	3.0 (1.0)	116 (15)
240°	2.8 (0.8)	14.5 (1.3)	1.2 (0.8)	2.3 (0.6)	4.4 (1.9)	108 (20)
300°	3.9 (0.8)	14.2 (1.5)	<2.3	1.6 (0.4)	3.6 (1.4)	59 (15)

The radionuclides are listed in the order of increasing mass.

were located near to each other at the top of the sample holder and thus were partly shielded by the carbon tube structure, which served as an obstacle for the charged particles. The distribution of ^{46}Sc in the lower Ti samples differed from this and had an almost constant value of 60 mBq, except at 60°. It appeared, therefore, that the activity occurring in the Ti samples at the tip of the BN-holder was produced mainly by the reaction ^{46}Ti(n,p)^{46}Sc induced at a low neutron energy level (with a threshold of about 3 MeV) in combination with the deuteron-induced reaction ^{48}Ti(d,α)^{46}Sc.

^{47}Sc was detected in two of the TiTop samples (of titanium), but due to its short half-life (3.35 days) it was only detected in the samples measured first. However, ^{47}Sc was found in the titanium samples while they were still mounted on the sample holder and was detected qualitatively at JET prior to the transport of the samples to the ULGS laboratories. Hence, it is assumed that most of the titanium samples had some ^{47}Sc content. Possible activation reactions for the production of ^{47}Sc are ^{47}Ti(n,p)^{47}Sc, ^{47}Ti(d,2p)^{47}Sc, ^{48}Ti(n,np)^{47}Sc, ^{48}Ti(n,np)^{47}Sc, ^{48}Ti(n,d)^{47} and ^{49}Ti(d,α)^{47}Sc. The two reactions with the highest $\theta\sigma$-products are ^{47}Ti(n,p)^{47}Sc and ^{48}Ti(n,np)^{47}Sc.

^{48}V was detected in the titanium samples Ti1 and Ti2 only, since these two samples were measured first. The short half-life of ^{48}V (16 days) precluded its detection in any of the other titanium samples. The possible reactions are ^{47}Ti(d,n)^{48}V, ^{48}Ti(p,n)^{48}V and ^{49}Ti(p,2n)^{48}V. The most

likely reaction is ^{48}Ti(p,n)^{48}V with a threshold of approximately 5 MeV. The range of 5 MeV protons in Ti is approximately 0.15 mm, whereas the range of 14 MeV protons is about 0.9 mm [21,22]. The reaction ^{47}Ti(d,n)^{48}V with a 2 MeV threshold and a lower $\theta\sigma$-product could also have played a role here.

The discovery of ^{124}Sb in the Ti samples (see Fig. 5c) was initially a mystery and entirely unexpected. Since the k_0-NAA procedure revealed a high concentration of Sb impurities in the Ti samples, the ^{124}Sb was obviously produced by the reaction ^{123}Sb(n,γ)^{124}Sb.

4.3. ^{7}Be found in the B_4C and LiF samples

^{7}Be was found in most of the B_4C and LiF samples (see Fig. 6a). It can be produced by the following activation reactions: ^{10}B(p,α)^{7}Be, ^{6}Li(d,n)^{7}Be, ^{7}Li(p,n)^{7}Be and ^{7}Li(d,2n)^{7}Be. In the B_4C samples, the activation reaction is ^{10}B(p,α)^{7}Be, with a threshold of about 0.5 MeV, whereas the major production channel in the LiF samples is ^{7}Li(p,n)^{7}Be. At energy levels above 5 MeV the ^{7}Li(d,2n)^{7}Be reaction is possible, although the $\theta\sigma$-product is very small compared to that of the ^{7}Li(p,n)^{7}Be reaction. The range of the 0.5 MeV protons in B_4C is approximately 5 μm, whereas the 14 MeV protons have a range of about 1.4 mm. In the LiF samples the range of 1.5 MeV protons is slightly less than a 100 μm, whereas the 14 MeV protons travel approximately 1.2 mm [21,22].

The ^{7}Be contained in the B_4C and LiF samples (~10–20 mBq) and the ^{48}V in the Ti samples (~50–80 mBq) are both proton-induced, although the activity of ^{7}Be is about four times lower than that of ^{48}V. The reaction cross-sections are strongly energy-dependent, which contributes to the variations in yield in the different reactions. The range in combination with the yield is approximately four times higher for ^{48}V than for ^{7}Be at a proton energy level of 14 MeV, which correlates with the measured activity levels of the two radionuclides. It can be concluded that 14 MeV protons were present and did indeed activate the B_4C, LiF and Ti samples.

^{7}Be was also produced in the cylindrical sample holder made of BN and could have been sputtered from the sample holder and then deposited on the surface of other samples. The only other samples with traces of ^{7}Be were Ti2 and Ti6, i.e. the Ti samples near the tip of the probe. This indicates that the surface deposition was very slight or was removed during cleaning, suggesting that the activity present in the B_4C and LiF samples originated from activation of the bulk materials.

4.4. ^{54}Mn

^{54}Mn was found in all of the TiTop samples but only in a few of the B_4C, Ti and LiF samples (see Fig. 6c). Table 3 shows that Fe was a major impurity in the samples and thus was probably the main source of ^{54}Mn. The following reactions are possible: ^{54}Fe(n,p)^{54}Mn, ^{56}Fe(d,α)^{54}Mn, ^{57}Fe(d,α+n)^{54}Mn, ^{57}Fe(p,α)^{54}Mn, ^{54}Cr(p,n)^{54}Mn, ^{59}Co(p,3n+3p)^{54}Mn. The two reactions with the highest $\theta\sigma$-product values are ^{54}Fe(n,p)^{54}Mn and ^{56}Fe(d,α)^{54}Mn. The Fe concentration was much lower in the LiF samples than in the TiTop and B_4C samples, which would explain why ^{54}Mn was only detected in a few of the LiF samples.

4.5. ^{56,57,58}Co

Three radionuclides of cobalt were detected: ^{56}Co, ^{57}Co and ^{58}Co. Some of the samples in each of the series except for W contained one or more of these radionuclides. Since the W samples were the purest samples and had no Co-activity, it can be concluded that the cobalt radionuclides were produced by activation of the Fe, Ni or Co impurities.

It is important to bear in mind that the impurity levels were measured in only one sample per series and that the individual samples in a series could differ slightly in their impurity level if they were not entirely homogenous. Since the same impurity level in all the samples in a series was assumed here, the conclusion is that the results produced by the activation of impurities are not as strong as those produced by activation of the bulk material, inasmuch as the individual abundances are not known. However, all samples from one series were from the same batch, so the differences should be small.

^{56}Co was detected in all but one of the B_4C and LiF samples. The graphs follow approximately the pattern for ^{7}Be discussed previously (see Fig. 6a and b). Possible activation reactions for ^{56}Co are those of ^{58}Ni(d,α)^{56}Co, ^{54}Fe(α,np)^{56}Co, ^{56}Fe(p,n)^{56}Co, ^{56}Fe(d,2n)^{56}Co and ^{57}Fe(p,2n)^{56}Co. Of these, the two reactions with the highest $\theta\sigma$-products are ^{56}Fe(d,2n)^{56}Co and ^{56}Fe(p,n)^{56}Co. The ^{58}Ni(d,α)^{56}Co reaction is deemed unlikely to occur since the $\theta\sigma$-product is very low compared to those for Fe.

^{57}Co was detected in four of the LiF samples, with the activity distribution resembling that of ^{56}Co and ^{7}Be (see Fig. 6a and b). The activation of Fe-impurities should not be a major source of ^{57}Co, since the levels of Fe-impurities in the LiF samples were lower than those in the B_4C and Ti samples. The detection limit for Ni in the LiF samples was 15 ppm, leading to rather high $\theta\sigma$-products for the Ni reactions compared to the Fe reactions. The possible activation reactions are: ^{58}Ni(n,d)^{57}Co, ^{58}Ni(n,np)^{57}Co, ^{58}Ni(d,n+2p)^{57}Co, ^{58}Ni(p,2p)^{57}Co, ^{60}Ni(p,α)^{57}Co, ^{54}Fe(α,p)^{57}Co, ^{56}Fe(d,n)^{57}Co, ^{57}Fe(d,2n)^{57}Co, ^{57}Fe(p,n)^{57}Co, ^{58}Fe(p,2n)^{57}Co and ^{59}Co(p, 2n+p)^{57}Co. The activation reactions with the highest $\theta\sigma$-products are: ^{58}Ni(n,np)^{57}Co (threshold 10 MeV), ^{56}Fe(d,n)^{57}Co (threshold about 5 MeV) and ^{60}Ni(p,α)^{57}Co (threshold 6.8 MeV).

The activity graphs for ^{56}Co and ^{57}Co in Fig. 6b resemble each other. Both of them have a clear angular distribution, making it reasonable to believe that they mainly originated from charged particle activation reactions of Ni or Fe, since both of these are capable of producing ^{56}Co and ^{57}Co and have rather high $\theta\sigma$-product values. However, the neutron reactions with

lower $\theta\sigma$-product values could make a small contribution here too. As indicated at the beginning of Section 3, neutrons were moderated in passing through the sample holder, resulting in a small angular distribution.

^{58}Co was found in all of the Ti and TiTop samples (of titanium) and was also found in the B_4C and LiF samples, but only to a slight degree (see Fig. 5b). Titanium contained the highest level of ^{59}Co impurities, which could produce ^{58}Co via the ^{59}Co(n,2n)^{58}Co reaction. In addition, since Fe and Ni impurities were present in the samples, the following activation reactions could occur: ^{58}Ni(n,p)^{58}Co, ^{58}Ni(d,2p)^{58}Co, ^{61}Ni(p,α)^{58}Co, ^{58}Fe(p,n)^{58}Co and ^{56}Fe(α,d)^{58}Co. The reactions with the highest $\theta\sigma$-product values are: ^{58}Ni(n,p)^{58}Co, ^{58}Ni(d,2p)^{58}Co and ^{58}Fe(p,n)^{58}Co, which have thresholds of 1–4 MeV. The $\theta\sigma$-products for the Ni reactions are actually much higher than that for the ^{59}Co reaction, while the thresholds of the Ni reactions are several MeV lower as compared with the ^{59}Co reaction threshold of approximately 10 MeV, which leads to the conclusion that the Ni impurities could be the main source of ^{58}Co.

5. Discussion

It is difficult to determine exactly how ^{54}Mn, ^{56}Co, ^{57}Co and ^{58}Co were produced unless one knows the exact amounts of impurities contained in the samples. The Fe, Co and Ni impurities found by the k_0-NAA procedure can be considered the main source of those detected radionuclides. Fe was a major impurity in all the sample materials, albeit to a lesser extent in the W samples. One should thus reject the idea that the radionuclides were activated in another part of the Tokamak and were then deposited on the surface of the samples where they remained after cleaning. The fact that cobalt is commonly found at ppm level as an impurity in titanium can explain why ^{58}Co was only detected in the Ti and TiTop samples, and not in the LiF and B_4C samples, despite the fact that these also contained Ni and Fe impurities.

The similarities of the activity distributions of ^{56}Co and ^{57}Co (Fig. 6b) could indicate that the radionuclides were produced in a similar way by deuterons and by protons.

^{7}Be was only detected in two of the Ti samples (Ti2 and Ti6). In the earlier experiment [4] the activity level was 27 times higher than in the present experiment, with the maximum activity levels of ^{7}Be being found in Ti2 and Ti6. Since the activity level was much lower this time, it is possible that ^{7}Be was below the detection limit in the other Ti samples, with only the maximum levels detected at positions 2 and 6.

The ^{48}V results are of considerable significance in the evaluations made here, since ^{48}V (found in the titanium samples) and ^{7}Be (found in the B_4C and LiF samples) are the two radionuclides detected which appear to have been produced solely by proton irradiation from the fusion plasma. This indicates that the titanium samples were penetrated by the 14 MeV protons from the fusion plasma, although the exact energy of the protons when they hit the samples is not known. The threshold for the ^{48}V activation reaction is 5 MeV.

The fact that the range of the protons from the fusion plasma depends on the sample material through which it travels is of particular interest here. The protons may be stopped completely by some materials, such that all of their energy is deposited, whereas in the case of other materials the protons travel through the material and deposit only a fraction of their energy there. The yield of an activation reaction depends on such factors as the range, energy threshold and cross-section of each reaction, as well as the differences in energy between the different incoming protons and the abundance of target atoms. Taken together, these factors could explain the variations found in the activity level detected in the different samples.

To speed up measurements and achieve lower detection limits, one can improve gamma-ray measurement techniques in a number of ways, especially when measuring small samples of this kind. The use of more advanced detector systems such as multiple HPGe-detectors can increase the solid angle and the detection efficiency. One alternative here is the use of the dual HPGe-detector system newly installed in HADES, which has its two germanium detectors facing each other, resulting in nearly double the detection efficiency compared to the detectors used for the measurements reported here.

To improve the study of such short-lived radionuclides as ^{47}Sc and ^{48}V, it would be advantageous to employ yet more underground detectors, for example one detector per sample. Such an approach is feasible since the number of underground HPGe-detectors has increased in recent years, as pointed out in a recent review [23], although the slight lack of robustness which would result from this would be a drawback. The method of studying the angular distribution of radionuclides by use of gamma-ray spectrometry, as described here, resulted in low uncertainties regarding the relative activity levels involved, since identical samples could be measured by one and the same detector. The efficiency is multiplied by the count rate, therefore an incorrect efficiency would mainly stretch the activity curve but not add bias. Careful calibration and validation of each detector should minimise this problem.

Various improvements in the sample composition could increase the power of the measurement technique. One such improvement could be the use of layered samples, i.e. thin samples stacked together so as to indicate the depth to which charged particles penetrate the sample. Enriched samples could also be used to obtain higher activity levels for certain reaction products. Specific mixtures of sample materials could also be used to produce several different activation reactions in one and the same sample.

Work is in progress aimed at calculating the level of activity of various activation products using Monte Carlo simulations, including simulations of both neutrons and charged particles [21]. On the basis of such simulations and measurements, it could be possible to reconstruct the

energy spectra of the neutrons, protons and deuterons inside the Tokamak using deconvolution techniques [24].

6. Conclusions

- The newly developed method investigated here was found to be successful in obtaining information on particle leaks from a fusion plasma; 12 different radionuclides were detected and identified as activation products of the bulk material in the various samples.
- The detection of ^{7}Be in LiF and B_4C samples and of ^{48}V in Ti samples indicates that the technique is able to provide quantitative data on charged particle emission from the fusion plasma.
- Several of the radionuclides detected were produced by a combination of proton, deuteron and neutron-induced reactions of the samples' bulk material.
- The new method studied here could be further developed into an important tool for fusion plasma diagnostics.

Acknowledgements

The work done by EURIDICE and the HADES crew of SCK•CEN in Mol, Belgium, is gratefully acknowledged.

References

[1] G. Bonheure, et al., Neutron diagnostics for reactor scale fusion experiments: a review of JET systems, in: Proceedings of International Workshop on Fast Neutron Detectors and Applications POS (FNDA2006) 064 ⟨http://pos.sissa.it⟩.
[2] G. Bonheure, S. Popovichev, L. Bertalot, A. Murari, S. Conroy, JET-EFSA Contributors, Rev. Sci. Instrum. 175 (10) (2004) 3540.
[3] M. Sasao, et al., Plasma Phys. Control. Fusion 46 (7) (2004) 107.
[4] J. Gasparro, M. Hult, G. Bonheure, P.N. Johnston, Appl. Radiat. Isot. 64 (2006) 1130.
[5] G. Bonheure, M. Hult, J. Gasparro, S. Popovichev, Phys. Scripta 75 (6) (2007) 769.
[6] N. Etxebarria, P. Robouch, J. Pauwels, S. Pomme, F. Hardeman, in: Proceedings of the Second International *k*0-Users Workshop, Ljubljana, Slovenia, 1996, pp. 137–141.
[7] M. Hult, W. Preuße, J. Gasparro, Acta Chim. Slov. 53 (2006) 1.
[8] M. Hult, M.J. Martínez Canet, M. Köhler, J. das Neves, P.N. Johnston, Appl. Radiat. Isot. 53 (1–2) (2000) 225.
[9] M. Hult, J. Gasparro, L. Johansson, P.N. Johnston, R. Vasselli, Environ. Radiochem. Anal. II (2003) 375.
[10] S. Neumaier, D. Arnold, J. Böhm, E. Funck, Appl. Radiat. Isot. 53 (1–2) (2000) 173.
[11] C. Arpesella, Appl. Radiat. Isot. 47 (1996) 991.
[12] M. Laubenstein, M. Hult, J. Gasparro, D. Arnold, S. Neumaier, G. Heusser, M. Köhler, P. Povinec, J.-L. Reyss, M. Schwaiger, P. Theodórsson, Appl. Radiat. Isot. 61 (2–3) (2004) 167.
[13] W.R. Nelson, H. Hirayama, D.W.O. Rogers, The EGS4 code system, SLAC Report, 1985.
[14] S. Agostinelli, et al., Nucl. Instr. and Meth. A 506 (3) (2003) 250.
[15] J. Allison, et al., IEEE Trans. Nucl. Sci. NS-53 (1) (2006) 270.
[16] O. Sima, D. Arnold, C. Dovlete, J. Radioanal. Nucl. Chem. 248 (2) (2001) 359.
[17] ⟨http://www.nucleide.org/DDEP.htm⟩.
[18] L.P. Ekström, R.B. Firestone, WWW table of radioactive isotopes, Database version 2/28/99 from ⟨http://ie.lbl.gov/toi/index.htm⟩.
[19] ISO/IEC/OIML/BIPM, Guide to the expression of uncertainty in measurement (1st corrected edition), International Organization for Standardization, Geneva, Switzerland, 1995.
[20] ISO, 11929-3, Determination of the detection limit and decision threshold for ionising radiation measurements—Part 3, first ed, International Organization for Standardization, Geneva, Switzerland, 2000.
[21] G. Bonheure, private communication, results to be published.
[22] H.H. Andersen, J.F. Ziegler, Hydrogen Stopping Powers and Ranges in All Elements, vol. 3, The Stopping and Ranges of Ions in Matter, Pergamon Press, New York, USA, 1977.
[23] M. Hult, Metrologia 44 (4) (2007) S87 (Erratum in Metrologia 44(5) (2007) 435).
[24] G. Lövestam, M. Hult, A. Fessler, J. Gasparro, P. Kockerols, K. Okkinga, H. Tagziria, F. Vanhavere, J.S.E. Wieslander, Neutron fluence spectrometry using disk activation, Radiat. Meas., submitted for publication.

Paper II

This article **was published** in Fusion Science and Technology (an international journal of the American Nuclear Society), volume 53(3), 806-815.

MEGA-ELECTRON-VOLT ION LOSS MEASUREMENTS IN JET D-^{3}He PLASMAS USING ACTIVATION TECHNIQUE

GEORGES BONHEURE,[a]* ELISABETH WIESLANDER,[b] MIKAEL HULT,[b]
JOËL GASPARRO,[b] GERD MARISSENS,[b] DIRK ARNOLD,[c] MATTHIAS LAUBENSTEIN,[d]
SERGEI POPOVICHEV,[e] ANDREA MURARI,[f] IGOR LENGAR,[g] and JET-EFDA CONTRIBUTORS
JET-EFDA Culham Science Centre, Abingdon OX14 3DB, United Kingdom

Received September 21, 2007
Accepted for Publication January 15, 2008

Measurements of mega-electron-volt charged-particle losses in the JET tokamak are reported. The technique is based on sample activation by nuclear reaction from mega-electron-volt particles. Samples are used as flux monitors for leaking fusion plasma particles in the mega-electron-volt energy range. Ultra-low-level gamma-ray measurements were performed at three underground facilities in order to significantly enhance detection levels. Two measured radionuclides (^{48}V and ^{7}Be) were identified as produced predominantly from charged-particle reactions. Quantitative data on charged-particle fluxes to the wall were obtained for the first time as well as angular distribution with respect to the magnetic field.

KEYWORDS: *nuclear fusion, tokamak, plasma diagnostics*

Note: Some figures in this paper are in color only in the electronic version.

*E-mail: georges.bonheure@jet.uk
[a]Laboratory for Plasma Physics, Association "Euratom-Belgian State," Royal Military Academy, Avenue de la Renaissance, 30, Kunstherlevinglaan, B-1000 Brussels, Belgium
[b]EC-JRC-IRMM, Institute for Reference Materials and Measurements, Retieseweg 111, B-2440 Geel, Belgium
[c]Physikalisch-Technische Bundesanstalt, 6.1 Radioactivity, Bundesallee 100, D-38116 Braunschweig, Germany
[d]Laboratori Nazionali del Gran Sasso, S.S, 17/bis, km 18+910, I-67010 Assergi (AQ), Italy
[e]Euratom/UKAEA Association, Culham Science Centre, Abingdon, Oxon, United Kingdom
[f]Consorzio RFX, Associazione ENEA-Euratom per la Fusione, Padova, Italy
[g]Slovenian Fusion Association, Jozef Stefan Institute, Jamova 39 SI-1000 Ljubljana, Slovenia

I. INTRODUCTION

Measurements of energetic particle losses from fusion plasmas, in particular alpha particles, remain difficult in large fusion devices, and further research and development is needed in view of ITER (Ref. 1) and future fusion reactors. The present paper describes new measurements using the activation technique.[2–4] Samples are activated because of nuclear reactions of type (z,n), $(z,\gamma),\ldots$, where z is a light charged particle p, t, d, ^{3}He, or α. After plasma exposure, samples are removed from the sample holder, and analysis of samples is performed using high counting efficiency, ultra-low-level, and high-energy-resolution gamma-ray spectrometry.[5] Earlier evidence in JET experiments of activation by charged particles was from a reversed toroidal field experiment in D-D plasmas in 2003. In this preliminary study, a large ^{7}Be (half-life 53.3 days) signal was detected.[4] In 2004, the first study performed with an activation probe was conducted on ^{4}He plasmas.[6] The new measurements reported in the present paper are from a first study conducted in D-^{3}He plasmas.

The main advantages of the activation technique are robustness, linear response, and immunity to electromagnetic noise and temperature variation and absence of saturation. A careful choice of the target allows particle identification and gives information on particle energy by selecting different nuclear reactions with different thresholds. Absolute measurements of fluence and spectral fluence (with the multifoil technique) can be performed. It is a well-established method at tokamaks for calibration of the neutron emission. The main limitation of the present method is time resolution. Online measurements are not possible. Two recently installed diagnostics are also available for particle loss measurements in JET, and first results have been obtained.[7,8] First, a set of ten faraday cup detectors with a 1-ms time resolution is

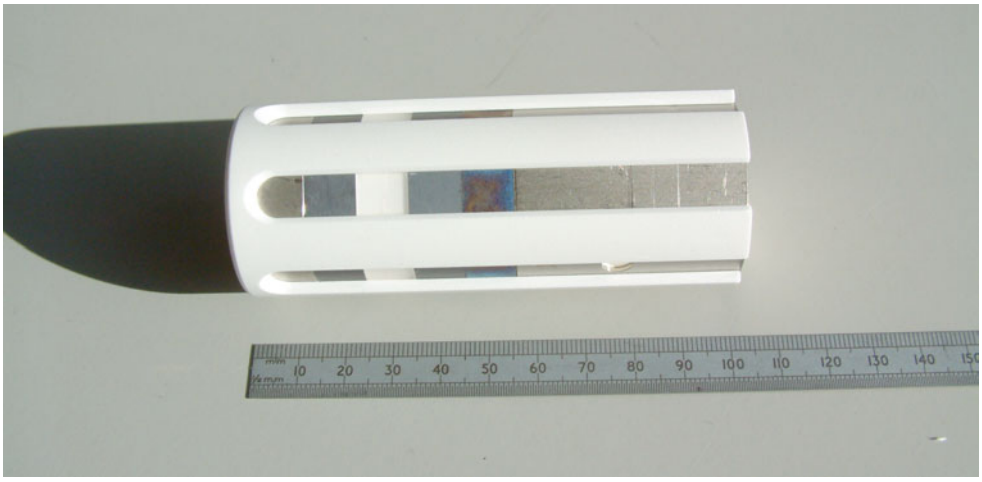

Fig. 1. Photograph of the activation probe.

mounted in-vessel and spread over five poloidal locations and three radial positions. Second, a scintillator probe is mounted slightly below midplane in a lower limiter guide tube. The scintillator probe provides two-dimensional (2-D) distribution in larmor radius and pitch angle space with a time resolution of 0.1 ms.

II. ACTIVATION PROBE

II.A. Sample Holder

The activation samples were mounted on an activation probe (Fig. 1), which can be introduced inside the JET tokamak vacuum chamber near the plasma edge. The activation probe is the first of its kind in a tokamak to be specifically designed for measuring charged-particle activation.[6] The probe head is 40 mm in diameter and 100 mm in length and has a hexagonal cross section. Each of the six sides has a slot that can be filled in with samples. Sample orientations are shown in Fig. 2. Samples in slot 1 are facing toward the inboard radial direction. The activation probe is mounted on a manipulator arm system located in the JET ceiling (see Fig. 3). This mechanical setup allows one to (a) position the samples close to plasma edge, (b) expose the samples only in dedicated plasma discharges, and (c) remove the samples after the desired exposure. The probe body is made of boron nitride (BN), which is a suitable material for the harsh environment inside the JET tokamak. Because of the extreme conditions inside the JET vacuum chamber, severe restrictions are put on sample materials used for the experiments. The material must be neither fragile nor brittle. It must be vacuum compatible and withstand a strong magnetic field and high temperature.

II.B. Sample Materials

Thirty-six samples with their sizes indicated in Table I were used. All samples were 10 mm in height, except one type of sample, which was 44 mm. Each sample is placed in its slot by sliding it down the holder. Because of the way it is fixed, the sample is partly covered by the edges of the slot, leaving the exposed area of the samples smaller than the total area. The uncovered width of the sample is 8.25 mm. Each slot was filled with six samples: (a) pure Ti near the tip of the sample holder (Ti1-6), (b) first set of B_4C (B1-6) located just above the Ti, (c) LiF (LiF1-6),

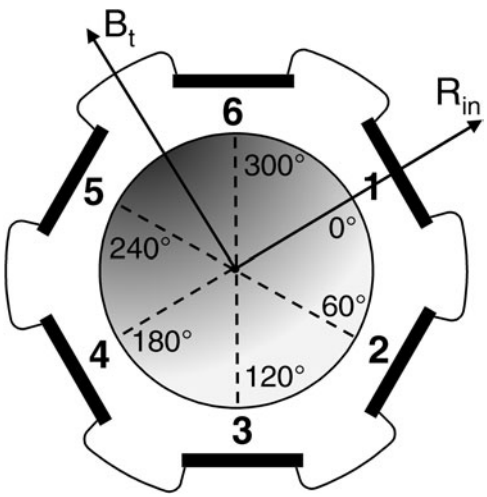

Fig. 2. A cross section of the activation probe holding all the samples. B_t = standard direction of the toroidal magnetic field and R_{in} = the direction along the major radius pointing radially inward. The numbers indicate the six sample positions.

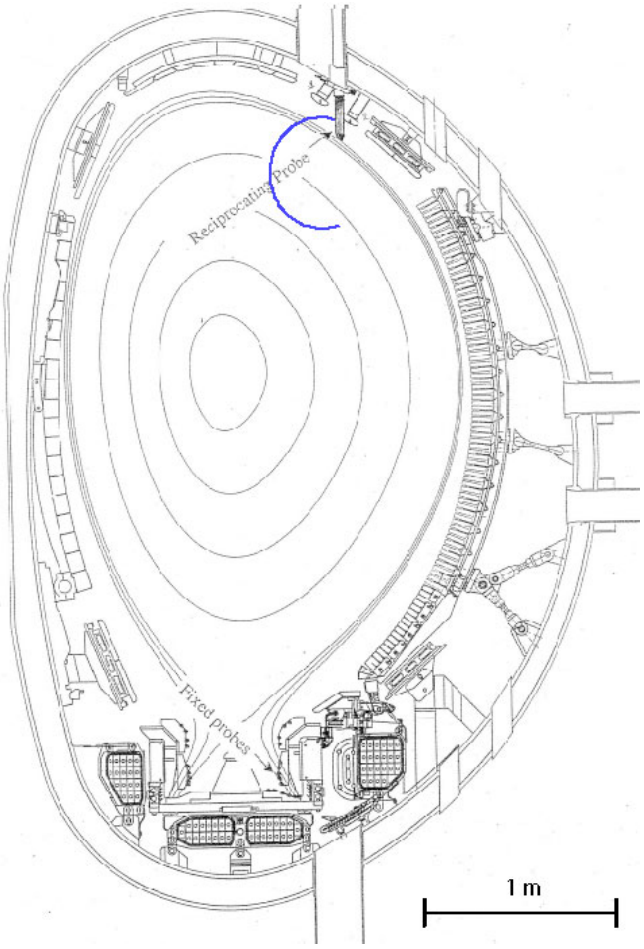

Fig. 3. A schematic drawing of the activation probe attached to the ceiling of the JET tokamak. The arrow pointed text "Reciprocating Probe" indicates the position of the activation probe. A typical trajectory in the JET plasma of a high-energy proton reaching the probe is shown.

TABLE I

Details of the Sample Material*

Label	Material	Number of Samples	Exposed Area (cm^2)	Mass (g)	Distance to Plasma (cm)
TiTop1-6	Ti	6	3.52	1.90	20
W1-6	W	6	0.825	1.95	19
B7-12	B_4C	6	0.825	0.26	18
LiF1-6	LiF	6	0.825	0.33	17
B1-6	B_4C	6	0.825	0.26	16
Ti1-6	Ti	6	0.914	0.39	15

*Material composition, geometry, and distance to plasma.

TABLE II

The Isotopic Abundance in the Samples Used in the JET Experiments

Isotope	Abundance (%)
^{6}Li	7.59
^{7}Li	92.41
^{10}B	19.9
^{11}B	80.1
^{12}C	98.93
^{13}C	1.07
^{19}F	100
^{46}Ti	8.25
^{47}Ti	7.44
^{48}Ti	73.7
^{49}Ti	5.5
^{50}Ti	5.2
^{180}W	0.12
^{182}W	26.5
^{183}W	14.3
^{184}W	30.6
^{186}W	28.4

(d) second set of B_4C (B7-12), (e) pure W (W1-6), and (f) long pure Ti samples (TiTop1-6). The short Ti samples were the nearest to the plasma edge while the long Ti samples were the farthest away. The distance between the samples and the plasma is indicated in the last column of Table I. The long Ti samples were located at the back of the sample holder and in the plasma shadow. All samples were of natural isotopic composition. Table II shows the list of the 17 different isotopes composing the sample materials.

III. EXPERIMENT

The samples were exposed for 4 days and were irradiated in a total of 63 JET plasma pulses. Most of the plasmas were in a D-^{3}He fuel mixture with the ^{3}He concentration ranging from 8 to 20%. In these plasmas, the toroidal magnetic fields were 2.2 to 3.4 T, and the plasma currents were 1.5 to 2.5 MA. The plasmas were heated with neutral beam injection NBI(D) heating with power up to 22 MW for 7 s and ion cyclotron resonance frequency heating (minority ^{3}He, mode conversion) with power up to 6.9 MW. The maximum total auxiliary input power applied was 29.2 MW. The total number of neutrons measured by the fission chambers[9] and summed over all plasmas was 5.08×10^{17} (with an uncertainty of

TABLE III

Larmor Radii of Charged Fusion Products

	Maximum Larmor Radius at 2.2 T (cm)	Maximum Larmor Radius at 3.4 T (cm)
^{3}He (0.82 MeV)	5	3.3
Tritons (1.01 MeV)	11	7.4
Proton (3.03 MeV)	11	7.4
Alpha (3.67 MeV)	12	8
Proton (14.68 MeV)	25	16.7

±10%). The neutron flux that reached the samples was calculated with the MCNP neutron transport code.[10] The main fusion reactions in the plasma were the following:

$$D + {}^3He \rightarrow p\ (14.7\ MeV) + \alpha\ (3.7\ MeV)$$

$$D + D \rightarrow p\ (3.0\ MeV) + T\ (1.0\ MeV)$$

$$D + D \rightarrow n\ (2.5\ MeV) + {}^3He\ (0.8\ MeV)$$

$$D + T \rightarrow n\ (14.1\ MeV) + \alpha\ (3.6\ MeV)\ .$$

The most important fusion reactions with the same order of magnitude were the D-^{3}He reaction and the two D-D reactions. The larmor radii of the charged fusion products are listed in Table III, and a typical orbit of a D-^{3}He proton that reaches the sample is shown in Fig. 3. The $D + T \rightarrow n\ (14.1\ MeV) + \alpha\ (3.6\ MeV)$ reaction occurred at a much lower level because of slowed-down tritons produced in D-D reactions and undergoing secondary reactions (triton burnup). The fraction of 14.1-MeV neutrons measured from the silicon diodes[9] was 1.18% (with an uncertainty of ±10%) of the total number of neutrons produced. The 14.1-MeV neutron flux that reached the samples was calculated with MCNP.

IV. MEASUREMENTS

After irradiation, the sample holder was removed from the vacuum chamber, and a preliminary gamma spectrometry analysis was performed after a cooling time of 20 days. Because of low sample activity, low detection levels are needed, and gamma-ray measurements are best performed in underground laboratories. The magnitude of the background reduction is up to 10^5 compared to a high-purity germanium detector used for neutron activation measurements at JET. As shown in previous work, JET samples are suitable for ultra-low-level gamma-ray spectrometry.[5] In collaboration with three underground laboratories, a detailed gamma-ray spectroscopy analysis of each individual sample was performed. The underground facilities are Institute for Reference Materials and Measurements (IRMM) in the 225-m-deep underground laboratory HADES located at the Belgian nuclear center StudieCentrum voor Kernenergie • Centre d'Etude de l'Energie Nucleaire (SCK•CEN) in Mol, Belgium[11]; Physikalisch-Technische Bundesanstalt (PTB) in the underground laboratory UDO located at a depth of 490 m in the ASSE salt mine close to Braunschweig, Germany[12]; and Laboratori Nazionali del Gran Sasso (LNGS) in the 3800 water meter equivalent low background counting facility located in the Gran Sasso nearby Assergi in Italy.[13]

V. RESULTS

V.A. Major Radionuclides

The major observed radionuclides are listed in Table IV. The massic activity value in mBq/g refers to the sample highest measured activity at the reference date. The main producing reactions and the samples on which these radionuclides were found are indicated. Vanadium-48 (half-life 15.98 days) was found on two samples (Ti1 and Ti2). Figure 4 shows a gamma-ray

TABLE IV

The Major Radionuclides Found in the Six Sets of Samples of Four Different Materials*

Radionuclide	Massic Activity (Max-mBq/g)	Main Production Reactions	Samples
$^{48}V_{(t_{1/2}=15.98\ days)}$	200 ± 30	$^{48}Ti(p,n)$, $^{47}Ti(d,n)$	Ti1, Ti2
$^{46}Sc_{(t_{1/2}=83.8\ days)}$	176 ± 5	$^{46}Ti(n,p)$, $^{47}Ti(n,d)$, $^{48}Ti(d,\alpha)$	Ti1-6, TiTop1-6
$^{7}Be_{(t_{1/2}=53.3\ days)}$	97 ± 5	$^{10}B(p,\alpha)$, $^{10}B(d,\alpha n)$ $^{7}Li(p,n)$, $^{6}Li(d,n)$	B1-3, B5-12 LiF1-3, LiF5-6, Ti2, Ti6

*The half-life $t_{1/2}$ is also listed for respective nuclide.[17] Massic activity refers to highest sample activity at the reference date. Main production reactions and samples on which these radionuclides were found are indicated. Note that ^{7}Be is listed under massic activity although it also probably contains a fraction of surface activity in the B_4C, LiF, and Ti samples.

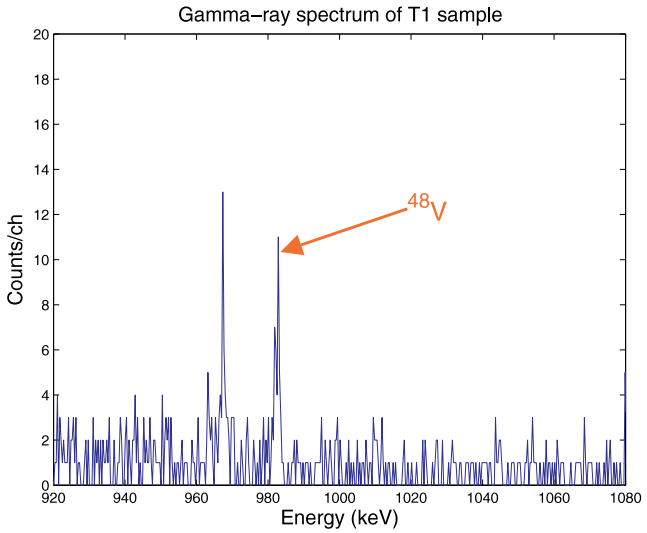

Fig. 4. A gamma-ray spectrum (Ti1 sample) showing a peak at 983.5 keV from the decay of ^{48}V (counting time ~7 days, 40 counts in peak). Such ultra-low-level activity could not have been detected using conventional above-ground gamma-ray spectrometry.

spectrum for the Ti1 sample. The peak at 983.5 keV from ^{48}V decay is clearly visible. The counting time for this spectrum was 7 days, and the total number of counts in the peak reached about 40. Such ultra-low-level activity could not have been detected above ground using conventional gamma-ray spectrometry. Scandium-46 (half-life 83.8 days) was found on all titanium samples (Ti1-6) located nearest to the tip of the probe and on all (Titop1-6) samples located at the back of the sample holder. These samples were shielded from the plasma particle flux. Beryllium-7 (half-life 53.3 days) was found on nearly all B_4C samples (B1-3 and B5-12) and on nearly all LiF samples (LiF1-3 and LiF5-6). Beryllium-7 was below threshold for samples B4 and LiF4. Ti2 and Ti6 had some ^{7}Be deposited on the surface.

Two radionuclides (^{48}V and ^{7}Be) were produced primarily from charged-particle reactions. Observation of ^{48}V (see Fig. 4) provides evidence of high-energy proton fluxes from the plasma. Vanadium-48 was not observed in previous experiments in D-D plasma[4] and helium plasma.[6] The ^{48}Ti(p,n) reaction energy threshold (~5 MeV) is too high for 3.02-MeV D-D fusion protons to contribute to ^{48}V production. Therefore, protons most likely originated in D-^{3}He fusion reactions and were born with an energy of 14.7 MeV. Confined 14.7-MeV protons were also observed by measuring 16.6-MeV gamma rays from the weak secondary branch D + ^{3}He → Li + γ of the D + ^{3}He fusion reaction. The gamma-ray spectrometer[14] consists of 125- × 125-mm-long sodium iodide NaI(Tl) scintillator and a 75- × 75-mm bismuth germanate BGO crystal. The 14.7-MeV protons have a very large larmor radius in the range of 0.2 m or above, as indicated in Table III, and are barely confined. The typical magnitude of first orbit losses is ~50%. Because of the direction of grad B drift, most of the first orbit losses occur in the lower outboard part of the vacuum vessel. A preliminary investigation of the 14.7-MeV proton trajectories and detection efficiency suggests the detected protons were born in the plasma region ($\rho \sim 0.8$) relatively close to the detector.

As indicated in Table IV, a deuteron contribution to ^{48}V production from ^{47}Ti(d,n) (energy threshold ~2 MeV) is possible as well.

The ^{7}Be angular distributions of massic activity on the lithium fluoride samples and the two sets of the boron carbide samples are shown in Fig. 5. Anisotropic angular distributions were found for the three sets of samples. In contrast, the angular distribution of ^{46}Sc massic activity (see Fig. 6), which is dominantly produced from neutron irradiation, was found to be nearly uniform. The activation variation versus sample orientation did not exceed 10% in the case of the Ti1-6 set and 15% in the case of the Titop1-6 set. In the latter case, the angular variation can be explained by neutron shielding due to the sample holder (see Sec. V.B). In case of the Ti1-6 set, neutron activation is mixed with a contribution from charged particles; hence, a different curve is observed. A low level of ^{7}Be was found on the Ti2 and Ti6 samples. It is sputtered particle deposition on the sample surface. The level was approximately 30 times less than in a previous experiment[6] in which two maxima were similarly found at the same sample orientation (Ti2 and Ti6). This suggests that the net deposition was lower compared to the previous experiment.

The uncertainty in the gamma-ray measurements is dominated by counting statistics, due to the low count rates. Another significant contribution to the uncertainty

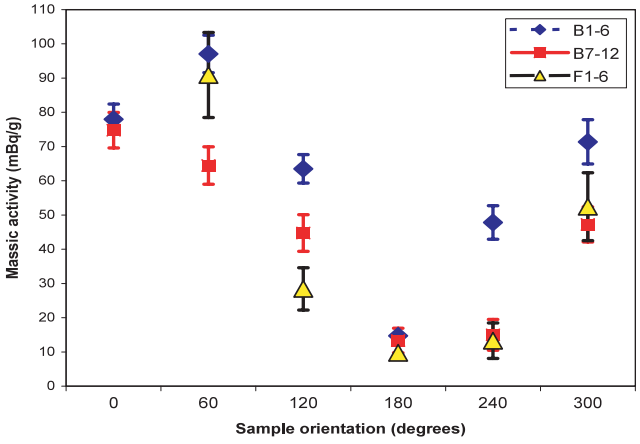

Fig. 5. The ^{7}Be angular distribution of the massic activity in mBq/g for three sets of samples. Anisotropic distributions are found in the case of charged-particle–induced reactions.

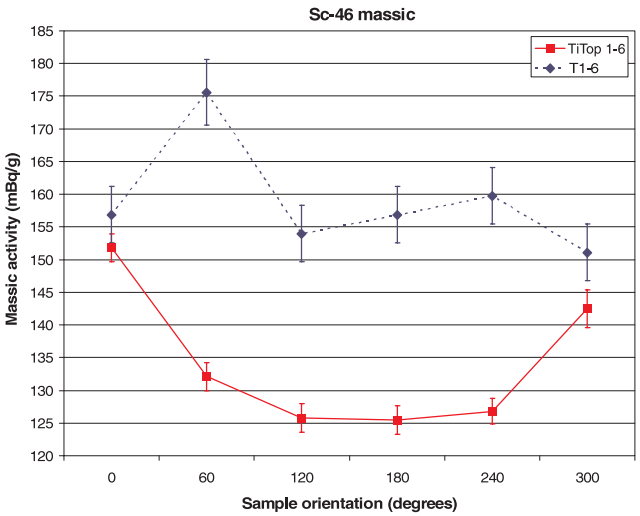

Fig. 6. Scandium-46 angular distribution of the massic activity in mBq/g for the two sets of titanium samples. The top samples are in the plasma shadow.

is the geometry due to the short distance between the sample and the detector and the unknown distribution of the source in the sample. Other minor error sources include gamma-ray emission probability and efficiency from counting statistics and from electron and photon transport and from precision of calibration sources.

V.B. Quantitative Analysis

Quantitative data on particle fluence could be deduced from the sample activity. The detailed elaboration of all the activation results required an algorithm that takes into account all possible nuclear reactions. The numerical method adopted in this work involved two steps. In the first step, the sample responses were determined from the nuclear properties of the material. In the second step, the particle fluence was determined using all sample responses, measured activity data, and prior spectral information. More than 100 reactions had already been examined including neutron-induced reactions, charged-particle–induced reactions, and photonuclear reactions, which all occur at various levels inside the tokamak. The level of photonuclear reactions was estimated from γ, n reactions in W samples with energy thresholds starting at 7 to 8 MeV and relatively significant cross sections (0.4 to 0.5 b). Products from these reactions were not detected, implying that gamma-induced activation was very low. The sample responses were studied in detail and calculated with the FISPACT code.[15] FISPACT is an inventory code that has been developed for neutron-induced activation calculations for materials in fusion devices. In addition to the neutron cross-section libraries, FISPACT runs also with proton and deuteron cross-section libraries. The accuracy of the calculated inventory is dependent on the quality of the input nuclear data, i.e., cross sections and decay data. For proton and deuteron irradiation, uncertainty of the material stopping power data gives an additional contribution to the total uncertainty.

Figure 7 shows a plot of activation coefficients calculated with FISPACT for several of the sample materials irradiated by neutrons at different neutron energies. The positions on the energy axis of the D-D and the D-T neutrons are indicated by arrows. The expected activity of a given radionuclide in the sample is calculated by integrating the yield curve (Fig. 7) over the neutron spectrum in the sample. A model of the activation probe suitable for MCNP neutron transport calculation was prepared. With the help of this model, it was possible to compute the neutron spectra in each of the 36 samples. More recently, a first set of MCNP calculations with the most up-to-date JET model was started. Using the measured activity data of the activation products dominantly produced by neutrons and the MCNP-calculated neutron spectrum, the inferred neutron fluence was found in good agreement with the neutron measurements from the time-resolved neutron yield monitors. The measured neutron-induced radionuclide activity was therefore consistent with the expected neutron-induced activity. Furthermore, these preliminary MCNP calculations showed an angular distribution fairly similar to the observed angular distribution of ^{46}Sc massic activity for the titanium sample Titop1-6 set (see Fig. 6), leading to the straightforward interpretation that the observed angular distribution is due to the interaction of the neutrons with the boron nitride sample holder. Because of this interaction, the highest reduction of direct neutron flux was in the case of samples directed radially outward (angular position 4 in Fig. 2), hence the observed minimum in activation (Fig. 6).

Figure 8 shows a plot of activation coefficients calculated with FISPACT for several of the sample materials irradiated by protons at different proton energies. The positions of 3-MeV D-D protons and 14.7-MeV D-^{3}He protons are indicated by arrows on the energy axis. The next step in order to determine the proton fluence is to specify the proton energy spectrum.

During this experiment, the scintillator probe[7] and the faraday cups[8] were also used in order to detect particle losses. The larmor radius of the 14.7-MeV protons exceeded the upper limit of the range of the scintillator probe, and therefore, these protons could not be detected, but particles with larmor radii corresponding to 3.02-MeV protons from D-D fusion reactions and 3.67-MeV alpha particles from D-^{3}He fusion reactions were detected by the scintillator. Both had similar larmor radii (see Table III) and could not be distinguished because of limited larmor radius resolution of the scintillator probe.

The most plausible proton energy spectrum had two peaks at 3.02 MeV from the D-D fusion reactions and 14.7 MeV from the D-^{3}He fusion reactions. The

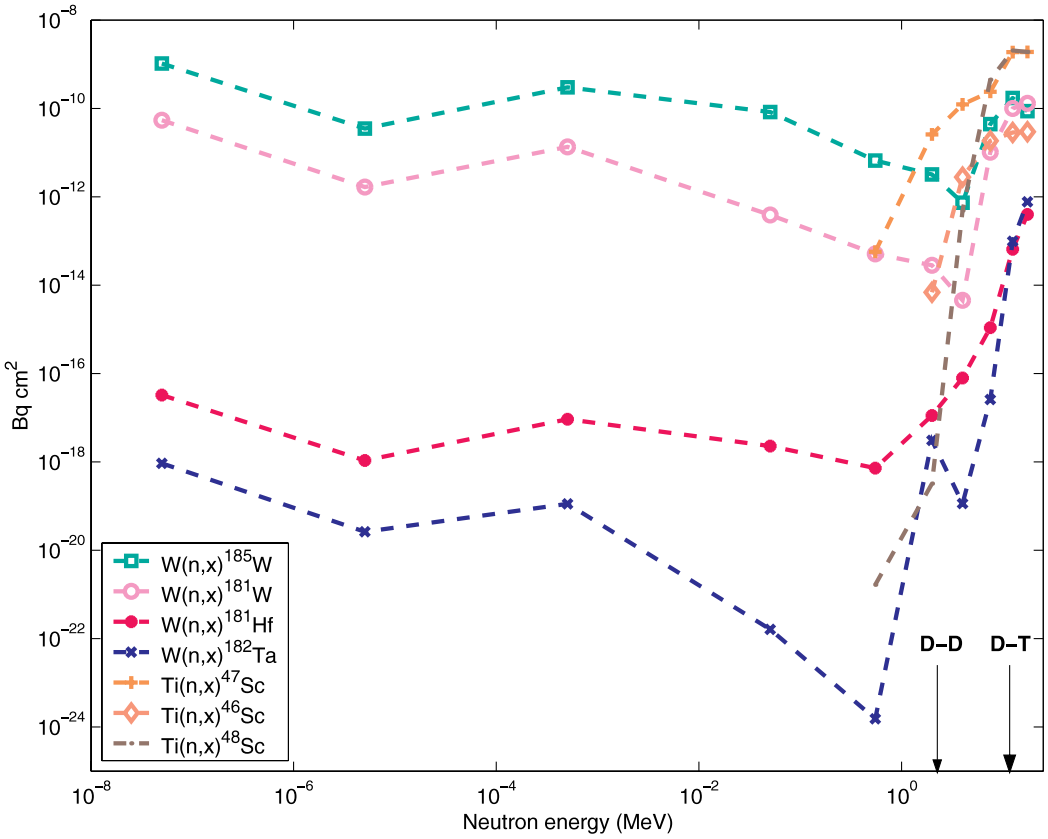

Fig. 7. Activation coefficients calculated with FISPACT (Ref. 15) for several materials irradiated by neutrons at different energies. The positions on the energy axis for D-D and D-T neutrons are indicated by arrows.

strongest evidence was the ratio of the measured yield ^{7}Be to ^{48}V. The ratio was found rather close to the expected ratio of the ^{7}Be to ^{48}V activation coefficients at D-^{3}He proton energy. This strongly suggests that most of the charged-particle–induced activation in the samples was due primarily to D-^{3}He protons. The inferred D-^{3}He proton fluence was 4.10^8 cm^{-2}. The best fit to the measured activity of ^{7}Be and ^{48}V was reached with a combined fusion proton source in a ratio p (3.02 MeV) / p (14.7 MeV) of ~17. This indicates that 3.02-MeV protons from the D-D fusion reactions were an additional significant contribution to the detected proton flux. Uncertainty due to the unknown spectrum is a factor of ~2.

For future experiments, it is proposed to better measure the proton energy spectrum by using a stack of foils and in a such a way that both types of protons could be identified experimentally and uncertainty could be significantly reduced.

The contribution from mega-electron-volt deuterons was not excluded by the measurements although it is likely a small contribution to the overall inventory. An assessment of the background contributions due to secondary particles in the samples was performed using FISPACT calculations. Secondary particles are charged particles p, t, d, ^{3}He, or α emerging from primary neutron interactions in the bulk of the samples. These secondary particles in turn contribute to the charged-particle activation and therefore are not leaking out of the plasma. Figure 9 shows the FISPACT calculations for the production of p, d, ^{3}He, and α as function of neutron energy in boron carbide samples. Note that the whole neutron spectrum must be considered as the yield from thermal neutrons can be very high. An upper limit in the case of these samples giving ~0.62% of proton fluence were secondary particles.

A complete model to quantify the charged-particle–induced activation in the samples and its angular distribution (Fig. 5) is currently under development. This model consists of three main parts. The first part is the model of the sample responses (see Figs. 7 and 8) and has been already described above. The second part, currently under elaboration, deals with the radiation transport (neutrons, charged particles, etc.) from the plasma to the detector. In the case of the neutrons, MCNP calculations were carried out, and preliminary simulations showed good agreement with the expected neutron-induced activation. In the case of charged particles, orbit-following techniques must be used. As was done in previous works,[4] first orbit loss simulations with the MCOrbit code were performed for this experiment. It was estimated from

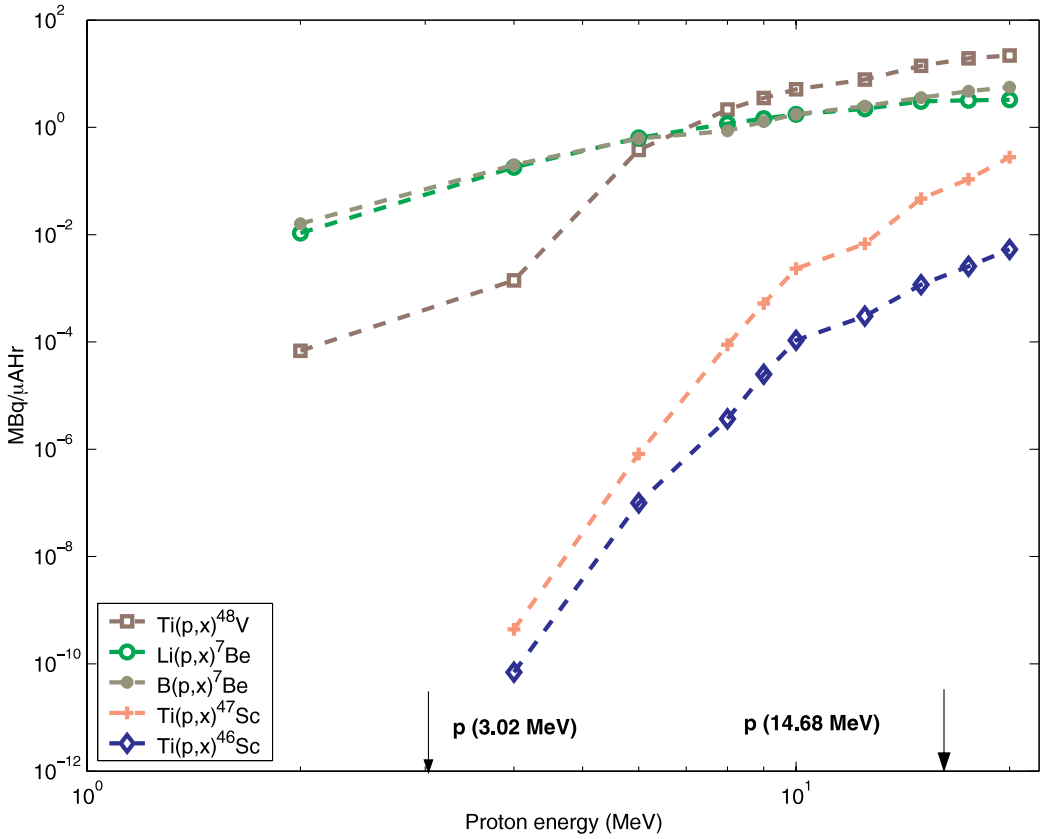

Fig. 8. Activation coefficients calculated with FISPACT (Ref. 15) for several materials irradiated by protons at different energies. The positions on the energy axis for D-D and D-^{3}He protons are indicated by arrows.

these simulations that the 14.68-MeV proton fluence in the detector region and integrated over all pitch angles could not exceed 10^9 to 10^{10} protons·cm^{-2}, which is above the measured 4.10^8 cm^{-2} D-^{3}He proton fluence. MCOrbit is a Monte Carlo code that forward propagates a packet of initial conditions. Although the MCOrbit code was useful to give an estimate of the order of magnitude of orbit losses, it was found inadequate for modeling further this activation experiment in detail. The main reasons are the following. First, the detailed geometry of the activation probe and some of the surrounding structures are currently not included in the code. Both the activation probe and some surrounding structures block some particles on their way to the samples. Second, statistical noise prevents getting an accurate answer. Basically, the Monte Carlo method becomes inefficient because very few particles reach the detector. Third, there is lack of flexibility in the code for prescribing the particle source and other effects not included in the model.

To compute the transport of charged particles to each sample more accurately, a suitable deterministic method initially proposed by Heidbrink,[16] and which is under development, is to calculate the detection efficiency distribution in phase-space. This method is valid for collisionless fast ions. The D-^{3}He proton source is the last part of the model and is relatively straightforward as tools are available (e.g., TRANSP) to compute the D-^{3}He fusion 2-D spatial distribution.

The measured losses of the D-^{3}He protons did not exceed our first estimate with MCOrbit. However, the above-described modeling issues need to be addressed before the observed angular distribution (Fig. 5) can be interpreted and more definite comparisons with theoretical predictions can be made.

V.C. Minor Radionuclides

These radionuclides, listed in Table V, are all the activation products that were found in very weak amounts, e.g., under the level of 10 mBq/g, with some very near the detection limits.

For the ^{181}Hf and ^{182}Ta in W samples, the most probable reaction is $^{184}\mathrm{W}(n,\alpha)^{181}\mathrm{Hf}$, with a threshold of ~10 MeV for ^{181}Hf production. Figure 10 shows the massic activity angular distribution for ^{181}Hf. A uniform distribution is possible within uncertainties. Furthermore, the D-T 14-MeV neutron fluence was measured with the 14-MeV time-resolved neutron yield monitor.[14] The value of 0.4 mBq/g is consistent with the measured number of 14-MeV neutrons.

TABLE V

The Minor Radionuclides Found in the Six Sets of Samples of Four Different Materials*

Radionuclide	Massic Activity (Max-mBq/g)	Main Production Reactions	Samples
$^{181}Hf_{(t_{1/2}=42.4\ days)}$	0.7 ± 0.3	$^{184}W(n,\alpha)^{181}Hf$	W1-6
$^{182}Ta_{(t_{1/2}=115.0\ days)}$	1.2 ± 0.2	$^{184}W(d,\alpha)^{182}Ta$, $^{182}W(n,p)^{182}Ta$, $^{183}W(n,pn)^{182}Ta$, $^{183}W(n,d)^{182}Ta$	W1-6
$^{54}Mn_{(t_{1/2}=312.2\ days)}$	0.7 ± 0.1	$^{54}Fe(n,p)^{54}Mn$	TiTop1-6, Ti5
$^{58}Co_{(t_{1/2}=70.916\ days)}$	6.1 ± 0.4	$^{58}Ni(n,p)^{58}Co$	Ti1-6, TiTop1-6
$^{56}Co_{(t_{1/2}=77.7\ days)}$	1.46 ± 0.15	$^{56}Fe(p,n)^{56}Co$, $^{58}Ni(d,\alpha)^{56}Co$, daughter ^{56}Ni	B2-3, B5-6 LiF1-3, LiF5-6
$^{57}Co_{(t_{1/2}=271.77\ days)}$	0.18 ± 0.05	$^{58}Ni(n,d)^{57}Co$, $^{58}Ni(n,np)^{57}Co$, $^{58}Ni(d,n+2p)^{57}Co$, $^{58}Ni(p,2p)^{57}Co$, $^{60}Ni(p,\alpha)^{57}Co$, $^{54}Fe(\alpha,p)^{57}Co$, $^{56}Fe(d,n)^{57}Co$, $^{57}Fe(d,2n)^{57}Co$, $^{57}Fe(p,n)^{57}Co$, $^{58}Fe(p,2n)^{57}Co$	LiF2-3, LiF5-6
$^{124}Sb_{(t_{1/2}=60.2\ days)}$	4.5 ± 0.4	$^{123}Sb(n,\gamma)^{124}Sb$	Ti1-6, TiTop1-6

*The half-life $t_{1/2}$ is also listed for the respective nuclide.[17] Massic activity refers to highest sample activity at the reference date. Main possible production reactions and samples on which these radionuclides were found are indicated.

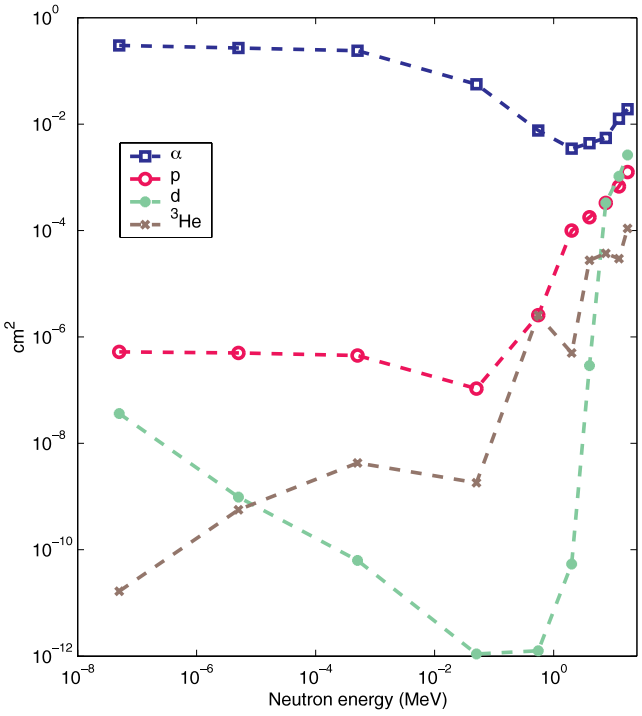

Fig. 9. The p, d, ^{3}He, and α yields calculated with FISPACT (Ref. 15) for B_4C boron carbide materials irradiated by neutrons at different energies.

Similar consistency was obtained for ^{182}Ta. FISPACT calculations including all channels of type $W(n,x)^{182}Ta$ indicated (see Fig. 7) an amount of ^{182}Ta larger than ^{181}Hf by a factor of ~2.

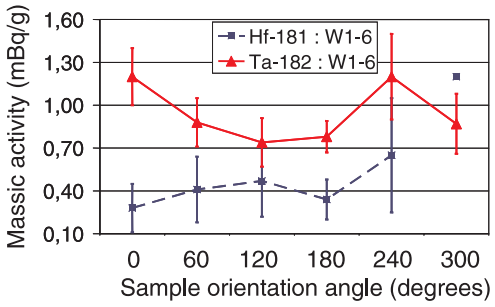

Fig. 10. The ^{181}Hf and ^{182}Ta angular distribution of the massic activity in mBq/g for the W1-6 samples.

Manganese-54 was most probably due to the neutron activation of sample impurities. In particular, the reaction $^{54}Fe(n,p)^{54}Mn$ is a highly likely production route. Manganese-54 was found in basically all the TiTop (titanium) and B_4C (boron carbide) samples but only in a few other samples. A nuclear activation analysis (NAA) of the samples was performed in a fission reactor in order to determine the level of impurities. The Fe impurity level was found to be the highest at 734 ± 35 mg/kg for the Ti sample, 600 ± 180 mg/kg for the B_4C sample, and much lower for all the other samples. Manganese-54 could also be deposited on sample surfaces as Ni, Cr, and Fe are elements usually eroded from the main chamber of JET due to sputtering by energetic charge-exchange neutrals.[6]

Four cobalt radionuclides were detected: ^{56}Co, ^{57}Co, ^{58}Co, and ^{60}Co. The ^{60}Co was detected on only one

sample (W5). The ^{58}Co was most probably due to neutron activation of sample impurities. $^{58}\mathrm{Ni}(n,p)^{58}\mathrm{Co}$ is a significant reaction for the production of ^{58}Co. The ^{58}Co was found in all the Ti and TiTop (titanium) samples but only scarcely in a few other samples. The measured level of ^{58}Co in the Ti samples was found consistent with the typical value for Ni impurity concentration.

Cobalt-56 and cobalt-57 were detected in B_4C (boron carbide) and LiF (lithium fluoride) samples at a level approximatively ten times less than ^{58}Co. Deposition on sample surfaces and/or production from charged particles are both likely pathways. Possible activation reactions for ^{56}Co are $^{58}\mathrm{Ni}(d,\alpha)^{56}\mathrm{Co}$, $^{54}\mathrm{Fe}(\alpha,np)^{56}\mathrm{Co}$, $^{56}\mathrm{Fe}(p,n)^{56}\mathrm{Co}$, $^{56}\mathrm{Fe}(d,2n)^{56}\mathrm{Co}$, and $^{57}\mathrm{Fe}(p,2n)^{56}\mathrm{Co}$. Possible activation reactions for ^{57}Co are $^{58}\mathrm{Ni}(n,d)^{57}\mathrm{Co}$, $^{58}\mathrm{Ni}(n,np)^{57}\mathrm{Co}$, $^{58}\mathrm{Ni}(d,n+2p)^{57}\mathrm{Co}$, $^{58}\mathrm{Ni}(p,2p)^{57}\mathrm{Co}$, $^{60}\mathrm{Ni}(p,\alpha)^{57}\mathrm{Co}$, $^{54}\mathrm{Fe}(\alpha,p)^{57}\mathrm{Co}$, $^{56}\mathrm{Fe}(d,n)^{57}\mathrm{Co}$, $^{57}\mathrm{Fe}(d,2n)^{57}\mathrm{Co}$, $^{57}\mathrm{Fe}(p,n)^{57}\mathrm{Co}$, and $^{58}\mathrm{Fe}(p,2n)^{57}\mathrm{Co}$.

Antimony-124 was found only in all Ti samples with levels comparable with ^{58}Co. Antimony-124 was unexpected as it had never been observed previously in tokamaks, e.g., from the postanalysis of in-vessel plasma-facing components. Antimony-124 was most probably due to neutron activation of impurities in titanium samples. $^{123}\mathrm{Sb}(n,\gamma)^{124}\mathrm{Sb}$ has a high cross section and is therefore a very significant production channel. The level of Sb impurities in the samples was measured with NAA. The NAA analysis gave a level of 9.9 ± 0.4 mg/kg in titanium and two to three orders of magnitude less in all other samples. This level is sufficiently high to yield the observed level of ^{124}Sb and thus confirms neutron activation as the production mechanism.

VI. SUMMARY

Charged-particle losses were observed for the first time in JET plasmas with a D-^{3}He fuel mixture using NAA. Ultra-low-level gamma-ray measurements performed at underground laboratories helped considerably to enhance detection levels. Production pathways were determined for all the measured radionuclides. Two radionuclides (^{48}V and ^{7}Be) were identified as produced dominantly from charged-particle reactions. Quantitative data on charged-particle losses were obtained for the first time. Angular distributions with respect to the magnetic field were measured as well. Observation of ^{48}V is clear evidence of high-energy proton fluxes (energy threshold of $\sim$5 MeV) from D-^{3}He fusion reactions. The best fit to the measured data was obtained with a modeled proton energy spectrum composed of both 3.02 MeV from D-D fusion reactions and 14.7 MeV from D-^{3}He fusion reactions. A ratio between the two peaks could be calculated. Ideas to better measure the proton energy spectrum in future experiments were suggested. Finally, in view of applications to ITER and future fusion reactors, further development and optimization of the use of activation monitors is planned at JET.

ACKNOWLEDGMENTS

We gratefully acknowledge the contribution of all team members of IRMM, PTB, and Gran Sasso and the support of the JET plasma boundary group, including M. Stamp, G. Matthews, J. Vince, G. Kaveney, B. Syme, and T. Edlington. Finally, we thank R. Forrest for his help with the FISPACT code, R. Cornille for the FISPACT calculations, and P. Vermaercke. This work was carried out under the European Fusion Development Agreement.

REFERENCES

1. A. J. H DONNE et al., *Nucl. Fusion*, **47**, S337 (2007).

2. R. E. CHRIEN et al., *Phys. Rev. Lett.*, **46**, 535 (1981).

3. E. CECIL et al., *Rev. Sci. Instrum.*, **57**, 1777 (1986).

4. G. BONHEURE et al., *Rev. Sci. Instrum.*, **75**, 3540 (2004).

5. J. GASPARRO et al., *Appl. Radiat. Isot.*, **64**, 1130 (2006).

6. G. BONHEURE et al., *Phys. Scr.*, **75**, 769 (2007).

7. M. REICH et al., in *Proc. 33rd European Physical Society Conf.*, Rome, Italy, June 19–23, 2006.

8. D. DARROW et al., in *Proc. 16th High Temperature Plasma Diagnostics Conf.*, Williamsburg, Virginia, May 7–11, 2006.

9. G. BONHEURE et al., in *Proc. Int. Workshop Fast Neutron Detectors and Applications*, University of Cape Town, South Africa, April 3–6, 2006; available on the Internet at http://pos.sissa.it (2006).

10. "Monte Carlo All-Particle Transport Code," available on the Internet at www-rsicc.ornl.gov/.

11. M. HULT et al., *Appl. Radiat. Isot.*, **53**, *1–2*, 225 (2000).

12. S. NEUMAIER et al., *Appl. Radiat. Isot.*, **53**, *1–2*, 173 (2000).

13. C. ARPESELLA et al., *Appl. Radiat. Isotopes*, **47**, 991 (1996).

14. V. KIPTILY et al., *Nucl. Fusion*, **42**, 999 (2002).

15. R. A. FORREST, UKAEA FUS 534, U.K. Atomic Energy Authority (2007).

16. W. W. HEIDBRINK, PhD Thesis, Chap. 2, Princeton University (1984).

17. M. M. BE et al., *Table of Radionuclides on CD-Rom*, Version 1-98, CEA/DAMRI, 91191, Commissariat à l'Energie Atomique (1999).

Paper III

This article **was published** in Applied Radiation and Isotopes,
DOI link: doi.org/10.1016/j.apradiso.2009.01.026.

The Sandwich spectrometer for ultra low-level γ-ray spectrometry

JS Elisabeth Wieslander[1,4], Mikael Hult[1,*], Joël Gasparro[1], Gerd Marissens[1], Marcin Misiaszek[2], Werner Preusse[3]

[1]*EC-JRC-IRMM,*

Institute for Reference Materials and Measurements,

Retieseweg 111, B-2440 Geel, Belgium

[2]*M. Smoluchowski Institute of Physics, Jagiellonian University, ul. Reymonta 4, 30-059 Krakow, Poland*

[3]*Saxon State Laboratories for Environmental Radioactivity, Dresdner Str. 183, D-09131, Chemnitz, Germany*

[4]*Department of Physics, P.O. Box 35, FIN-40014 University of Jyväskylä, Finland*

Abstract

The technical details and performance of the newly developed Sandwich spectrometer for ultra low-level γ-ray spectrometry are presented. The spectrometer, which consists of two HPGe detectors, an active muon shield and a lead/copper shield with a convenient and rapid opening mechanism, is located in an underground laboratory at a depth of 225 m. The data is collected in list mode, which enables off-line data analysis to identify muon-induced events and possible Ge detector crosstalk due to Compton scattering. The background count-rate from 40 to 2700 keV normalised to the mass of the Ge crystals is 220 day^{-1} kg^{-1}.

Keywords: Ultra low-level gamma-ray spectrometry, muon, underground laboratory, HPGe detectors, low background measurements

* Corresponding Author: Phone +32 14 571 269; FAX +32 14 584 273; E-mail mikael.hult@ec.europa.eu, elisabeth.wieslander@gmail.com

1. Introduction

In the quest for lower detection limits in γ-ray spectrometry (Hult, 2007), a new spectrometer for Ultra Low-level Gamma-ray Spectrometry (ULGS) has been developed and characterized in an underground laboratory. Since the detection limit in γ-ray spectrometry is inversely proportional to the detection efficiency, it is of interest to design low-level detection systems with high efficiency. The detector presented here includes two Ge detectors facing each other between which the sample is placed: this approach effectively doubles the detection efficiency compared to using a single Ge detector. The new spectrometer design is intended for measurements of levels of activity in the mBq to μBq range in small samples. The high efficiency allows faster measurements, which is suitable for a wide range of applications.

2. Properties of the Sandwich spectrometer

The Sandwich spectrometer is located in the underground laboratory HADES (Hult et al., 2006 and 2003) at a depth of 500 metres water equivalent and located at the premises of the Belgian nuclear Centre SCK•CEN in Mol, Belgium. Fig. 1 shows a side and a top view of the Sandwich spectrometer while the electronics are described in Fig 2.

During the design process for the Sandwich spectrometer extra attention was paid to the following points that affect system performance:

- Use of radiopure materials for the detectors and shielding.
- Radon reduction by minimising the empty cavities inside the shield and by flushing with liquid nitrogen boil-off from the two dewars.
- Easy access for changing samples as well as installing/removing detectors.

2.1. HPGe detectors

The technical details of the two coaxial p-type HPGe detectors in Fig.1, Ge-6 and Ge-7, are listed in Table 1. The samples are placed on Ge-6, which is always in a fixed position. Ge-7 can be moved vertically to accommodate bigger or smaller samples, which minimises not only the distance to the sample for both detectors but also the amount of air inside the measurement volume.

The relatively thick dead layer of Ge-6 in combination with the Cu endcap has the advantage of lower background and summing effects from low energy x-rays. The benefit of the Al endcap of Ge-7 in combination with the thin dead layer of its crystal is

generally improved detection limits for γ-rays below 100 keV. Both detectors were well calibrated since they had been in use in the underground laboratory before they were installed in the Sandwich spectrometer, for which they were made available. Due to the multifunctional design of the lead shield, the Ge-detectors can easily be exchanged if necessary.

2.2. Lead shield with Cu lining

The lead for the Sandwich spectrometer was produced by the Polish company Plombom and cast in the right shape by the company Von Gahlen. The innermost part of the lead shield is 4.0 cm thick with an activity of 2.5 Bq/kg (^{210}Pb) while the outer part of the shield is 14.5 cm thick with an activity of 20 Bq/kg (^{210}Pb).

To achieve lower background there is a 3.5 cm thick lining of radiopure electrolytic Cu closest to the measurement volume, within the lead shield, that shields against radiation from ^{210}Pb in the lead. The activity of ^{60}Co in freshly produced electrolytic copper could not be detected in a small test sample, so an estimate based on the fact that the copper was stored above ground for less than three weeks indicates that the ^{60}Co activity should be less than 15 μBq/kg (Laubenstein and Heusser, 2009). The activity of ^{228}Th in the electrolytic copper is estimated to be less than 20 μBq/kg.

The lead shield splits in two when it is opened, see Fig. 1b, and the front part is motor-driven along a rail which gives the advantage of making it fast and easy to open the shield to access samples and detectors. The diameter of the sample volume is slightly bigger than the diameter of the endcaps of the two Ge detectors, which is 102 mm. The upper Ge-detector (Ge-7) can be vertically moved in steps of 0.1 mm, resulting in a sample cavity height between 0 mm and 70 mm.

2.3. Active muon shield

Directly on top of the lead shield are two plastic scintillators (PS) as depicted in Fig. 1a and with details as listed in Table 2. The detectors are 2.54 cm thick and cover an area of 80 × 80 cm^2. Fig. 2 shows all Sandwich spectrometer electronics, including the coincidence circuit used for the hardware muon-gating pulse and the connection to the DAQ2000 multi-parameter system. The scintillator detectors are not shielded, which inevitably results in accidental coincidences originating from the environmental γ-background. Compared to the energy deposited by the muons, the γ-background is

located in the low energy part of the spectrum and the hardware coincidence criteria reduce the background as seen in Fig. 3. The LLD (low level discriminator) on the ADC is set high enough to filter out most of the γ-background but low enough to clearly see the valley between the muon and gamma background parts of the spectrum. The final muon signal is obtained by cutting off the γ-background at channel 840 in Fig. 3 during the off-line data analysis. Muons depositing high energy in the detectors cause saturation of the amplifier output and these are counted and collected at the end of the spectrum.

2.4. Electronics

The electronics included in the Sandwich spectrometer, see Fig. 2, consist of standard NIM modules together with the DAQ2000 multi-parameter system. The DAQ2000, which is based on LabView and designed and manufactured by IRMM, registers up to four input channels and time-stamps all events with 100 ns time resolution.

The coincidence signal from the two plastic scintillators is used as a hardware gating signal *only* for the muon spectrum from the lower plastic scintillator, PS4. *The coincidence circuit ensures that only gated signals are sampled from PS4 while all data from the two Ge detectors is collected*. For every event in any of the three detectors, Ge-6, Ge-7 or PS4, the time stamp is registered and the signal from all three detectors is read. There is no hardware delay ensuring that the signals from the Ge detectors and the plastic scintillator arrive at the same time. This is not needed because the coincidence criterion is set in the software during off-line analysis.

3. Data analysis and background reduction

The output from the DAQ2000 multi-parameter system consists of files with time-stamped list-mode data in binary format. The list files are converted to the CERN standard for ROOT files (CERN, 2008) and the data is analysed using a custom-made software tool based on the ROOT environment. Since all events are collected and time-stamped, there are many choices for the off-line data analysis. The software is used for the usual γ-ray measurement analysis, for summing spectra from many measurements, performing energy calibration, studying time-interval distributions and finding coincidences or anti-coincidences between detectors for any chosen time window. Using the software, the coincidences with the muons are filtered out from the Ge detectors spectra, i.e. the muon-induced events are removed. The time window between the arrival of the signal from the plastic scintillator to the arrival of the slower pulse from the Ge

detectors used for these anti-coincidences can be selected freely. In this work it is taken to be 1 ms. The crosstalk due to Compton scattering between the two Ge detectors can also be reduced with software analysis.

3.1. Uncertainties

The uncertainties are expressed as combined standard uncertainties following the BIPM Guide to the Expression of Uncertainty in Measurement (1995) while detection limits and decision thresholds are in accordance with ISO 11929-3 (2000), see Table 3. All results are compared to the decision threshold using $\alpha = 0.05$. The uncertainty is given in brackets after each measurement value and the last digit(s) of their numerical value correspond(s) to the last digit(s) of the quoted result. The major contribution to the uncertainty budget in this work originates from counting statistics. The reference date and measurement times must be precisely recorded.

4. The Sandwich Spectrometer performance

4.1. Solid angle

The maximum solid angle for the Ge detectors in the Sandwich spectrometer has been calculated to 3.0 sr (corresponding to 24% of 4π) using the following approximations:

- The end-caps of the two detectors are so close that they touch each other.
- An infinitesimally thin sample of 1 cm in diameter is placed between the end-caps, i.e. in contact with each detector's end-cap.
- The dead layers are excluded in the calculation of the solid angle and only the active crystal volume is included.

4.2. Efficiency

Generally, the FEP (full energy peak) efficiency for a given sample is a factor of two higher for the Sandwich spectrometer as compared to a single Ge detector. For examples see the decay data measurements of a thick tantalum metal disc given by Hult et al. (2009).

4.3. Muons in HADES

The average count-rate of muons in the active muon shield of the Sandwich spectrometer, see Fig. 3, is 0.138 muons m^{-2} s^{-1} during the period July 2007 to May 2008. The count-rates of muon-induced events in the two Ge detectors are 72 muons day^{-1} and 52 muons day^{-1} for Ge-6 and Ge-7 respectively.

4.4. Background reduction with the active muon shield

In Fig. 4 the background spectrum for the Sandwich spectrometer is shown without the muon-induced events. The events that were filtered out are shown in Fig. 5. The background count-rates of the Sandwich spectrometer in the energy interval 40-2400 keV are 992 counts day^{-1} with the muons included and 868 counts day^{-1} without muons, the muons being 124 counts day^{-1}, see Table 3. Extrapolating the background from 2400 keV to 2700 keV enables comparison with other underground spectrometers. The count-rate normalised to the Ge-crystal mass in the region 40-2700 keV is 220 day^{-1} $kg_{(Ge)}^{-1}$, which is lower than the previous best detector in the HADES laboratory: Ge-3 with a background index of 280 day^{-1} $kg_{(Ge)}^{-1}$. During the measurement of a tantalum sample with a diameter of 100 mm (Hult et al., 2009) the count-rates were reduced by about 10% compared to the background, especially below 500 keV due to the shielding effect of the tantalum sample that was 12 mm thick. Generally the background count-rates from the two detectors are very similar, the major contribution being the ^{222}Rn daughters. It is likely that the main source of the ^{222}Rn daughters is ^{226}Ra inside the detectors. The 186 keV peak from ^{226}Ra is below the detection limits in the background measurements but can be seen in the sum spectrum from the tantalum measurements (Hult et al., 2009), which leads to the conclusion that the contribution to the background from ^{222}Rn transported via air from outside the shield is not a major factor.

5. Discussion

The new Sandwich spectrometer with its high efficiency and low background is faster in producing results and is ideal for many applications involving small samples or radionuclides with relatively short half-lives. In several applications it is necessary to measure activation products in small metal samples, such as: (i) neutron cross-section measurements using the traditional activation approach (Reimer et al., 2002), (ii) neutron cross-section curve measurements using broad beams (Lövestam et al., 2007), (iii) fast neutron spectrum characterisation using the DONA technique (dosimetry using neutron activation) (Lövestam et al., 2008), (iv) samples activated by charged particle leakage from fusion plasma (Wieslander et al., 2008) and decay measurements of rare decays such as in ^{180m}Ta (Hult et al., 2009) or the ββ-decay in Sn (Dawson et al., 2008). The Sandwich spectrometer is also an efficient way of using resources, since less lead and copper is needed in comparison to two single systems. Based on the experiences from this spectrometer, the next generation of HADES Sandwich spectrometers is being designed. The developments include a larger sample cavity, for which it is necessary to

further develop the active radon-reduction inside the shield. In addition to enabling measurements of larger volume samples, a larger sample cavity would also open up the possibility of placing other types of detectors, such as small scintillator cells, inside the shield for special coincidence or anti-coincidence measurements.

Acknowledgements

The work done by EURIDICE and the HADES crew of SCK•CEN in Mol, Belgium, is gratefully acknowledged.

References

CERN, 2008.< www.root.cern.ch/ >, accessed 2008.

Dawson, J., Degering, D., Kohler, M., Ramaswamy, R., Reeve, C., Wilson, J.R., Zuber, K., 2008. Search for double beta decays of tin isotopes with enhanced sensitivity. Accepted for publication in Physical Review C.

Hult, M., 2007. Low-level gamma-ray spectrometry using Ge-detectors. Metrologia 44, S87-S94. (Erratum in Metrologia 44, 425.)

Hult, M., Gasparro, J., Johansson, L., Johnston, P.N., Vasselli, R., 2003. Ultra sensitive measurements of gamma-ray emitting radionuclides using HPGe-detectors in the underground laboratory HADES. Royal Society of Chemistry, Cambridge, UK. Environmental Radiochemical Analysis II, 375-382.

Hult, M., Preuße, W., Gasparro, J., 2006. Underground Gamma-ray spectrometry. Acta Chimica Slovenica 53, 1-7.

Hult, M., Wieslander, J.S.E., Marissens, G., Gasparro, J., Wätjen, U., Misiaszek, M., 2009. Search for the radioactivity of ^{180m}Ta using an underground HPGe sandwich spectrometer. Applied Radiation and Isotopes, these proceedings.

ISO/IEC/OIML/BIPM, 1995. Guide to the expression of uncertainty in measurement, (1st corrected edition). International Standard Organisation, Geneva, Switzerland.

ISO, 11929-3, 2000. Determination of the detection limit and decision threshold for ionising radiation measurements – Part 3. 1st edition. International Standards Organisation, Geneva, Switzerland.

Laubenstein, M., Heusser, G., 2009. Cosmogenic radionuclides in metals as indicator for sea level exposure. Applied Radiation and Isotopes, these proceedings.

Lövestam, G., Hult, M., Fessler, A., Gamboni, T., Gasparro, J., Geerts, W., Jaime, R., Lindahl, P., Oberstedt, S., Tagziria, H., 2007. A novel technique for measuring neutron activation cross section curves. Nucl. Instr. Meth A. 580, 1400-1409.

Lövestam, G., Hult, M., Fessler, A., Gasparro, J., Kockerols, P., Okkinga, K., Tagziria, H., Vanhavere, F., Wieslander, J.S.E. Neutron fluence spectrometry using disk activation. Submitted for publication in Radiat. Meas.

Reimer, P., Hult, M., Plompen, A.J.M., Johnston, P. N., Avrigeanu, V., Qaim, S.M., 2002. Measurement of the ^{nat}Mo(n, x)^{94}Nb cross section using ultra low-level γ -ray spectrometry at HADES. Nuclear Physics A 705, p. 265–278.

Wieslander, J.S.E., Hult, M., Bonheure, G., Arnold, D., Dombrowski, H., Gasparro, J., Laubenstein, M., Marissens, G., Vermaercke, P., 2008. Low-level gamma-ray spectrometry for analysing fusion plasma conditions. Nucl. Instr. Meth. A 591, 383-393.

Fig. 1. The sandwich spectrometer set-up including dimensions a) side view, b) top view.

Fig. 2. The Sandwich spectrometer's electronics set-up showing how the two plastic scintillators, PS3 and PS4, and the two HPGe detectors, Ge-6 and Ge-7, are connected to the DAQ2000 multi-parameter system.

Fig. 3. The muon spectrum in HADES using the coincidence signal from PS3 and PS4 as gate for the spectrum from PS4.

Fig. 4. The background spectrum from the Sandwich spectrometer with the Ge detectors Ge-6 and Ge-7 summed together and the muon-induced events filtered out.

Fig. 5. The energy spectrum of muon-induced events which are filtered out from the background spectrum Fig. 4.

Table 1. Details of the two HPGe detectors included in the Sandwich spectrometer set-up.

Details	Ge-6	Ge-7
Crystal diameter × thickness (cm)	7.80 × 8.40	8.05 × 6.65
Detector relative efficiency (%)	80	90
FWHM at 1332 keV (keV)	2.3	2.2
Dead layer (front)	0.9 mm	0.3 μm
End-cap material	Cu	Al
Bias voltage (Volt)	+ 3000	+ 4500
Year of manufacturing / refurbished	2004	2004 / 2007

Table 2. Details of the plastic scintillators from Scionix, PS3 and PS4, included in the active muon shield.

Details	**PS 3**	**PS 4**
Model Number	R25 x 800 B 800 / 2M – X + VD 14 – E2 with built-in Voltage divider / preamplifier	
Size (mm)	800 × 800 × 25.4	
Plastic type	EJ-200: PVT (Polyvinyltoluene)	
Rise / Decay time (ns)	0.9 / 2.1	
Photomultiplier tube	Type 2" ETL 9266, diameter 51 mm, 14 pins connector, Al housing	
Maximum signal height (Volt)	+/- 10	
Spectrum sampled	No	yes
PM high voltage (V)	+1000	+1000
Coincidence sampling	The coincidence signal between PS3 and PS4 is used as gating pulse to sample the muon spectrum from PS4.	

Table 3. List of background γ-ray peaks in the Sandwich detector with the uncertainties in brackets. The last rows show the count-rate in the background for different energy ranges, with the number of removed muons in brackets.

Eγ (keV)	**Radionuclide**	**Ge-7 without muons** (counts day^{-1})	**Ge-6 without muons** (counts day^{-1})
46	^{210}Pb	2.1 (3)	< 0.5
63	^{234}Th	< 0.6	< 0.6
93	^{234}Th	< 0.6	< 0.6
186	^{226}Ra + ^{235}U	< 0.7	< 0.7
238	^{212}Pb	2.2 (3)	2.1 (4)
242	^{214}Pb	0.34 (25)	< 0.8
295	^{214}Pb	0.70 (29)	0.56 (26)
338	^{228}Ac	0.28 (17)	< 0.6
351	^{214}Pb	2.1 (3)	2.3 (3)
511	Annihilation	2.51 (28)	2.9 (4)
583	^{208}Tl	1.05 (19)	0.61 (19)
609	^{214}Bi	2.37 (25)	2.5 (0.3)
661	^{137}Cs	< 0.3	< 0.4
911	^{228}Ac	0.48 (14)	0.79 (20)
969	^{228}Ac	0.22 (11)	0.26 (14)
1120	^{214}Bi	0.50 (13)	0.86 (19)
1173	^{60}Co	1.44 (17)	0.85 (18)
1332	^{60}Co	1.24 (16)	1.32 (20)
1460	^{40}K	1.31 (16)	0.84 (17)
1764	^{214}Bi	0.41 (10)	0.72 (14)
40-2400 keV		428 (72 muons)	441 (52muons)
40-400 keV		264 (35 muons)	268 (39 muons)
400-1400 keV		136 (28 muons)	145 (19 muons)
1400-2400 keV		28 (9 muons)	28 (5 muons)
Measurement time		46.4 days	63.4 days

Fig. 1a

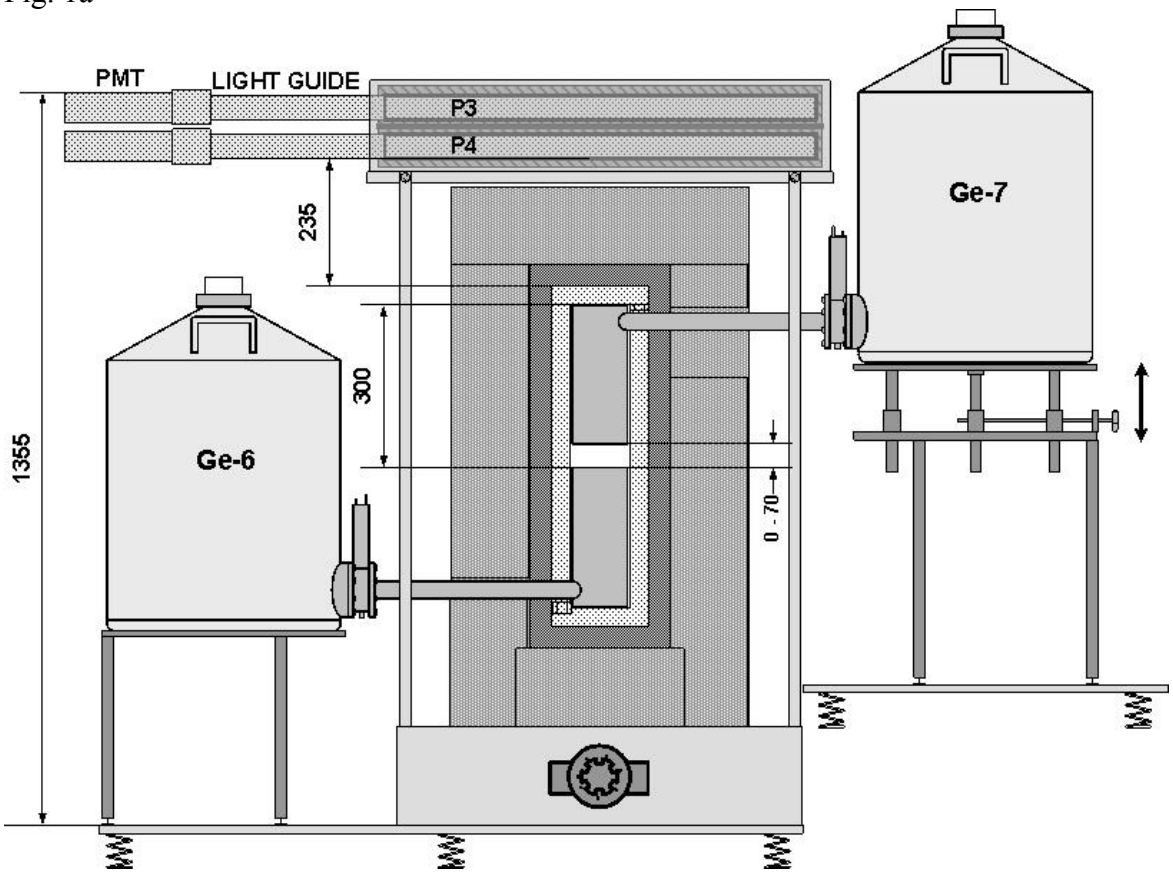

Fig. 1b

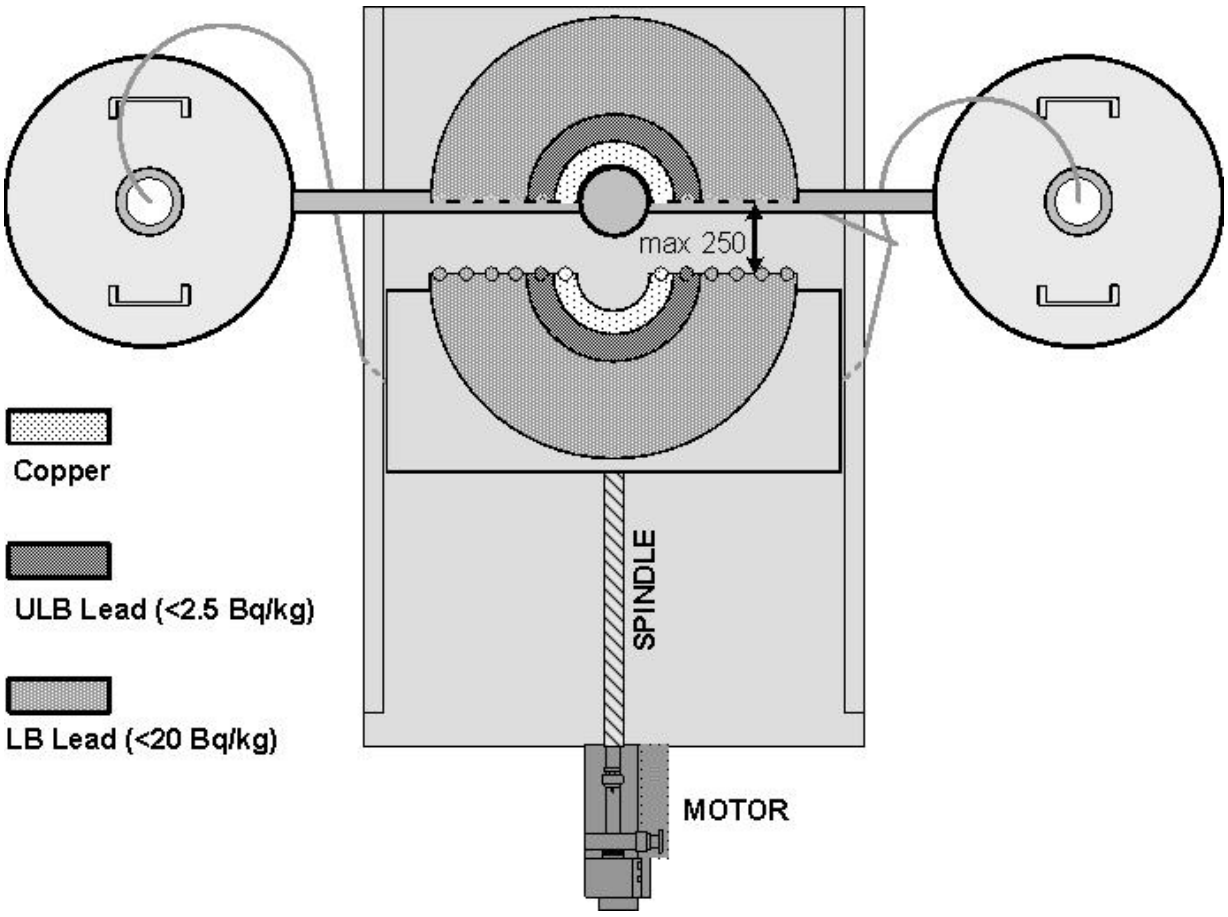

Fig. 2

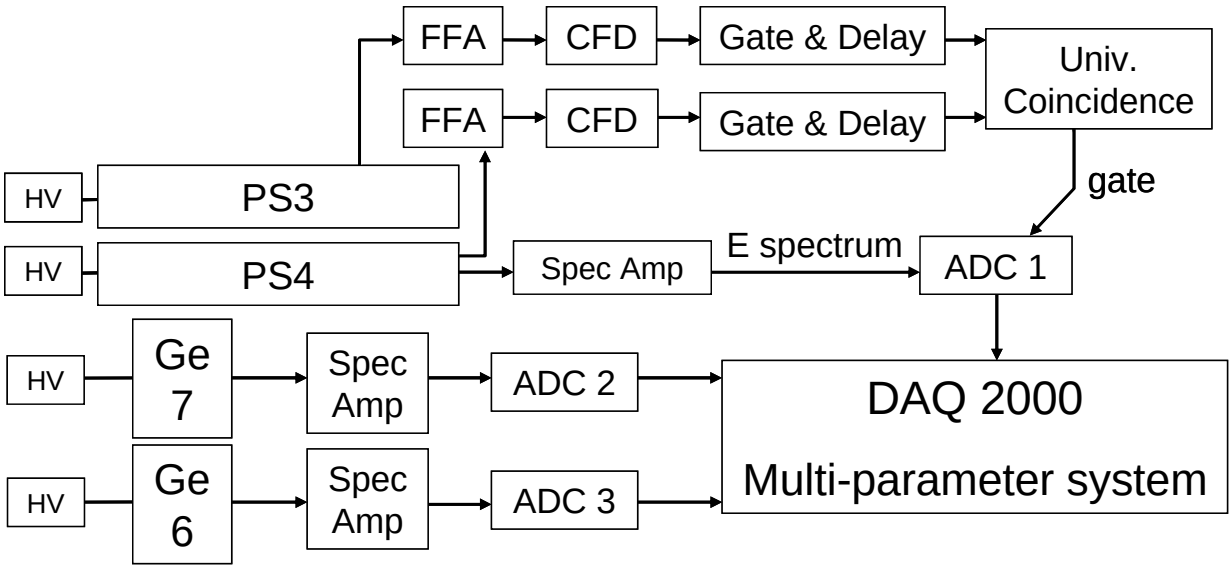
FFA
CFD
Gate & Delay
Univ.
Coincidence
FFA
CFD
Gate & Delay
HV
PS3
gate
HV
PS4
Spec Amp
E spectrum
ADC 1
HV
Ge
7
Spec
Amp
ADC 2
DAQ 2000
Multi-parameter system
HV
Ge
6
Spec
Amp
ADC 3

Fig. 3

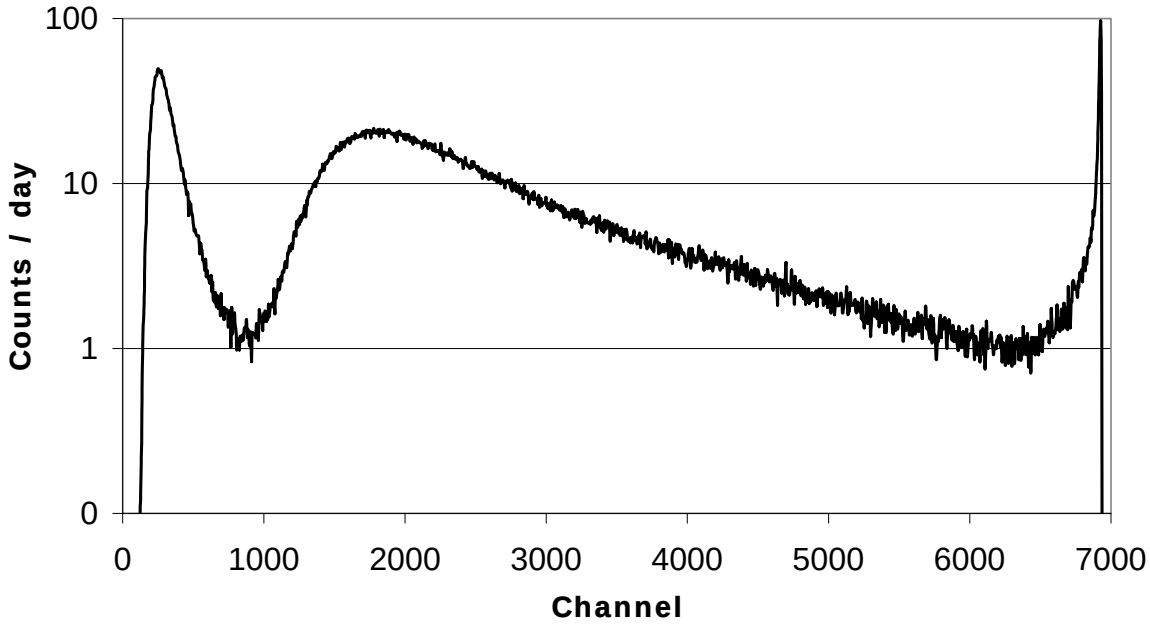
100
10
1
0
Counts / day
0
1000
2000
3000
4000
5000
6000
7000
Channel

Fig. 4

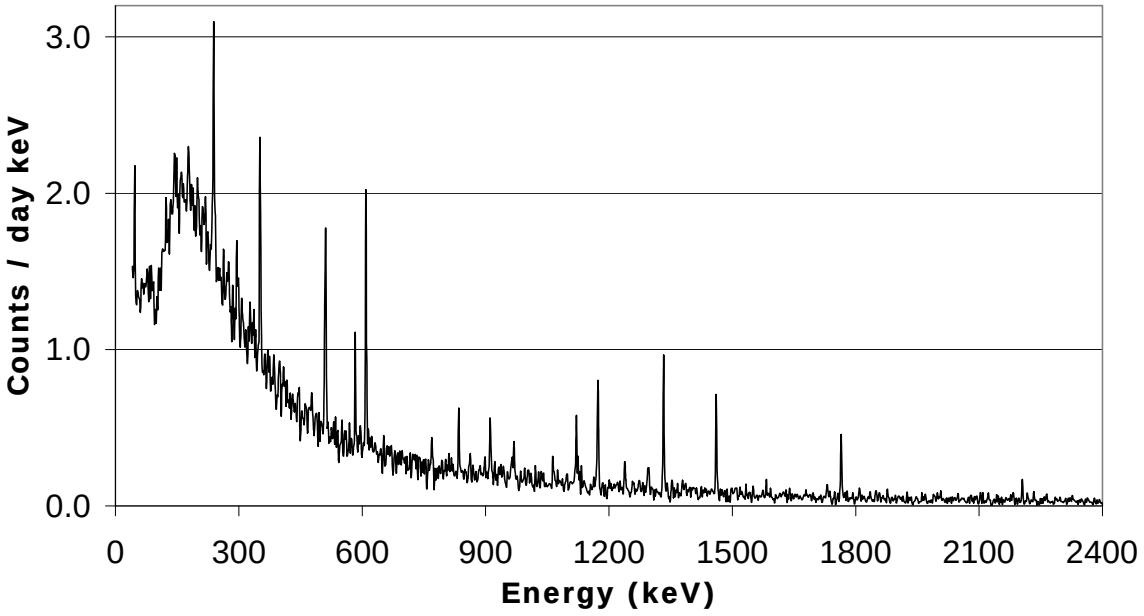
3.0
2.0
1.0
0.0
Counts / day keV
0
300
600
900
1200
1500
1800
2100
2400
Energy (keV)

Fig. 5

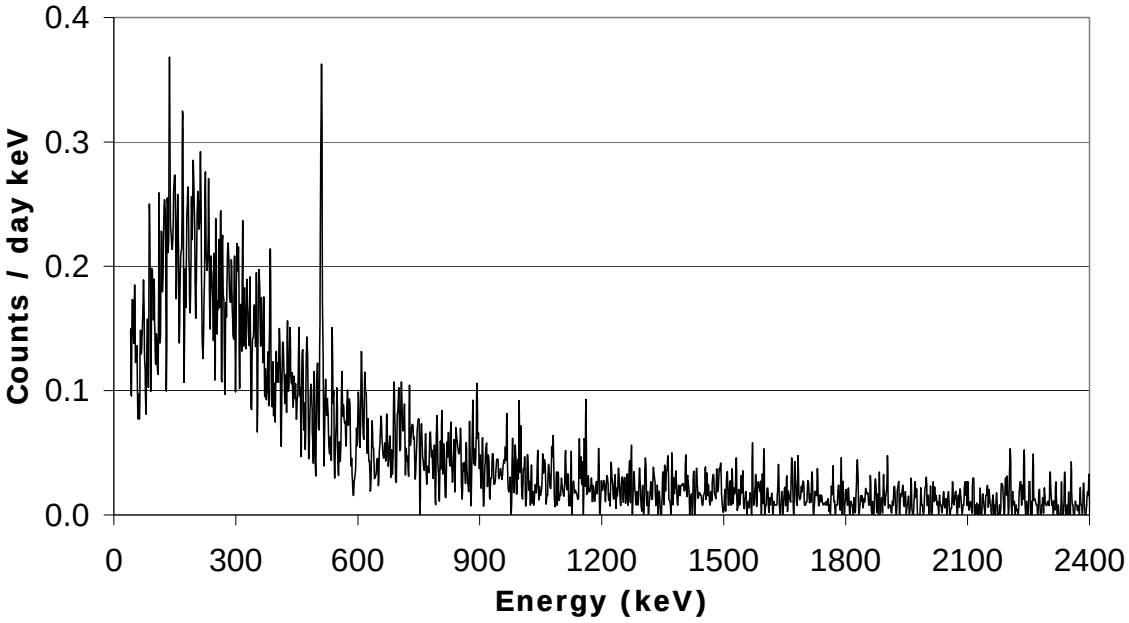
0.4
0.3
0.2
0.1
0.0
Counts / day keV
0
300
600
900
1200
1500
1800
2100
2400
Energy (keV)

Paper IV

This article **was published** in Applied Radiation and Isotopes.
DOI link: doi:10.1016/j.apradiso.2009.01.057

SEARCH FOR THE RADIOACTIVITY OF ^{180m}Ta USING AN UNDERGROUND HPGe SANDWICH SPECTROMETER

Mikael Hult[1, *], J. S. Elisabeth Wieslander[1,3], Gerd Marissens[1], Joël Gasparro[1], Uwe Wätjen[1], Marcin Misiaszek [2]

[1]*European Commission, Joint Research Centre, Institute for Reference Materials and Measurements, Retieseweg 111, B-2440 Geel, Belgium*

[2]*M. Smoluchowski Institute of Physics, Jagiellonian University, ul. Reymona 4, 30-059 Krakow, Poland*

[3]*Department of Physics, P.O. Box 35 (YFL), FIN-40014 University of Jyväskylä, Finland*

Abstract

The radioactivity of ^{180m}Ta has never been detected. This attempt to detect it was carried out using a newly developed HPGe sandwich spectrometer installed 225 m underground in the HADES laboratory. The sample consisted of 6 disks of tantalum of natural isotopic composition with a total mass of 1500 g and a total mass for ^{180}Ta of 180 mg. The sample was measured for 68 days and the resulting lower bound for the half-life of ^{180m}Ta was 2.0×10^{16} y, which is a factor of 2.8 higher than the previous highest value.

Keywords: low-level, underground, tantalum, 180m, half-life, gamma-ray spectrometry, muons

---

[*]Corresponding author: Mikael Hult, EC-JRC-IRMM, Retieseweg 111, B-2440 Geel, Belgium, Tel. No. +32-14-571269, Fax No. +32-14-584273, mikael.hult@ec.europa.eu

1. Introduction

Tantalum-180m is a radionuclide that has generated a lot of interest in recent years for various reasons. The ground state of ^{180}Ta has a short half-life of only 8.1 h but its metastable state is the most long-lived metastable state known to man. Tantalum-180 is the rarest isotope of nature's rarest element and its isotopic abundance was measured recently with high precision by de Laeter and Bukilic (2005) to only 0.01201(8)%. This gives a Solar System abundance of ^{180m}Ta of 2.49×10^{-6} where the reference Si equals 10^6. Recent interest for this nuclide has been due to its potential use in gamma-ray lasers (Carroll, 2007; Coussement et al., 2004) and the debate on its production in the stellar nucleosynthesis (Moher et al., 2007; Loewe et al., 2003) as well as its wide use in studies of nuclear structures of nuclei with high spin state (Wendel et al., 2001).

The decay scheme of ^{180m}Ta can be considered to be well understood and was recently (2003) updated in the ENSDF data base, (Nuclear Data Sheets, 2008). The part of the decay scheme essential for this investigation is presented in Fig. 1. The decay is composed of an electron capture branch and a β^--decay branch. There is also the possibility for isomeric transition from the 9^+ level to the 2^+ or 1^+ levels. Norman (1981) claims that the decay by isomeric transition should have a half-life greater than 10^{27} y and that the β decays are expected to have higher probabilities.

The radioactivity of ^{180m}Ta is yet to be detected. There are eight attempts to detect it reported in literature (Hult *et al.*, 2006) starting shortly after it was first discovered in 1955 by White, Collins and Rourke. Presently, the highest value for the lower bound of the half-life is 7.1×10^{15} y. This value was determined in the first underground measurement of the nuclide although the experiment was not optimised for this task (Hult *et al.*, 2006). The experiment reported here was the first ever underground measurement specially designed for searching for the decay of ^{180m}Ta. The measurement was carried out using a newly developed HPGe sandwich spectrometer (Wieslander et al., 2009) installed in the underground laboratory HADES, which is located 225 m underground.

2. Materials and Methods

2.1 Sample

The sample consisted of 6 disks of high purity tantalum of natural isotopic composition. The disks were 1 dm in diameter and together they had a mass of 1500.33 g. Using the natural isotopic abundance of 0.01201% (de Laeter and Bukilic, 2005) gives the total mass for ^{180}Ta of 180 mg. This is to be compared with 73 mg used in the previous underground experiment (Hult et al., 2006) and 8 mg used in the enriched sample by Cumming and Alburger (1985). In order to minimise the background contribution from surface impurities the Ta disks underwent a thorough surface cleaning procedure in a bright dipping solution. This procedure involved degreasing in Perchloroethylene, ultrasound rinsing in soapy solutions as well as in ultrapure water, immersion and stirring in the bright dipping solution, rinsing several times with ultra pure water and finally drying in ethylic alcohol. This cleaning resulted in a drastic change in surface colour from grey to silver and a loss of mass of 10%. The disks were kept almost 2 years in HADES prior to starting the measurement in order to reduce the activity of the cosmogenically produced ^{182}Ta (half-life: 114 d). However, during disk cleaning the disks spent 3 weeks above ground 3.5 months prior to commencing the measurements. This generated some ^{182}Ta that contributed to the background of this measurement.

2.2 Detection system

The measurements took place in the HADES underground laboratory (Hult et al., 2006), which is operated by EURIDICE (European Underground Research Infrastructure for Disposal of nuclear waste In Clay Environment) and located at the premises of the Belgian Nuclear Centre SCK•CEN in Mol, Belgium

The tantalum sample was placed between two ultra low-background HPGe-detectors as depicted in Figure 2. The shape of the sample enabled a very tight fit and thus minimizing the air volume inside the shield, which consequently limited the radon induced background. The average radon activity concentration in the laboratory was 7 Bq/m^3 during the measurement. Inside the detector-shield, the radon level is expected to be lower than 7 Bq/m^3 because of the flushing with boil-off nitrogen from

the Dewars. For this measurement two p-type coaxial crystals were used. The upper detector (Ge-7) has a submicron deadlayer (~ 0.3 μm) and a relative efficiency of 89.4%. The lower detector (Ge-6) has a deadlayer of 0.9 mm and a relative efficiency of 80.5%. The germanium sandwich spectrometer is described in detail by Wieslander et al. (2009). The background reduction is achieved through (i) placement of the system underground at 500 m water equivalent (w.e.), (ii) use of two plastic scintillators as a muon shield and (iii) time stamped list-mode data in order to enable anti-coincidence background reduction off line from e.g. Compton scattering.

Spectra were collected in 24 h intervals and an energy calibration was performed generally every 7 days. All spectra were looked at and checked for inconsistencies and energy calibration. The measurements were interrupted at several occasions in order to measure samples from other projects so the time difference between the first spectrum and the last spectrum was 258 days. The energy calibration was very stable over each measurement period for one or two weeks. But due to change of hardware the energy calibration changed at some occasions of the 258 day period. This was taken care of by adding spectra after converting the x-axis to energy in keV.

2.3 Efficiency calculation

The full energy peak (FEP) efficiencies per decay were calculated using the Monte Carlo code EGS4. A computer model of the sandwich spectrometer that was used in the Monte Carlo code was based on radiographs of the detectors. The thicknesses of the deadlayers on the front, side and back of the HPGe-detectors in the model were adjusted in an iterative procedure in which the FEP efficiency for a number of point sources measured at three different distances were compared with the efficiency calculated using the Monte Carlo code. The iterative procedure was stopped when the relative differences were better than 3%. The computer simulation also contained the complete decay scheme of ^{180m}Ta including conversion and X-rays. The expected cascading gamma-rays following the decay of ^{180m}Ta will result in a loss of counts in the FEP peaks due to coincidence summing. For a small sample in a well detector (Cumming and Alburger, 1985) it would be advantageous to detect the sum peaks. In this case, the large sample and sandwich design with independent detection using two detectors favored detection of the single lines. The efficiencies for the two major sum peaks are also stated in Table 1. This approach has been validated by using

a ^{176}Lu reference source consisting of a liquid solution with 8.95 g of $LuCl_3 \cdot 6(H_2O)$ of natural isotopic abundance (104 mg of ^{176}Lu). It was contained in a cylindrical Teflon container with an O-ring seal. The inside of the container was 80 mm in diameter and 10 mm in height, while the outside measures where 110 mm and 14 mm, respectively. ^{176}Lu has a long half-life ($3.6 \cdot 10^{10}$ y) and a decay scheme for the β^- decay that is similar to that of ^{180m}Ta. The relative difference of the calculated and measured full energy peak (FEP) efficiencies for the peaks at 88 keV, 202 keV and 307 keV were 12%, -6% and -1% respectively.

3. Results

The relevant part of the resulting sum spectrum with muon induced counts subtracted is shown in Figure 3. The resolution of the final spectrum was about 20% worse than in the previous measurement (Hult et al., 2006) due to stability problems with the electronics, which marginally degrades the data. There is no sign of the expected peaks and there were no unidentified peaks in the rest of the spectrum. The only peaks that are not amongst the normal background peaks are from ^{182}Ta, which was produced by neutron activation in the Ta-disks when they were stored above ground. In Figure 3 (below the spectrum curve) is indicated the location of the visible background peaks. At 122 keV is a peak-like structure that is likely to be attributed to background from ^{57}Co located in copper parts and possibly also in the Ge-crystals as that peak is also seen (but below decision threshold) in the background spectrum. It is worth noting that the count-rate in the region below 300 keV is lower when the Ta-sample is present. This tells us that the sample is very radiopure and improves the shielding. The decision thresholds for the peaks in question were calculated using the formula given in the international standard with the error of first kind (α) set to 0.05 (ISO, 2000). The upper bound of the disintegration constant (λ) was calculated for each decay branch (EC or β^-) by taking the ratio of the decision threshold of the activity and the number of ^{180}Ta atoms in the sample ($n=6.0 \cdot 10^{20}$). More details on the calculation are given in the paper describing the previous underground attempt to detect the radioactivity of ^{180m}Ta by Hult et al. (2006). The resulting lower bounds for the half-life calculated for each gamma-line are presented in Table 1. Due to self-

absorption in the sample and conversion, the efficiencies for the 93.3 keV and 103.5 keV peaks, and their respective sum-peaks, are very low and consequently the corresponding half-life limits are also relatively low. The combined lower bound for each decay branch and the total half-life and the corresponding log*ft* values calculated for third-forbidden non-unique transitions are reported in Table 2. The background count-rate of the background peak at 351.9 keV from ^{214}Pb is 4.4(4) d^{-1}. In this experiment (Fig. 3) the count-rate of that peak was 4.0(4) d^{-1}, which is consistent with the background value. This peak hampers detection of the expected 350.9 keV gamma-ray[1] from ^{180}W. However, the peak count-rate is more or less equal to the count-rate of the continuous background under the peak, so the effect of the background peak is not so severe. Because of (i) the minute quantities of air near the detectors, (ii) the high purity of the thick copper lining, (iii) the low radon concentration in the laboratory air and (iv) the flushing of the sample volume with boil-off liquid nitrogen, the main contribution to this peak is expected to come from ^{226}Ra impurities inside the detectors. This should thus alleviate great variations in the background count-rate, which is also what has been observed so far with this relatively new detection system. The peak count-rates of the 242 keV and 295 keV peaks (from the decay of ^{214}Pb) were 1.3(4) d^{-1} and 2.0(2) d^{-1}, respectively, which is somewhat higher than in the background spectrum. The same applies to other radon induced background peaks at 609 keV and 1764 keV. This indicates that the count-rate in the peak at 351.9 keV is due to decay of ^{214}Pb and not ^{180m}Ta.

4. Discussion

The new sandwich spectrometer is a very useful instrument in many projects requiring detection of mBq activities and will be fully occupied for many years to come. Even so it is hoped that there will be time slots available to continue the search for the decay of ^{180m}Ta using this set-up. Another 300 days of data-taking with the present background would result in a detection limit of about 5.2×10^{16} y for the total half-life and 1.15×10^{17} y for the EC branch solely. In order to reach a total half-life limit of 10^{17} y, it would be necessary to measure during 3.75 y, assuming a constant background. This could be considered the uppermost limit of what this detection

[1] The energy of this gamma transition was until 2003 in the ENSDF evaluation with a value of 350.4 keV.

system can reach. It is possible to improve the present concept somewhat. Recent developments in producing large HPGe-crystals may continue (Hult, 2007) and the background can be reduced further. Simulations show that by using two detectors with crystals of 9 cm in diameter (instead of 8 cm as in this experiment) combined with using a bigger Ta-disk of 12 cm diameter and assuming a background reduction of a factor of 2, would result in a lower bound of the total half-life of 10^{17} y after a measuring time of 1.7 y. Should it be considered worth the effort to search beyond 10^{17} y, other more highly performing systems can be designed by using enriched samples with ^{180}Ta masses of a few hundreds of mg and/or using big detector systems used for detection of rare events like e.g. the GERDA detector (Schönert et al., 2005).

5. Conclusions

- A new underground experiment designed for measuring the decay of ^{180m}Ta could not detect its radioactivity. It resulted, however, in a new lower bound of its half-life by 2.0×10^{16} y, which is a factor of 2.8 higher than the previous lower bound.
- The present system has the possibility of increasing the lower bound of the half-life to 10^{17} y after 3.7 years of data taking.

Acknowledgements

The authors wish to acknowledge the HADES crew of EURIDICE at SCK•CEN in Mol, Belgium. Prof. Vincenzo Palmeiri and his staff at INFN, Padua, are acknowledged for performing the surface cleaning of the tantalum disks and Prof. Kai Zuber (Technical University, Dresden) and Dr. Tim Vidmar (Jožef Stefan Institute, Ljubljana) for constructive comments.

References

Carroll, J. J., 2007. Nuclear structure and the search for inducedenergy release from isomers. Nuclear Instruments and Methods in Physics Research B 261 960–964.

Coussement, R., Shahkmouratov, R., Neyens, G. and Odeurs, J., 2004. Quantum optics with gamma radiation. Europhysics News 34/5, 190.

Cumming, J. B., and Alburger, D. E., 1985. Search for the deacy of $^{180}Ta^{m}$. Physical Review C 31, 1494.

Hult, M., Gasparro, J., Marissens, G., Lindahl, P., Wätjen, U., Johnston, P.N., Wagemans, C. and Köhler, M., 2006. Underground search for the decay of $^{180}Ta^{m}$. Physical Review C 74, 054311, 1-5.

Hult, M., Preusse, W., Gasparro, J., Köhler, M., 2006. Underground Gamma-ray spectrometry. Acta Chimica Slovenica 53, 1-7.

Hult, M., 2007. Low-level gamma-ray spectrometry using Ge-detectors. Metrologia 44, No.4, S87-S94. (Erratum in Metrologia 44, No.5, 425.)

ISO, 2000. International Standard 11929-3. Determination of the detection limit and decision threshold for ionizing radiation measurements. International Standards Organization, Geneva, Switzerland.

de Laeter, J. R. and Bukilic, N., 2005. Isotope abundance of $^{180}Ta^{m}$ and p-process nucleosynthesis. Physical Review C 72, 025801.

Loewe, M., Alexa, P., de Boer, J. and Würkner, M., 2003. The ^{180}Ta production puzzle and the classical s-process. Nuclear Physics A719, 275c.

Mohr, P., Käppeler, F., and Gallino, R., 2007. Survival of nature's rarest isotope ^{180}Ta under stellar conditions. Physical Review C 75, 012802.

Norman, E.B., 1981. Half-life of ^{180}Ta. Physical Review C 24, 2334.

Nuclear Data Sheets, http://www.nndc.bnl.gov/nds/, accessed, September 25, 2008.

Schönert, S. and the GERDA collaboration, 2006. Status of the Germanium Detector Array (GERDA) for the search of neutrinoless ββ decays of 76Ge at LNGS. Progress in Particle and Nuclear Physics 57, 241–250.

Wendel, T. et al., 2001. Low-K two-quasiparticle states in ^{180}Ta. Physical Review C 65, 65.

White, F. A., Collins, T. L. and Rourke, F. M., 1955. New naturally occurring isotope of tantalim. Physical Review 97, 566.

Wieslander, J.S.E., Hult, M., Gasparro, J., Marissens, G., Preusse, W. and Misiaszek, M., 2009. An ultra low-background HPGe-detector system in a sandwich configuration. Applied Radiation and Isotopes, these proceedings.

Table 1. Half-life limits obtained from the different energy intervals of interest from the measurements of the Ta-disk. The full energy peak efficiency per decay is also shown.

Energy of expected peak (keV) and decay mode	Full energy peak efficiency per decay (%)	Lower bound of half-life (y)
93.3 (EC)	0.020(2)	3.68×10^{14}
215.3 (EC)	0.96(10)	1.44×10^{16}
332.3 (EC)	2.40(24)	4.45×10^{16}
215.3+332.3 (EC)	0.087(9)	2.39×10^{15}
103.5 (β^-)	0.035(4)	5.27×10^{14}
234.0 (β^-)	1.16(12)	1.79×10^{16}
350.9 (β^-)	2.54(25)	3.65×10^{16}
234.0+350.9(β^-)	0.099(10)	2.17×10^{15}

Table 2. The new lower bounds of the half-life and corresponding log*ft* values for ^{180m}Ta arising from this work.

	EC decay	β^- decay	Total
Lower bound for half-life (year)	4.45×10^{16}	3.65×10^{16}	2.0×10^{16}
Lower bound for log*ft*	24.1	22.9	

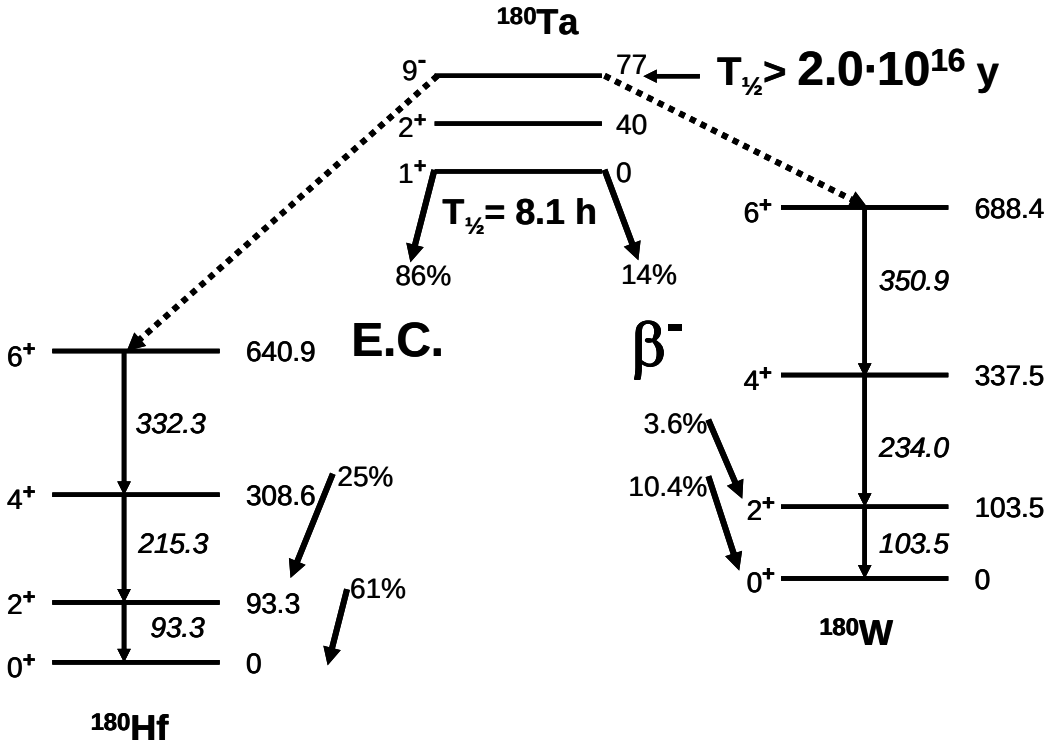

Figure 1. The decay scheme of ^{180}Ta

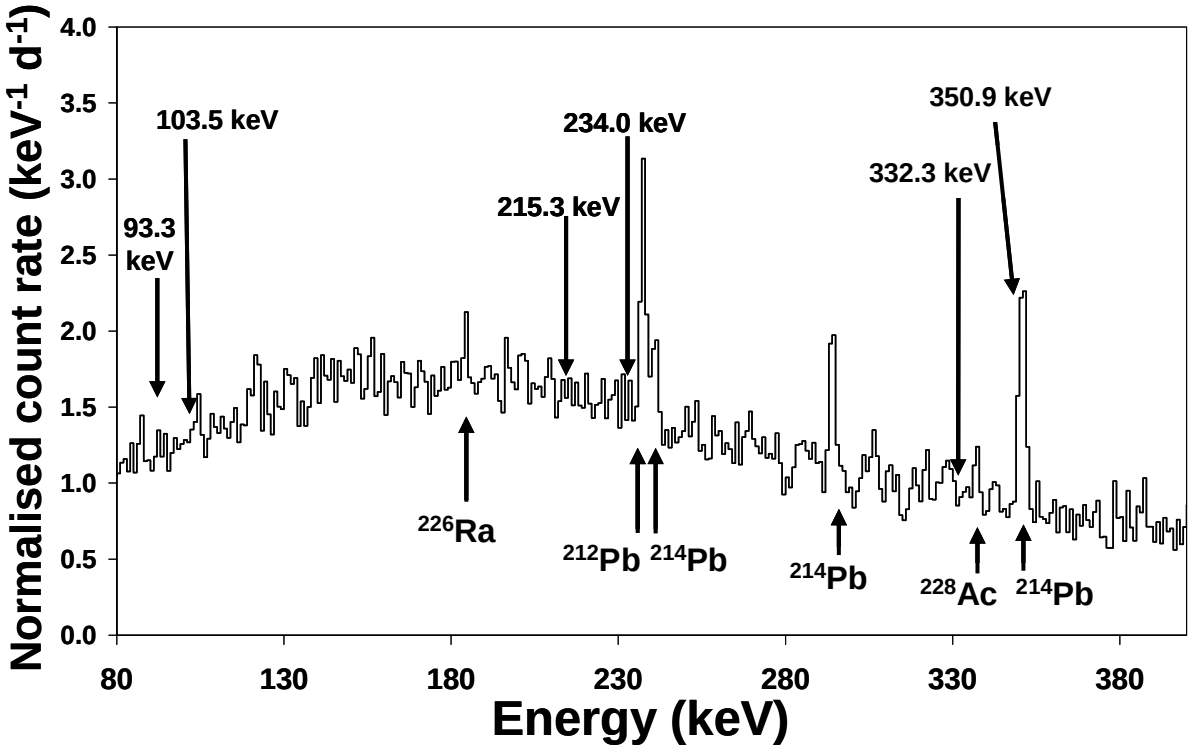

Figure 3. The part of the γ-ray spectrum collected for 68 days that encompasses the energy regions with the γ-rays expected from the decay of ^{180m}Ta. The spectrum has been re-binned to enhance visibility. The peaks are all from background of the naturally occurring decay chains and the radionuclides being the major contributors to those peaks are indicated.

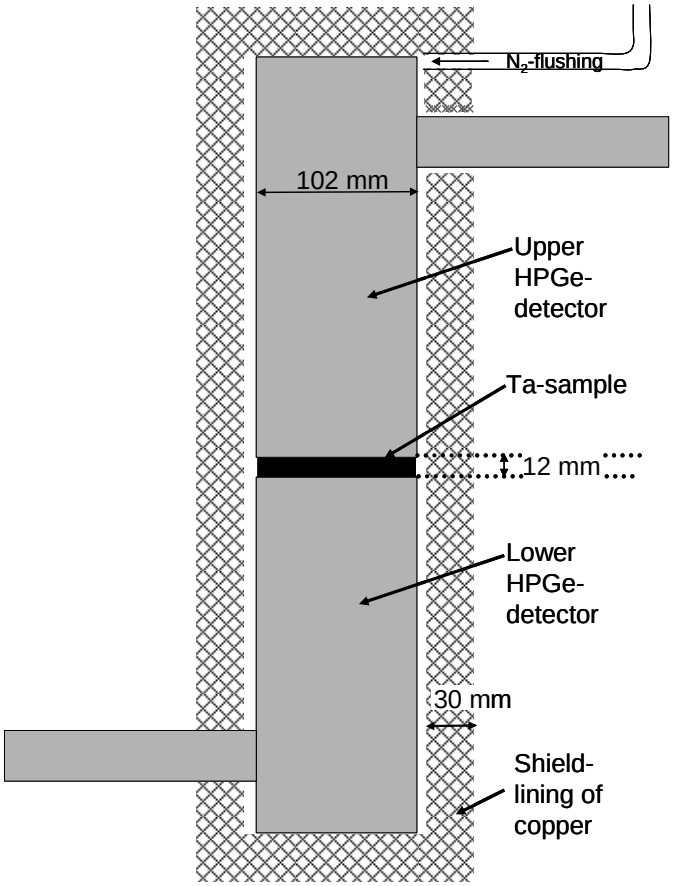

Figure 2. Sketch of the sample, the detector configuration and innermost shield at a cross section taken where the detector cryostat arms enter the shield. Outside the copper lining there is 17 cm of lead. The drawing is to scale and describes a cylindrical geometry.

Paper V

This article **was published** in Radiation Measurements, doi:10.1016/j.radmeas.2008.10.012.

Radiation Measurements xxx (2008) 1–8

Contents lists available at ScienceDirect

Radiation Measurements

journal homepage: www.elsevier.com/locate/radmeas

Neutron fluence spectrometry using disk activation

Göran Lövestam [a,*], Mikael Hult [a], Andreas Fessler [a], Joël Gasparro [a], Pierre Kockerols [a], Klaas Okkinga [a], Hamid Tagziria [b], Filip Vanhavere [c], J.S. Elisabeth Wieslander [a,d]

[a] EC-JRC-Institute for Reference Materials and Measurements (IRMM), Retieseweg 111, B-2440 Geel, Belgium
[b] EC-JRC-Institute for the Protection and the Security of the Citizen (IPSC), Via E. Fermi 1, I-21020 Ispra (VA), Italy
[c] SCK•CEN, Boeretang, 2400 Mol, Belgium
[d] Department of Physics, P.O. Box 35 (YFL), FIN-40014, University of Jyväskylä, Finland

ARTICLE INFO

Article history:
Received 9 March 2007
Received in revised form
11 March 2008
Accepted 22 October 2008

Keywords:
Neutron fluence spectrometry
Activation
Spectrum unfolding
Neutron detector

ABSTRACT

A simple and robust detector for spectrometry of environmental neutrons has been developed. The technique is based on neutron activation of a series of different metal disks followed by low-level gamma-ray spectrometry of the activated disks and subsequent neutron spectrum unfolding. The technique is similar to foil activation but here the applied neutron fluence rates are much lower than usually in the case of foil activation. The detector has been tested in quasi mono-energetic neutron fields with fluence rates in the order of 1000–10000 cm^{-2} s^{-1}, where the obtained spectra showed good agreement with spectra measured using a Bonner sphere spectrometer. The detector has also been tested using an AmBe source and at a neutron fluence rate of about 40 cm^{-2} s^{-1}, again, a good agreement with the assumed spectrum was achieved.

1. Introduction

Considering the increasing number of nuclear installations world-wide it is imperative to ensure that adequate techniques to monitor environmental neutron radiation and doses are available. Important issues like environmental and personal safety, safety at work, benchmarking of existing monitoring techniques and unveiling of terrorist threats are sometimes directly linked to whether neutron spectrometry is possible. The techniques used today for measurement of environmental neutron energy spectra include Bonner sphere spectrometry (Bramblett et al., 1960) which is rather accurate but bulky and time consuming to carry out, and bubble detectors (Roy et al., 1987) which suffer from high uncertainties for spectrometry.

In this work, a novel approach is tested. It is based on measuring the neutron activity induced in a series of small metal disks followed by spectrum unfolding to obtain a neutron energy spectrum from the measurement site. A similar technique, usually referred to as the foil activation technique, is widely used for the characterisation of high neutron fluence rates, for example inside nuclear reactors and at neutron research institutes, see for example Negoita (2004). The detector discussed here, however, is aimed for the measurement of much lower fluxes which is facilitated by using thicker disks and low-background gamma-ray detectors for measuring the activation products. Due to the more complex geometry (a ring with several thick disks) neutron scattering corrections and thick target gamma measurement efficiencies need to be determined. This gives a slightly higher uncertainty compared to the foil activation technique but the contribution to the total uncertainty is limited to about 1% for a typical measurement.

As an environmental neutron-flux detector, the proposed detector possesses a number of distinct advantages. The detector

- is practically only sensitive to neutron radiation,
- is small and robust,
- requires no electrical power at the measurement site,
- can be placed at remote locations or locations with difficult access and/or in hazardous environments,
- sensitivity can be increased by using more and bigger disks and by using underground gamma-ray detectors for measuring the induced activity in the disks,
- is energy sensitive over a large neutron energy region, and
- is of relatively low cost.

A few limitations should, however, also be noted:

- The measurement of the activation products can be time consuming, especially if low detection limits are sought.
- The necessary time between the end of an activation and the start of gamma-ray measurements limits the possible disk materials to isotopes with long half-lives relative to the transport time.

* Corresponding author. Tel.: +32 (0) 14 571373; fax: +32 (0) 14 571376.
E-mail address: goeran.loevestam@ec.europa.eu (G. Lövestam).

1350-4487/$ – see front matter © 2008 Elsevier Ltd. All rights reserved.
doi:10.1016/j.radmeas.2008.10.012

- Only constant neutron fields can be accurately measured, no information about flux-changes in the spectrum during the irradiation time is obtained.

For applications there are numerous situations where a better knowledge of the neutron spectrum would give a better understanding of the origin of the neutrons, scattering effects, possible shielding effects, etc. Although in this study, the detector is designed as a neutron spectrometer, its extension to neutron dosimetry using a different design is anticipated.

2. Materials and methods

The main concept of the technique consists of three parts: 1) the neutron sensitive device consisting of a number of metal disks arranged in a holder, 2) a low-background gamma-ray measurement station and 3) a spectrum unfolding procedure.

2.1. Materials for the detector device

For the actual detector device a number of different metals are chosen depending on the prospected irradiation time and the expected neutron energy distribution. To generate adequate data for spectrum unfolding at least 6 neutron activation reactions are necessary and about 8–10 are recommended. The detector used for the measurements discussed here comprised 8 disks and the elements Mg, Al, Ti, Fe, Ni, Co, Cu and In. Each disk was 5 mm thick and 20 mm in diameter and had been analysed for possible prior activation by means of low-background gamma-ray spectrometry. The disks were geometrically arranged in a circle as in Fig. 1 on a circular piece of sticky hard paper.

The detector disk materials must be chemically stable, robust and not hygroscopic so as to facilitate the placement of the detector in rough, hostile environments. The mass as well as the isotopic and chemical composition must be well known and with high purity, which is critical. As an example, a manganese impurity in an iron disk produces via the $^{55}Mn(n,\gamma)^{56}Mn$ reaction the same reaction product as the $^{56}Fe(n,p)^{56}Mn$ reaction.

Activated pure metal disks are highly suited for gamma-ray measurements due to the well defined sample geometry, easy sample preparation and clean gamma-ray spectra that are relatively easy to analyse. Using pure metals eases the peak identification as well as minimises the background contribution from the sample itself. This results in a technique with low detection limits that can benefit from using low-background (or even ultra low-background) gamma-ray detection systems in order to further reduce the detection limits. An alternative to pure elemental metals is the use of alloys. By using several elements in each disk, fewer disks have to be used and measured by gamma-ray spectrometry, giving a faster technique with fewer detectors. The disadvantages are (i) the activation can lead to decay products with similar or overlapping gamma lines, (ii) the less material of each metal results in a lower activity and higher detection limits and (iii) each gamma-ray spectrum will have more peaks which could give higher detection limits.

It should be noted that the re-use of disks is, of course, only possible after an elapsed time corresponding to a number of half-lives for the produced radionuclides, depending on the sensitivity sought. For all measurements in this study, the disks were irradiated only once.

The neutron cross sections for the disk materials must be well known and large enough in order to produce sufficient activation products for gamma-ray measurements with appropriate statistics. The excitation functions should have different thresholds and together cover the full energy interval of interest in order to allow for the spectrum unfolding. It is desirable to avoid disk materials where different reactions produce the same radionuclide in one disk. Data for the activation reactions used in this study are given in Table 1.

A general requirement of an activation product is that its decay should be followed by at least one gamma-ray with energy between about 50 keV and 2 MeV and with a precisely known high emission probability. In addition, it is essential that the corresponding half-lives are short enough for all disks to be measured in a reasonable time span after the irradiation, but also long enough to transport the disks from the activation site to the gamma-ray detector. If several gamma-ray detectors are available and the disks can be retrieved and measured shortly after the neutron irradiation, radionuclides with shorter half-lives can be used. If the fluence rate varies during the irradiation the half-lives must be chosen long with respect to the irradiation time in order to not to reach the saturation activity. For a constant neutron field this is not the case. Furthermore, if the neutron fluence varies but the variations are known, reactions with shorter half-lives can be used since a correction can be applied to account for the variations.

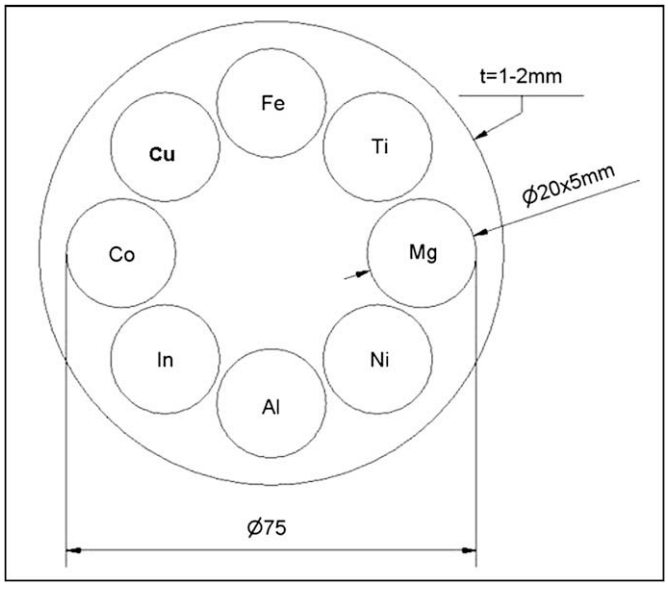

Fig. 1. Schematic drawing of the detector arrangement as viewed from the front. The disks are arranged in a circle on a sticky paper holder with a thickness of about 1–2 mm.

Table 1
Nuclear reactions used for the tested detector units. $T_{1/2}$ is the half-life, E_g is the gamma-ray energy, P_γ is the intensity of the most prominent gamma-ray, and I_{ab} is the natural isotopic abundance.

Reaction	Threshold (MeV)	$T_{1/2}$ (d)	E_g (keV)	P_γ (%)	I_{ab} (%)
$^{24}Mg(n,p)^{24}Na$	5.70	0.62	1368 (and 2753)	100.0	78.99
$^{27}Al(n,p)^{27}Mg$	2.00	0.0066	844 (and 1014)	71.80	100
$^{27}Al(n,\alpha)^{24}Na$	5.10	0.62	1368 (and 2753)	100.00	100
$^{46}Ti(n,p)^{46}Sc$	3.00	83.79	889 (and 1021)	100.0	8.25
$^{47}Ti(n,p)^{47}Sc$	0.80	3.35	159	68.30	7.44
$^{48}Ti(n,p)^{48}Sc$	3.60	1.82	983 (and 1037, 1312)	100.0	73.72
$^{54}Fe(n,p)^{54}Mn$	1.10	312.30	835	99.97	5.845
$^{56}Fe(n,p)^{56}Mn$	3.20	0.11	847 (and 1810, 2113)	98.9	91.754
$^{58}Ni(n,p)^{58}Co$	0.80	70.78	811	99.49	68.27
$^{58}Ni(n,d+np)^{57}Co$	6.10	271.77	122	85.5	68.27
$^{59}Co(n,\alpha)^{56}Mn$	4.00	0.11	847 (and 1810, 2113)	98.9	100
$^{59}Co(n,2n)^{58}Co$	10.70	70.78	811	99.45	100
$^{59}Co(n,p)^{59}Fe$	1.60	44.5	1099	56.59	100
$^{63}Cu(n,\gamma)^{64}Cu$	0.00	0.529	1346	0.5	69.17
$^{115}In(n,n')^{115}In$	0.40	0.19	336.2 (and X-ray at 24)	45.8	95.7
$^{115}In(n,\gamma)^{116m}In$	0.00	0.03764	1293.5	84.4	95.7

Please cite this article in press as: Lövestam et al., Neutron fluence spectrometry using disk activation, Radiation Measurements (2008), doi:10.1016/j.radmeas.2008.10.012

2.2. Gamma-ray measurements

Due to the relatively low neutron fluence applications aimed for in this study the metal disks need to be measured using low-level gamma-ray spectrometry (LGS) or ultra low-level gamma-ray spectrometry (ULGS). The LGS set-up includes an HPGe-detector made from selected radiopure materials installed in a specially designed shield made from e.g. very old lead. For the ULGS, additional measures such as using a muon shield or measuring underground are necessary. In this work some of the measurements were performed in the underground laboratory HADES, situated 225 m below ground (Hult et al., 2006).

Traditionally when using the foil activation method, the beta–gamma coincidence technique has been widely used. For thicker disks, as used here, it is not useful to measure the beta particles in a beta–gamma coincidence spectrometer since only the beta particles from the surface part of the disk will enter the beta-counter. In certain cases it is possible to reach low detection limits by using radiochemical methods. This was not considered an option here since the detector concept requires a method with simple sample preparation. Gamma-ray spectrometry has the advantages of requiring very little sample preparation and the measurement is easy to start and can run unattended for longer time periods. When special low-background or ultra low-background gamma-ray detection systems are used, the detection limits can reach the μBq kg^{-1} range (Hult, 2007). In recent years there has been a significant increase of the commercially available sizes of HPGe-detectors, which in combination with the use of underground laboratories has triggered a new field of gamma-ray spectrometry where very low activities are now routinely measured. Table 2 gives details for the HPGe-detectors used in this study.

For the gamma-ray spectra, the net peak areas, C, were determined using manual subtraction of background in a region of interest around the peak of interest. The specific activity, a, in Bq for a certain radionuclide, per gram of the activated isotope at the time of the end of the irradiation, was calculated from:

$$a = \frac{C\lambda}{(1-e^{-\lambda t_m})P_\gamma \varepsilon_{Ref}} \frac{1}{m\theta\xi} \cdot e^{\lambda t_d}$$

where λ is the decay constant, t_m the measurement time, t_d the decay time from the end of the irradiation to the start of the gamma-ray measurement, ε_{Ref} the full energy peak efficiency per γ-ray of the γ-ray peak in question derived from measuring a reference sample, m the mass of the sample, θ the isotopic abundance of the isotope and P_γ the gamma-ray emission probability. ξ is the efficiency correction factor, here the ratio of the efficiencies calculated using a Monte Carlo code for the reference sample and the real sample. Reference samples were not available for all radionuclides in which cases the factor ξ was set to unity and the full energy peak (FEP) efficiency was calculated using the EGS4 Monte Carlo code (Nelson et al., 1985).

Of the radionuclides included, ^{46}Sc, ^{48}Sc and ^{116m}In have decay schemes involving cascading gamma-rays. These gamma-rays are uncorrelated and there is a high probability that two or more in the cascade interacts in the Ge-crystal simultaneously. This probability increases as the sample gets closer to the detector. In this study, due to low-level activations, only close geometry measurements were carried out and, thus it was necessary to correct for the so called true coincidence summing effect. For ^{48}Sc and ^{116m}In, this correction was done directly in the Monte Carlo code when calculating the FEP efficiency. For the ^{46}Sc radionuclide the coincidence summing correction was done using the formula given by Debertin and Helmer (1988) based on the total efficiency, calculated using the EGS4 Monte Carlo code.

As input the Monte Carlo code uses the dimension and composition of the disks, the detector and the shield. The detector dimensions were determined from a radiograph made at two angles. For the window thickness the value given by the manufacturer was used. The dead layer thicknesses (front, side and bottom) were determined experimentally using calibration sources and adjusting the thicknesses until a good match was achieved. In the simulations the gamma-ray emissions are assumed to be isotropic and uncorrelated.

This measurement technique has been validated through participation in several international proficiency tests and proved to be able to produce results with an uncertainty of better than 3% when the counting statistics is not the limiting factor. It is essential for the subsequent deconvolution process that the uncertainty in the measured gamma data is as low as possible.

Table 2
Data for the HPGe-detectors used for the gamma-ray measurements. HADES is the underground laboratory and Lab indicates a detector located above ground at IRMM.

Detector	Relative efficiency (%)	Crystal mass (kg)	Crystal configuration	Dead layer thickness (mm)	Window thickness (mm) and material	Location
Ge-2	8	0.209	Semi-planar	0.0005	0.7, Al	HADES
Ge-3	60	1.337	Coaxial	1	0.7, Al	HADES
Ge-4	106	2.195	Coaxial	0.0005	1.5, Al	HADES
Ge-5	50	0.803	Planar	0.0002	1.0, Al	HADES
Ge-6	80	2.106	Coaxial	0.7	1.0, Cu	HADES
Ge-T2	20	0.423	Coaxial	0.7	1.5, Al	Lab

2.3. Neutron spectrum unfolding

The measured and corrected activation data was unfolded using the Gravel unfolding code (Matzke, 1994), which is a modified version of the SAND-II code (Jacobs and van den Bosch, 1980). The Gravel code requires an input default spectrum representing a first "guess" of the neutron fluence spectrum. All response functions used were the evaluated excitation functions data files obtained from the international Reactor Dosimetry File IRDF-2002 (http://www-nds.iaea.or.at/irdf2002/), except for the ^{58}Ni(n,d + np) ^{57}Co excitation function that was obtained from the IAEA Reference Neutron Activation Library, RNAL (http://www-nds.iaea.org/ndspub/rnal/www/), and the ^{59}Co(n,p)^{59}Fe excitation function that was obtained from the ENDF/B-VII.0 (http://www.nndc.bnl.gov/exfor/endf00.htm).

For all activation cross sections, the excitation function was extracted from the respective evaluated data file and interpolated using cubic spline to cover the energy region 0.0–20.0 MeV in steps of 0.1 MeV, i.e. 200 data points per reaction, see Fig. 2. An adequate overlap is achieved for the energy region up to 20 MeV neutrons. The cross section data from the ^{115}In(n,γ)^{116}In^{m} and ^{63}Cu(n,γ)^{64}Cu reactions have been included to cover the low-energy part of the neutron spectra (<0.4 MeV). However, this includes the resonance region which was averaged out to a smooth curve to fit the bin structure for the unfolding calculations.

The measure of how well the spectrum is unfolded is given by the chi-2 value calculated as:

$$\chi^2_{n-1} \sim \frac{\sum_k^n \left(\sum_i^m \sigma_{ki}\Phi_i - A_k \right)^2}{s^2}$$

where Φ_i is the unfolded (calculated) spectrum, σ_{ki} the corresponding activation cross sections (the response functions), A_k the measured activation data, s the standard deviation, n the number of measurements (reactions) and m the number of bins in the neutron spectrum.

Please cite this article in press as: Lövestam et al., Neutron fluence spectrometry using disk activation, Radiation Measurements (2008), doi:10.1016/j.radmeas.2008.10.012

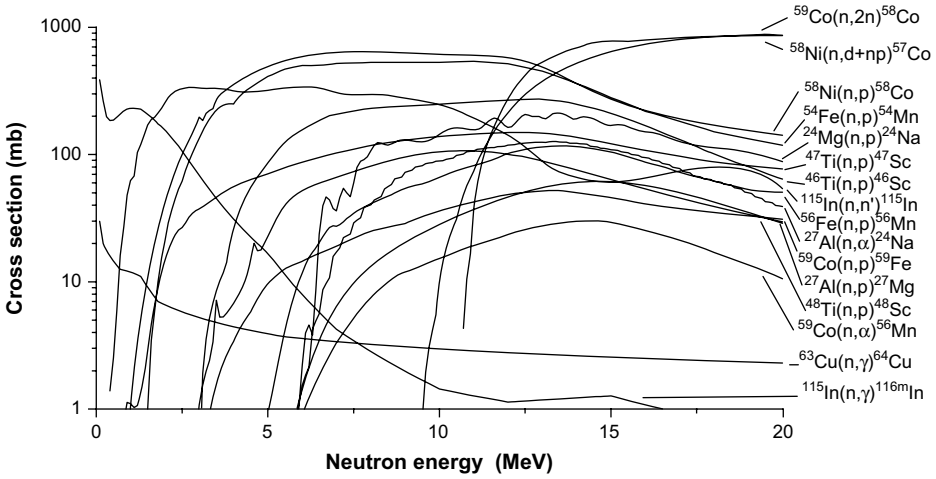

Fig. 2. Interpolated evaluated cross section data used for the unfolding of neutron spectra. All data is from the international Reactor Dosimetry File, IRDF-2002, except for the ^{58}Ni(n,d + np)^{57}Co reaction that is from the IAEA Reference Neutron Activation Library and the ^{59}Co(n,p)^{59}Fe reaction that is from the ENDF/B-VII.0 data library. See text for references.

3. Activations

Four test detectors were prepared using the selected disks with the materials arranged as shown in Fig. 1. The detectors were irradiated with quasi mono-energetic neutron fields of energy 5.0, 7.0 and 17.0 MeV (irradiations #1, #2 and #3) and with an AmBe source (irradiation #4). The first three irradiations were carried out in high intensity neutron fluence fields at the IRMM Van de Graaff (VdG) neutron data laboratory and the fourth detector was irradiated in a low intensity field at the Belgian nuclear research centre SCK•CEN. The three high intensity irradiations, #1–#3, were included to test the detector at "point-wise" energies and the fourth irradiation (#4) was included as a test in a continuous neutron spectrum with a relatively low flux.

3.1. Irradiations in high intensity quasi mono-energetic neutron fields

For the irradiations #1–#3 the neutron fluence fields were created using the nuclear reactions listed in Table 3. The neutron fields were energy characterised using the IRMM Bonner sphere neutron spectrometer of type PTB-C (Bramblett et al., 1960; Thomas and Alevra, 2002; Lövestam et al., 2004) and the fluence characterised using the IRMM recoil proton telescopes (Thomas and Axton, 1980; Chen et al., 2007). For all irradiations the measurement sequence was: recoil proton telescope–detector irradiation–Bonner sphere spectrometry, with the laboratory stationary long counter monitor used for normalisation between measurements.

For the measurements #1 and #2 the D(d,n)^{3}He reaction was used by means of a solid deuterium–titanium target with a thickness of 2.065 mg cm^{-2} and for measurement #3 the T(d,n)^{4}He reaction was used with a 2.075 mg cm^{-2} thick tritium–titanium target. Both targets were mounted on 0.5 mm thick silver backings. The deuterium–titanium target had about 150 h of usage and the tritium–titanium target about 800 h. This is a considerable time and some low-energy contaminations are expected in the neutron spectra. For the activations #1 and #2 the detector was positioned 1.0 m in front of the neutron producing target and for activation #3, 0.5 m in front of the target. The recoil proton telescope measurements were done using the IRMM RPT2 telescope with a silicon end-detector for irradiations #1 and #2 and for irradiation #3 the IRMM RPT3 telescope with a CsI scintillator end-detector.

Table 3
Experimental data for the neutron irradiations #1–#3. Neutron producing reaction is the utilised reaction for neutron production using the Van de Graaff accelerator.

Measurement	#1	#2	#3
Neutron producing reaction	D(d,n)^{3}He	D(d,n)^{3}He	T(d,n)^{4}He
Ion energy (MeV)	1.94	3.84	1.35
Peak neutron energy (MeV)	5.0	7.0	17.0
Distance (mm), neutron source to detector surface	1000	1000	500
Total neutron fluence at the position of the detector (cm^{-2})	1.0×10^8	4.1×10^8	1.3×10^8
Irradiation time (h)	20.9	18.0	17.5

3.2. Irradiation using low intensity AmBe neutron field

For irradiation #4, the neutron spectrum consisted of a pure AmBe spectrum directly from the source with the addition of a component from neutrons in-scattered by the room, the air and surrounding materials. The spectrum of the scattered neutrons was not fully known at the detector location. The detector was mounted on a plastic slab phantom believed to give an extra contribution to the low-energy part of the neutron spectrum due to scattered neutrons. However, for the higher energy part a standard ^{241}AmBe spectrum was assumed. The direct neutron fluence rate had previously been calibrated to about 40 cm^{-2} s^{-1} at the position of the detector. The irradiation time was 3.8 days.

4. Result and discussion

4.1. Activity measurements

The dominating uncertainty contributions to the specific activity are from the gamma detector efficiency and counting statistics. The uncertainty of the detector efficiency is assumed to be less than 3% and mainly due to uncertainties in the geometrical description of the detector as well as the used photon and electron interaction cross sections. The expressed uncertainties are given as the combined standard uncertainty estimated following the ISO/BIPM Guide to the Expression of Uncertainty in Measurement, ISO, 1995. Nuclear decay data was taken from the PC based interactive database Nucléide V.2.0, supplied by DAMRI/LPRI and developed under the Decay Data Evaluation Project (DDEP) (http://www.nucleide.org/DDEP.htm).

Please cite this article in press as: Lövestam et al., Neutron fluence spectrometry using disk activation, Radiation Measurements (2008), doi:10.1016/j.radmeas.2008.10.012

The activity data used as input for the unfolding programme is given in Table 4 as the saturation activity, calculated by multiplying the activity with the factor $(1-e^{-\lambda t_i})^{-1}$, where t_i is the irradiation time and λ is the decay constant of the radionuclide in question.

4.2. Corrections

The neutron detector (i.e. the disks) themselves disturb the neutron field measured. Corrections for this included correction for self shielding and neutron multiple scattering as well as in-scattering from neighbouring disks. For calculating the corrections, the Monte Carlo software MCNP-4C2 (Briesmeister, 1993) was used.

For the irradiations #1, #2 and #3 corrections were calculated also for variations in the accelerator beam current during activation. The accelerator instability was monitored by recording the integrated ion beam charge during irradiations with an integration time set to 1 s. The corresponding correction factor c_{fluence} was calculated for each radionuclide from:

$$c_{\text{fluence}} = \frac{\Phi\left(1-e^{-\lambda t_i}\right)}{\sum_{i=1}^{n}\Phi_i\left(1-e^{-\lambda \Delta t}\right)e^{-\lambda(n-i)\Delta t}}$$

Here, Φ is the mean fluence of the irradiation, Φ_i the fluence at time-bin i, n the total number of time-bins, t_i the irradiation time, Δt the dwell time and λ the decay constant for the radionuclide in question.

The importance of this fluence correction depends on the half life of the radionuclide studied. If the half life is very long in comparison to the total irradiation time, the correction is very small whereas it is larger for half-lives similar or shorter than the irradiation time.

4.3. Measurements of Sc-impurities in Ti

The radionuclide ^{46}Sc can be produced in different ways and in this study the reaction ^{46}Ti(n,p)^{46}Sc was of most interest. However, the cross section for the reaction ^{45}Sc(n,γ)^{46}Sc is very high for thermal neutrons, about 17 b, and thus, scandium impurities in the titanium disks of the order of mg g^{-1} would cause a potential problem. To measure possible impurities, a titanium disk was irradiated in a thermal field at the BR1 nuclear reactor at SCK•CEN. The neutron fluence rate was 7×10^8 cm^{-2} s^{-1}, and the irradiation time was 1.5 h.

^{46}Sc has two strong gamma lines at 889 and 1120 keV ($P_\gamma = 1.0$) with a rather long half life (83.81 d) making it possible to let short-lived radionuclides decay in order to reduce the background. The only radionuclides detected were ^{24}Na ($T_{½}$ = 14.66 h), ^{54}Mn ($T_{½}$ = 312 d), ^{56}Mn ($T_{½}$ = 2.58 h) and ^{76}As ($T_{½}$ = 1.10 d). This indicates trace impurities at μg g^{-1} level of Na, Mn, Fe and As while any trace impurity of Sc is less than 1 μg g^{-1}. The conclusion is that the contribution from thermal activation of scandium impurities in the titanium disks can be neglected.

4.4. Detection limits

Table 5 gives the detection limits calculated for two specific detectors using the disk arrangement employed in this study and some realistic times for irradiation, cooling and gamma measurement.

It is difficult to give a well defined detection limit for what neutron fluence rates can be measured as it depends on the shape of the applied neutron spectrum. The values given in Table 5 cannot be obtained across a wide energy range unless the neutron activation cross section curve is flat. The deconvolution technique requires at least 6 reactions to be determined which means that for a realistic broad neutron spectrum, the detection limits will be determined by nuclear reactions with higher detection limits than given in Table 5.

For radionuclides with long half-lives (>several days), very low detection limits can be obtained if long irradiation and measurement times are used. For these radionuclides the cooling time is not so critical and the gamma-ray measurements may start some days after the irradiation ended provided that no significant additional activation takes place during cooling. In cases where the disks have to be transported a long distance from the activation site to the gamma measurement station, it could be necessary to use a special transport container filled with a moderator like water or paraffin surrounding an inner cadmium shield.

In order to obtain as good results as possible, information from both short-lived and long-lived reaction products should preferably be obtained. It is thus recommended to access the measurement station in as short time as possible following the activation. However, considering the number of available radionuclides with half life over one day, a transport time of a day or two would still enable for an acceptable neutron spectrum determination.

4.5. Unfolding results

Fig. 3 shows calculated neutron spectra for the respective neutron irradiation energy using the Monte Carlo code Target (Schlegel-Bickman et al., 1980), the respective spectra measured using the IRMM Bonner sphere system and the unfolded data from the irradiations #1–#3. For the unfolding the respective calculated

Table 4
The specific saturation activity in Bq/g of activated isotope multiplied with correction factors for neutron scattering between discs and neutron self-absorption. The values were used as input data for the unfolding calculations after conversion to Bq/atom.

Reaction	5 MeV	7 MeV	17 MeV	Am–Be
^{24}Mg(n,p)^{24}Na		1.7(6)	1.9(3)	
^{27}Al(n,p)^{27}Mg	1.8(5)	5.7(23)	0.67(12)	
^{27}Al(n,α)^{24}Na		0.7(5)	2.6(2)	
^{46}Ti(n,p)^{46}Sc[a]	0.85(17)	11.3(9)	4.2(6)	0.027(12)
^{47}Ti(n,p)^{47}Sc[b]	1.03(7)	5.0(3)	14.7(9)	
^{48}Ti(n,p)^{48}Sc	0.0025(10)	0.35(3)	1.29(7)	0.0014(3)
^{54}Fe(n,p)^{54}Mn	6.0(8)		5.3(7)	0.09(4)
^{56}Fe(n,p)^{56}Mn	0.014(2)	0.9(3)	1.63(10)	0.0037(12)
^{58}Ni(n,p)^{58}Co	3.91(25)	28(3)	3.02(18)	0.100(5)
^{58}Ni(n,d + np)^{57}Co			13.6(8)	
^{59}Co(n,α)^{56}Mn		0.08(4)	0.45(3)	
^{59}Co(n,2n)^{58}Co			12.7(8)	
^{59}Co(n,p)^{59}Fe			0.61(5)	
^{63}Cu(n,γ)^{64}Cu		1.1(3)		
^{115}In(n,n′)^{115}In	3.03(18)	10.0(9)	1.31(8)	0.064(5)
^{115}In(n,γ)^{116m}In	0.86(13)	8.1(10)	0.85(6)	1.10(6)

[a] Cannot be distinguished from ^{47}Ti(n,np + d)^{46}Sc for irradiation #3 (17 MeV neutrons).
[b] Cannot be distinguished from ^{48}Ti(n,np + d)^{47}Sc for irradiation #3 (17 MeV neutrons).

Table 5
Example of detection limits for neutron fluence rates calculated at a neutron energy where the respective cross section is high. The assumptions used are 14 h irradiation time and 1 h decay time. The gamma-ray measurement time varies according to the half life of the respective radionuclide. HADES is the underground laboratory and Lab indicates a detector located above ground at IRMM.

Reaction	Neutron detection limits (s^{-1} cm^{-2})	
	HADES (Ge-4)	Lab (Ge-T2)
^{27}Al(n,p)^{27}Mg	1.3	46
^{27}Al(n,α)^{24}Na	0.14	5.5
^{59}Co(n,α)^{56}Mn	0.45	18
^{115}In(n,n′)^{115}In	0.15	5.0
^{115}In(n,γ)^{116m}In	0.0013	0.068

Please cite this article in press as: Lövestam et al., Neutron fluence spectrometry using disk activation, Radiation Measurements (2008), doi:10.1016/j.radmeas.2008.10.012

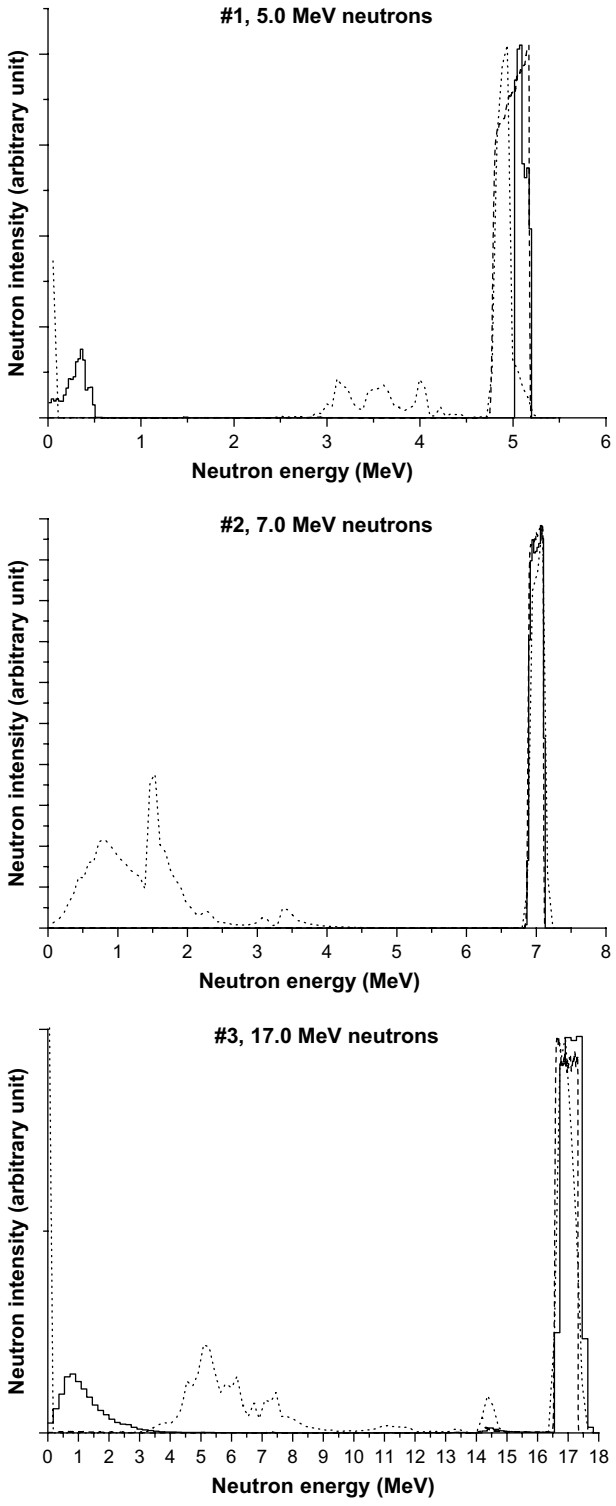

Fig. 3. Unfolded neutron spectra for the neutron irradiations #1–#3 (solid lines), together with the corresponding calculated spectra (dashed lines) and the spectra measured using Bonner spheres (dotted lines). The spectra have been normalised for every energy to the respective maximum number of counts in the high-energy peak.

spectrum was used as default spectrum. The obtained chi-2 values were 1.43 (#1), 1.21 (#2) and 1.00 (#3). The Target code calculates neutron scattering in the neutron producing target as well as air in/out-scattering but not room in-scattering. The Bonner sphere measurements were done about 2.5 m from the neutron producing target, which is the closest distance the spectrometer is accurate due to the size of the larger spheres and the double differential character of the neutron field produced using an ion beam and nuclear reactions, as reported by Lövestam et al. (2004). The Bonner sphere data were normalised to the laboratory stationary long counter, dead time corrected and unfolded using the Gravel code with the respective calculated spectrum as default input spectrum.

The calculated spectra, the spectra measured using the Bonner spheres and the spectra obtained from the test detectors agree well for the main neutron peak, particularly for the 7.0 and 17.0 MeV measurements. For the 5.0 MeV measurement both the peak measured using the Bonner spheres and the peak measured using the test detector have a full width half maximum of about 50% compared to the calculated peak. Furthermore, the Bonner sphere measured peak is shifted about 200 keV to the low-energy side. The reason for this is not known. The lower energy contributions in the measured spectra are believed to be due to in-scattering from surrounding materials, particularly from a 50 cm concrete protective wall surrounding the laboratory building and about 6 m away from the activation point. All Bonner sphere spectra show a mid-energy region, which is not visible in the test detector spectra. A plausible explanation is that the Bonner sphere spectra were recorded at a greater distance from the neutron producing target (2.5 m) than the test detector spectra (0.5–1.0 m) and thus, closer to the surrounding shielding wall. This would also create a low-energy contribution believed to have a large uncertainty as the cross section data below 100 keV is grouped in one single energy bin. This

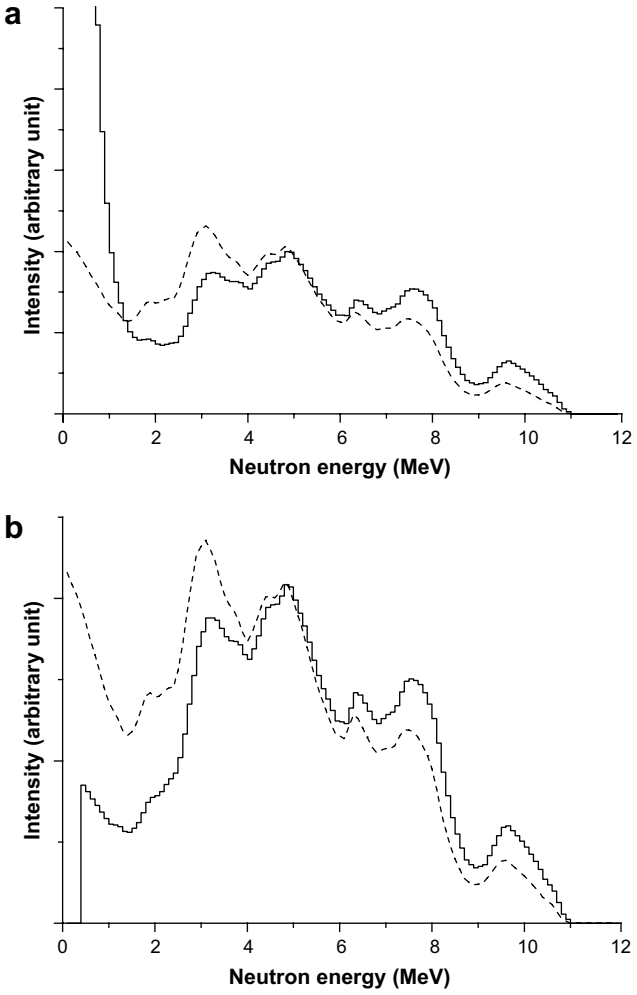

Fig. 4. Unfolded spectra from the AmBe irradiation (solid line) and a typical AmBe spectrum used as default input spectrum for the unfolding (dashed line). The unfolding was done with (a) and without (b) the reaction $^{115}In(n,\gamma)^{116}In^{m}$ included. The ordinate is the neutron intensity in arbitrary unit.

Please cite this article in press as: Lövestam et al., Neutron fluence spectrometry using disk activation, Radiation Measurements (2008), doi:10.1016/j.radmeas.2008.10.012

bin contains both the resonance area and the thermal component of the cross section curve for the $^{115}In(n,\gamma)^{116}In^m$ reaction.

In Fig. 4a the unfolded spectrum from the AmBe irradiation together with a typical AmBe spectrum is given. Here, the typical AmBe spectrum has been entered as default spectrum for the unfolding procedure. The calculated chi-2 value is 0.43. From Fig. 4a the conclusion is that the typical spectrum is well represented above 2.0 MeV but not at lower neutron energies. The reason for this is believed to be a plausible low-energy part in the spectrum irradiating the test detector which is not included in the typical spectrum. Since the detector was mounted on a polyethylene body phantom which in turn is mounted on a concrete wall about 5.8 m from the AmBe source, a considerable low energy and thermal energy contribution is expected. The thermal and lower neutron energy region (<0.4 MeV) is not well unfolded since it is only covered by one reaction, $^{115}In(n,\gamma)^{116}In^m$, which, as discussed above, has been smoothened and will affect the rest of the unfolded spectrum. The only conclusion that can be drawn is that a low-energy spectrum component is present. If the $^{115}In(n,\gamma)^{116}In^m$ reaction is removed from the input data to the unfolding procedure, the reconstructed spectrum is more similar to the default also in the higher energy part as seen in Fig. 4b. Here a chi-2 value of 0.48 is achieved from the unfolding. The spectrum is, however, unfolded using only six reactions, which is at the limit of feasibility and makes the procedure rather dependant on the default spectrum, in this case the typical AmBe spectrum. Moreover, the high uncertainties in the measurement data make the unfolding even more dependent on the default spectrum. Nevertheless, the results show that the AmBe spectrum is a candidate as a solution spectrum.

The good match of the unfolded spectrum to the default AmBe spectrum, as shown in Fig. 4a and b, raises the question what spectrum is obtained when the "true" spectrum is not well known and hence not available as default spectrum. The IAEA has collected more than 400 operational neutron spectra (IAEA, 2001) for radiation protection purposes. The collection includes the reference spectrum recommended by ISO-8529 for AmBe, as shown in Fig. 5. The spectra are given in fluence per unit log energy (lethargy) and therefore not very detailed in the higher energy region but, nevertheless, when using AmBe as default input spectrum for unfolding and using the data measured in this study, the resulting spectrum is in better agreement with the more detailed AmBe spectrum from Fig. 4, see Fig. 5. Here, the $^{115}In(n,\gamma)^{116}In^m$ reaction has been included and the chi-2 value is 0.47. The spectrum is rather crude in the high-energy region due to the lack of data points in the default spectrum in this region.

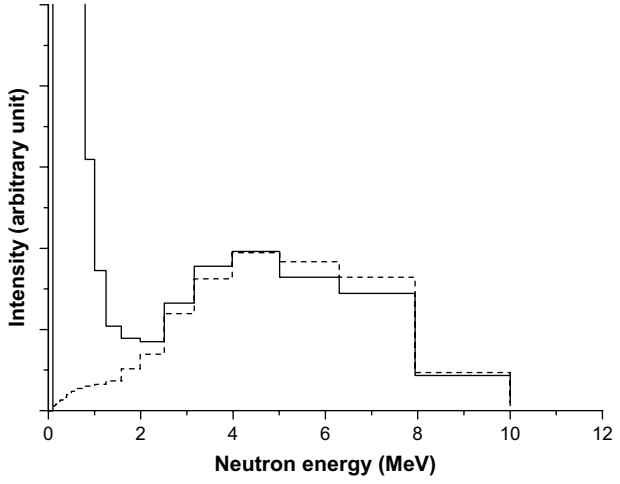

Fig. 5. The reference spectrum recommended by ISO-8529 for AmBe from the IAEA library of operational neutron fluence spectra (IAEA, 2001) (dashed line) used as default spectrum and the resulting unfolded spectrum from the AmBe irradiation (solid line). The unfolding was done with the reaction $^{115}In(n,\gamma)^{116}In^m$ included. The ordinate is the neutron intensity in arbitrary unit.

For a "sharp case", when the detector has been exposed to an unknown neutron fluence field, the IAEA library of operational spectra may be very useful as they can be "tested" as default spectra to seek the lowest chi-2 value.

4.6. Future developments

Further detector development work includes precise tests of detector units in well characterised neutron fields, preferably from ^{252}Cf and AmBe sources, to select the best excitation functions available also for other isotopes not used in this study. A single erroneous excitation function may obscure the resulting neutron spectrum considerably in a similar way as a single badly modelled or characterised response function to a Bonner sphere spectrometer. Thus, it is crucial for the technique that the set-up of isotopes and the corresponding excitation functions are carefully selected.

A new HPGe-detector system, including two HPGe-detectors, has been installed in the IRMM underground laboratory HADES. This effectively increases the gamma-ray detection efficiency by a factor of two. Since the new detector system has better background reduction compared to previously used detectors, the detection limits are reduced even further.

Additionally, the development of a dedicated gamma-ray detector station comprising several low-level gamma-ray detectors, an automatic disk changer and an integrated data evaluation software is foreseen. A study is underway looking into the critical task of optimising the gamma-ray measurement sequence for the included isotopes while using a limited number of gamma-ray detectors during a limited measurement time. A dedicated disk holder has been designed which eases positioning of the holder at the neutron fluence measurement site.

5. Conclusions

Prototypes of a novel neutron detector, based on neutron activation of eight metal disks mounted in a circular pattern, have been shown to successfully measure neutron energy distribution over a wide energy range. The paper shows that also low neutron fluences rates can be measured in the order of 40 s^{-1} cm^{-2}. The demonstrated technique reconstructs both simple mono-energetic high flux spectra at different energies and a more complicated low-flux spectrum from an AmBe source.

The technique opens for more convenient measurements of environmental neutron fluence fields than conventional techniques used today, mainly Bonner sphere spectrometry and bubble detectors. The actual detector unit, i.e. the metal disks supported by a disk holder, can be placed virtually anywhere, also in hazardous environments or in areas difficult to access, as it is small, not fragile and needs no electronics. The moderate price of a detector unit also opens for mass usage where the loss of an individual unit very well can be accepted. In practice two modes of utilisations have been foreseen:

- The stationary mode. The detector is "pre-installed" at certain locations and only used and transported to the gamma-ray measurement laboratory for activation measurements if and when a neutron fluence field have been suspected.
- The dynamic mode. For a more conventional measurement use where one or several detector units are positioned occasionally in a suspected or known neutron fluence field.

The stationary mode is applicable wherever increased neutron radiation normally should not occur but for some reason could occur by accident or deliberately, for example at nuclear power plants, thermonuclear fusion facilities, high-energy accelerators,

Please cite this article in press as: Lövestam et al., Neutron fluence spectrometry using disk activation, Radiation Measurements (2008), doi:10.1016/j.radmeas.2008.10.012

nuclear research laboratories, at nuclear materials storage sites, and medical installations employing neutrons for cancer treatments. The dynamic mode targets situations whenever a known or suspected neutron field should be characterised, for example at nuclear research installations, after a nuclear accident and at border and custom controls.

Acknowldegements

Peter Vermaercke at SCK•CEN is acknowledged for neutron activation measurements. Staff from SCK•CEN and EURIDICE are acknowledged for technical support at the underground laboratory HADES.

References

Bramblett, R.L., Ewing, R.I., Bonner, T.W., 1960. A new type of neutron spectrometer. Nucl. Instrum. Methods 9, 1–12.

Briesmeister, J.F. (Ed.), 1993. MCNP – A General Monte Carlo N-Particle Transport Code. Los Alamos, USA Version 4A. LA-12625.

Chen, J., Wang, Z., Rong, C., et al., 2007. International key comparison of neutron fluence measurements in mono-energetic neutron fields: CCRI(III)-K10. Metrologia 44, 06005.

Debertin, K., Helmer, R.G., 1988. Gamma- and X-ray Spectrometry with Semiconductor Detectors. North-Holland Publishing, Amsterdam, ISBN 0 444 871071 (Chapter 4.5.1).

Hult, M., Preusse, W., Gasparro, J., Köhler, M., 2006. Underground gamma-ray spectrometry. Acta Chim. Slov. 53, 1–7.

Hult, M., 2007. Low-level gamma-ray spectrometry using Ge-detectors. Metrologia 44, S87–S94. Erratum at Metrologia 44, 425.

IAEA, 2001. Compendium of Neutron Spectra and Detector Responses for Radiation Protection Purposes. In: Technical Reports, no. 403. International Atomic Energy Acency, Vienna, ISBN 92-0-102201-8.

Jacobs, G., van den Bosch, R., 1980. Calibration measurements with the multisphere and neutron spectrum analyses using the SAND-II program. Nucl. Instrum. Methods 175, 483–489.

Lövestam, G., Cserpak, F., Geerts, W., Plompen, A., 2004. The IRMM Bonner sphere system for neutron spectroscopy. IRMM internal report GE/NP/07/2004/11/29.

Matzke, M., 1994. Unfolding of pulse height spectra: the HEPRO program system. PTB Bericht 19, Braunschweig, Germany.

Negoita, C.C., 2004. Measurement of Neutron Flux Spectra in a Tungsten Benchmark by Neutron Foil Activation Method. Shaker Verlag GmbH, Aachen, Germany, ISBN 3-8322-3519-1, 120 pp.

Nelson, W.R., Hirayama, H., Rogers, D.W.O., 1985. The EGS4 code system. SLAC Report 265.

Roy, S.C., Apfel, R.E., Lo, Y.-C., 1987. Superheated drop detector: a potential tool in neutron research. Nucl. Instrum. Methods A255, 199.

Schlegel-Bickman, D., Dietze, G., Schölermann, H., 1980. A collimator system for fast neutron scattering experiments. Nucl. Instrum. Methods 169, 517–526.

Thomas, D.J., Axton, E.J., 1980. The need for a relativistic approach when calculating proton recoil telescope efficiencies. Nucl. Instrum. Methods 174, 321–322.

Thomas, D.J., Alevra, A.V., 2002. Bonner sphere spectrometers – a critical review. Nucl. Instrum. Methods A 476, 12–20.

Please cite this article in press as: Lövestam et al., Neutron fluence spectrometry using disk activation, Radiation Measurements (2008), doi:10.1016/j.radmeas.2008.10.012

Paper VI

This article **will be submitted 2009** to Radiation Protection Dosimetry (Oxford Journals), this is a paper ready to be submitted.

J.S.E. Wieslander, G. Lövestam, M. Hult, D. Arnold, A. Fessler, J. Gasparro, P. Kockerols, A. Zimbal, *A neutron dosimetry and spectrometry method using activation of thick metal discs.*

Radiation Protection Dosimetry (2009), Vol. 0, No. 0, pp. 0–0
DOI: 10.1093/rpd/nc0000

A NEUTRON DOSIMETRY AND SPECTROMETRY METHOD USING ACTIVATION OF THICK METAL DISCS

J.S. Elisabeth Wieslander[1,3], Göran Löwestam[1], Mikael Hult[1,*], Dirk Arnold[2], Andreas Fessler[1], Joël Gasparro[1], Pierre Kockerols[1], Andreas Zimbal[2]
[1]EC-JRC-IRMM, Institute for Reference Materials and Measurements, Retieseweg 111, B-2440 Geel, Belgium
[2]Physikalisch-Technische Bundesanstalt, Bundesallee 100, D-38116 Braunschweig, Germany
[3]Department of Physics, P.O. Box 35, FIN-40014 University of Jyväskylä, Finland

Received month date year, amended month date year, accepted month date year

A technique for neutron dosimetry and spectrometry based on neutron activation of metal discs has been studied. After exposure to a neutron field the activated radionuclides in the discs are detected using low-level γ-ray spectrometry and the neutron spectrum is obtained by using a spectrum unfolding technique. In order to validate the method an irradiation was performed in a well-characterized ^{252}Cf neutron reference field. Furthermore, the detector was used to determine the neutron fluence rate at a storage place for MOX nuclear fuel. The results of these two experiments are reported and discussed.

INTRODUCTION

Accurate monitoring of environmental neutron radiation in the fast neutron energy region is becoming important due to an increased level of awareness of personal safety, safety of nuclear installations and possible terrorist threats. The accident in the nuclear reprocessing plant Tokai-mura (Japan) in 1999 (1, 2, 3) highlighted the need for a low cost backup system for monitoring neutrons. One method to retrospectively determine the neutron fluence at different locations around the Tokai-mura site was to perform measurements of the neutron activation induced in various metal objects found in the nearby surroundings, such as jewellery and table spoons (2, 3). This method was also used to estimate the doses received by the Hiroshima victims (4). These measurements indicate the need and usefulness of a passive pre-defined neutron detection device, based on neutron activation of metal discs, that is preferably mounted in advance at a potential measurement site.

The technique employed here is based on measuring the neutron induced activity in a series of small discs of different metals, followed by spectrum unfolding to obtain the neutron energy spectrum. A similar technique, usually referred to as the foil activation technique, is used for characterization of high neutron fluence rates present at facilities such as nuclear research laboratories and nuclear reactors. The detector studied in this work is aimed at detecting much lower environmental fluence rates, which is facilitated by using thicker metal disks in combination with low-background γ-ray spectrometry for detection of the activation products. The method was first described by Lövestam et al. (2008) (5) together with results from the initial tests. The present paper discusses recent improvements, the results from a validation experiment performed at the Physikalisch-Technische Bundesanstalt (PTB) in Braunschweig, Germany, as well as the results from an environmental measurement performed at the MOX nuclear fuel fabrication facility Belgonucleaire in Dessel, Belgium.

The most common environmental neutron spectrometer used today is the Bonner sphere system (6), which makes use of a traditional low-energy neutron detector (for example a BF_3 or ^{3}He type detector) together with a set of polyethylene moderators that have to be subsequently applied by the user during the measurement. In comparison to the Bonner spheres, there are several advantages with the detector described in this paper: the detector unit is small, robust, easy to handle and to mount, does not need any external power supply at the measurement site, can be placed for long periods of time in harsh environments and is of relatively low cost. However, the technique described here is only useful in neutron energy region 0.3-20 MeV, which is the energy region where the neutron radiation weighting factor is the highest. A few limitations of the technique should also be mentioned and these are time consuming γ-ray measurements following an activation, the need of relatively short transport time to the γ-ray measurement laboratory in order to detect radionuclides with short half-lives and, finally, variations in the neutron fluence rate during an irradiation can not be detected.

MATERIALS AND METHODS

The neutron detector unit

The actual detector unit consists of a set of small metal discs placed in a circular plastic holder, which is 120 mm in diameter. The holder was re-designed after the initial tests described by Lövestam et al. (2008) (5), see Figure 1. The holder has 10 disc positions in a ring pattern with one additional position in the middle.

A critical design consideration is the selection of activation materials, i.e. metal discs. Parameters to consider are the thresholds of the excitation functions, the half-lives of the activation products and their suitability for γ-ray spectrometry (5). It is also important to consider the quality of the available cross section data for the included activation reactions. For this study the following metal discs were selected: Ti, Ni, Fe, Co, In, Mg, Al, Zr and Au. All discs were pure and of natural isotopic composition and not previously activated. Each disc was 20 mm in diameter with a thickness of 5 mm, except the Au disc which was only 2 mm thick.

γ-ray measurements

The order in which the γ-ray measurements are performed is crucial and depends on the half-life of the activated radionuclides in a metal disc in combination with the level of activity and the number of available γ-ray spectrometers. Relatively long-lived radionuclides with very low levels of activity benefit from longer measurements and are preferably measured in a low-level γ-ray spectrometry laboratory.

In this study the γ-ray measurements were performed at two research institutes: Physikalische-Technische Bundesanstalt (PTB) in Braunschweig, Germany, and Institute for Reference Materials and Measurements (IRMM), in Geel, Belgium. After the irradiation by the ^{252}Cf reference source at PTB, the short-lived activation products were detected using three HPGe detectors in the PTB low-background laboratory at ground level. All other γ-ray measurements were performed at IRMM using two low-background HPGe spectrometers at ground level and three ultra low-background spectrometers in the underground laboratory HADES (7).

The full energy peak efficiency (ε) was derived from efficiency curves by calculating correction factors using Monte Carlo codes. At IRMM the EGS4 code (8) was used, while PTB used GESPECOR (9). Both computer codes include models of the HPGe-crystal and its holder, the detector endcap, the sample and the sample holder for both the reference source and the metal disc. For the coincidence summing calculations the computer codes also include the complete decay schemes of radionuclides with cascading γ-rays. In the simulations it is assumed that the distribution of radionuclides in the samples is homogenous.

The specific saturation activity, A_s, per atom of the activated isotope at the end of activation was calculated:

$$A_s = \frac{\lambda C e^{\lambda t_d}}{\varepsilon P_\gamma \left(1-e^{-\lambda t_m}\right)\left(1-e^{-\lambda t_a}\right)} \frac{M}{m\theta N_A} \xi$$

where λ is the decay constant, C the net-number of counts in the peak, t_d is the decay time, t_a is the activation time, t_m is the measurement time, ε is the full energy peak efficiency, P_γ is the γ-ray emission probability, M is the atomic mass of the isotope, m is the mass of the disc, θ is the natural isotopic abundance, ξ is the efficiency correction factor (5) and N_A is Avogadro's number. The nuclear decay data used in this work was taken from the DDEP website (10) or from the ENSDF database (11) when no DDEP data was available. When several γ-ray energies from one radionuclide were detected, the weighted mean of the activity for these peaks was calculated.

The dominating uncertainty contribution when measuring low intensity neutron fields originates from counting statistics in the γ-ray measurements. The combined standard uncertainty of all other sources of uncertainty is generally less than 3%. The validity of this value for the γ-ray efficiency calculations has been verified through the laboratories' participation in several proficiency-testing schemes.

Neutron spectrum unfolding

The relation between the neutron fluence rate and the saturation activity, A_s, is given by:

$$A_s = N \cdot \sigma \cdot \Phi$$

where N is the number of target atoms of the isotope, σ is the cross section and Φ is the neutron fluence rate (neutrons cm^{-2} s^{-1}). Equation (2) can be written in the form of a discrete neutron spectrum:

$$A_{sk} + u_{sk} = \sum_i \sigma_{ki} \Phi_i$$

where k is the activation reaction, the index i refers to the energy-bin, A_{sk} is the detected saturation activity (per atom of the isotope) for each k, u_{sk} is the uncertainty of A_{sk}, σ_{ki} is the corresponding activation

*Corresponding author: Phone +32 14 571 269,
FAX +32 14 584 273, e-mail mikael.hult@ec.europa.eu

excitation function and Φ_i is the unfolded (calculated) neutron spectrum. Since normally $k << i$, equation (3) is under-determined and can be solved by applying an unfolding technique. In this work the MAXED unfolding code (12) (maximum entropy code) is used in combination with the IQU error propagation code ccording to the procedure described by Lövestam et al (2008) (5).

The cross section data files of the selected nuclear reactions are used as response functions for the unfolding of the neutron spectrum. The excitation functions together with their corresponding saturated activity value and total uncertainty are listed in Tables 1 and 3, which are used as input data to the unfolding software. For comparison, the calculated to measured value (**c-m value**) is given in the tables. When the different cross section databases for a nuclear reaction contain identical or almost identical data, they are all listed for that particular reaction in Table 2. The measured data is normalised using the data from the ^{58}Ni(n,p)^{58}Co reaction because it is available in all cross section data bases, has no substantial discrepancies and has a rather low threshold (~0.8 MeV). Unless anything else is stated, all spectra have been normalised to 1 neutron for the summed data above 0.3 MeV. The unfolded spectra are truncated at 0.3 MeV since none of the included excitation functions have a threshold below this neutron energy.

Dose rate calculations

When the neutron spectrum is known it is possible to calculate the dose rate in pSv h^{-1} at the location of the neutron spectrometer:

$$Total\ Dose\ Rate = F \cdot \left(\sum_i P_i \cdot \Phi_i \right) \cdot 3600$$

where Φ_i is the calculated neutron spectrum normalised to 1 neutron, P_i is the dose conversion factor in pSv cm^2 given in the ISO standard 8529-3 (13), F is a normalisation factor calculated in the unit of neutrons cm^{-2} s^{-1} by using the unfolded spectrum and cross section:

$$F = \frac{A_S}{\sum_i (\Phi_i \cdot \sigma_i) \cdot 10^{-24}}$$

and finally the expression in equation (4) is multiplied with 3600 seconds to have the *Total Dose Rate* in pSv h^{-1}. For the irradiation with the ^{252}Cf reference source, the ISO report (13) gives the conversion factor of 385(8) pSv cm^2 for such a reference source, which thus in the validation experiment substitutes the middle factor in parenthesis in equation (4).

Uncertainties and corrections

The contributions to the uncertainty of the neutron spectrum are (i) neutron scattering and self-shielding correction factors, (ii) corrections for interfering reactions, (iii) uncertainties in the cross sections and (iv) the uncertainties in the γ-ray activity measurements. The uncertainties in the γ-ray activity were determined following the *Guide to the expression of uncertainty in measurement* (14) and were discussed in section 2.2. The neutron field was assumed to be constant in the experiments. Correction factors for neutron scattering between discs and neutron self-shielding in discs were calculated using the MCNP-4C2 code, while no corrections for interfering reactions were needed in this work. The specific saturation activity was multiplied with the mentioned neutron correction factors before they were entered into the unfolding software to calculate the neutron spectrum.

The combined standard uncertainty of the contributions (i)-(iii) was estimated to 5%, which should be added to the uncertainty of the γ-ray measurements (iv) to give the total input uncertainty of the neutron energy distribution. In this study the uncertainty of the default ^{252}Cf reference fluence was given by PTB (15) to be 1.3%. In addition, the output spectrum contains uncertainties related to the unfolding procedure.

There is no standard method for determining the detection limit for a neutron spectrum calculated using unfolding techniques. Based on the previous work by Lövestam et al. (2008) (5) as well as the work in this paper, the authors have formulated an empirical definition applicable to different types of neutron spectra. The minimum requirements for determining a neutron spectrum are that at least six excitation functions are available with different shapes and thresholds as well as covering the neutron energy region of interest. In addition, the uncertainty of the specific saturation activity must be less than 20% for all reactions.

Activation irradiations

Validation experiment with a ^{252}Cf source at PTB

The validation experiment was done at PTB using a ^{252}Cf reference source in a low scattering room (16, 17). The neutron detection unit was mounted on an aluminium holder with a clamp of the same material, see Figure 2. The centre of the unit front plane was at a distance of 500 mm from the ^{252}Cf source and the normal between the front plane and the source was 0°.

The fluence rate of the direct neutrons at the location of the detector was calculated by PTB to be 8000(50) cm^{-2} s^{-1} for energies >0.3 MeV, taking into account the source strength, the distance, the measured anisotropy of the source and the attenuation due to the intermediate air. An additional spectral component from in-scattered neutrons was determined with the PTB Bonner sphere spectrometer (13) to about 8% of the direct neutrons, but in this study left without consideration as only 30% of the scattered neutrons have energies above 0.3 MeV, which is the minimum threshold energy for the included excitation functions (18). The irradiation time was 24 hours.

Application experiment with MOX fuel

During the years 1986 to 2006 Belgonucleaire (19, 20) in Dessel, Belgium, produced annually 35-38 tons of MOX fuel for fast breeders and light water nuclear reactors, but today the facility is closed. A MOX fuel element is a mixture of depleted uranium oxide (approx. 415 kg per container) and plutonium oxide (approx. 35 kg per container).

The MOX fuel rods are kept in leak-proof metal boxes with dimensions of approximately 4.5 m x 30 cm x 30 cm with 264 fuel elements in each (19). At Belgonucleaire all boxes are stored in a concrete bunker inside a warehouse. One box with fuel rods was taken out from the storage place and one neutron detector unit was positioned on the top surface at the centre of the box. The neutron radiation from the MOX fuel originates from spontaneous fission of plutonium nuclides and by (α,n) reactions with the oxygen nuclei. The detector unit was irradiated for 4.7 days and then transported to the low-level γ-ray laboratories at IRMM.

RESULTS AND DISCUSSION

Results from the experiment with the ^{252}Cf

Calculated data for the neutron irradiations were obtained by folding the data file for respective excitation function with the ^{252}Cf ISO spectrum (21). These results are similar to those obtained when unfolding with a flat default spectra. In Table 1 general information of each excitation function is listed together with the measured saturated radioactivity per atom (A_s), the total uncertainty (u_{total}) and the uncertainty in the γ-ray measurement (u_γ). The excitation data files were selected according to the c-m values, see Table 2. The following cross section data files were investigated for the excitation functions used in this work: Irdf-2002, ENDF VI, ENDF VII, JEFF 2.2, JEFF 3.0, JEFF 3.0/A, JEFF 3.1, JENDL 3.3, FENDL 2.1, BROND 2.2.

From the calculated c-m values it was obvious that the reactions ^{46}Ti(n,p)^{46}Sc and ^{48}Ti(n,p)^{48}Sc should not be used, but the reason for this is not known. The isotopic composition of the Ti discs was verified using secondary ion mass spectrometry (SIMS) and the result deviated less than 1% from the assumed natural composition of the included isotopes. Also neutron activation analysis was performed to assess the level of impurities in the Ti discs and particularly the concentration of scandium impurities since the cross section of the ^{46}Sc(n,γ)^{46}Sc reaction is relatively high for thermal neutrons. However, scandium was not detected and any levels under the detection limit of 1 μg/g were not considered to have any influence on the activation experiment. The only identified impurities were Na, Mn, Fe and As, all at μg/g level.

Using the ^{252}Cf energy spectrum from Ref. (21), the calculations show that the ^{47}Ti(n,np+d)^{46}Sc and ^{48}Ti(n,p,np+d)^{48}Sc reactions contribute with less than 0.2% to the final result and can thus be discarded. The (n,2n)-reactions with higher energy thresholds, ^{59}Co(n,2n)^{58}Co and ^{90}Zr(n,2n)^{89}Zr, have unexpectedly low c-m values while the ^{197}Au(n,2n)^{196}Au reaction has a value of 0.99. This can be du to the threshold energy of the ^{197}Au(n,2n)^{196}Au reaction (8.3 MeV) is lower than that of the ^{59}Co(n,2n)^{58}Co (10.7 MeV) and ^{90}Zr(n,2n)^{89}Zr (12.7 MeV) reactions, in a region where the ^{252}Cf spectrum is very low in intensity. Hence, those reactions were kept. The ^{54}Fe(n,p)^{54}Mn reaction also gives a low c-m value (0.82), which is discussed below.

Figure 3 shows the unfolded neutron spectrum together with the ISO ^{252}Cf spectrum. The step size is 0.1 MeV. The edges in the two spectra is explained by the reference spectrum having larger step size. When investigating the experimental spectrum in detail with a 0.1 MeV stepsize the disturbing effect of the larger steps in the reference spectrum is increased results in edges. An almost perfect agreement between the experimentally determined spectrum and the reference is obtained, except at very high energies, where the fluence rate is very low. The effect of including the ^{54}Fe(n,p)^{54}Mn reaction is seen in Figure 4 where the relative deviation of the unfolded curve, with and without the ^{54}Fe(n,p)^{54}Mn excitation function data, to the ISO ^{252}Cf spectrum is plotted. Below approximately 3 MeV the ^{54}Fe-reaction makes no difference while a small discrepancy up to maximum 5% at the neutron energy of 6 MeV can be discerned. Above the neutron energy of 8 MeV the relative difference increases dramatically, which is in the energy region where the ^{252}Cf spectrum is low in intensity. The ^{54}Fe(n,p)^{54}Mn reaction may be included if there is a lack of other reaction data, particularly for low energy spectra, but should otherwise be avoided.

The experimentally calculated neutron fluence rate for neutron energies >0.3 MeV in the validation experiment at PTB was determined to 8500 neutrons

cm^{-2} s^{-1}, which can be compared to the value given by PTB of 8000(50) neutrons cm^{-2} s^{-1}. The measured dose rate was determined to 11.7 mSv h^{-1}, which compares well to the value reported from PTB of 11.12(13) mSv h^{-1}.

Results from the MOX fuel experiment

The results from the irradiation are listed in Table 3. For the unfolding the spectrum "*Bare MOX fuel at 20 cm*" from IAEA's technical report 403 (22), was used as default input spectrum as described in section 2.3 and with uncertainties described in section 2.5. Due to the low neutron intensity, γ-ray data from only eight excitation reactions could be detected. In this experiment the $^{54}Fe(n,p)^{54}Mn$ reaction is included since higher energy neutrons are not expected. Also the $^{46}Ti(n,p)^{46}Sc$ and $^{48}Ti(n,p)^{48}Sc$ reactions are included, despite the absence of a plausible explanation for the large discrepancy when verifying the neutron spectrometer, as discussed in section *Results from the experiment with the ^{252}Cf.*

In Figure 5 the "*Bare MOX fuel at 20 cm*" spectrum as well as the "*MOX fuel at storage place*" spectrum from the IAEA report (22) are plotted together with the experimentally determined spectrum. The experimentally determined spectrum is similar to the one for "*Bare MOX fuel at 20 cm*", but with less pronounced peaks at 1 and 3 MeV, which is rather likely to be the case since the measured spectrum has been shielded by the metal box in contrast to the default spectrum. It is interesting to note that the experimentally determined unfolded spectrum is in remarkable agreement with the "*MOX fuel at storage place*". The experimentally determined neutron flux was 2200 neutrons cm^{-2} s^{-1} and the corresponding dose rate was determined to 3.1 mSv h^{-1}.

DISCUSSION

It is an advantage to perform the γ-ray measurements in an underground facility since the cosmically induced background radiation is significantly reduced. But, for this technique to become widely used it is for practical reasons required to develop a low-background γ-ray spectrometry set-up with low detection limits also above ground. Recent developments in low-level γ-ray spectrometry (23) with bigger crystals and lower levels of background have significantly decreased the detection limits, which should open for an increase in the numbers of low-level systems available above ground. The neutron detector described in this work can be used for fluence rates in the order of 1000 cm^{-2} s^{-1}. For lower fluence rates, in the range of about 40 cm^{-2} s^{-1}, as that detected by Lövestam et al (2008) (5), an underground laboratory would still be required. Provided that the impurities of the metal discs are on μg/g level or less it is possible to detect radionuclides that have well separated γ-ray lines by using low-background NaI-detectors, which in certain cases can render very low detection limits.

Further improvements of the neutron spectrometer would include investigations of the detection limits for different types of neutron spectra and tests in different activation conditions. Finally, a thorough evaluation of the available cross section data files should be performed in order to identify additional suitable activation reactions.

Acknowledgements

The work done by EURIDICE and the HADES crew of SCK•CEN in Mol, Belgium, is gratefully acknowledged.

The authors thank Magnus Hedberg at the European Commission Joint Research Centre, Institute for Transuranium Elements, Karlsruhe, Germany, for the investigation of the isotopic composition of the titanium discs.

REFERENCES

1. IAEA, Vienna, Austria. Report on the Preliminary Fact Finding Mission Following the Accident at the Nuclear Fuel Processing Facility in Tokaimura, Japan (1999).
2. Komura, K., Yousef, A.M., Murata, Y., Mitsugashira, T., Seki, R., Imanaka, T. Activation of gold by the neutrons from the JCO accident. J. Env. Rad. 50 (1), 77-82 (2000).
3. Gasparro, J., Hult, M., Komura, K., Arnold, D., Holmes, L., Johnston, P.N., Laubenstein, M., Neumaier, S., Reyss, J.L., Schillebeeckx, P., Tagziria, H., Van Britsom, G., Vasselli, R. Measurements of ^{60}Co in spoons activated by neutrons during the JCO criticality accident at Tokai-mura in 1999. J. Env. Rad. 73(3), 307-321 (2004).
4. Hult, M., Gasparro, J., Shizuma, K., Vasselli, R., Neumaier, S., Arnold, D. Deep underground measurements of ^{60}Co in steel exposed to the Hiroshima atomic bomb explosion. Appl. Rad. Isot. 61, 173-177 (2004).
5. Lövestam, G., Hult, M., Fessler, A., Gasparro, J., Kockerols, P., Okkinga, K., Tagziria, H., Vanhavere, F., Wieslander, J.S.E. Neutron fluence spectrometry using disk activation. Accepted to Radiation Measurements (2008).
6. Thomas, D.J., Alevra, A.V. Bonner sphere spectrometers – a critical review. Nucl. Inst. and Meth. A 476, 12-20 (2002).
7. Hult, M., Preuße, W., Gasparro, J. Underground Gamma-ray spectrometry. Acta Chimica Slovenica 53, 1-7 (2006).
8. Nelson, W.R., Hirayama, H., Rogers, D.W.O. The EGS4 code system. SLAC Report (1985).
9. Sima, O., Arnold, D., Dovlete, C. GESPECOR: a versatile tool in gamma-ray spectrometry. J. Radioanal. Nucl. Chem. 248(2), 359-364 (2001).
10. www.nucleide.org/DDEP.htm
11. www.nndc.bnl.gov/ensdf/
12. Reginatto, M. and Goldhagen, P. MAXED, A computer code for maximum entropy deconvolution of

multisphere neutron spectrometer data. Health Phys. 77 (5), 579-583 (1999).
13. International Standard Organisation, Geneva, Switzerland, ISO 8529-3. Reference neutron radiations: Calibration of area and personal dosimeters and determination of their response as a function of neutron energy and angle of incidence (1998).
14. International Standard Organisation, Geneva, Switzerland, ISO/IEC/OIML/BIPM. Guide to the expression of uncertainty in measurement, (1st corrected edition) (1995).
15. Private Communication, Andreas Zimbal, Physikalisch-Technische Bundesanstalt, PTB, Braunschweig, Germany.
16. International Standard Organisation, Geneva, Switzerland, ISO 8529-1. Reference neutron radiations: Characteristics and Methods of production (2001).
17. Kluge, H., Irradiation facility with radioactive reference neutron sources: Basic principles, PTB Report, PTB-N-34, ISBN 3-89701-192-1 (1998).
18. Kluge, H., Alevra, A.V., Jetzke, S., Knauf, K., Matzke, M., Weise, K. and Wittstock, J. Scattered neutron reference fields produced by radionuclide sources. Radiat. Prot. Dosim. 70, 327-330 (1997).
19. www.belgonucleaire.be/uk/mox.htm
20. Olaerts, R., Kockerols, P., Renard, A., Rosenstock, W., Köble, T., Vanhavere, F. Determination of neutron spectra in a MOX plant for the qualification of the BD-PND bubble detector. Health Physics Society, 77 (2), 200-206 (1999).
21. International Standard Organisation, Geneva, Switzerland, ISO 8529-1, (E) p.7 (2001).
22. IAEA, Vienna, Austria. Compendium of Neutron Spectra and Detector Responses for Radiation Protection Purposes. Technical Report Series 403, ISBN 92-0-102201-8 (2001).
23. Hult, M. Low-level gamma-ray spectrometry using Ge-detectors. Metrologia 44 S87-S94 (Erratum in Metrologia 44, 425) (2007).

Table 1. The nuclear reactions used in the validation experiment at PTB. A_s is the saturated activity at the end of activation, u_γ is the relative uncertainty for the γ-ray measurement and u_{total} is the total calculated total relative uncertainty.

Activation reaction	Threshold (MeV)	$t_{1/2}$	γ-ray energy (keV)	A_s (10^{-24} Bq·atom^{-1})	u_γ (%)	u_{total} (%)
^{24}Mg(n,p)^{24}Na	0.6	15.0 h	1369	8.3	6.5	7.2
^{27}Al(n,α)^{24}Na	5.1	15.0 h	1369	49	18.2	18.5
^{46}Ti(n,p)^{46}Sc	3.0	84 d	889	3.0	11.1	11.5
^{47}Ti(n,p)^{47}Sc	0.8	3.35 d	159.3	1.9	15.1	15.4
^{48}Ti(n,p)^{48}Sc	3.6	1.82 d	175.3, 983.5, 1038, 1312	13.6	4.6	5.5
^{54}Fe(n,p)^{54}Mn	1.1	312 d	834.8	474	7.4	8.0
^{56}Fe(n,p)^{56}Mn	3.2	2.58 d	847	14.7	7.1	7.7
^{59}Co(n,α)^{56}Mn	4.0	2.58 h	847	1467	12.1	12.5
^{59}Co(n,2n)^{58}Co	10.7	70.9 d	811	1794	2.1	3.7
^{59}Co(n,p)^{59}Fe	1.6	44.5 d	1099, 1292	20.0	5.7	6.4
^{58}Ni(n,p)^{58}Co	0.8	70.8 d	810	959	4.3	5.2
^{90}Zr(n,2n)^{89}Zr	12.7	3.27 d	909.2	64	11.4	11.8
^{113}In(n,n')^{113}In	0.4	1.66 h	392	166	5.5	6.2
^{115}In(n,n')^{115}In	0.4	4.49 h	336.3	2.3	9.1	9.6
^{197}Au(n,2n)^{196}Au[1]	8.3	6.18 d	333.0, 355.7	1.2	20.3	20.5

[1]Significant contribution from a short-lived isomeric state.

Table 2. Evaluated data files used for respective excitation function in the validation experiment at PTB. The reactions ^{46}Ti(n,p)^{46}Sc and ^{48}Ti(n,p)^{48}Sc were not included in the unfolding. The c-m value is the ratio of the calculated to measured data. The c-m value of the ^{54}Fe(n,p)^{54}Mn reaction is taken from the second irradiation experiment at PTB.

Activation reaction	Data file	c-m value for default spectrum
^{24}Mg(n,p)^{24}Na	ENDF VII, JEFF 3.1, JENDL 3.3	1.00
^{27}Al(n,α)^{24}Na	JENDL 3.3	0.92
^{46}Ti(n,p)^{46}Sc	JEFF 3.1	0.57
^{47}Ti(n,p)^{47}Sc	JEFF 3.1	0.98
^{48}Ti(n,p)^{48}Sc	JEFF 3.1	0.66
^{54}Fe(n,p)^{54}Mn	JEFF 3.1	0.82
^{56}Fe(n,p)^{56}Mn	JEFF 2.2	0.92
^{59}Co(n,α)^{56}Mn	JENDL 3.3	0.98
^{59}Co(n,2n)^{58}Co	JEFF 3.0/A	0.78
^{59}Co(n,p)^{59}Fe	ENDF VII, FENDL 2.1, JEFF 3.1	0.95
^{58}Ni(n,p)^{58}Co	ENDF VI, FENDL 2.1, JEFF 3.1	1.00
^{90}Zr(n,2n)^{89}Zr	JEFF 3.0/A	0.58
^{113}In(n,n')^{113}In	JEFF 3.0/A	1.23
^{115}In(n,n')^{115}In	JEFF 3.0/A	1.15
^{197}Au(n,2n)^{196}Au	ENDF VII, FENDL 2.1, JEFF 3.1	0.99

Table 3. The measured specific saturation activity from irradiation by a MOX nuclear fuel box. A_s is the specific saturated activity at the end of the irradiation, u_γ is the uncertainty from the γ-ray measurement, u_{other} is the additional estimated uncertainty and finally u_{total} is the combination of u_γ and u_{other}.

Activation reaction	A_s (10^{-24} Bq·atom^{-1})	u_γ (%)	u_{other} (%)	u_{total} (%)
^{24}Mg(n,p)^{24}Na	0.70	13.4	5.0	14.3
^{46}Ti(n,p)^{46}Sc	4.13	25.5	5.0	26.0
^{47}Ti(n,p)^{47}Sc	19.24	4.9	5.0	7.0
^{48}Ti(n,p)^{48}Sc	0.12	11.8	5.0	12.8
^{54}Fe(n,p)^{54}Mn	79.99	9.1	5.0	10.4
^{58}Ni(n,p)^{58}Co	84.87	4.2	5.0	6.5
^{113}In(n,n')^{113}In	235.21	24.7	5.0	25.2
^{115}In(n,n')^{115}In	283.93	4.6	5.0	6.8

FIGURES

Figure 1. Photo of the second-generation neutron detector unit. The overall diameter of the detector unit is 120 mm.

Figure 2. Close up photo of the neutron spectrometer during activation with the calibrated ^{252}Cf source at PTB, Braunschweig, Germany.

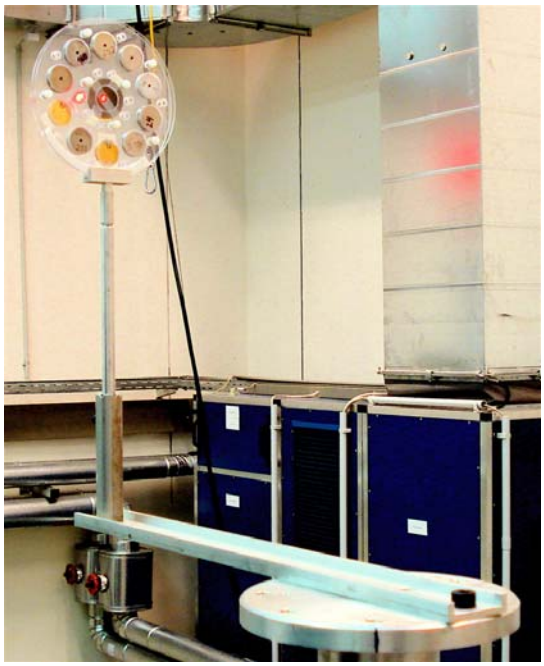

Figure 3. The unfolded spectrum for the validation experiment at PTB, together with the ISO ^{252}Cf spectrum. The data is plotted with stepsize 0.1 MeV.

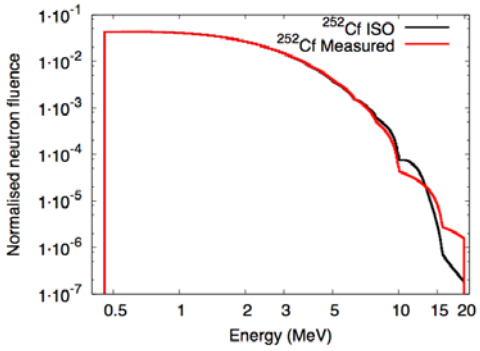

Figure 4. The effect of including the ^{54}Fe(n,p)^{54}Mn reaction in the unfolded spectrum in Figure 3. The relative difference (in %) to the ISO spectrum is shown for the experimentally determined spectra with and without the ^{54}Fe(n,p)^{54}Mn reaction.

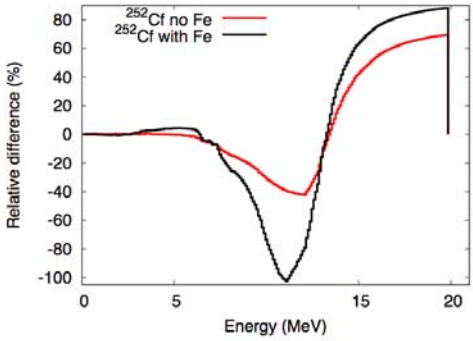

Figure 5. The experimentally determined MOX nuclear fuel spectrum (red) from the experiment at Belgonucleaire together with the "*MOX fuel at storage place*" (black) and "*Bare MOX fuel at 20 cm*" (blue) spectrum from the IAEA report (22).

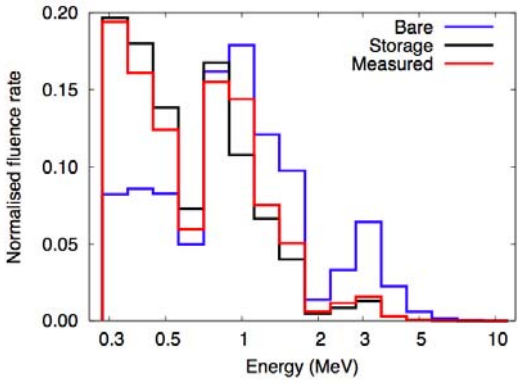

Paper VII a

This paper **will be submitted 2009** to Physical Review Letters (American Physical Society), this is an almost complete paper.

J.S.E. Wieslander, M. Hult, J, Suhonen, T. Eronen, M.T. Mustonen, V.V. Elomaa, A. Jokinen, G. Marissens, M. Misiaszek, S. Rahaman, C. Weber and J. Äystö, *The smallest known Q value of a nuclear decay: the rare β decay of $^{115}In(9/2^{+})$ to $^{115}Sn(3/2^{+})$.*

The smallest known Q value of a nuclear decay: the rare β^- decay of ^{115}In$(9/2^+) \rightarrow {}^{115}Sn(3/2^+)$

J.S.E. Wieslander,[1,2] M. Hult,[1] J. Suhonen,[2] T. Eronen,[2] M.T. Mustonen,[2] V.-V. Elomaa,[2] A. Jokinen,[2] G. Marissens,[1] M. Misiaszek,[3] S. Rahaman,[2] C. Weber,[2] and J. Äystö[2]

[1] *EC-JRC-IRMM, Institute for Reference Materials and Measurements, Retieseweg 111, B-2440 Geel, Belgium*
[2] *Department of Physics, P.O. Box 35 (YFL), FI-40014 University of Jyväskylä, Finland*
[3] *M. Smoluchowski Institute of Physics, Jagiellonian University, ul. Reymonta 4, 30-059 Krakow, Poland*

(Dated: February 20, 2009)

The ground-state-to-ground-state Q_{β^-} value of ^{115}In was determined to 497.68(17) keV using a high precision Penning trap facility. From this, a Q_{β^-} value of 0.35(17) keV is obtained for the *rare β^- decay* to the first excited state of ^{115}Sn at 497.334(22) keV. The first underground measurement specifically designed to detect the 497.334 keV γ-ray from this rare decay was performed and the corresponding half-life and branching ratio were determined to $4.1(6)\times10^{20}$ y and $1.07(17)\times10^{-6}$ respectively. Due to uncertainties in description of such ultra-low Q values the theoretical modelling of this 2^{nd}-forbidden unique β^- transition yields only the lower limit $Q_{\beta^-} > 0.039$ keV using the measured half-life. Both the theory and the measurements imply the discovery of the lowest Q value of a known nuclear β decay.

PACS numbers: 21.10.Dr, 23.40.Bw, 23.40.-s, 27.60.+j, 29.30.Kv

It is debatable whether the β^- decay ^{115}In$(9/2^+) \rightarrow {}^{115}Sn(3/2^+)$ is energetically possible or not. From the most recent mass evaluation [1], the energy of the ground-state-to-ground-state β^- decay of ^{115}In is 499(4) keV. Given that the energy of the first excited state in ^{115}Sn is 497.334(22) keV [2], the available β^- decay energy to this excited state ^{115}Sn$(3/2^+)$ is only 1.7(40) keV. Cattadori et al. [3] detected this *rare decay* by measuring the 497.334 keV γ-ray from a 929 g pure indium rod using an ultra low-background γ-ray spectrometer in the Gran Sasso National Laboratory 3800 m water equivalent (m w.e.) below ground. The measurement was a spin-off from experiments to characterise the bremsstrahlung spectrum of ^{115}In, as a part of the LENS neutrino project. Fig. 1 shows the decay scheme of ^{115}In based on ENSDF [2] with the inclusion of the β^-decay to ^{115}Sn(3/2+), which is the focus of this study. In the work presented here this decay is examined through: (i) measurements of the cyclotron frequency of ^{115}In and ^{115}Sn in order to determine the ground-state-to-ground-state Q_{β^-} value of ^{115}In, which in turn is used to obtain the Q_{β^-} value for the rare decay, (ii) underground γ-ray spectrometry measurements to detect the 497.334 keV γ-ray from which the partial half-life of the decay is accurately determined and (iii) a theoretical calculation of the transition energy, the Q_{β^-} value, for the rare decay.

The ground-state-to-ground-state Q_{β^-} value of ^{115}In to ^{115}Sn was measured with the JYFLTRAP Penning trap facility [4] at the accelerator laboratory of the University of Jyväskylä. The measurement procedure was similar to the Q value measurements of superallowed β emitters [5]. The Q_{β^-} value was determined by high precision measurements of the cyclotron frequency ratio of

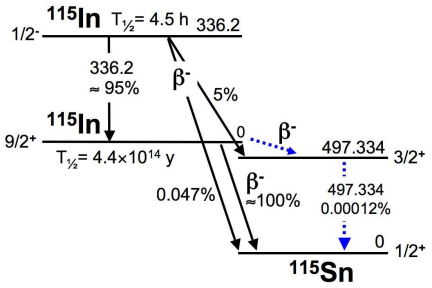

FIG. 1: The decay level scheme of ^{115}In, including the decay to the first excited state of ^{115}Sn (dotted blue line).

the parent and daughter ions:

$$Q_{\beta^-} = m_1 - m_2 = \left(\frac{\nu_2}{\nu_1} - 1\right)(m_d - q m_e)\,, \qquad (1)$$

where m_1, m_2 and m_e are the masses of the parent atom, the daughter atom and an electron respectively, $\frac{\nu_2}{\nu_1}$ is the cyclotron frequency ratio of corresponding ions having the charge state q. The binding energies of the atomic electrons can be neglected. The ions were produced using a spark ion source [6]. The composition of the spark electrode was prepared such that roughly the same intensity of ion beam was simultaneously produced for both ion species. A clean sample of either ^{115}Sn or ^{115}In was prepared using the Ramsey cleaning technique [7]. This was done prior to the frequency measurement of the selected species, using time-of-flight ion-cyclotron resonance technique [8, 9] in combination with the time-separated oscillatory fields technique [10].

The determination of the cyclotron frequency of one ion species took approximately one hour and a representative resonance is shown in Fig. 2. The frequency ratio was determined by interleaving the measurements of the two species to account for the drift of the magnetic field.

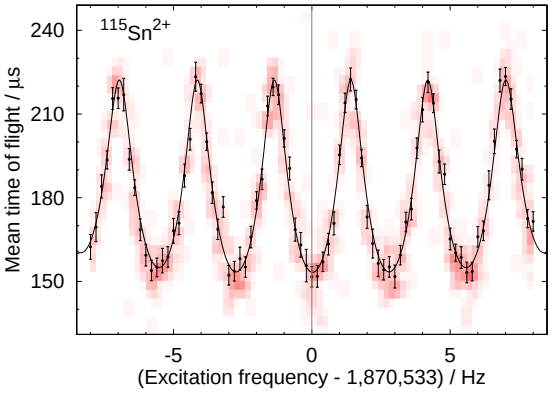

FIG. 2: A representative time-of-flight ion-cyclotron resonance obtained for $^{115}Sn^{2+}$ ions using the excitation time pattern of (50-350-50) ms (On-Off-On).

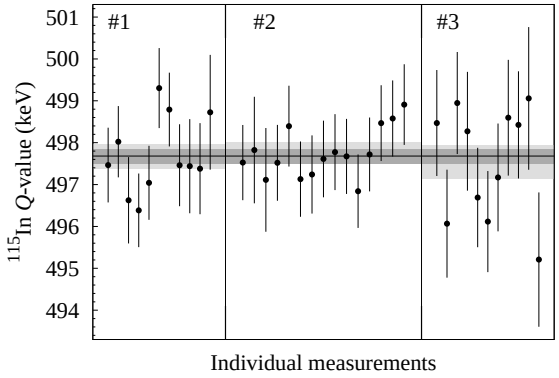

FIG. 3: The individual Q_{β^-} values. The values are grouped in sets (denoted with $\#N$). The light grey band is the average of each set with one standard deviation. The dark grey horizontal line is the total average with one standard deviation.

In this way, a weighted mean Q_{β^-} value could be calculated from several individual frequency ratios. Three sets of data were collected consisting of 11, 15, and 11 individual frequency ratios. The Q_{β^-} values derived from these individual ratios are plotted in Fig.3. The first and second set were measured with single charged ions while the third set was measured with doubly charged ions. The obtained frequency ratios and Q values are given in table I. Finally, the Q_{β^-} value 0.35(17) keV of the transition $^{115}\mathrm{In}(9/2^+) \rightarrow {}^{115}\mathrm{Sn}(3/2^+)$ is deduced from the value in table I, given that the energy of the excited state $^{115}\mathrm{Sn}(3/2^+)$ is 497.334(22) keV [2]. This indicates that the rare β^- decay is energetically possible.

TABLE I: Results of the measurements. Column "q" denotes the charge state of the ions used and column "No." the number of obtained individual frequency ratios.

Set	q	No.	Frequency ratio, $\frac{\nu_{\mathrm{Sn}}}{\nu_{\mathrm{In}}}$	Q_{β^-} (keV)
#1	1	11	1.0000046497(27)	497.66(29)
#2	1	15	1.0000046506(23)	497.76(24)
#3	2	11	1.0000046484(37)	497.53(40)
Final Q_{β^-} of ^{115}In(gs)–^{115}Sn(gs) decay				**497.68(17)**

Three γ-ray spectrometry measurements of a radiopure indium sample were carried out in the underground laboratory HADES located at a depth of 500 m w.e. [11]. The objective was to confirm or dispute the observation of the rare decay done by Cattadori et al. [3], as well as to perform a dedicated measurement in a simple geometry and thereby reduce the final uncertainty. To detect this low level of activity it is important to perform the measurements in a deep (Gran Sasso) or semi-deep (HADES) underground γ-ray laboratory in order to reduce the cosmogenic activation of the sample and detectors.

The indium disc was of natural isotopic abundance with 95.71(5)% of the isotope ^{115}In [12]. After surface cleaning the disc dimensions were 10.6 cm (diameter), 4.0 cm (thickness) and 2566.13 g (total mass). Three different ultra low-background γ-ray spectrometers were made available in HADES for these measurements (measurement time in brackets): Ge-4 (48 days), Ge-7 (15 days) [13] and the Sandwich Spectrometer (14 days) [13]. Ge-4 is a p-type, coaxial HPGe detector with a submicron dead layer, the other detectors are described in [13].

The bremsstrahlung spectrum from the ground-state-to-ground-state β^-decay is clearly visible in the γ-ray spectrum in Fig. 4. However, the excited state of ^{115}In was not present in the sample at the time of measurement, since the 336 keV γ-ray line from the main branch was not detected. The peak of interest, 497.334 keV, is located in a favourable energy region with low continous background and without any interfering background peaks. The count rate is low, typically 456 d^{-1} in the interval 10–2700 keV for Ge-4. There are no pile-up effects from the bremsstrahlung. The decision threshold (α=0.05 [14]) for the rare decay was in these measurements 500 μBq for the Sandwich Spectrometer and 280 μBq for Ge-4. The decision thresholds for the following naturally occuring contaminants indicate the radiopurity of the sample: ^{40}K 2 mBq/kg, ^{228}Ra 0.5 mBq/kg, ^{228}Th 0.4 mBq/kg. Careful analysis confirmed the absence of any unknown γ-ray emitters in the spectra, which was also the conclusion of Cattadori et al. after a thorough study of alternative sources of the detected 497 keV γ-ray line in their experiment. The full energy peak (FEP)

TABLE II: Results from the γ-ray measurements on spectrometers Ge-4, Ge-7 and the Sandwich Spectrometer (SW) [13]. The only previous measurement by Cattadori et al. [3] is included for comparison. BR is the branching ratio, $t_{1/2}$ is the partial half-life and Rel.U is the relative uncertainty.

Spectrometer	BR	$t_{1/2}(10^{20}$ y)	Rel.U(%)
Ge-4	1.06(17)	4.2(7)	17
Ge-7	1.0(5)	4.4(2.0)	45
SW	1.2(4)	3.6(1.2)	42
HADES final	**1.07(17)**	**4.1(6)**	**15**
For comparison			
Cattadori et al.	1.2(3)	3.7(1.0)	26

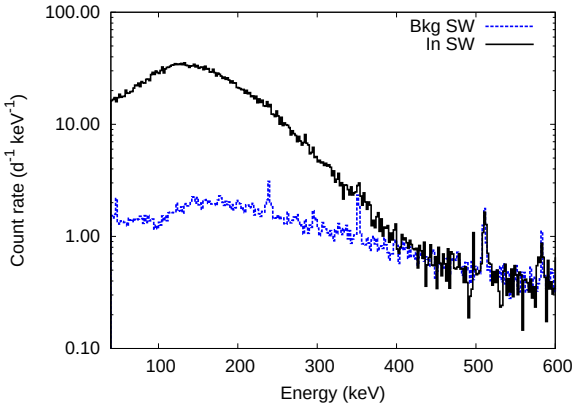

FIG. 4: γ-ray spectrum of indium (In, black solid line) and the background (Bkg, blue dotted line) on the Sandwich Spectrometer (SW).

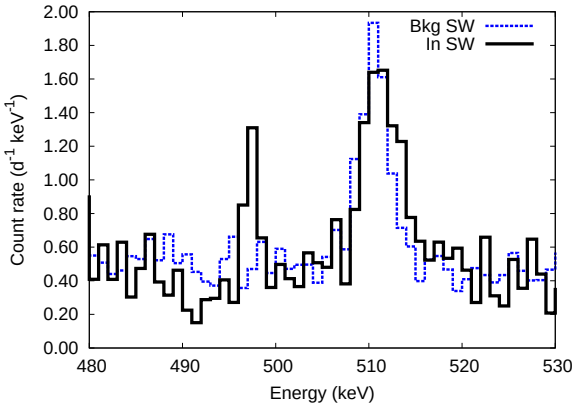

FIG. 5: γ-ray spectrm of indium (In, black solid line) and the background (Bkg, blue dotted line) on the Sandwich Spectrometer (SW).

detection efficiencies were calculated using the Monte Carlo technique and the EGS4 simulation software. The geometrical model used for the Monte Carlo simulations was validated by measuring point sources (^{85}Sr, ^{137}Cs, ^{134}Cs) sandwiched between indium discs of 3, 6 and 12 mm thickness. These measurements confirmed that the calculated FEP detection efficiencies agree within 3%.

The weighted mean activity of the three measurements was 0.69(9) mBq. Using the natural isotopic abundance of ^{115}In this converts to a partial half-life of $4.1(6)\times10^{20}$ y. The relative combined standard uncertainty was determined to 15% and is dominated by counting statistics (14%). Other major contributions to the total uncertainty are: the FEP detection efficiency (3%), the isotopic abundance (0.05%) and the internal conversion coefficient (0.12%). The branching ratio was calculated to $1.07(17)\times10^{-6}$, which contains an additional uncertainty of 5.7% from the half-life of the ground-state-to-ground-state β^-decay. The measurements in this work are in agreement with that of Cattadori et al., see table II.

The β^- decay of the ground state of ^{115}In to the first excited state in ^{115}Sn is 2^{nd}-forbidden unique. For a

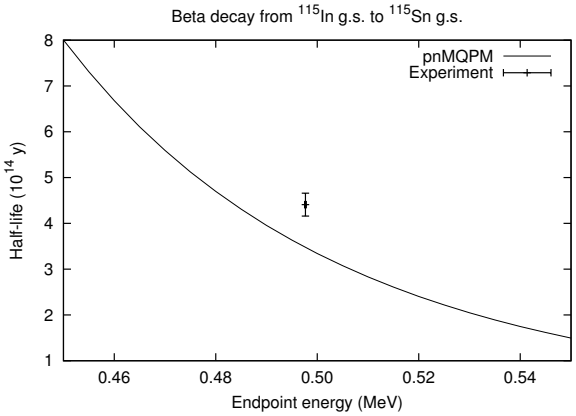

FIG. 6: Calculated half-life of the ground-state-to-ground-state β^- decay of ^{115}In as the function of the endpoint energy. The experimental bars combine the half-life range from Ref. [20] and the Q-value range extracted in the present trap measurement.

unique decay the nuclear-structure information is contained in only one nuclear matrix element (NME), as seen from the following expression for the half-life of the Kth forbidden unique β^- transition

$$T_{1/2} = \frac{1}{M^2 f_K(w_0, Z_f, R)}. \qquad (2)$$

Here M is the NME (equivalent to M_4 in Refs. [15, 16] and ${}^A\mathcal{M}^{(0)}_{K+1,K,1}$ in Ref. [17]) and $f_K(w_0, Z_f, R)$ is a phase-space function which only depends on the endpoint energy $W_0 = w_0 m_e c^2$, the charge Z_f of the daughter nucleus and the nuclear radius R. The detailed expression for the function f_K reads [15, 17]

$$\begin{aligned} f_K(w_0, Z, R) =& \frac{g_A^2 (6.706\times10^{-6})^K}{\kappa} \frac{(2K)!!}{(2K+1)!!} \\ & \times \int_1^{w_0} dw_e \sum_{k_e+k_\nu=K+2} F_{k_e-1}(Z, w_e) \\ & \times \frac{w_e p^{2k_e-1} (w_0 - w_e)^{2k_\nu}}{(2k_e-1)!(2k_\nu-1)!} \ , \end{aligned}$$

where g_A stands for the axial coupling constant, $F_{k_e-1}(Z, w_e)$ is the generalized Fermi function as defined in Ref. [15], w_e is the electron energy in units of electron rest mass, $p = \sqrt{w_e^2 - 1}$ and the constant $\kappa = 6147$ s [18].

We have calculated the NME M using the same pnMQPM description of the initial and final nuclei as in Ref. [19], where the model was applied to the fourth-forbidden non-unique ground-state-to-ground-state decay of ^{115}In. The theoretical curve for the half-life of that decay as a function of the Q value is shown in Fig. 6. The calculation marginally disagrees with the data shown in the figure, showing that our calculation reproduces reasonably well the features of the ground-state transition.

In Fig. 7 we plot the endpoint energy dependence of the partial half-life for the transition ^{115}In$(9/2^+) \rightarrow$

^{115}Sn($3/2^+$) by using our calculated NME and its estimated conservative 30% error. The deviation of the calculated curve from the present data, shown in the figure, is much larger than in the case of the ground-state transition. This difference between the calculation and the data can stem either from the nuclear or the phase-space uncertainties. From the nuclear-structure point of view all crystalizes in the value of the one and only participating NME. Based on the experience with the ground-state transition we do not expect the magnitude of this computed NME to be very far from the correct one. On the other hand, the involved small decay energy poses a challenge to the phase-space calculations. One problem relates to the electron screening corrections that are known [17] to be very important for the β^+ and electron-capture decays. These corrections seem to be small for the allowed β^- decays even at vanishingly small Q values [22**?**]. For the forbidden decays these corrections obviously increase the half-life but we do not know how much. A second source of correction to the phase-space is the mismatch between the initial and final *atomic* states in β decay. In β decay the nucleus changes its charge by one unit so that the initial atomic state is not any more a stationary state of the final nucleus and its surrounding electrons. This leads to an incomplete overlap of the initial and final atomic states and thus reduces the β decay rate [23]. Further corrections come from exchange effects [23, 24] and final-state interactions [25].

What is common to all the above mentioned corrections is that the theories behind them have not been designed to apply to ultra-low Q values as in the case here. It seems, however, that the bulk of these corrections shifts the shaded theory band in Fig. 7 upwards by a yet unknown amount. Thus, from Fig. 7 we can produce only the lower limit $Q_{\beta^-} > 0.039$ keV for the Q_{β^-} value.

The principal conclusion emerging from the present study is that the combined efforts of the two measurements and the theoretical investigation of the β^-transition ^{115}In($9/2^+$) $\rightarrow$ ^{115}Sn($3/2^+$) suggest that this *rare decay* may have the lowest Q value discovered for any nuclear beta decay so far, about one order of magnitude smaller than that of ^{187}Re [26].

This work was supported by the EU 6th Framework programme "Integrating Infrastructure Initiative - Transnational Access", Contr. No. 506065 (EURONS, JRA TRAPSPEC) and by the Finnish Center of Excellence Prog. 2006–2011 (Proj. No. 213503, Nuclear and Accelerator Based Physics Programme at JYFL).

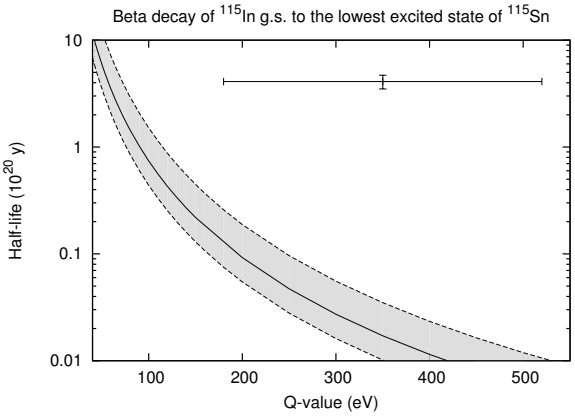

FIG. 7: Calculated relation between the Q value and partial half-life for the β^- decay ^{115}In($9/2^+$) $\rightarrow$ ^{115}Sn($3/2^+$). The pnMQPM description of Ref. [19] has been used to obtain the required NME. The grey band indicates a conservative 30% error estimate for the NME. The experimental bars combine the half-life and Q-value ranges extracted in the present underground and trap measurements.

[1] G. Audi A.H. Wapstra and C. Thibault, Nucl. Phys. A **729**, 337 (2003).
[2] Nuclear Data Sheets, **104(4)**, 967 (2005).
[3] C. Cattadori *et al.*, Nucl. Phys. A **748**, 333 (2005).
[4] A. Jokinen *et al.*, Int. J. Mass Spectr. **251**, 204 (2006).
[5] T. Eronen *et al.*, Phys. Rev. Lett. **100**, 132502 (2008).
[6] S. Rahaman *et al.*, Phys. Lett. B **662**, 111 (2008).
[7] T. Eronen *et al.*, Nucl. Instr. Meth. B **266**, 4527 (2008).
[8] M. König *et al.*, Int. J. Mass Spectr. Ion Processes **142**, 95 (1995).
[9] G. Gräff, H. Kalinowsky, and J. Traut, Z. Phys. A **297**, 35 (1980).
[10] S. George *et al.*, Int. J. Mass Spectrom. **264**, 110 (2007).
[11] M. Hult, W. Preuβe and J. Gasparro, Acta Chim. Slov. **53**, 1-7 (2006).
[12] IUPAC, Pure and Appl. Chem. **70(1)**, 217-235 (1998).
[13] J.S.E Wieslander *et al.*, Appl. Rad. Isot. (2009), doi:10.1016/j.apradiso.2009.01.026.
[14] ISO 11929-3, (2000).
[15] M.T. Mustonen, M. Aunola, and J. Suhonen, Phys. Rev. C **73** (2006) 054301; Phys. Rev. C **76**, 019901(E) (2007).
[16] H. Heiskanen, M.T. Mustonen, and J. Suhonen, J. Phys. G: Nucl. Part. Phys. **34**, 837 (2007).
[17] H. Behrens and W. Bühring, *Electron Radial Wave Functions and Nuclear Beta-Decay* (Clarendon, Oxford, 1982).
[18] J. Hardy *et al.*, Nucl. Phys. A **509**, 429 (1990).
[19] M.T. Mustonen and J. Suhonen, Phys. Lett. B **657**, 38 (2007).
[20] L. Pfeiffer *et al.*, Phys. Rev. C **19**, 1035 (1979); L. Pfeiffer *et al.*, Phys. Rev. Lett. **41**, 63 (1978).
[21] J.J. Matese and W.R. Johnson, Phys. Rev **150**, 846 (1966).
[22] J.L. Lopez and L. Durand, Phys. Rev. C **37**, 535 (1988).
[23] J.N. Bachcall, Phys. Rev. C **129**, 2683 (1963).
[24] M.R. Harston and N.C. Pyper, Phys. Rev. A **45**, 6282 (1992).
[25] A. Saenz and P. Froelich, Phys. Rev. C **56**, 2132 (1997).
[26] M. Galeazzi *et al.*, Phys. Rev. C **63**, 014302 (2000).

Paper VII b

This paper **will be submitted 2009** to Physical Review C or similar later, this is a draft version of a long detailed paper.

J.S.E. Wieslander, M. Hult, J, Suhonen, T. Eronen, M.T. Mustonen, V.V. Elomaa, A. Jokinen, G. Marissens, M. Misiaszek, S. Rahaman, C. Weber and J. Äystö, *Underground measurement of the rare β^- decay of the ^{115}In ground state to the first excited state of ^{115}Sn*.

Underground measurement of the rare β^- decay of the ^{115}In ground state to the first excited state of ^{115}Sn

J. S. E. Wieslander[1,2], M. Hult[1]*, J. Suhonen[2], T. Eronen[2], V-V. Elomaa[2], A. Jokinen[2], G. Marissens[1], M. Misiaszek[3], M.T. Mustonen[2], S. Rahaman[2], J. Suhonen[2], C. Weber[2] and J. Äystö[2]

[1]*EC-JRC-IRMM, Institute for Reference Materials and Measurements, Retieseweg 111, B-2440 Geel, Belgium*

[2]*Department of Physics, P.O. Box 35, FIN-40014 University of Jyväskylä, Finland*

[3]*M. Smoluchowski Institute of Physics, Jagiellonian University, ul. Reymonta 4, 30-059 Krakow, Poland*

* Corresponding Author: Phone +32 14 571 269, FAX +32 14 584 273, e-mail mikael.hult@ec.europa.eu, elisabeth.wieslander@gmail.com

Abstract

The β^- decay of ^{115}In to the first excited state of ^{115}Sn is a rare decay that is discovered in this work to have the lowest Q value (57±3) eV known to man, a value two orders of magnitude lower than the previously lowest value determined for ^{187}Re. The first underground measurement specifically designed to detect the 497.4 keV γ-ray from this rare decay is presented and the partial half-life and branching ratio were determined to $(4.1\pm0.6)\cdot10^{20}$ years and $(1.07\pm0.17)\cdot10^{-6}$ respectively. Using a recently developed implementation of the complex theoretical model of the rare decay, the pnMQPM formalism, the Q value was determined as well as the logarithm of the comparative half-life, $\log ft_{1/2}$ (12.9±0.8).

Keywords: Ultra low-level γ-ray spectrometry, branching ratio, underground laboratory, HPGe detectors, low background measurements, decay data, indium

PACS:
23.20.Lv, 23.40.-s, 07.85.Fv and Nc, 29.30.Kv, 27.60.+j, 29.40.Wk

1. Introduction

In 1967 Murri et al observed for the first time a 497 keV γ-ray following the β^- decay from the first excited state in ^{115}In to the first excited state of ^{115}Sn. In the late 1970's interest around the decays of indium grew as research was done to investigate the usefulness of indium in liquid scintillators for low-background measurements of solar neutrinos and the present data in ENSDF is mainly a result of that (Pfeiffer et al 1979). Figure 1 shows the decay scheme based on data taken from ENSDF (2008) with the addition of the rare β^- decay from the ground state of ^{115}In to the first excited state in ^{115}Sn, which is the focus of this work. This transition is a 2nd-forbidden unique decay ($\Delta J = 3$, with no change of parity). Cattadori et al (2005) published the first value of the rare decay branching ratio $(1.18 \pm 0.31)\cdot 10^{-6}$ from a measurement performed underground in the Gran Sasso National Labratories, Italy. The observation of the rare decay was a spin-off from a measurement to characterize the bremsstrahlung spectrum of the β^- decay from the ground state in ^{115}In to the ground state in ^{115}Sn, which was done to support the LENS solar neutrino experiment. In their experiment, a 929 g rod of indium with natural isotopic abundance was measured for 115 days using an HPGe detector with 4 crystals in one cryostat.

The progress in low-level γ-ray spectrometry in recent years (Hult 2007) and particularly the developments in underground measurements (Hult et al 2006) has brought along great possibilities regarding measurements of rare decay events. The branching ratio in this case is considered a rare decay since it is 10^6 times less common than that of the main branch. This work presents the first underground measurements targeted for this specific β^- decay and seeks to both confirm the observation done by Cattadori and co-workers, as well as to perform a measurement in a simpler geometry and thereby reduce the final uncertainty. Additionally, recent developments regarding the theoretical model of this rare 2nd-forbidden unique decay by Mustonen and Suhonen (2007) finally makes it possible to accurately determine the released decay energy, Q, and comparative half-life, ft.

2. Materials and methods

2.1 Sample

The sample used for these measurements is a disc of ultra pure indium of natural isotopic abundance. The isotopic abundance of the isotope with mass number 115 is according to IUPAC (1998) 95.71(5)%. In order to remove any surface impurities, the sample was submerged for 10 minutes in a solution of 65% HNO_3. This resulted in a loss of 90 g of material and a somewhat uneven surface. After cleaning the disc mass is 2566.13 g, the diameter 10.6 cm and the thickness 4.0 cm. The sample was stored in the underground laboratory before the measurement to ensure that there would be no contribution to the 497.4 keV line from the decay of the excited state of ^{115}In via the excited state in ^{115}Sn to the ground state of ^{115}Sn, see figure 1. The excited state of ^{115}In was not present in this sample at the time of measurement, since the 336 keV gamma-ray line from the main branch was not detected in the spectrum.

2.2 γ-ray measurements in an underground laboratory

The γ-ray measurements were performed in the HADES laboratory in Belgium 223 m underground (Hult et al 2006) where IRMM operates 7 custom designed ultra low background γ-ray spectrometers. Three p-type HPGe detectors were made available for these measurements: Ge-4 (Hult et al 2002), Ge-7 (one of the detectors in the Sandwich Spectrometer) and the Sandwich spectrometer (Wieslander et al 2009). In the Sandwich Spectrometer the two detectors Ge-6 and Ge-7 are facing each other, see figure 2, which effectively doubles the detection efficiency compared to using a single Ge detector. The Sandwich Spectrometer's active muon shield is used to deduct the muon-induced events from

the background of the two Ge detectors. The main characteristics of the detectors are listed in table 1.

While waiting for the Sandwich Spectrometer to become available the first measurement was performed for approximately 48 days on detector Ge-4, which is a coaxial detector with a sub-micron dead layer. The second measurement was carried out on the Sandwich spectrometer with one detector (Ge-6) unavailable due to technical problems, resulting in about 15 days measurements with detector Ge-7. Finally, the third measurement lasted for almost 14 days on a fully working Sandwich Spectrometer. From a robustness point of view it can be seen as an advantage to have several measurements from different detectors provided that the results agree, so the upcoming situation with three separate measurements was in the end not considered a disadvantage.

2.3 Detection efficiency

The full energy peak efficiencies (FEP) were calculated using the Monte Carlo technique with the computer code EGS4 (Nelson et al 1985). The Monte Carlo code includes a model of the Ge detector crystal, crystal holder, cryostat, the inner 5 cm of the shield and the sample. The computer models were first set-up based on information from the manufacturer complemented with radiographs. Then the dead layer thicknesses (at the front and side) were optimised in the model by comparing the measured and the calculated efficiencies of reference sources while varying the thicknesses iteratively until a match was reached within the uncertainty of the reference sources. Acquiring exact values requires the use of coincidence summing corrections and for radionuclides with cascading γ-rays the computer models include the complete decay schemes. Although good results (±3%) have been achieved in proficiency testing using the absolute detection efficiency from Monte Carlo simulations, it is generally preferred to use a suitable reference source to obtain the absolute efficiency or to validate a computer model. For the indium measurements in this work, the computer models were validated by measuring point sources of ^{85}Sr (514 keV), ^{137}Cs (662 keV) and ^{134}Cs (475 keV) sandwiched between indium discs of 0, 3, 6 and 12 mm thicknesses. The measurements of the point sources agreed within 2% uncertainty to the simulated values, which led to the assignment of a 3% final uncertainty of the absolute detection efficiency for the 497.4 keV line from the indium sample.

2.4 Calculations

The activity measured in each detector, A_{ind} (Bq), was calculated as

$$A_{ind} = \frac{C}{\varepsilon\, t\, P_\gamma} \qquad (1)$$

where C is the net peak counts in the 497.4 keV peak, ε is the detection efficiency, t is the measurement time and P_γ is the γ-ray emission probability. The weighted mean activity, A_{mean}, for the three measurements was calculated and the half-life for the rare decay branch is then given by

$$t_{1/2}(r) = \ln 2 \left(\frac{A_{mean}\, M}{m\, \theta\, N_A} \right)^{-1} \qquad (2)$$

where $t_{1/2}(r)$ is the half-life of the rare β^- decay, M is the atomic mass, m is the mass of the sample, θ is the isotopic abundance, N_A is the Avogadro number and the the time is finally converted to years. The branching ratio, BR, of the rare decay was determined as

$$BR = \frac{t_{1/2}(r)}{t_{1/2}(d) + t_{1/2}(r)} \tag{3}$$

where $t_{1/2}$ is given for the rare (r) and the dominating (d) β^- decay respectively.

The β^- decay of the ground state of ^{115}In to the first excited state in ^{115}Sn is 2nd-forbidden unique. From a theoretical point of view, the unique forbidden beta decays are relatively simple to calculate. This is due to the fact that the dependence of the half-life on nuclear structure is, to a very good approximation, contained in only one nuclear matrix element. This nuclear matrix element has no effect on the beta-decay spectrum shape except for an overall scale. The half-life for K^{th} forbidden unique β^- decay can be simply written in the form

$$T_{1/2} = \frac{1}{M^2 f_K(w_0, Z_f, R)} \tag{4}$$

where M is the nuclear matrix element (equivalent to M_4 (Mustonen et al 2006, Heiskanen et al 2007) and $^A M^{(0)}_{K+1,\ K,\ 1}$ (Behrens and Bühring, 1982) and $f_K(w_0, Z_f, R)$ is a phase-space function which only depends on the end-point energy $W_0 = w_0\ m_e\ c^2$, the charge Z_f of the daughter nucleus and the nuclear radius R.

The detailed expression for the function f_K reads

$$f_K(w_0, Z, R) = \frac{g_A^2 (6.706 \times 10^{-6})^K}{\kappa} \sqrt{\frac{(2K)!!}{(2K+1)!!}} \times \int_1^{w_0} dw_e \sum_{k_e + k_\nu = K+2} F_{k_e - 1}(Z, w_e) \frac{w_e p^{2k_e - 1} (w_0 - w_e)^{2k_\nu}}{\sqrt{(2k_e - 1)!(2k_\nu - 1)!}} \tag{5}$$

This is easily derived from the equations from Mustonen et al (2006) or slightly more tediously from the general beta-decay formalism of Behrens and Bühring (1982). Here g_A stands for the axial coupling constant, $F_{ke\text{-}1}(Z,\ w_e)$ is the generalized Fermi function as defined in Ref. (Mustonen et al 2006), w_e is the electron energy in units of electron rest mass, $p = \sqrt{(w_e^2 - 1)}$ and the constant κ = 6147 s (Hardy et al 1990).

The nuclear matrix element M has been calculated using the same pnMQPM description of the initial and final nuclei as in Ref. (Mustonen and Suhonen 2007), where the model was successfully applied to the fourth-forbidden non-unique ground-state-to-ground-state decay of ^{115}In. The theoretical curve for the half-life of that decay as a function of the Q value is in perfect agreement with the latest joint measurement (Pfeiffer et al 1978) of the decay Q value and the half-life, as seen in figure 6. This figure, together with the comparison between the experimental and pnMQPM energy spectra in Ref. (Mustonen and Suhonen 2007), indicates that our theoretical wave functions for the low-energy states of these nuclei are reasonably good.

3. Results

The indium and background spectra in the range from 40-600 keV from detector Ge-4 and the Sandwich Spectrometer are shown in figure 3, in which the bremsstrahlung from the continuous β^- radiation from the dominating decay branch of ^{115}In is clearly visible. In figure 4 the spectra from all three measurements are displayed in the interesting region around the peak 497.4 keV. In figure 5a-c the spectra from Ge-4, Ge-7 and the Sandwich spectrometer are shown in the interesting region together with the background of each detector respectively.

The results from the calculations of the half-life and the branching ratio are presented in table 2. The final relative combined standard uncertainty was determined to 15% and is dominated by counting statistics (14%). Apart from the counting statistics, the other main contributions to the final uncertainty are: the half-life of the dominating β^- decay to the ground state of ^{115}Sn (5.7%), the detection efficiency (3%), the isotopic abundance (0.05%) and the internal conversion coefficient (0.12%). The uncertainties are expressed as standard uncertainties following the *Guide to the Expression of Uncertainty in Measurement* (ISO 1995) given in brackets after each measurement value and the last digit(s) of their numerical value correspond(s) to the last digit(s) of the quoted result.

By using equation (5) the logarithm of the comparative half-life can be calculated as

$$\log f t_{1/2} = 12.9 \pm 0.8$$

where $t_{1/2}$ is the half-life for the rare decay, see table 2, in seconds and f (Z=49, E_0=57eV) is determined from eq. (5) for ^{115}In. Using equation (4) we can plot the endpoint energy dependence of the partial half-life for the 2nd-forbidden unique decay to the first excited state of ^{115}Sn, see figure 7, and deduce that the experimentally determined partial half-life of $(4.1 \pm 0.6)\cdot 10^{20}$ y (table 2) corresponds to the Q value (57±3) eV.

4. Discussion

The three measurements in this work and the final result of the branching ratio compares well to the value given by Cattadori et al (2005). In addition, the measurement set-up in this work was designed for this particular measurement and hence the value has, as expected, lower uncertainty i.e. a relative uncertainty of 15% in comparison to Cattadori's earlier measurement of 26%. The main part of the uncertainty in these measurements originates from counting statistics and consequently would a longer measurement reduce this uncertainty. By producing reference samples that are similar to the sample used in this measurement, it should be possible to reduce the uncertainty of the efficiency determination to approximately 1%. However, better accuracy in the current value of the half-life of the dominating β^- decay, $(4.14\pm0.25)\cdot 10^{14}$, is required in order to significantly improve the value of the rare decay branching ratio.

Since no unknown radionuclides above the decision threshold could be detected it is concluded that no significant impurities were present in the sample. The strong bremsstrahlung continuum from the indium disc disturbs the detection limits at gamma-ray energies below approximately 400 keV. But, at energies above 400 keV the decision thresholds (using α=0.05) for some of the common primordial radionuclides were caluclated: ^{40}K 2 mBq/kg, ^{228}Ra 0.5 mBq/kg and ^{228}Th 0.4 mBq/kg.

The Q value of the rare decay is determined by using equations and until the Q value is verified with mass measurements, there is a some uncertainty in the correctness of the model equations.

5. Conclusions

A 497.4 keV γ-ray was detected when measuring a 2.57 kg ultra pure indium sample in the underground laboratory HADES. The γ-ray is attributed to the de-excitation of ^{115}Sn, which follows from the rare β^- decay branch from the ground state of ^{115}In to the first excited state in ^{115}Sn. The partial half-life of the rare decay branch was determined to $(4.1 \pm 0.6)\cdot10^{20}$ years and the branching ratio to $(1.07 \pm 0.17)\cdot10^{-6}$, which agree with the only previously reported value $(1.18 \pm 0.31)\cdot10^{-6}$ by Cattadori et al (2005). By using recently developed model equations by Mustonen and Suhonen (2007) the comparative half-life, $\log(ft_{1/2})$, was determined to (12.9 ± 0.8) and, finally, the Q value to (57 ± 3) eV. This suggests that the decay of ^{115}In to the excited state of ^{115}Sn may have the lowest beta-decay Q value discovered so far, two orders of magnitude smaller than that of ^{187}Re (Galeazzi et al 2000).

Acknowledgements

The work done by EURIDICE and the HADES crew of SCK•CEN in Mol, Belgium, is gratefully acknowledged.

References

Behrens H and Bühring W 1982 *Electron Radial Wave Functions and Nuclear Beta-Decay*, Clarendon Press, Oxford.

Cattadori C M, De Deo M, Laubenstein M, Pandola L and Tretyak V I 2005 Observation of β decay of ^{115}In to the first excited level of ^{115}Sn *Nucl. Phys. A* **748** 333-347

Galeazzi M, Fontanelli F, Gatti F and Vitale S 2000 The end-point energy and half-life of the ^{187}Re β decay *Phys. Rev. C* **63** 014302

Hardy J C, Towner I S, Koslowsky V T, Hagberg E and Schmeing H 1990 Superallowed $0^+ \rightarrow 0^+$ nuclear β-decays: A critical survey with tests of CVC and the standard model *Nucl. Phys. A* **509** 429-460

Heiskanen H, Mustonen M T and Suhonen J 2007 Theoretical half-life for beta decay of ^{96}Zr *J. Phys. G: Nucl. Part. Phys.* **34** (5) 837-843

Hult M 2007 Low-level gamma-ray spectrometry using Ge-detectors *Metrologia* **44** S87-S94 (Erratum in Metrologia **44** 425.)

Hult M, Preuße W and Gasparro J 2006 Underground Gamma-ray spectrometry *Acta Chimica Slovenica* **53** 1-7

International Standard Organisation, Geneva, Switzerland 1995 Guide to the expression of uncertainty in measurement *ISO/IEC/OIML/BIPM* (1st corrected edition)

IUPAC, Inorganic Chemistry Division, Commission on atomic weights and isotopic abundances, Subcommittee for isotopic abundance measurements 1998 Isotopic compositions of the elements 1997 *Pure and Applied Chemistry* **70** (1) 217-235

Murri E L, McIsaac L D and Helmer R G 1967 Decay of In^{115m} *Phys. Rev.* **155** (4) 1263-1264

Mustonen M T, Aunola M and Suhonen J 2006 Theoretical description of the fourth-forbidden non-unique decays of ^{113}Cd and ^{115}In *Phys. Rev C* **73** 054301 (Erratum in Phys. Rev. C **76** 019901)

Mustonen M T and Suhonen J 2007 Microscopic quasiparticle-phonon description of beta decays of ^{113}Cd and ^{115}In using proton-neutron phonons *Phys. Lett. B* **657** 38-42

Nelson W R, Hirayama H and Rogers D W O 1985 The EGS4 code system, *SLAC Report*.

Pfeiffer L, Mills A P Jr, Chandross E A and Kovacs T 1979 Beta spectrum of ^{115}In *Phys. Rev.* **19** (3) 1035-1041

Pfeiffer L, Mills A P Jr, Raghavan R S and Chandross E A 1978 Indium-Loaded Liquid Scintillator for Low-Energy Solar-Neutrino Spectroscopy *Phys. Rev. Lett.* **41** 63-66

Wieslander J S E, Hult M, Gasparro J, Marissens G, Misiaszek M and Preuβe W 2009 Accepted for publication in *Appl. Radiat. Isotopes*.

Tables

Table 1. Characteristics of the 3 HPGe detectors used in this study. The uncertainties are in brackets.

	Ge-4	Ge-6	Ge-7	Sandwich detector (Ge6 + Ge7)
Relative efficiency	106%	80%	90%	See Ge6 and Ge7
Diameter × thickness (cm)	8.25×7.8	7.80×8.40	8.05×6.65	See Ge6 and Ge7
Endcap material	Al	Cu	Al	See Ge6 and Ge7
Thickness of copper lining (cm)	10	3.5		See Ge6 and Ge7
Thickness of lead shield (cm)	15	18.5 cm		See Ge6 and Ge7
Background count rate at 497.4 keV (counts d^{-1})	0.20(3)	0.38(12) [a]	0.42(15) [a]	0.80(19) [a]
FEP efficiency for the In-disc at 497.4 keV	1.71%	0.70%	1.69%	2.39%
Measurement time (days)	47.9	-	14.7	13.8

[a]Data for which the muon induced events are removed.

Table 2. Results from the γ-ray measurements of the indium disc on detectors Ge-4, Ge-7 and the Sandwich spectrometer. The results from the only previous measurement by Cattadori et al (2005) is included for comparison.

	Branching ratio $\cdot 10^{-6}$	Half-life $\cdot 10^{20}$ (y)	Relative uncertainty (%)
Ge-4	1.06(17)	4.2(7)	17
Ge-7	1.0(5)	4.4(2.0)	45
Sandwich spectrometer	1.2(4)	3.6(1.2)	42
Combined final results HADES	**1.07(17)**	**4.1(6)**	**15**
For comparison Cattadori et al. (2005)	1.2(3)	3.73(1.0)	26

Figures and figure captions

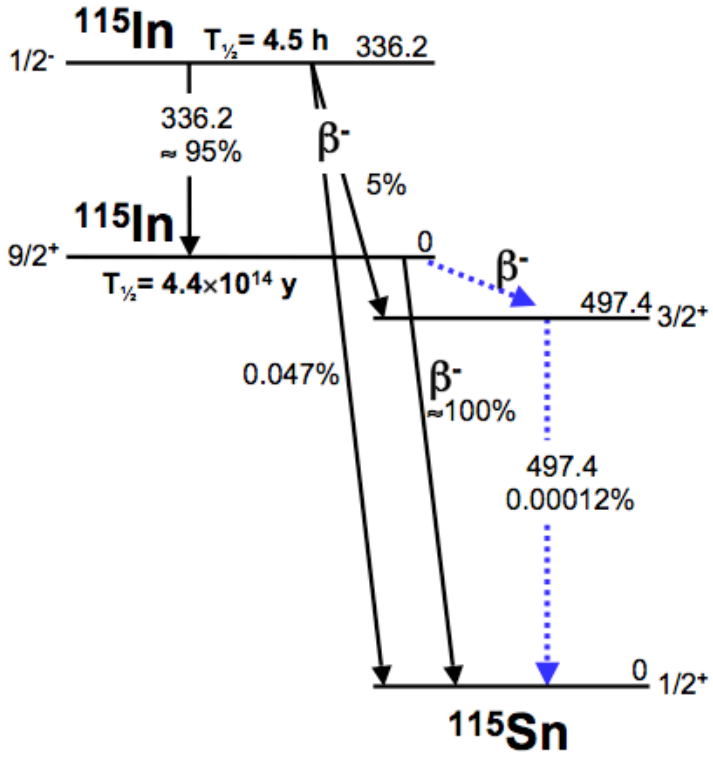

Figure 1. The level scheme of ^{115}In and its decay to the first excited state in ^{115}Sn.

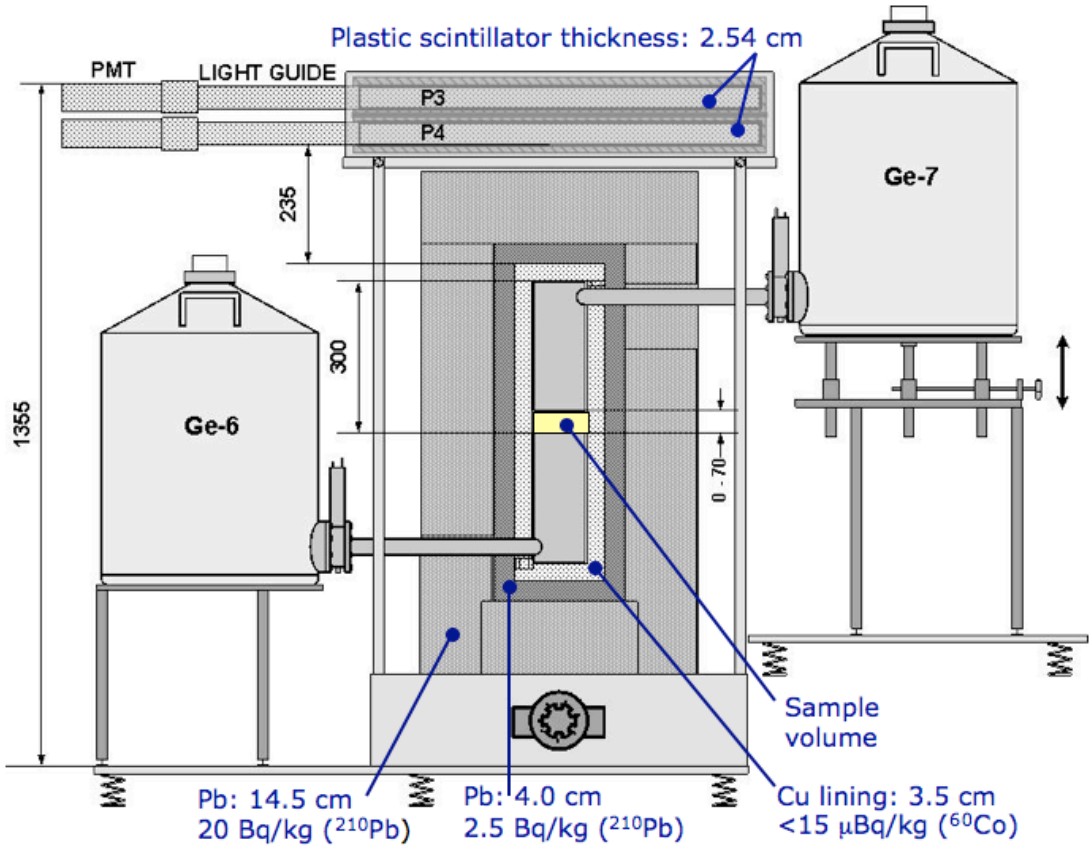

Figure 2. The Sandwich spectrometer set-up with two germanium detectors (Ge-6 and Ge-7) and the two plastic scintillators (P3 and P4) working as active muon shield.

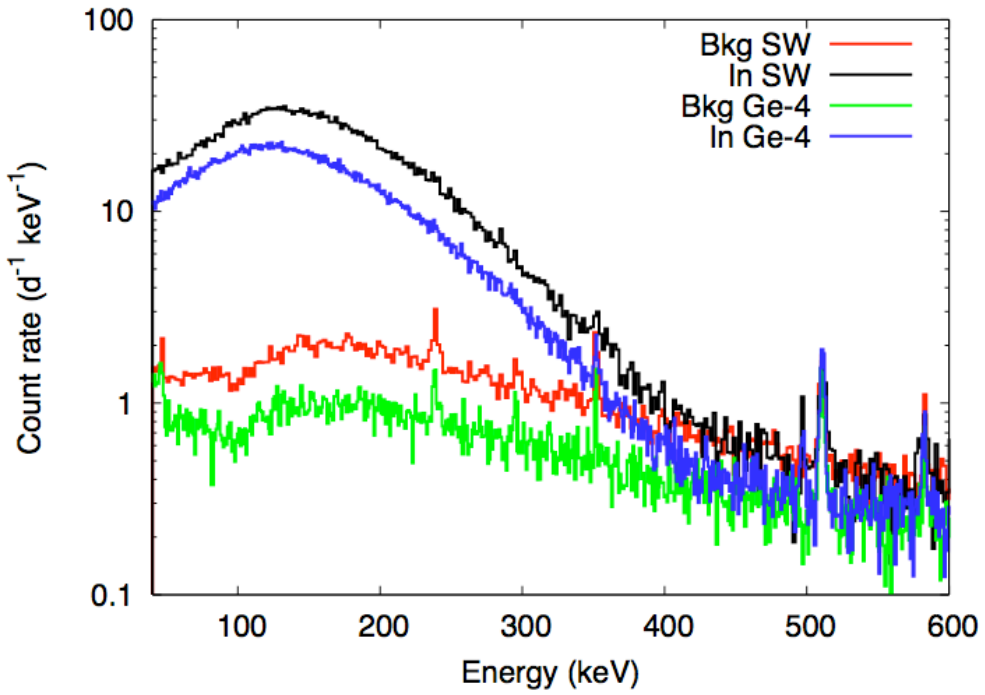

Figure 3. Indium (In) and background (Bkg) for the range 40-600 keV on the Ge-4 detector (Bkg Ge-4 and In Ge-4) and the Sandwich spectrometer (Bkg SW and In SW).

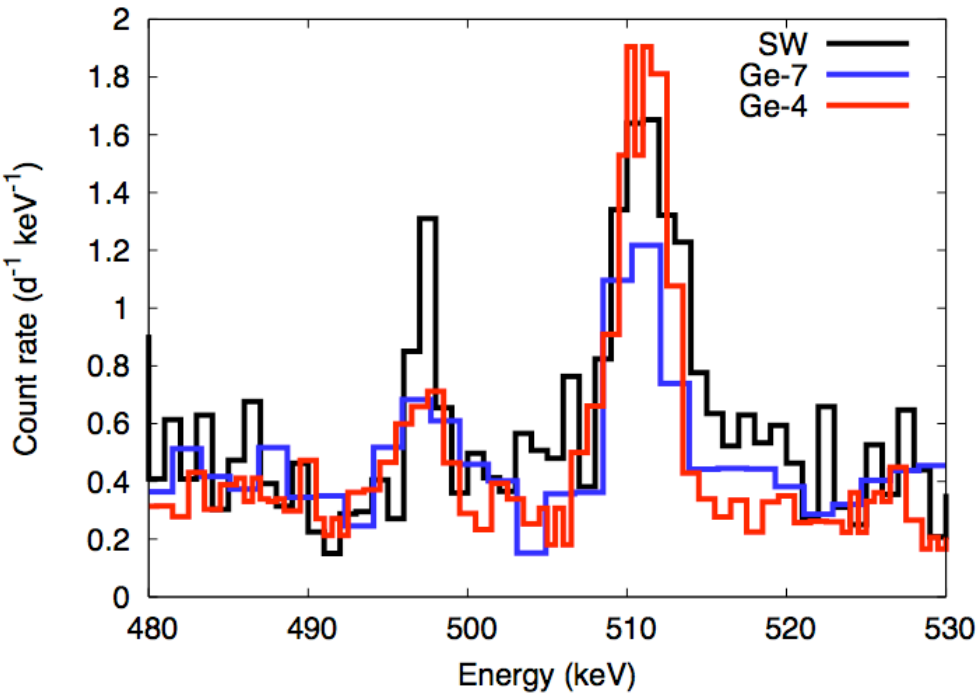

Figure 4. The indium spectra from all three measurements on the Sandwich spectrometer (SW, black), detector Ge-7 (Ge-7, blue) and Ge-4 (Ge-4, red).

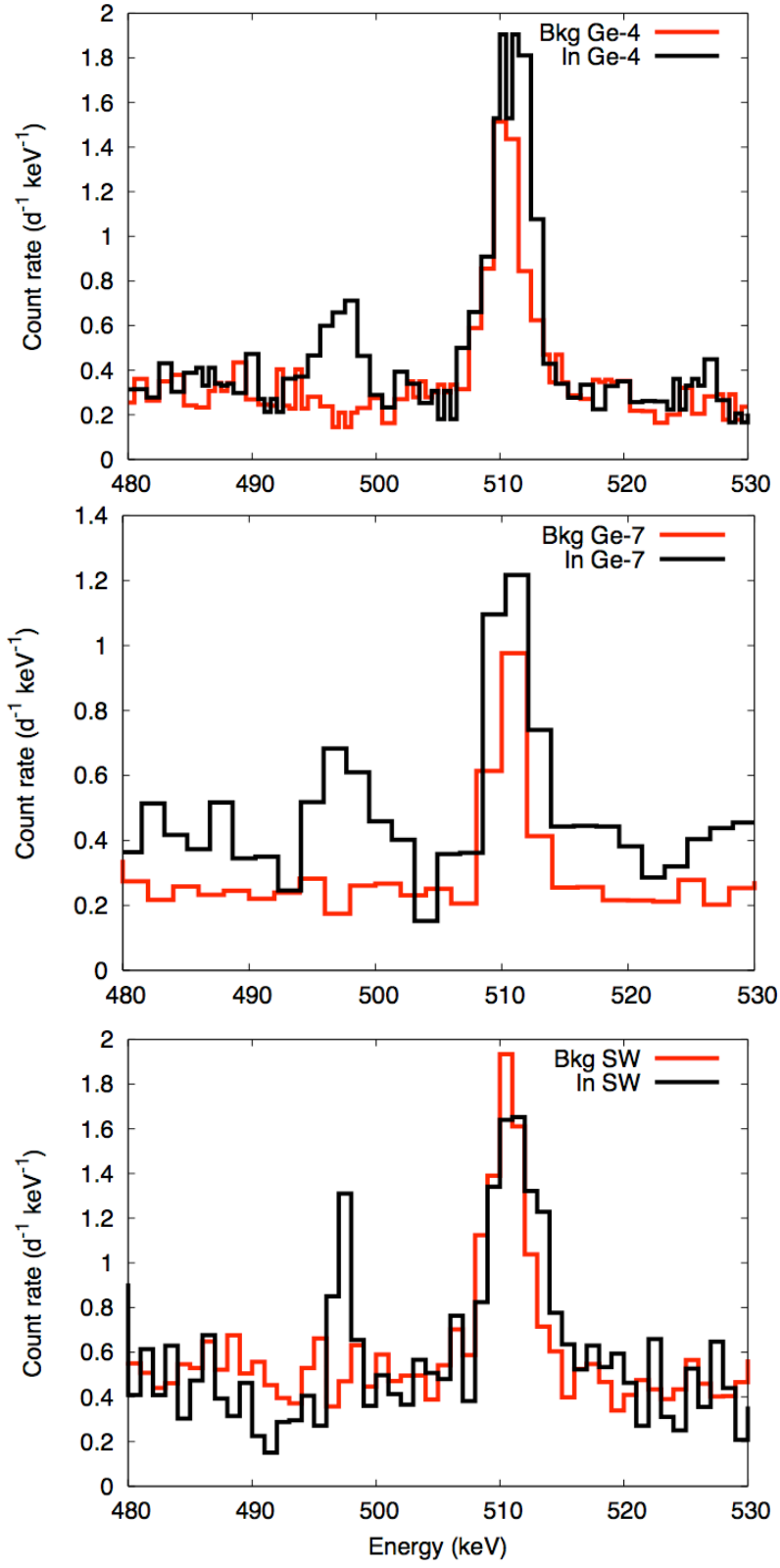

Figure 5. Indium (In) spectra and background (Bkg) for the measurements on the a) Ge-4 detector, b) Ge-7 detector and c) the Sandwich spectrometer (SW).

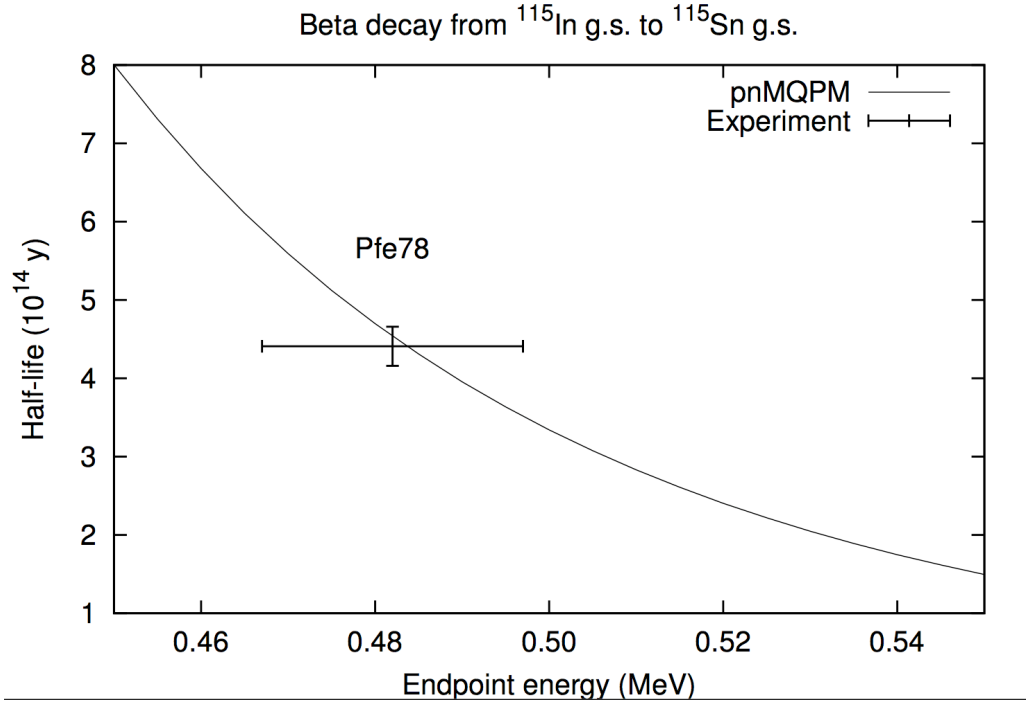

Figure 6. The theoretical half-life of the ground-state-to-ground-state β^- decay of ^{115}In as the function of the endpoint energy. The pnMQPM description of Ref. (Mustonen et al 2007) has been used. The experimental point has been taken from Ref. (Pfeiffer et al 1978).

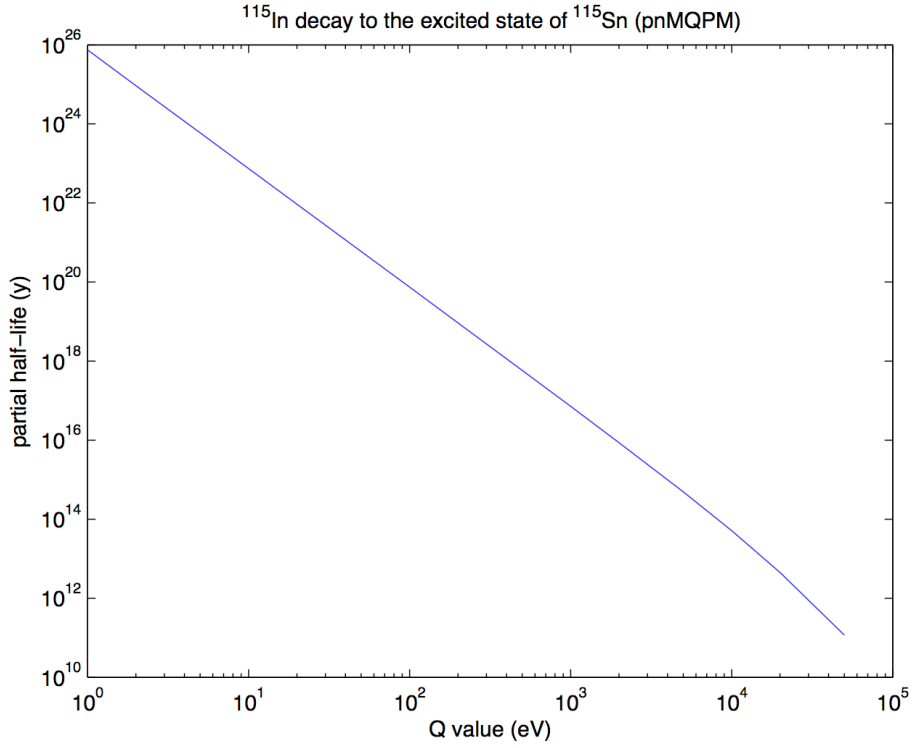

Figure 7. The theoretical half-life of the ground-state-to-first-excited-state β^- decay of ^{115}In as the function of the endpoint energy. The pnMQPM description of Ref. (Mustonen et al 2007) has been used to obtain the required nuclear matrix element.